MOLECULAR MECHANISMS OF MEASLES VIRUS ENTRY AND EXIT

by

VÍTOR DANIEL GONÇALVES CARNEIRO

A thesis submitted to the University of Birmingham

For the degree of DOCTOR OF PHILOSOPHY

Institute of Immunology and Immunotherapy

College of Medical and Dental Sciences

University of Birmingham

November 2016

ABSTRACT

Measles is a leading cause of mortality in infants in countries with suboptimal vaccination coverage. This disease is caused by a negative-strand RNA virus, measles virus (MeV). Wild-type strains of the virus use two cellular receptors to invade cells and establish infection: the signalling lymphocyte activation molecule f1 (SLAMF1), which is present on certain immune cells, and nectin-4, which is expressed in the lung epithelium. During infection, MeV can spread through the release of virions or by inducing cell-cell fusion. The aim of this thesis is to determine the molecular mechanism underlying viral entry and exit. Herein, I observed that, upon attachment to SLAMF1+ cells, MeV particles induce extensive but transient membrane blebbing and cytoskeleton contraction. MeV entry occurred simultaneously with fluid-uptake and was sensitive to inhibitors of macropinocytosis and cytoskeleton dynamics. In contrast, the cortical actin network restricted the early stages of MeV-induced cell-cell fusion, in RhoGTPases, ezrin and moesin dependent manner. By resolving the proteome of infected cells, conserved phosphorylated residues in the viral haemagglutinin were also shown to impact on dimerization and cell-cell fusion. These results suggest the manipulation of several cellular components and pathways during entry and exit of MeV.

“

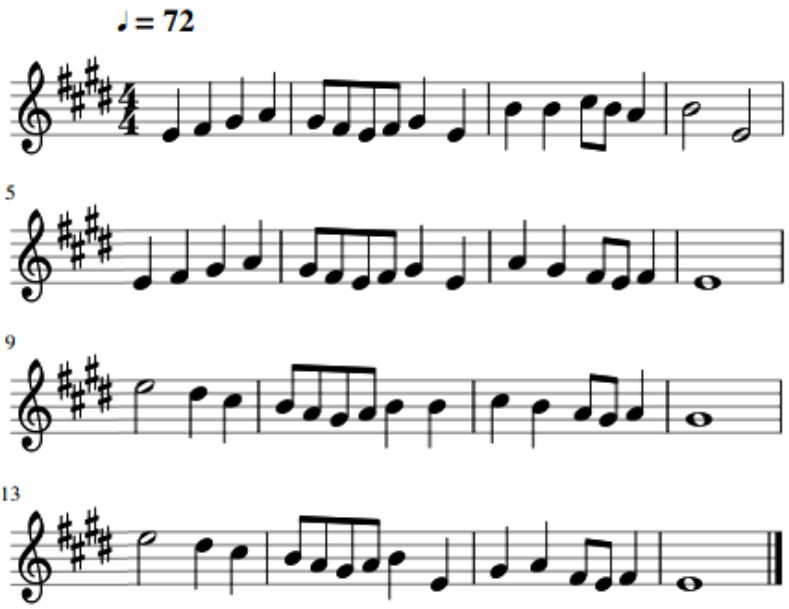

Joly Braga Santos – Symphony No. 4

Opus 16 Lento

ACKNOWLEDGEMENTS

Most of all, I would like to thank Dr Dalan Bailey, my supervisor and mentor, whose guidance, dedication and creativity have supported and inspired me throughout the past 3 years. I feel very privileged to have been his student and I can only hope that I can recreate his ingenuity and passion for science for the rest of my career. Secondly, I would like to acknowledge my co-supervisor Professor Jane McKeating for her guidance, patience and kindness throughout my PhD and to be a role model of inventiveness and excellence in virology research that I hope I can follow.

I would also like to thank the present and previous members of our group, Joe, Corwin, Naz, Clare, Phil, Callum, Salman, Sha, Edouard and Tayo, for all the experimental help and enjoyable times we had together. A special thank you to Machaela and Johnny, two very talented students that I had the pleasure to supervise, whose unbelievable hard work and dedication contributed to some of the results in this thesis. A big thank you to everyone in the McKeating's group for their help and expertise throughout my doctorate. I would also like to thank the people in Zania Stamataki's group, Sudha, Ben, Susan, Kostas and my partner in crime Scott for their support and friendship. To my friends in and outside of Birmingham, Isa, Jaclyn, Luca, Cami, Francis, Malwina, Chris and Raquel, for making my time in the UK unforgettable.

I would like to acknowledge the University of Birmingham for funding me, as well as the Microbiology Society, Biochemical Society and PrimerDesign Ltd for additional funding. Thank you to everyone in Professor Ian Goodfellow's lab group, at the University of Cambridge, for welcoming me and teaching me so much about proteomics.

Lastly, I would like to thank all my friends and family, particularly my mother and my sister, for always believing in me.

TABLE OF CONTENTS

Chapter 1: General Introduction

Chapter 2: Materials and Methods

LIST OF FIGURES

Chapter 1

Chapter 2

Chapter 3

Chapter 4

Chapter 5

Chapter 6

Chapter 7

LIST OF TABLES

Chapter 2

LIST OF ABBREVIATIONS

+	Positive
A	Adenosine
AD	Anno domini
ADAR-1	Adenosine deaminase actin on RNA-1
BC	Before Christ
Bleb	Blebbistatin
C	Cytosine
Cav1	Caveolin-1
CD	Cluster of differentiation
CDV	Caninde distemper virus
CDV	Canine distemper virus
CeMV	Cetacean morbillivirus
CHC	Clathrin heavy chain
CytoD	Cytochalasin D
DC	Dendritic cell
DMEM	Dulbecco’s modified Eagle’s medium
DNA	Deoxyribonucleic acid
Dyn2	Dynamin-2
ECHS	Mitochondrial short chain enoyl-CoA hydratase
EDTA	Ethylenediaminetetraacetic acid
EGFP	Enhanced Green Fluorescent Protein
EIPA	5-(N,N-Dimethyl)amiloride

EPS15	Epidermal growth factor receptor pathway 15
ESCRT	Endosomal sorting complexes required for transport
F	Fusion protein
FAO	Food and Agriculture Organisation
FBS	Foetal bovine serum
FBS	Foetal bovine serum
FcγRII	Fc receptor for immunoglobulin G
FDR	False discovery rate
FL	Full-length
Fluc	Firefly luciferase
FmoPV	Feline morbillivirus
G	Guanine
GAPDH	Glyceraldehyde 3-phosphate dehydrogenase
GMQE	Global Model Quality Estimate
GP	Glycoprotein
H	Haemagglutinin
HBSS	Hank’s balanced salt solution
HEK293T	Human Embryonic Kidney 293T cells
HEPES	4-(2-hydroxyethyl)-1-piperazineethanesulfonic acid
HIV	Human Immunodeficiency virus
ICAM	Intercellular adhesion molecule
IgG	Immunoglobulin G
IgM	Immunoglobulin M
IL	Interleukin

IRGM	Immunity-related GTPase M
Jasp	Jasplakinolide
L	Large protein
LB	Lysogenic broth/Luria Bertani
LCL	lymphoblastoid cell line
M	Matrix protein
MEK1/2	Mitogen-activated protein kinase kinases 1 and 2
MeV	Measles virus
MIBE	Measles inclusion body encephalitis
Moesin	DC-SIGN
MOI	Multiplicity of infection
MS	Mass spectrometry
MTT	3-(4,5-dimethylthiazol-2-yl)-2,5-diphenyltetrazolium bromide
N	Nucleocapsid
NE	Non envelope
NF-κB	Nuclear factor κ-B
nt	nucleotides
OIE	World Organization for Animal Health
ORF	Open reading frame
P	Phosphoprotein
PAK-1	P21 activated kinase 1
PCR	Polymerase chain reaction
PDV	Phocine distemper virus
PFA	Paraformaldehyde

PFU	Plaque-forming-unit
PI3P	Phosphotidyinositol-2-phosphate
PP	Pseudotyped particles
PPRV	Peste des petits ruminants virus
PVDF	Polyvinylidene difluoride
RdRp	RNA-dependent RNA polymerase
RFP	Red fluorescent protein
RIPA	Radioimmunoprecipitation assay buffer
RLuc	Renilla luciferase
RLuc	Renilla renifmorfis luciferase
RNA	Ribonucleic acid
RNP	Ribonucleoprotein
ROCKI	RhoA kinase
RPD	Rinderpest virus
RPMI	Roswell Park Memorial Institute
RSV	Respiratory syncytial virus
RT	Reverse transcriptase
SDM	Site directed mutagenesis
SDS-PAGE	Sodium dodecyl sulphate-polyacrylamide gel electrophoresis
siRNA	short interfering RNA
SOC	Super optimal broth with catabolite repression
SSPE	Subacute sclerosing panencephalitis
T	Thymine
TBE	Trizma Base, boric acid and EDTA

TBS	Tris-buffered saline
TCID50	tissue culture infectious dose 50
TLR	Toll-like receptor
TNE	Tris/EDTA saline
U	Uracyl
UV	Ultraviolet
V	Variable
VLP	Virus-like particle
VPS	Vesicular protein sorting
VSV-G	Vesicular stomatitis virus glycoprotein
WHO	World health organisation

Chapter 1

GENERAL INTRODUCTION

Viruses are a leading cause of mortality and morbidity for humankind. Since the birth of the first civilisations, infectious diseases have had a significant impact on the public health, economy and development of nations. Together with smallpox, measles virus (MeV) is one of the first pathogens known to infect humans in record, being firstly described and distinguished from smallpox infection by the Persian physician Rhazes, in the 10th century AD. MeV's origin is proposed to coincide with the domestication of cattle in Mesopotamia, in approximately 10,000 BC; MeV is thought to have jumped from an ancient common ancestor of the bovine pathogen, rinderpest virus (RPV) [1]. Spreading during the expansion of the Roman empire, MeV was probably endemic in Europe, North Africa and the Middle East in the 1st century BC [2]. Some speculate that the disease had reached China and Southeast Asia by the 7th century, transmitted by merchants via the Silk Road [3]. MeV did not spread to the New World until the 15th century, when Portuguese and Spanish explorers colonised the Americas. The introduction of this pathogen, in combination with smallpox, had a devastating impact on the naïve populations of the continent, with some estimates suggesting they reduced the indigenous populations by 90%. In 1758, in Scotland, MeV was first identified as the causative agent of measles by Francis Home [4]. True global spread was finally achieved in the 1850s, when British sailors introduced the disease in Australia [5]. After centuries of causing morbidity and mortality in human populations, the first efficacious measles vaccine was developed in 1963 by John Enders and colleagues, a live attenuated vaccine derived from the original isolation of the virus (made from an 11-year-old boy, David Edmonston) [6]. The number of people affected by measles has progressively

reduced since the introduction and wide-distribution of this vaccine, a trend that is supported by ongoing international efforts to eradicate MeV.

1.1 The *Morbillivirus* genus

Taxonomically, MeV belongs to the genus *Morbillivirus*, and by extension to the *Paramyxoviridae* family, two groups that classify enveloped, non-segmented, negative-sense, single-stranded RNA viruses. Aside from MeV the genus *Morbillivirus* contains viruses that infect several species of mammals, including carnivores, ruminants, cetaceans and primates. RPV was the causal agent of a plague in cattle and other ungulates, and, while extant, had a profound impact on livestock throughout the centuries [7]. In infected cattle this virus caused a substantial mucosal degradation of the oral-nasal cavity and digestive tract together with prolonged leukopenia; symptoms that were coincident with severe dehydration and diarrhoea that commonly led to death [8]. After extensive vaccination campaigns, the Food and Agriculture Organisation (FAO) together with the World Organization for Animal Health (OIE) achieved the global elimination of RPV, becoming the second viral disease ever to be eradicated, after smallpox [9]. Other ruminants are infected by a closely related virus, Peste des petits ruminants virus (PPRV) which causes a similar disease in sheep and goats. This disease is endemic in several regions of Africa, Southeast Asia, India and Middle East where it is responsible for a vast economic burden [10]. Although PPRV is also able to infect cattle asymptomatically, propagation of the disease is limited by cross-reaction with RPV-induced antibodies [11]. Several control campaigns are already underway, and some authors consider PPRV the most likely next eradicable pathogen [12-14].

1.1.1 Hosts and disease

Members of the *Morbillivirus* genus can infect a wide range of animals, including humans, dogs, cats, whales, sheep and goats, cattle, dolphins, bears, etc., causing a transient immunosuppression and several respiratory and neurological illnesses. Morbilliviral infections are wide spread among carnivores, with major pathogens including canine distemper virus (CDV), phocine distemper virus (PDV) and the recently identified feline morbillivirus (FmoPV). CDV's natural hosts include several families of the *Carnivora* order, including dogs, foxes, racoons, skunks, hyenas, and tigers [15, 16]. It causes similar symptoms to RDV and PPRV infections, as well as a profound, rapidly-progressing encephalitis [17]. Due to its prominent neurotropism, CDV is used as model to study multiple sclerosis [18]. In the last decade an expansion of the already broad spectrum of CDV hosts has been observed, suggesting a propensity for the virus to quickly adapt to new host species [19]. After an outbreak in a monkey population in China, studies showed that CDV can rapidly adapt *in vitro* to human receptors, raising concerns about the possible adaptation of this virus to humans in nature [20-22]. Although CDV has been shown to infect domestic cats [23], a distinctive feline-specific morbillivirus, FmoPV, was first identified in domestic cats in China and Japan associated with tubulointerstitial nephritis, and it is now assumed to have a global distribution [24-26]. PDV outbreaks have been reported in seal populations, especially in Northern and Western Europe, with recorded mortality rates up to 60% [27, 28]. This disease is symptomatically related to CDV in dogs, causing a severe demyelinating disease [29, 30].

Morbilliviruses have also been identified in other marine mammals. These are described as cetacean morbilliviruses (CeMV) and infect porpoises, dolphins and whales [31, 32]. Genetic comparison studies show that CeMV is more similar to RPV than to PDV and CDV, suggesting a different route for its evolution [33]. Mortality in CeMV infection is associated with severe pneumonia and lung failure, accompanied by general immunosuppression and multifocal encephalitis [34].

Finally, several morbillivirus-like RNA sequences have been identified in tropical bats and rodents [35]. Despite the lack of infectious viruses isolated from these animals, these data suggest a much broader tropism for morbilliviruses than previously thought, and may also represent possible zoonotic transmissions to humans, which may collide with MeV eradication efforts. The global burden of morbillivirus infections in humans and livestock, combined with the potential for zoonotic transfer, highlight the importance of this genus of viruses. Improving our understanding of virus infection and transmission will generate better control mechanisms and therapeutic approaches for measles and other morbilliviruses.

1.2 Measles virus: the causative agent of measles

The morbillivirus that infects humans, MeV, causes a disease of the same name, known as measles. Humans are the natural host of MeV, but other primates can be experimentally infected [36]. Although public health actions, mainly vaccination, have decreased the number of cases reported worldwide, measles is still a leading cause of morbidity and mortality among young children in Africa and Asia [37]. Secondary

infections also contribute to the mortality rate, i.e. when opportunistic pathogens take advantage of the long-term immune suppression induced by MeV [38, 39].

1.2.1 Measles, the disease

1.2.1.1 Transmission

Measles is an airborne disease and MeV is transmitted via aerosols through the respiratory route (**Fig.1-1A**). Once in its host, the virus first infects resident alveolar macrophages and dendritic cells of the airway tract. Infection later spreads to local lymph nodes before being finally transmitted to the epithelial cells of the lungs and trachea. After viremia, the virus infects the airway epithelium and releases infectious viral particles into the lumen which are expelled into the environment and transmitted to new hosts [36, 40]. In addition, mesenchymal and neuroendocrine cells are also important target cells for MeV, and are likely to be involved in the immune- and neuropathologies associated with infection [16].

1.2.1.2 Symptoms

Measles is commonly diagnosed through the characteristic rash it causes, but it is also associated with general cold-like symptoms and an increase in complications related to secondary infections, such as pneumonia. Measles has a latent period of 10 to 14 days, and symptomatically initially presents with fever, conjunctivitis and a cough, as well as small white lesions on the mucosa

Fig.1-1. Measles virus is the causative agent of measles. (**A**) Droplets containing MeV particles inhaled by the host interact with resident dendritic cells and macrophages of the lung. Infection spreads to the local lymph nodes where it develops and causes viremia. After systemic distribution of the virus, circulating lymphocytes infected with MeV interact with the basal surface of the airway epithelium, which becomes infected. New viral particles are then released into the lumen of the lung and expelled. Adapted from [41]. (**B**) Koplik's spots are one of the earliest signs of MeV infection and are characterised by small white spots on the internal epithelia of the cheek. Adapted from [42]. (**C**) The maculopapular rash of measles appears later on during infection, initially presenting on the neck and face before spreading through the rest of the body. Adapted from [42].

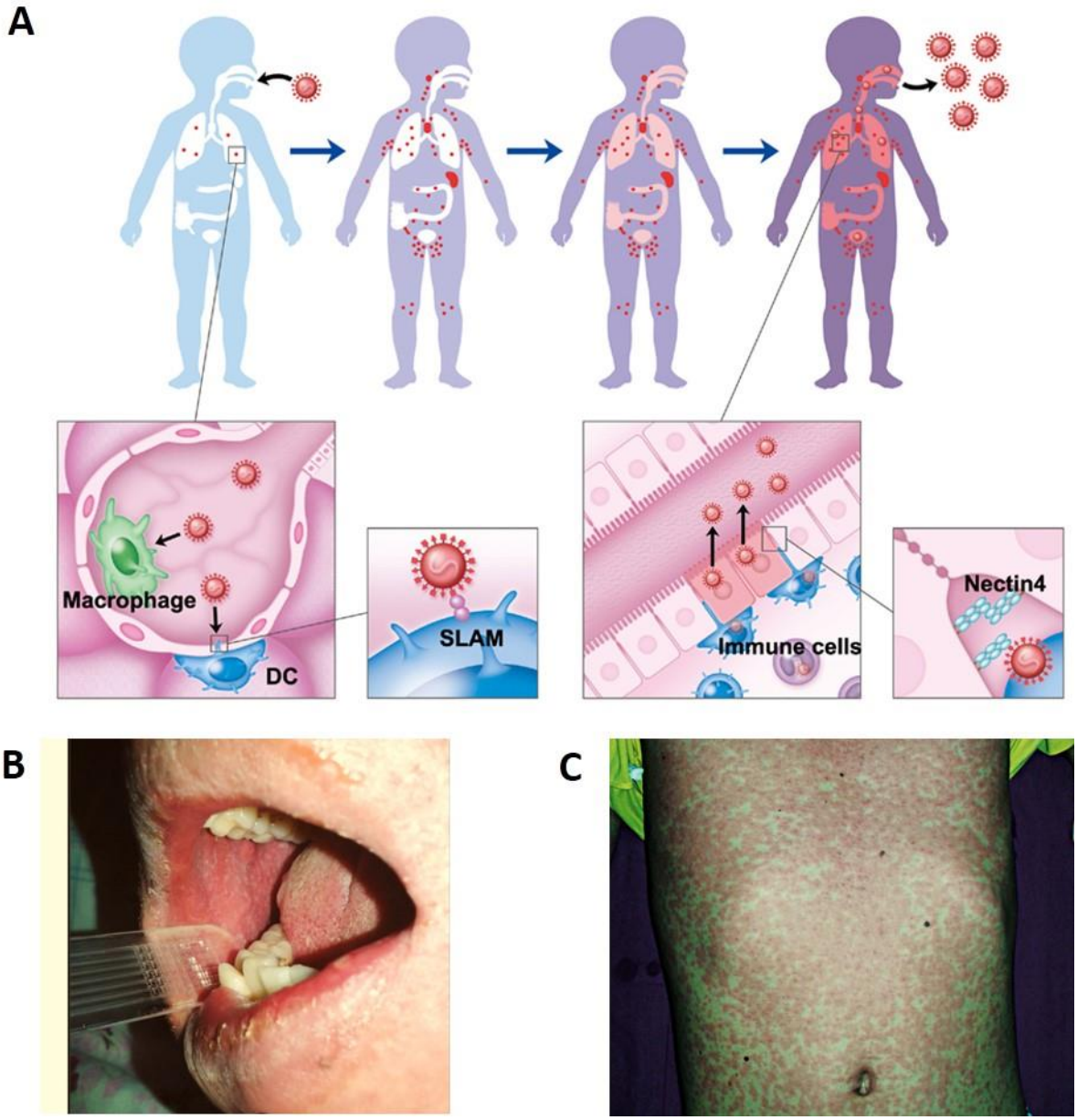
A
Macrophage
DC
SLAM
Immune cells
Nectin4
B
C

of the mouth known as Koplik's spots (**Fig.1-1B**). This is followed by a maculopapular rash with concentrated distribution on the face and chest (**Fig.1-1C**) [1, 43]. The typical maculopapular rash caused by MeV results from an inflammatory reaction where deposits of viral proteins complexed with MeV-specific antigens. Accordingly, no infectious viral particles can be recovered from the rash. Histological analysis of the rash has shown that epithelial cells infected with MeV are closely associated with infiltrated T lymphocytes [44], while no rash is observed in patients lacking a strong immune response [45, 46]. Concurrent to the manifestation of the maculopapular rash is the development of an adaptive immune response. Immune reactions are usually sufficient to clear infection, and after this period infectious virus particles cannot be recovered from the blood [47-49]. Interestingly, viral RNA can still be detected in lymph nodes and lung epithelial cells for up to three months, suggesting a persistence of viral genetic material after the resolution of infection [50]. Although life-long immunity is achieved, a prolonged immunosuppression, which lasts for several months, increases the susceptibility to secondary infections. In fact, bacterial and viral-associated pneumonia are responsible for the majority of fatal cases during measles infection [1, 51].

1.2.1.2 Rare complications

Other severe, yet rarer, complications of MeV infection are related to the central nervous system and present as a distinct range of sequelae and symptoms. Acute demyelinating encephalomyelitis, an autoimmune disease, can occur one month after the initial infection. Although associated with MeV infection, viral proteins and RNA cannot be detected in the brain [52]. In other cases, a persistent infection of MeV can

develop causing severe forms of encephalitis that only manifest several months, or even years, after the initial infection. Subacute sclerosing panencephalitis (SSPE) and measles inclusion body encephalitis (MIBE) are the most common complications in this context. While MIBE only occurs in immunocompromised patients, within nine months after infection, SSPE manifests several years after acute infection. In both cases, neurological damage of the brain is a consequence of virus-derived pathogenesis (demyelination, astrogliosis, infiltration of lymphocytes, etc.) and leads to dementia, seizures, spasms and death [53, 54]. Treatment is limited for measles-related encephalopathies, and there is no current cure.

1.2.2 Epidemiology

Despite an efficacious vaccine being available, measles still has a global incidence and causes thousands of deaths per year. The majority of cases in recent years have been documented in South East Asia, the West Pacific region and Africa [55]. Furthermore, measles is still a leading cause of death among children in Africa and some parts of Asia. In 2014, there were 266,701 cases of measles reported worldwide with over 145,000 estimated deaths in 2013 [56] and 114,900 in 2014 [55]. Measles is a disease characterized by both high mortality and morbidity [57]. However the number of reported cases of measles has been steadily decreasing since 1980, as a consequence of widespread immunization with most countries undertaking national vaccination programmes [56]. After the introduction of immunization, measles incidence dropped from 70.9 cases/100,000 individuals/year to 0.9 cases/100,000/year. Models have shown that a 1% increase in vaccine coverage equates to a 2% decrease in incidence [58]. Prior to routine vaccination,

measles caused an estimated 2.6 million deaths per year and it was estimated that 90% of children had contracted the disease by the age of 10 [59]. According to WHO, over 95% of measles deaths occur in countries with low income and weak healthcare infrastructure.

Measles is sustained through an unbroken chain of human-to-human transmission, and no animal or environmental reservoir is known to exist [60]. Although persistent infection occurs in the population, especially within cases of SSPE, as described above, these are not considered reservoirs for onward infection, since neurons and glial cells infected with measles produce defective virions. Interestingly, some serological studies have presented evidence of measles virus infection in wild populations of primates in India and Indonesia [61, 62]. These cases are assumed to be the result of transmission from human to primates [60].

1.2.2.1 Transmission

The transmission of measles occurs through contaminated respiratory aerosols, i.e. those produced by sneezing, coughing or alternatively through direct contact with the throat phlegm, nasal secretions or other contaminated body fluids of infected people, such as excretions from the eye and urine. Environmental transmission of MeV is also possible, e.g. in closed spaces, such as medical examination rooms and aeroplanes, because the virus remains contagious on fomites and in the air for up to 2 hours [63, 64]. In fact, measles is one of the most communicable human diseases and can be transmitted as early as 4 days prior to the onset of the maculopapular rash, with the peak of transmission occurring a week later [1]. Most measles cases occur in late winter and spring in temperate regions, and after the rainy season in

tropical regions [56, 65]. The most likely cause of these observed seasonal peaks is overcrowding induced by the winter or rainy seasons.

1.2.2.2 Molecular epidemiology

Despite the existence of a single serotype, various circulating genotypes of MeV have been reported. Measles surveillance is mainly provided by a network of WHO laboratories. Additionally, the online database, Measles Nucleotide Surveillance, provides a repository as well as bioinformatics tools to analyse measles sequences (http://www.hpa-bioinformatics.org.uk/Measles/Public/Web_Front/main.php).

Molecular epidemiological studies often examine the complete sequence of the *nucleocapsid* (*N*) or *haemagglutinin* (*H*) genes (see **chapter 1 section 1.3**) or, more frequently, the C-terminal 450 nucleotides of *N*, which is the most variable region of the MeV genome [66]. Currently, field isolates are classified into 8 clades (A to H) and 24 genotypes, indicated with numbers. To date, the identified MeV genotypes are A, B1, B2, B3, C1, C2, D1, D2, D3, D4, D5, D6, D7, D8, D9, D10, D11, E, F, G1, G2, G3, H1 and H2 [67]. All genotypes belong to wild-type virus isolates that have caused epidemics apart, from genotype A, which comprises all the vaccine strains of MeV [68]. A study of global MeV genotype distribution identified three main regions where certain genotypes are predominant: in Africa genotype B3 is most common, apart from Namibia where genotype B2 prevails; in Southeast and Eastern Asia genotypes D9 and H1 are commonly detected, while in Europe and the Americas, D4 and D5 genotypes are predominant [69].

1.2.3 Diagnosis

There are several approaches to aid the diagnosis of measles, such as the unique clinical symptoms, virus neutralisation tests with patient's sera or genotyping of the virus. Early clinical symptoms, such as Koplik's spots, can be used to diagnose the disease. When incidence is low, diagnosis is more difficult, since other respiratory pathogens or inflammatory diseases may offer differential diagnoses (because of the fever and rash symptoms) [60]. In addition, clinical diagnosis might also be hindered since the maculopapular rash associated with measles does not always occur in individuals with weakened immune responses, i.e. those caused by underlying malnutrition or immunosuppressive diseases [70].

The detection of MeV-specific antibodies, present in blood sera or oral fluids, is the most common method applied for measles diagnosis. Levels of immunoglobulin M (IgM), during acute infection, or immunoglobulin G (IgG), in the convalescent phase, are used for serological detection of MeV infection [56, 71]. Since the production of IgM precedes IgG, MeV-specific antibodies might not be detected until 4 days after the onset of the maculopapular rash [52, 70]. As a result, false positives or false negative results can be potentiated by the low concentration of IgM and the under-sensitivity of the assays used for serological tests [12].

Depending on the health infrastructure, cases of measles can also be confirmed by culturing MeV in permissive cell lines isolated from body fluids. Preferentially, Epstein-Barr virus-transformed B lymphocyte cell lines should be used for diagnosis, since it has enhanced sensitivity to wild-type strains of the virus. MeV has been detected in oral and nasopharyngeal swabs [72], blood [73], eye rheum [74] and urine [75].

Finally, to simultaneously evaluate the genotype of MeV and diagnose disease, detection, amplification and sequencing of MeV RNA through reverse-transcriptase-polymerase chain reaction (RT-PCR) should be performed. This method is used to study the molecular epidemiology and phylogenetics of MeV and to classify isolates into respective genotypes.

1.2.4 Vaccination

The burden of measles disease worldwide has significantly decreased in the last 50 years, after successive vaccination campaigns. The main measles vaccine is derived from the first isolation of the virus [76], the Edmonston strain. To generate this vaccine the virus underwent a total of 71 passages in a series of primary human cell lines and embryonated chicken eggs [77]; an inactivation process similar to that used during the development of the poliomyelitis vaccine. In Europe the measles vaccine is administered as a trivalent vaccine, MMR (measles, mumps and rubella). It is administered in two doses: the first one administered between 9 and 15 months of age and the second dose when the child is 4 to 6 years old [78]. The recent re-emergence of measles in Europe has mainly been caused by suboptimal vaccination coverage, i.e. less than the minimum 95% coverage stipulated by the WHO, and importation of the virus from countries in which the disease is endemic. Accordingly, unvaccinated individuals represent the majority of measles cases in Europe [79]. Susceptible individuals comprise people who (1) were not previously affected by measles, (2) immunosuppressed people or pregnant women, (3) people that despite being vaccinated fail to produce an immune response and (4) people who are under the age to be vaccinated or older unvaccinated people [80]. In addition, several

people are not eligible for vaccination, namely if they have allergies to any of the vaccine's components or have underlying severe illness or immunodeficiency, since measles-related fatalities have occurred in immunocompromised people [80, 81].

1.2.5 Treatment

There are no specifically approved antiviral treatments for measles although several antiviral compounds have been discovered [82]. Severe complications from measles can be avoided through good healthcare, ensuring adequate nutrition, fluid intake and the treatment of dehydration. Secondary infections associated with measles can be treated through the administration of antibiotics. The WHO also recommends vitamin A supplements to children diagnosed with measles. This treatment restores low vitamin A levels during measles that occur even in well-nourished children and can help prevent eye damage and blindness. Vitamin A supplements have been shown to reduce the number of deaths from measles by 50% [83].

1.3 Genome structure

The genome of MeV shares similarities with other paramyxoviruses, which are non-segmented, single-stranded, negative-sense RNA viruses. MeV genomes comprise an RNA molecule of 15,894 nucleotides with negative polarity [84]. They are composed of six transcription units, in *cis*, sequentially encoding for the N, the phosphoprotein (P), the matrix (M) protein, the fusion (F) protein, H and the large (L) protein, the order of which was first deduced in 1985 (**Fig.1-2**) [85]. Two additional proteins are also produced by MeV genomes: the C protein, which is produced from

Fig.1-2 Organisation of the MeV genome. Genomes of MeV are a single molecule of RNA in the negative-sense and contain six transcription units *in cis*. From 3' to 5', the transcription units encode for the nucleocapsid protein (N), phosphoprotein (P), matrix protein (M), fusion (F) protein, haemagglutinin (H) and the large (L) protein. Additionally, MeV genomes can produce two additional protein, C and V, by leaky scanning of the optimal Kozak sequence or editing of the P mRNA transcript, respectively. A typical MeV genome contains 15,894 nucleotides (nt). Adapted from ViralZone, ExPASy Swiss Institute of Bioinformatics Bioinformatics Resources Portal

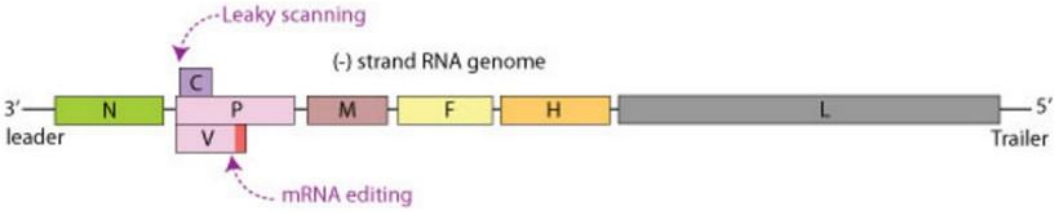
Leaky scanning
(-) strand RNA genome
C
3′
leader
N
P
V
M
F
H
L
5′
Trailer
mRNA editing

15,894 nt

the P transcription unit as an alternative ORF [85], and the V protein, whose production results from editing of the viral mRNA transcript of P [86]. The P and L protein, together with the N protein and the genome form the ribonucleoprotein (RNP) complex. The L and the P proteins form the RNA-dependent RNA polymerase (RdRp) complex, responsible for viral replication and transcription, of which L is the main component and P is a co-factor. The RNP also protects the viral RNA from the activity of RNAses [87]. The M protein's function is classically attributed to viral budding while the two envelope glycoproteins (GPs) F and H are responsible for viral attachment and fusion of the viral envelope with the cell [1]. A specific intergenic region consisting of three nucleotides separates each open reading frame (ORF); the sequence 3'-GAA-5' (as the genome is negative sense) marks the intergenic regions between N, P, M, F and H, while the sequence 3'-GCA-5' is found at the intergenic region between H and L. Of note, the untranslated region between M and F is much longer than the others and comprises around 1000nt [85, 88]. This region is unique to morbilliviruses and has a high GC content and variability. Furthermore, two promoters are located at the termini of the genome: the 3'end leader or genome promoter, which is comprised of 56nt, and the 5' trailer or antigenome promoter, composed of 40nt [84].

1.3.1 Molecular evolution

MeV genomes undergo very little variation both *in vitro* and in the field compared to other negative-sense RNA viruses [66, 69]. Two estimations of mutation rate for MeV in the field have been made: 5×10^{-4} and 4×10^{-4} substitutions per base per year [89, 90]. Both estimations are much lower than the calculated error rates of other RNA

viruses, such as 8×10^{-4} for hepatitis C virus, $1.8\times10^{-3}$for influenza A virus and 2.5×10^{-3} for the human immunodeficiency virus 1 (HIV-1) [90], a feature that is shared by other paramyxoviruses [91]. Interestingly, the mutation rate of MeV polymerase *in vitro* is similar to other RNA viruses [92, 93], suggesting significant biological or structural pressures that might be applied during the MeV life cycle in nature. A recent studied used random insertional mutagenesis to study how various sections of the MeV genome tolerated insertions in MeV genome [94]. They concluded that although N, P and M protein could tolerate small insertions, F, H and L were highly sensitive to mutagenesis. The L gene is the most conserved gene in the MeV genome followed by the F gene. Although MeV glycoproteins might be under intense antigenic pressure, MeV F and H sequences are very stable during *in vivo* passage [95]. The M gene is also well conserved among the morbilliviruses, and paramyxoviruses in general [96]. This might be due to the high number of interactions with other viral components and cellular proteins. In conclusion, MeV undergoes very little variation, in comparison to other RNA viruses, which suggests a high selective pressure environment upon infection.

1.4 Virion structure

Measles virions are large pleomorphic particles with sizes ranging from 120nm to 1µm (**Fig.1-3**) [97, 98]. The envelope is heavily decorated with the two glycoproteins (forming spikes at the viral envelope of ~15nm from the membrane [97]) while the interior is composed of an RNP, complexed or wrapped in helices of the M protein [99]. Although densely packed viral envelopes have been observed for the majority, if not all, of paramyxoviruses, this RNP-associated structure formed by MeV M proteins

Fig.1-3 Structure of virions of measles. (**A**) Micrograph of MeV particles observed by transmission electron microscopy and negative stain. [100] (**B**) Representation of a MeV particle. Measles virions contain two viral glycoproteins in their envelope, F and H, while the interior contains the viral genome wrapped into a helix with N and subsequently with M. M can also interact with the inner leaflet of the lipid bilayer. Additionally, L and P protein are present in close association with the nucleocapsid. Adapted from [99]. (**C**) Diagram of the N, P and L interactions. Adapted from [101].

A

B

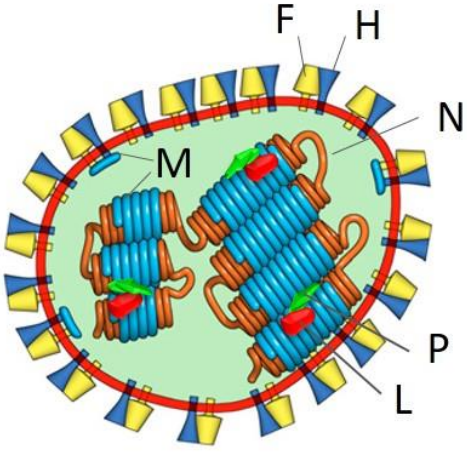

C

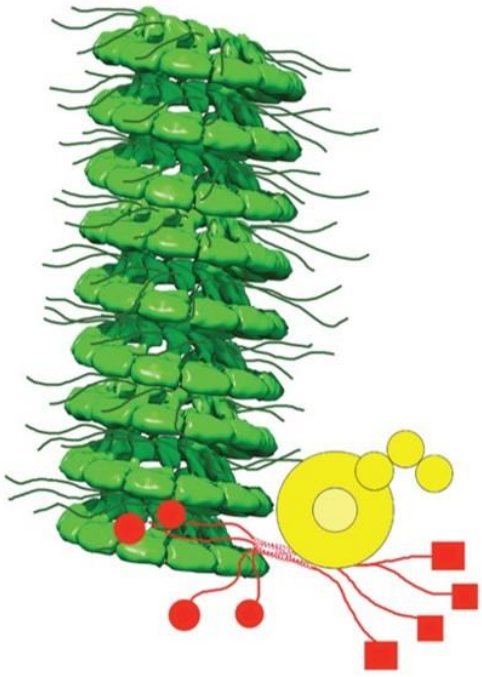

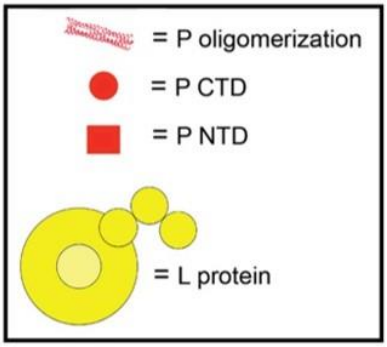

has not been observed in other viruses. MeV is polyploid, i.e. it can incorporate more than one RNP per particle; if this is an artefact of *in vitro* infection or relevant to the biology of the virus while *in vivo* is not clear [102]. Some studies that investigated generating segmented viral genomes, show that MeV can incorporate several RNPs with different sizes, suggesting the packaging of RNPs into the particle might not be a highly selective process [103].

The RNP complex is a helical arrangement of the N protein bound to the RNA genome and is approximately 1µm in length, 19.5nm in diameter and has a central empty core of 5nm [104] (**Fig.1-3C**). When negative-stained and visualised under electron microscopy (EM), the RNP complex has a herringbone structure similar to other paramyxo- and pneumoviruses [105]. CryoEM studies on the RNP revealed that the structure has significant flexibility, and it has been suggested that the N-terminal domain of N is responsible for this conformational plasticity [106]. The polarity of the genome within the RNP structure has also been determined: with the "pointy end" of the herringbone representing the 5'-terminus [105]. The RNP complex was shown to be composed of 97% protein with a density of 1.30g/cm3 in CsCl gradients [107]. The exact stoichiometry of the MeV RNP has not been defined yet, but assuming some similarly to other paramyxoviruses, it is estimated that the RNP complex is composed of 2649 monomers of N [108], ~260 monomers of P and approximately 25 copies of L [109]. The precise number of N monomers required to encapsidate a genome is easily deduced because all paramyxo- obey the "rule of six" [108, 110]. This rule, which means the genome must be a multiple of six nucleotides in length is explained by the interaction of N with the RNA molecule: each monomer of N binds to six nucleotides at once. It is assumed that an excess or deficit of

nucleotides (in the genome) will interfere with the interaction of N at the genome termini and destabilise the RNP complex [111].

1.4.1 Particle to plaque-forming unit ratio

In vitro, the particle to plaque-forming-unit (PFU) infectivity ratio for MeV is relatively high and has been suggested to be greater than 10 (>10:1) [112]. Even though MeV is one the most infectious pathogens known, it is intriguing that the particle-to-PFU ratio is so high. Presumably, this number might be due to the formation of defective particles. A common feature of *in vitro* MeV infections is the formation of defective RNPs that can lead to the formation of defective-interfering particles, which are known to be present in vaccine stocks [113]. These faulty RNPs contain large deletions of the original RNA sequence or positive-sense RNA molecules. A common topology for these defective RNAs is the 3' copy-back structure, where 5' to 3' replication of the antigenome stops at a specific point, reverses the reading sense orientation and copies back the initial part of the genome again. Interestingly, the budding process of MeV does not seem able to distinguish antigenomic, genomic or partial (defective) RNPs, since all these types can be found in virions [114].

1.5 Transcription

MeV gene expression is accomplished by the action of the RdRp complex, which synthesises viral mRNAs directly from the negative-sense RNA genome. The leader, or genome promoter, of MeV genomes located at the 3' end of the RNA molecule acts as the transcriptional promoter sequence. The polymerase complex, composed

of L and its co-factor P, recognises this region and generates a nascent molecule of RNA. This nascent mRNA molecule is capped at the same time of transcription by the L protein. The polyadenylation of the 3' end of viral mRNAs is thought to be the result of "stuttering" of the transcription complex on the sequence 5'-RUUAUAAAACUU-3' located at the 3' end of the transcription unit, where R is a purine [115]. Polyadenosine tails are composed of 70 to 140 A residues, and although the exact mechanism by which L+P stop polyadenylating is not known, cellular mRNAs have similar length polyA tails.

As mentioned previously, the transcript of the protein P can be edited to allow translation of the V protein. In the middle of the P ORF, a sequence similar to the gene end element (3'UAAUUUUUCCC-GUG-5') instructs the viral transcription complex to introduce an extra G residue, that is not present in the template. Even though morbilliviruses only express one edited transcript, leading to the production of V, other paramyxoviruses can produce V and W proteins depending on the insertion of one or two G residues, respectively [116]. The lack of expression of W proteins in morbilliviruses could be a result of tight regulation of the editing process.

1.5.1 Regulation of gene expression

The main mechanism for regulation of morbillivirus gene expression is the transcriptional gradient, formed during viral mRNA synthesis, i.e. transcription initiation and viral mRNA production is proportional to the distance of the transcription unit from the 3' promoter of the genome (**Fig.1-4**). This can be explained by the stop-restart feature of the L+P complex during transcription, and governed by the

Fig.1-4 MeV transcription generates an mRNA gradient. (A) The L and P protein complex binds to the 3’ terminus of MeV genome and initiates transcription. After the first transcription unit is complete, the polymerase can either continue to the next ORF and start its transcription or abandon the RNA molecule and bind to the 3’ end of the same or other genome molecules. The same happens at the end of all transcription units. This feature of the RdRp, known as the stop-and-restart function, leads to the formation of a gradient of viral mRNA, in which the most abundant transcripts are 3’ terminal, i.e. N, followed by P, M, F, H and L.

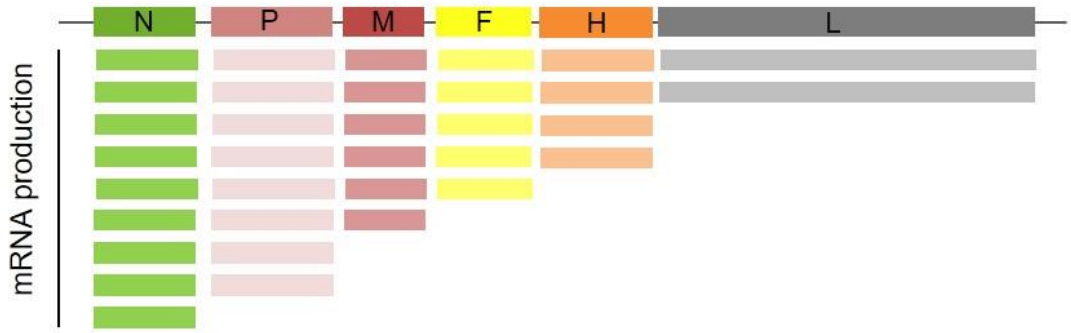
N
P
M
F
H
L
mRNA production

probability of the complex to abandon the template RNA molecule and re-start from 3' terminus. At the end of each transcription unit the polymerase either ceases transcription altogether and disassociates from the genome, or continues to transcribe the next gene. Since the polymerase is thought to only begin transcription at the 3' end of the genome the result is a gradient of transcription. Several studies have attempted to determine the characteristics of this gradient. In particular, during an acute infection, all viral transcripts decay at a similar rate [117], which in general is very low [118]. Two studies showed a steep attenuation of gene expression from N to P by analysing mRNA abundance [119, 120] - a threefold reduction in mRNA copy numbers – but this degree of change is attenuated for the genes further downstream (approximately 0.8 times of the previous ORF). However, there is another transition where continued transcription dramatically attenuates in likelihood, the H-L interface, where the total number of L nascent transcripts is approximately 10 times less than H.

Recent evidence has suggested a role for the C protein as a "quality control" factor in measles replication [121]. Recombinant MeVs that lack the expression of C generate increased levels of defective RNAs. Analysis of the "breakpoints" between correct and copy-back RNA showed accumulation of specific A→G and U→C mutations, while the sequences flanking these mutations match to the binding sites of adenosine deaminase actin on RNA-1 (ADAR-1), a protein that acts on double strand RNA and edits it. Since viral dsRNA accumulates during viral infections lacking C protein, along with phosphorylation of the dsRNA-dependent protein kinase [122], which leads to the activation of immune responses, it is possible that C mediates N-RNA

interactions during transcription to avoid the formation of defective RNPs and activation of innate immunity [123].

1.6 Regulation of translation

Little is known about the mechanisms that regulate translation during the MeV lifecycle. Frequently, untranslated regions located downstream or upstream of the ORF play a role in stabilisation of the mRNA molecule. The M and F genes are the only two genes that have significant untranslated regions (UTRs), located at the 3' end of M and the 5' terminus of F. This long UTR is a unique feature of morbilliviruses and is highly variable and also has a high GpC dinucleotide content. Some have speculated that this region might fold into complex secondary structures. In studies with CDV genomes, viruses that carried deletions in this region had increased replication and reduced virulence [124]. The role of the MeV M-F UTR in the MeV lifecycle is not completely understood yet and is likely to affect several steps of the virus; nevertheless, it has been show that this region is not required for MeV growth *in vitro* and *in vivo*, but has been shown to alter translation rates of the F mRNA [125].

Interestingly, in a random mutagenesis insertional study of the MeV genome, non-coding regions were much more tolerant to insertions than ORFs [94]. In particular, the 5' UTRs of each gene were less tolerant to insertions than the 3'UTRs, suggesting a putative regulatory role for the 5' UTRs in the regulation of the MeV lifecycle.

1.6.1 Location of transcription and replication

In other viral infections, such as positive-sense RNA viruses, viral transcription and replication occur in dedicated structures, such as membranous replication factories [126]. However, similar structures have not been observed for negative-strand viruses, including MeV. Transcription and replication of MeV is thought to occur in the cytoplasm, since MeV can replicate in anucleated cells [127]. Immunofluorescence staining of several components of the viral RNP shows a punctate pattern of N and P proteins near the nucleus of the cell, co-localising with viral mRNA [95, 128]. Similarly, the L protein, known to co-localise with N, P and M, also shows a perinuclear punctate pattern [129], suggesting the existence of specific replication sites within the cell. Even though MeV can replicate in the presence of cytochalasin B, a drug that inhibits polymerisation of actin filaments, suggesting replication does not require the cytoskeleton [130], several cytoskeletal components have been shown to interact with the RNP. In particular, MeV L proteins interact with tubulin, the major constituent of the microtubules, to increase viral RNA synthesis [131], while cofilin, a protein involved in the severing of actin filaments, was shown to interact with N and be required for assembly of the RNP [132]. Although a specific site for RNA synthesis has not been described for MeV, it is possible that interaction with cytoskeletal components might help to concentrate viral proteins.

1.7 Replication

Replication is the process of producing full-length negative-sense RNA copies of the genome, using a positive-sense RNA template (the antigenome) (**Fig.1-5**). Briefly,

Fig.1-5 Schematic diagram of MeV transcription and replication. To initiate transcription, the RdRp complex binds to the 3’ end of a negative-sense (genome) RNA copy of MeV and starts mRNA synthesis. To initiate genome replication, the RdRp complex must produce a positive-sense copy of the genome (antigenome) which is encapsidated by N monomers. After this molecule is produced, the RdRp then synthesises a full-length copy of the genome, using the antigenome as a template, which is also immediately encapsidated by N.

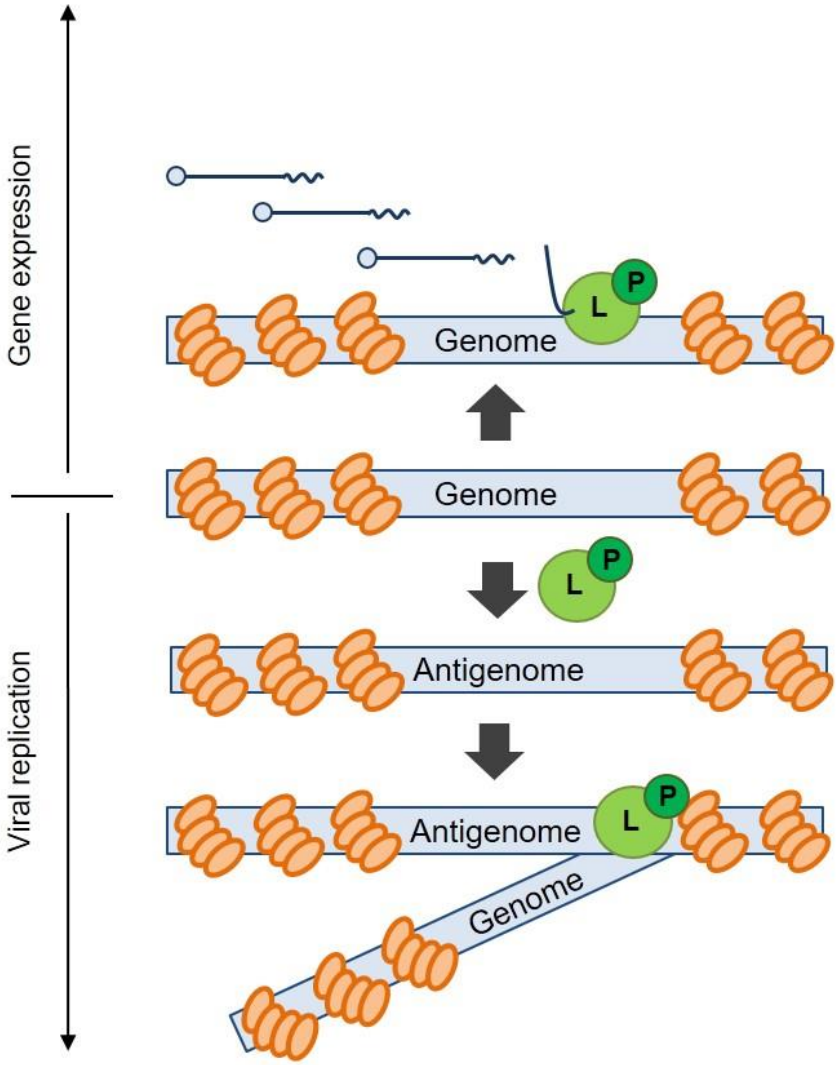
Gene expression
Viral replication
L
P
Genome
Genome
L
P
Antigenome
Antigenome
L
P
Genome

during this process the RdRp complex produces a positive-sense copy of the genome, which is immediately encapsidated by N monomers. Subsequently, the same protein complex binds to the 3' terminus of the antigenome molecule (via the antigenome promoter) and starts synthesising a complementary RNA molecule (the nascent genome) that is also immediately encapsidated by N. The molecular mechanisms behind the switch between transcription and replication are not well characterised. Some hypothesise that certain conformational changes in L lead to the intergenic regions (that may direct the disengagement of L during transcription) being ignored by L, so a full-length transcript is made [133].

Although both positive and negative RNPs are produced during the replication phase of the life cycle, genomes are produced at a greater proportion than antigenomes [120, 134]. This is due to an apparently stronger promoter at the 3' of the antigenome, in comparison to the genome promoter on the negative sense RNP. In related viruses, such as Sendai virus, the ratio of genome to antigenome is governed by expression of C protein; in this model, early infection is dominated by the synthesis of antigenomes since the total amount of C is low, but later in infection, with accumulation of C, this protein binds to the leader of the genome blocking its replication [135].

1.8 Translation

MeV does not encode its own translation machinery and relies on host ribosomes to produce viral proteins. During acute infection, viral RNA accounts for 25% of the total RNA in the cell [133]. Concurrently, MeV induces the complete shut-off of host protein synthesis. MeV translation was found to be independent of several translation

initiation factors, including eIF4G, eIF4E and 4E-BP1 [136]. It has also been reported that host translation was blocked by binding of the N protein to eIF3-p40 [137]. Nevertheless, it is thought that MeV translation is dependent on the phosphorylation of eIF2α [136], an initiation factor.

MeV 5'UTRs are composed of only short 20 to 60 stretches of nts and lack recognisable functional structures. However, a predictive study suggested the existence of a short hairpin in the 5' UTR of the N ORF [138]. This region was found to bind to the La/SSB antigen, and depletion or over-expression of this protein impacted on the translation of N [138].

1.9 Immune Response

During the initial stages of infection MeV primarily infects cells of the immune system. As a result immune responses to MeV can be affected by this tropism and long-lasting effects occur that impact on immune function long after infection is cleared. Some studies have shown that vaccine strains of MeV have a reduced tropism for lymphocyte populations [139, 140], and this perhaps explains the success of the attenuated virus in inducing a long-term immunity without the manifestation of clinic symptoms – even though the vaccine strain of MeV has been detected in a patient suffering from MIBE [141]. After initial contact with immune resident cells in the upper respiratory tract, MeV infection is transported to the lymph nodes where it replicates very efficiently. Viruses then enter the bloodstream through the circulation of infected peripheral blood mononuclear cells [47, 142].

1.9.1 Innate Immunity

The first response to viral infection, including infection with MeV, is an innate immune response. Infection of lung epithelial cells leads to the production of interleukin-8 [143] and interferon-β [144]. The production of IL1 and IL8 was also shown to be increased in patients infected with MeV [145]. MeV-induced IFN-β production is dependent on viral replication [146] since viral RNA is thought to be recognised by the pattern recognition receptors RIG-I and MDA5 [147, 148]. As opposed to this, MeV infection of $CD4^+$ T lymphocytes leads to inhibition of type I IFN production [144]. Other viral components were shown to induce immune responses, i.e. upon interaction with the Toll-like receptor 2 (TLR2) [149], MeV H induces the production of IL-6, while the N protein interacts with interferon regulation factor 3 (IRF3), activating it and leading to IFN-β production [150, 151]. Finally, defective interfering particles can also induce the production of IFN-β [152]. Interestingly, vaccine strains of MeV are more potent inducers of IFN-β production then wild-type viruses, and this could be another important mechanism that explains the attenuation of the virus [153].

MeV accessory proteins C and V have been implicated in virulence and in distinctive differences in the immune response to wild-type and attenuated viral infections [154, 155]. As discussed previously, the C protein might be implicated in RNA synthesis and production of defective interfering particles, and although C is not required for *in vitro* infection, it's deletion in a recombinant virus decreased replication *in vivo* [156, 157]. The V protein prevents type I IFN production by direct binding to IKKα, a regulator of the NF-κB signal transduction cascade [158] and interferes with IFN signalling by binding to MDA5 [159, 160] and the STAT1 and STAT2 proteins [161,

162]. V protein has also been shown to be associated with reduced cytopathic effect *in vitro* and fast replication [163].

1.9.2 Adaptive Immunity

The emergence of an adaptive immune response, comprising humoral antibodies specific for MeV proteins and committed T cells, occurs concurrently with the development of the maculopapular rash, ~10 days after infection [164]. In monkeys, the most important control mechanism for viral infection appears to be $CD8^+$ T lymphocytes, since depletion of this population sustains viremia for longer periods of time and leads to higher viral titres in the blood [44]. While CD4+ cells remain in the blood for longer periods of time after infection is cleared, the CD8+ T cell population rapidly decreases [165-167]. Along with this shift in cellular immunity, humoral immunity also shifts after the resolution of infection. Along with the activation of CD8+ T cells and CD4+ Th1 cells, an increase in the production of IL-2 and IFN-γ is observed, but this rapidly decreases after the establishment of memory B cells [166, 168]. During recovery, regulatory CD4+ T lymphocytes remain activated for a long period of time [169].

After efficient clearance of infection, MeV causes a prolonged immunosuppression that can last up to nine months [1, 39]. Although no infectious particles can be recovered from convalescent individuals, viral RNA can still be detected in circulating blood cells for several months. Interestingly, only wildtype strains of MeV cause this dysregulation of the immune system after infection, even though a similar long-term immunity is achieved with vaccine strains of MeV. The mechanisms underpinning this

immunosuppression are still not known however, some suggest that a combination of temporary leukopenia, dysregulated functions of antigen presenting cells and permanent type 2 cytokine production contributes [164].

1.10 Cellular targets of viral infection

Several MeV proteins have been implicated in virulence and pathogenesis of MeV infections, most prominently the C and V proteins. In a yeast two hybrid screen [170]. MeV C protein was shown to interact with the immunity-related GTPase M (IRGM), a protein that is known to interact with pattern recognition receptors and the autophagy machinery to induce antimicrobial responses [171]. Interestingly, MeV infections increased the formation of autophagosomes in cells and targeting IRGM was shown to decrease the formation of viral particles [170]. Furthermore, MeV infection was shown to induce two waves of autophagy in the cell, the first one soon after attachment and the second occurring 12 to 24 hours post-infection [172]. MeV C is also involved in the later phases of autophagy. In this study, viral proteins escape autophagic protein degradation and the induction of autophagy was shown to increase the formation of viral particles. Even though vaccine strains of MeV can induce autophagy during entry, by activation of the CD46-GOPC pathway [173], virulent strains (that do not use the CD46) could also induce autophagy [172]. Although some have suggested that the induction of autophagy by MeV prevents cell death [172], other reports show MeV-induced apoptosis. MeV infection was demonstrated to induce apoptosis in HeLa cells [174] and MeV H protein (from the vaccine strain) alone could induce apoptosis via the TRAIL-mediated pathway and the mitochondrial-controlled pathway [175].

MeV infection has also been shown to induce the downregulation of housekeeping genes [144]. In particular, the protein phosphatase 5 (PP5) was inactivated during infection, leading to the suppression of the DNA-dependent protein kinase activity, the reduction of SP1 phosphorylation levels and c-Myc degradation, all of which are involved in the regulation of expression of several housekeeping genes [176]. Although the mechanism behind this downregulation is unknown, it is possible that the accumulation of N leads to the inactivation of PP5.

Another study that looked at gene expression in persistently infected human glioblastoma cells observed a downregulation of the mitochondrial short chain enoyl-CoA hydratase (ECHS) [177], which is involved in the β-oxidation of fatty acids. siRNA knockdown of this protein leads to reduced cytopathic effects and MeV replication. Similarly, in persistently infected neuronal cells, genes regulating cholesterol biosynthesis were dysregulated when compared to uninfected cells [178]. Furthermore, knock-down of cholesterol biosynthesis impaired MeV budding in acute infection. These reports suggest that MeV might exploit lipid biogenesis pathways to promote viral budding. Such pathways might be dysregulated in persistently infected cells where viral exit is impaired.

1.11 Entry and exit

MeV exploits several cellular molecules and pathways to spread within the host. Particularly, the two envelope proteins of the virus, F and H, are involved in attachment and invasion of permissive cells to MeV, interacting with several receptors and controlling the fusion of the viral envelope to the plasma membrane.

The present thesis is focused on the mechanisms underlying viral spread; following sections therefore summarise what is currently known of MeV entry and exit.

1.11.1 Envelope proteins

1.11.1.1 Haemagglutinin

MeV encodes two envelope proteins, H and F, whose function is to direct viral entry and exit. MeV H is a type II transmembrane protein composed of an N-terminal cytoplasmic tail (37 residues), a single pass transmembrane domain, a long extracellular stalk domain and a C-terminal cube-shaped globular head (**Fig.1-6A**) [179, 180]. In contrast to the majority of paramyxovirus haemagglutinin proteins, MeV H lacks neuraminidase function and it does not bind to sialic acids [181]. In spite of this, the globular head of H still resembles the sialidase conformation of other viruses, characterised by a β-propeller structure composed of six β-sheets (**Fig.1-6B**). The globular head is thought to be the main region for attachment and interaction with cellular receptors, while the stalk domain interacts with F. The cytoplasmic tail of H was shown to modulate fusion activity and surface expression [182]. MeV H is thought to be present at the virus envelope as a dimer-of-dimers, although some studies have described both monomeric and dimeric forms of H [181, 183]. Dimerization was demonstrated to occur via the formation of two disulphide bonds at two cysteine residues, C139 and C154 [184].

Fig.1-6 Structure of MeV haemagglutinin. (A) MeV H is a transmembrane protein composed of an intravirion tail, a transmembrane domain, a long stalk and a globular head. MeV H is present at the surface as a dimer-of-dimers. The globular head interacts with cellular receptors while the stalk domain is known to interact with F. (B) A crystal structure of the globular head of H (inset in A). The H ectodomain has six β-propeller blades, named β1 to β6. The β1 blade interacts with the other monomer of H, while blades 4 to 6 interact with cellular receptors. H is *N*-glycosylated and two carbohydrate moieties have been resolved in this structure [181].

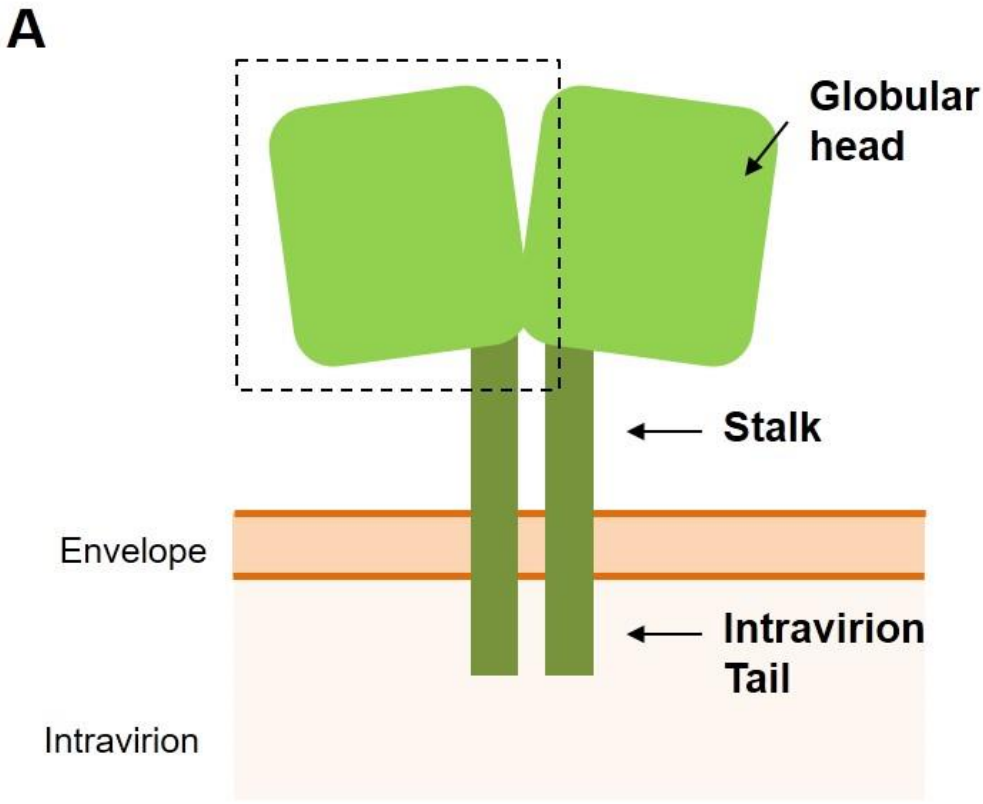
A
Globular head
Stalk
Envelope
Intravirion Tail
Intravirion

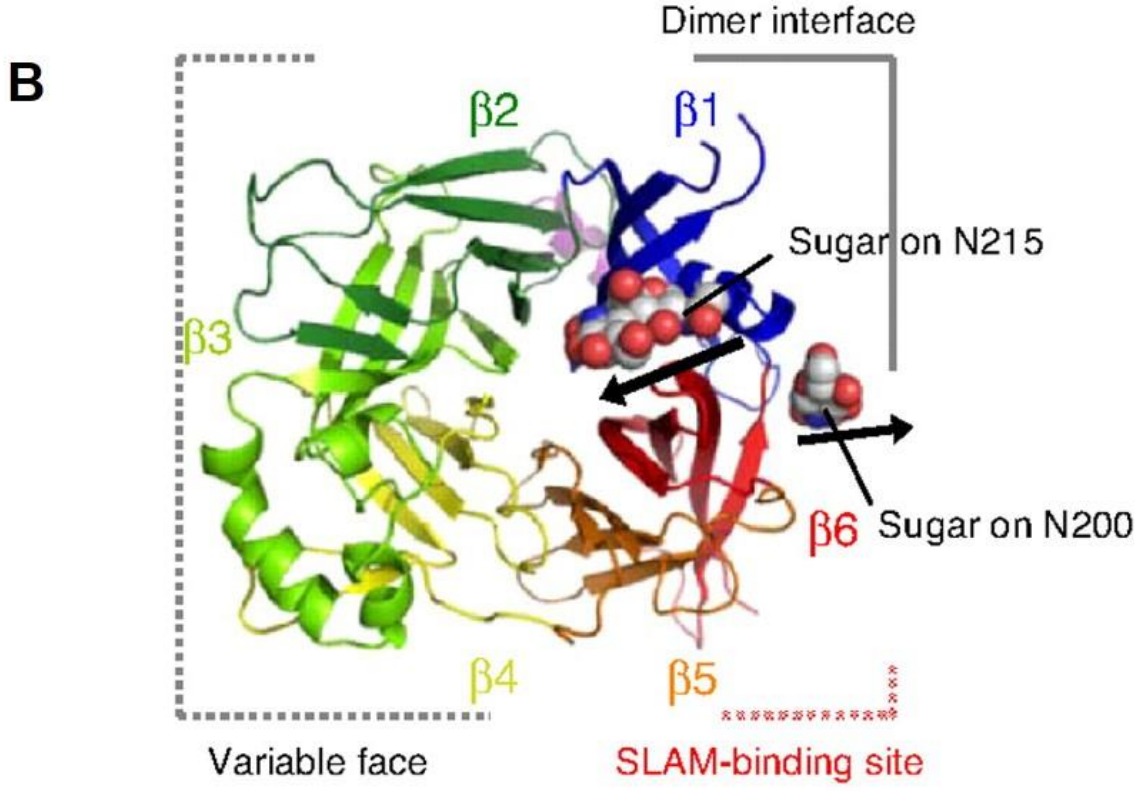
B
Dimer interface
β2
β1
Sugar on N215
β3
β6
Sugar on N200
β4
β5
Variable face
SLAM-binding site

1.11.1.2 Fusion protein

The F protein of MeV, and by inference the fusion proteins of all morbilliviruses, is a type I transmembrane protein that contains several glycosylated residues in its ectodomain [185]. Although the structure of MeV F has not been resolved yet, comparisons with the crystal structure of the related paramyxovirus, human parainfluenza virus type 5, as well as mutagenic studies have allowed the identification of several structural domains [186, 187]. The structure of F is described as a large globular head supported by short stalk, a single-pass membrane spanning domain and a short cytoplasmic tail of 33 amino acids. (**Fig.1-7**). The ectodomain of F is composed of three heptad repeat regions (HR): HRA and HRC are well conversed domains and are located in domain III (D3) which is the top and furthermost region of F in relation to the viral envelope, and HRB, which comprises the stalk domain in the pre-fusion conformation. Domains I and II (DI and DII) comprise the base of the globular head, while DII contains the region that interacts with H. The N-terminal domain contains a highly hydrophobic, leucine zipper structure – known as the fusion peptide – which is thought to be the fusion element of F [188]. The transmembrane domain was shown to impact on fusion activation [186] but this was not seen for the cytoplasmic tail [182]. This protein is translated in the endoplasmic reticulum and its location is encoded by an N-terminal signal peptide of 28 amino acids [189]. Initially, F is synthesised as a single peptide of 60 kDa, known as F0, which is fusion incompetent. Further proteolytic processing in the trans-Golgi network, catalysed by the furin protease, leads to the formation of two peptides – F1 of 40 kDa and F2 of 20 kDa - which are covalently linked by a disulphide bond [190, 191]. This process is calcium-dependent and furin acts on a polybasic site of F.

Fig.1-7 Structure of MeV fusion protein. (A) MeV F is a transmembrane protein present on the virus envelope as a trimer. F is composed of an intravirion tail, a transmembrane domain, a short stalk and a small globular head. The globular head is further dived into four domains: the top of F is composed of the DIII domain, while the bottom part is comprised of DI and DII; the fusion peptide is located between the DII and DIII domains. (B) Although the crystal structure of MeV F has not been resolved, a model based on the structure of the paramyxovirus human parainfluenza virus type 5 was generated and the relevant domains identified. Adapted from [192].

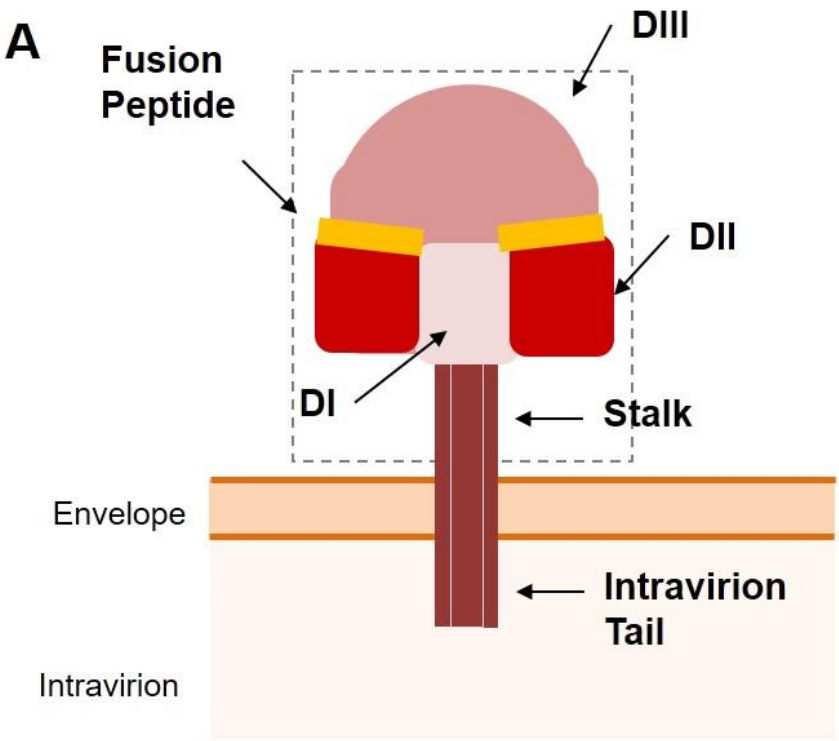
A
Fusion Peptide
DIII
DII
DI
Stalk
Envelope
Intravirion Tail
Intravirion

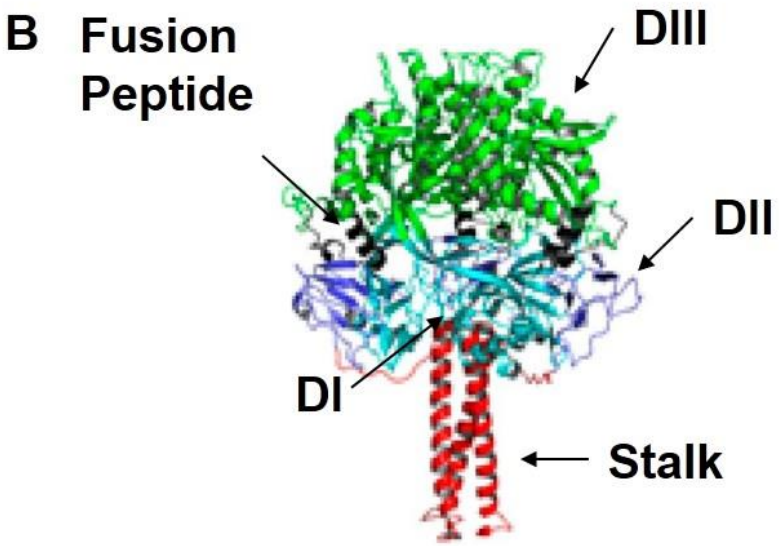
B
Fusion Peptide
DIII
DII
DI
Stalk

Proteolytic activation of F proteins of related viruses has been shown to be accomplished by several mechanisms. For example, Hendra virus F is cleaved by protease cathepsin L [193] and is dependent on an endocytosis motif present in its cytoplasmic tail [194], while RSV F is cleaved in the macropinosome upon viral entry [195].

1.11.1.3 Assembly and protein processing

As mentioned previously, F and H are glycosylated. In particular, two asparagine residues in F2 peptide were found to be N-glycosylated [196]. These modifications are important for subsequent protein cleavage and correct transport to the plasma membrane. Meanwhile, several residues of MeV H have also been shown to be glycosylated, including residues N200 and N215 [181]. In CDV, the *N*-glycans of H were shown to impact on virulence [197]. Glycosylation of paramyxoviral proteins is very common e.g. studies have shown that Hendra and Nipah virus glycoproteins contain several N-glycosylated residues, some of which impact on fusion activity and antibody neutralisation evasion [198], however there have also been O-glycosylated residues recorded as well [199].

MeV F and H proteins are thought to interact with each other in the endoplasmic reticulum [189]. In particular, the stalk of MeV H is known to interact with F and play a fundamental part in the triggering of F [200]. MeV F is a trimer, similarly to other paramyxoviral F protein. An exception to this rule was recently described for Nipah virus F, which is present as a hexamer[201].

Similarly to other enveloped viruses, morbilliviruses can spread by particle formation and by cell-cell fusion - a phenomenon called syncytium formation. Both processes are thought to rely on the same fusion mechanism, accomplished through the interaction of the viral GPs with virus specific cellular receptors. Recent crystallography and site-directed mutagenesis studies of the H protein-receptor interaction have elucidated the fusion mechanism of morbilliviruses. The H-protein is presented in two different tetramers when interacting with the receptor; the ectodomain is composed by a membrane-proximal stalk formed by a four-helical bundle, with an upper straight part and a lower supercoiled region, and a membrane-distal six-blade β-propeller structure [202].

1.11.2 Cellular receptors

Several viruses interact with proteins or carbohydrates present at the plasma membrane of the cell to promote its entry and access the cytoplasm. Interaction with specific protein molecules, known as viral receptors, is fundamental to the spread of virus infection and virulence. Consequently, the tissue tropism of MeV is greatly explained by the interactions between the two GPs present at the envelope of the virus and a set of proteinaceous receptors expressed in different cells of the host. At present, two receptors are known to be responsible for the permissivity of different cells to wild-type MeV: the signalling lymphocyte activation molecule f1 (SLAMF1) or CD150, which is expressed at the surface of activated T and B lymphocytes and other cells of the immune system [23, 203], and Nectin-4 (or poliovirus receptor-related 4), found the basolateral surface of epithelial cells [204, 205]. For attenuated

strains, CD46 also functions as a receptor for MeV. SLAMF1 is considered the main cellular entry receptor for wild-type strains [206, 207].

1.11.2.1 SLAMF1

The discovery of SLAMF1 as a receptor for MeV was pivotal to the understanding of MeV tropism and pathogenesis but also brought insights into the MeV fusion process. SLAMF1, also known as SLAM or CD150, was first identified by Tatsuo *et al.* and it was the first recognised receptor to be used by both attenuated and wild-type strains of MeV. Subsequently it has also shown to be a universal morbillivirus receptor used by the rest of the members of the genus [203, 208]. SLAMF1 was identified using a cDNA library transfected into HEK293T cells - ordinarily refractory to MeV infection - in conjugation with VSV-based pseudoparticles typed with wild-type MeV H and F.

SLAMF1 belongs to a superfamily of proteins whose members are important immunomodulators involved in lymphocyte maturation. This family is composed of nine members, classified as SLAMF1 to 9, that are present on the cell surface as dimers and function as cell ligands with signalling ability. Their tissue distribution is restricted to haematopoietic cells [209]. Recently, antimicrobial functions have been attributed to several members of this family, including SLAMF1 [210], SLAMF2[211] and SLAMF6 [209]. This molecule acts as a self-ligand and is involved in the stimulation and activation of T and B cells [212]. SLAMF1 is an integral membrane protein and its cytoplasmic tail contains three SRC homology 2 (SH2) binding domains (**Fig.1-8**). The membrane-proximal domain interacts with the SLAM-

Fig.1-8 Schematic representation of SLAMF1. SLAMF1 is a transmembrane protein that contains two immunoglobulin-(Ig)-like domains, a membrane distal variable (V) domain and membrane proximal constant C2 domain. This protein has a single membrane spanning domain and a long cytoplasmic tail. Its cytoplasmic tail contains three Src homology 2 (SH2)-binding motifs that are known to interact with several cellular proteins.

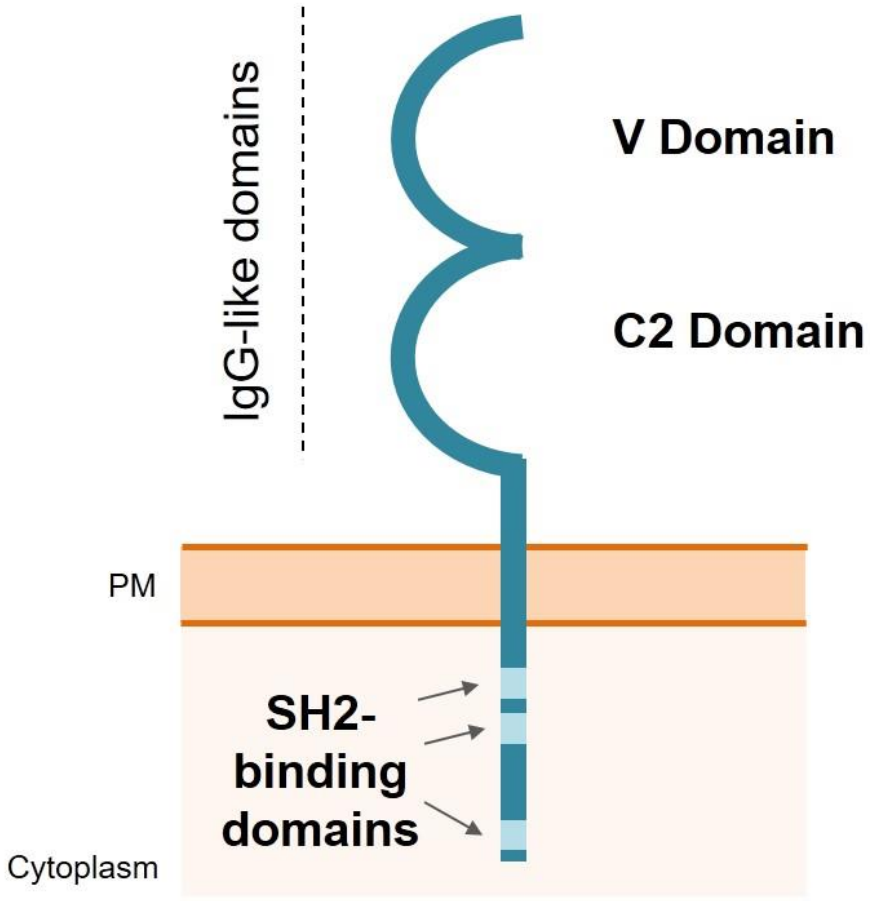
IgG-like domains
V Domain
C2 Domain
PM
SH2-
binding
domains
Cytoplasm

associated protein (SAP), recruiting FYN that phosphorylates the membrane-distal tyrosine initiating a signalling cascade that culminates in activation of NF-κB and cytokine production [213]. Similarly, the membrane-proximal domain can interact with Ewing's sarcoma associated transcript 2 (EAT-2) protein, which is expressed in macrophages and dendritic cells, possibly leading to cytokine production in these cells without interaction with the membrane-distal tyrosines [214]. The cytoplasmic tails of these receptors contain several signalling motifs known to interact with a myriad of proteins. One interaction partner is the SLAM-associated protein (SAP) which is known to interact with at least six members of this family [209]. SAP interaction can be both dependent and independent on the phosphorylation of tyrosine-containing motifs, such as the SH2 domains in the cytoplasmic tail of SLAMF1. This primary interaction between SAP and the cytoplasmic tail of SLAMF1 governs SAP-mediated signalling. SAP interaction with these SH2 domains can block the binding of SHP-1 and SHP-2, two tyrosine phosphatases, and recruit the Src kinase Fyn[215]. The congenital truncation of SAP is associated with the X-linked lymphoproliferative disease [216].

SLAMF1's antimicrobial functions are centred on the sensing of incoming bacteria, recruitment of the autophagy machinery and clearance of the microbe [210]. SLAMF1 in macrophages recognises the outer membrane porins C and F present at the surface of Gram-negative bacteria. This interaction leads to the recruitment of Beclin-1, a protein involved in the scaffolding of the autophagic complex, and later the formation of UVRAG, VPS34 and VPS35. This process was shown to be dependent on the production of phosphotidyinositol-2-phosphate (PI3P), which leads to the formation of the NAPDH oxidase complex and recruitment of EEA1, necessary for

phagocytosis and clearance of the microbe. The SLAMF6 protein was reported to recognise *E. coli* with potential roles in colitis [217]. Interestingly, macrophages that lack the expression of SLAMF1 have defective responses to LPS, while in dendritic cells SLAMF1 might also play a role in cytokine production.

1.11.2.2 Nectin-4

After the discovery of SLAMF1 receptor, a new paradigm emerged. Wild-type strains of MeV were known to infect several types of tissues, such as the lung epithelium, upper respiratory tract, mouth, nose, bladder, intestines and the liver, that lack expression of SLAMF1 [218-220]. This was clear evidence for the existence of at least another receptor that granted MeV tropism for these cell types. In 2011, Noyce *et al.* discovered that MeV infection was sensitive to the loss of tight junctions and later identified Nectin-4 (also known as poliovirus-receptor-like 4) as the epithelial receptor of MeV [221]. This molecule belongs to the family of nectin proteins which are components of adherens junctions and contribute to cell adhesion. This molecule has been identified in several cancer cell lines [222] and has recently been recognised as a lung and breast tumour cell marker [223, 224] . Nectin-4 contains a short cytoplasmic tail and a transmembrane domain, while its extracellular domain is composed of three immunoglobulin-like loops: two conserved C2 domains and a variable (V) region (**Fig.1-9**) [225]. Its cytoplasmic tail is known to interact with afadin and confer attachment to the cortical cytoskeleton.

Fig.1-9 Schematic diagram of nectin-4. Nectin-4 is present as dimer and is a transmembrane protein that contains three immunoglobulin (Ig)-like domains and a cytoplasmic tail. MeV interacts with the ectodomain of nectin-4 to gain access to epithelial cells and establish infection. Nectin-4 is a component of the adherens junctions, forming *cis*- and *trans*-dimers between neighbouring cells.

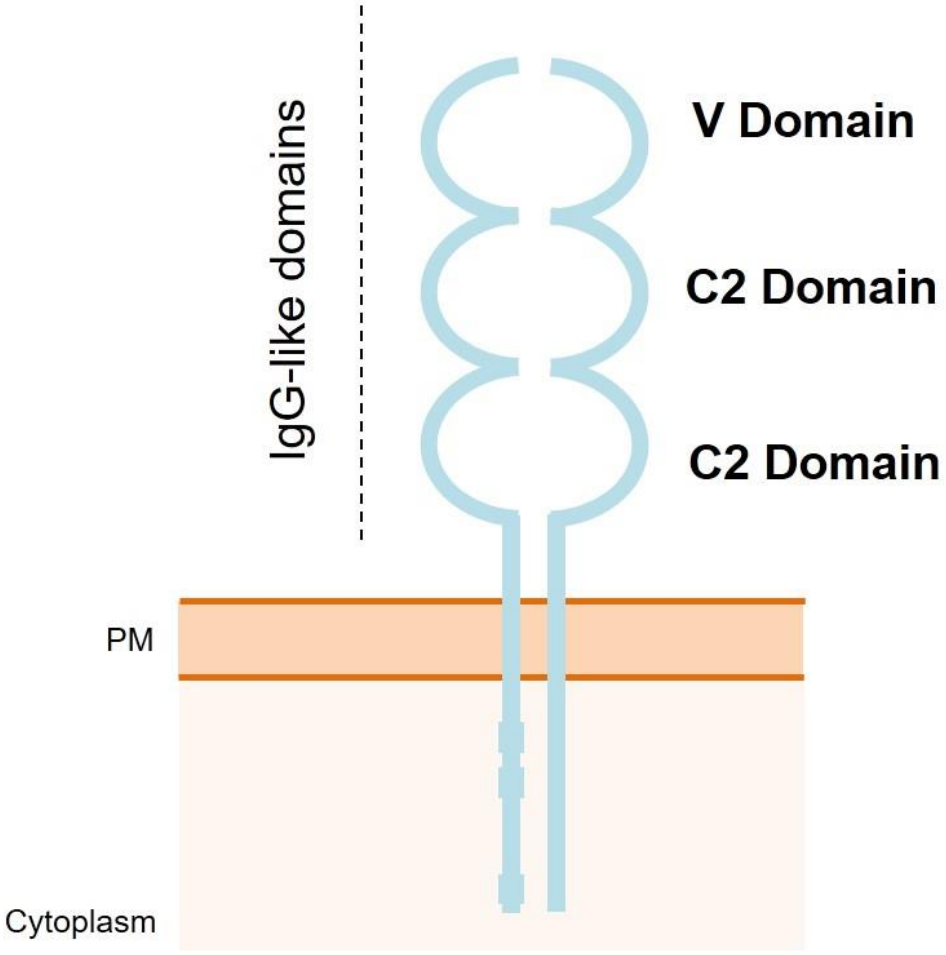
IgG-like domains
V Domain
C2 Domain
C2 Domain
PM
Cytoplasm

This protein can interact with other monomers of nectin-4 as well as several members of its wider family [225]. Although its predicted molecular weight is 55.5 kDa, post-translation modifications, such as *N*-glycosylation of its ectodomain, are responsible for a shift in molecular weight. Despite the suggestive name, nectin family members do not function as poliovirus receptors [226]. Nevertheless, nectin-1 and nectin-2 have been shown to function as receptors for several alphaherpesviruses [227, 228]. Although SLAMF1 and nectin-4 were initially identified as MeV receptors, they have also been shown to act as viral receptors for the other established morbilliviruses [203, 205, 229-232]. It is therefore interesting to analyse the ability of different morbilliviruses to use non-host receptors. CDV, in particular, was found to readily use human Nectin-4 where adaptation to human SLAMF1 required only a single amino acid substitution in the H protein, D540G [22].

1.11.2.3 CD46

Despite its restricted use by only attenuated but not wild-type strains of MeV, cluster of differentiation 46 (CD46) was the first MeV receptor identified [233, 234]. CD46 is a regulatory protein of the complement system and is ubiquitously expressed except for on erythrocytes [235]. As part of the innate immune response, the complement system is a collection of humoral proteins present in the blood that catalyse inflammatory reactions and mediate the lysis of cellular pathogens or promote the opsonisation of microbes and their uptake by phagocytic cells [236]. CD46 is an important regulator of complement and is part of a larger family of complement regulatory membrane proteins. In particular CD46 plays a role in the inactivation of C3b and C4b opsonins [237, 238]. CD46 is a transmembrane protein composed of a

cytoplasmic domain (two known isoforms, CYT-1 or CYT-2), a transmembrane domain and two extracellular regions: (1) a membrane-proximal region that contains two glycosylated, serine-, threonine- and proline-rich domains known as the B and C domains, and (2) a membrane-distal region that contains four complement control (CCP) domains, also known as short consensus repeat 1 to 4 (**Fig.1-10**) [237].

Mutations in, or deficiency of, CD46 are associated with over-activation of complement due to a reduced capacity for inactivating C3b and C4b. Additionally, the accumulation of C3b onto the surface of endothelial cells can lead to the formation of thrombi, causing macroangiopathic anaemia and renal failure [239, 240]. This protein has also been shown to be involved in certain reproductive processes. In particular, the expression of CD46 on the surface of spermatozoa is associated with the fusion process between the oocyte and the sperm [241, 242]. Consequently, a deficiency in CD46 expression in males is linked to infertility [243, 244].

Similarly to several SLAM and nectin family members, CD46 has also been shown to interact with several other pathogens. In particular CD46 is a cellular receptor for human herpes virus 6 [245], group B adenoviruses [246] and for the bovine viral diarrhoea virus [247]. The Gram-negative bacteria *Neisseria gonorrhoeae* [248] and *Neisseria meningitis* [249] as well as the Gram-positive bacterium *Streptococcus pyogenes* [250] also establish interactions through CD46. In the context of bacterial infection via CD46, it has been suggested that CD46-mediated signalling leads to rearrangements of the cytoskeleton that permit the invasion of these pathogens [251]. Particularly, *Neisseria* infection leads to the phosphorylation of the cytoplasmic tail of CD46 by the Src-tyrosin kinase c-Yes; these phosphorylated residues then interact with ezrin – a protein involved in the crosslinking of plasma membrane to

Fig.1-10 Schematic diagram of CD46. The molecule CD46 is a membrane protein comprised of a cytoplasmic tail, a transmembrane domain and an ectodomain. There are two isoforms of CD46 with different cytoplasmic tails, known as CYT-1 and CYT-2. In the ectodomain, the membrane-proximal B and C domain are rich in serine, threonine and proline (STP). The membrane-distal region contains four short consensus repeat (SCR) domains named 1 to 4. Domains SCR1 and 2 are known to interact with MeV [252].

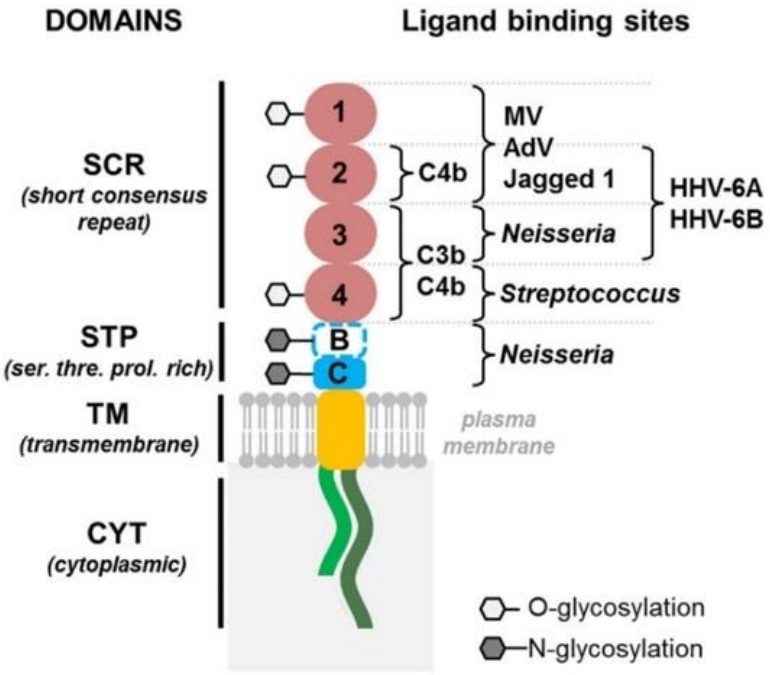
DOMAINS
Ligand binding sites
SCR
(short consensus repeat)
STP
(ser. thre. prol. rich)
TM
(transmembrane)
CYT
(cytoplasmic)
1
2
3
4
B
C
MV
AdV
Jagged 1
C4b
HHV-6A
HHV-6B
Neisseria
C3b
C4b
Streptococcus
Neisseria
plasma membrane
O-glycosylation
N-glycosylation

actin filaments – and the accumulation of cytoskeletal components facilitate pathogen entry [253, 254]. Phosphorylated residues in the cytoplasmic tail of CD46 have also been implicated in the cortical actin network and the modulation of cell polarity and integrity of the epithelial barrier [255, 256]. In recent years, with the elucidation of autophagy mechanisms, the activity of the cytoplasmic tail of CD46 has been linked with the formation of autophagosomes through the recruitment of Golgi-associated PDZ and coiled-coil motif-containing (GOPC) protein [173, 257].

1.11.2.4 Other receptors and entry co-factors

1.11.2.4.1 Moesin

Several other molecules have been linked to the entry step of the MeV life cycle, even though they do not function as viral receptors. One such protein is the membrane organising extension spike protein (moesin), a protein that bridges actin filaments of the cell cortex to plasma membrane proteins [258]. Although this protein was initially thought to be a receptor for MeV [259], this was subsequently disproved by other groups and its role in MeV remains unclear. In the study performed by Dunter *et al.*, the authors used an antibody that specifically inhibited MeV infection in certain cell lines [259, 260]. Further incubation of this antibody with surface-labelled cells and subsequent immunoprecipitation pulled down a 75kDa protein, with sequence similarity to moesin. The same research group later described that moesin and CD46 may act as a complex during MeV entry [261]. Studies by other groups showed that cells lacking moesin are still permissive to MeV [262] and the antibody used previously has cross-reactivity to CD46 [263]. The commonly attributed localisation of moesin is to the inner leaflet of the plasma membrane in association

with the cytoskeleton of cell cortex; and it is therefore hard to imagine how it could act as a primary viral receptor. Nevertheless, two reports on the localisation of moesin suggest its presence at the cell surface [264, 265]. More recently, a report highlights the important of this protein in the transmission of MeV infection between dendritic cells and lymphocytes [266]. Although moesin is not seen as a MeV receptor, it is possible that it plays a yet undetermined role in MeV entry.

1.11.2.4.2 NK-1

Another example of a protein that might be involved in the entry of MeV is the substance P receptor neurokinin-1 receptor (NK-1). Substance P is a small peptide (11 amino acids) that functions as a neurotransmitter and is associated with pain and inflammatory responses [267]. NK-1 is the receptor for substance P and is expressed at the synaptic neuronal endings of neurons in the brain and spinal cord [268]. The initial work of Harrowe *et al.* showed that MeV F protein shares sequence similarity to substance P and incubation with substance P reduced MeV-induced cell-cell fusion [269]. This is particularly relevant to MeV transmission to the nervous system. It has been documented that cell-to-cell fusion induced by MeV infection in neurons, that occurs primarily at synapses, does not require the activity of H protein or expression of known receptors [270-272]. Further studies demonstrated that interfering with the expression or activity of NK-1 reduced MeV infection in susceptible mice [273]. It is possible that MeV spread to neurons might be regulated by NK-1, where F might be triggered by this interaction. Nevertheless, the search for a neuronal receptor is a topic of current investigation [274].

1.11.2.4.3 TLR2

As part of cellular innate immunity, pattern recognition receptors, such as RIG-I-like receptors or Toll-like receptor (TLRs), play a crucial role in recognizing pathogens and subsequently activating immune responses [275]. One such receptor is TLR2, which is a cell surface receptor present on several immune cells, such as macrophages, dendritic cells, T and B lymphocytes, as well as epithelial and microglial cells. This receptor is known to recognise pathogen-derived molecules including lipoproteins, lipotechoic acid and peptidoglycans [276]. Although its mechanism of action is dependent on the cell in which it is expressed, TLR2 activation leads to several inflammatory responses: increased production of reactive oxygen species [277], NF-κB activation [278], stress responses [279], etc. Interestingly, wild-type strains of MeV H were reported to interact with TLR2 on dendritic cells, leading to the production of IL-6 and upregulation of SLAMF1 [149]. This interaction between H and SLAMF1 was specific to virulent strains and sensitive to one single amino acid substitution (N481Y), which is also involved in CD46-mediated entry of attenuated strains. TLR2 activation during MeV infection is associated with virus-induced immune suppression and viral tropism.

1.11.2.4.4 DC-SIGN

Similarly, the dendritic cell-specific intercellular adhesion molecule-3-grabbing non-integrin (DC-SIGN) molecule has been shown to interact with MeV H and F during the initial stages of immune cell infection [280]. DC-SIGN is C-type lectin pattern recognition receptor, expressed on dendritic cells (DCs) and macrophages, that recognises endogenous glycoproteins, such as intercellular adhesion molecule 2 (ICAM2) and 3 (ICAM3) which impact on cell migration and cell-cell communications [281, 282], but also interacts with pathogens, mediating phagocytosis and immune

responses [283, 284]. In studies performed by de Witte *et al*. in 2006 and 2008, DC-SIGN activity was shown to be necessary for infection even though its expression in non-permissive cells does not permit MeV entry. Furthermore, they showed that this molecule mediates the spread of MeV from DCs to T lymphocytes. In particular DC-SIGN appears to be involved in trans-infection of MeV into T cells in a process that is independent of both SLAMF1 expression and DC infection [280, 285]. Consequently, in the macaque model, lung-resident DCs expressing DC-SIGN were shown to be initial targets of MeV and pivotal to subsequent spread of the infection [286]. DC-SIGN is now seen as an important attachment factor and pivotal molecule in the establishment of MeV infection. Interestingly, this molecule has been implicated in the attachment and entry of numerous viruses, including RSV [287], Ebola virus [288], Influenza A virus [289], herpes simplex virus 1 [290], HIV-1 [291], etc. This association of DC-SIGN with a broad collection of viral envelope proteins is likely to be related to the ability of this receptor to recognise glycosylated proteins – as viral envelope proteins usually are – and the role it plays in antigen presentation.

These examples of interactions between MeV envelope proteins and cellular receptors are likely to impact, at some level, on the steps of viral attachment and entry. Reports have shown that atypical interaction of intravirion proteins with cell surface proteins might aid the establishment of infection. Despite a growing list of interaction partners for MeV proteins and their putative functions as cellular receptors, researchers have predicted the existence of at least two other receptors. As mentioned previously, MeV can also infect the nervous system, particularly neurons and astrocytes [141, 272, 292]. Although F interaction with NK-1 may contribute to infection of these cells, it is possible that a specific H-interacting

receptor exists on these cells. In addition, endothelial cells can also become infected with MeV [174, 219]. Since endothelial cells lack the expression of any of the identified receptors for virulent strains of MeV (SLAMF1 and nectin-4) it is possible that another cellular protein grants permissivity to these cells.

1.11.3 Virus Entry

The initial stages of MeV infection are likely to involve the interaction of several proteins and the exact stoichiometry of this process is not known. Nevertheless, mutagenic studies of viral proteins, crystallographic approaches and the biochemical characterisation of receptors and viral H and F proteins have unravelled some of the details of virus entry. The measles virion is decorated with H tetramers and F trimers; each tetramer of H ad trimer of F form a complex called the “fusion complex” and it is considered the minimum requirement for MeV entry. When a virion is adsorbed onto the plasma membrane of a permissive cell, H interacts with SLAMF1 leading to a series of conformational changes in this protein and, subsequently, in the F protein. A dramatic refolding of F exposes a highly hydrophobic peptide that penetrates the plasma membrane of the cell. The reconfiguration of the structure of F brings the two membranes together, leading to the coalescence of the outer lipid leaflets of both membranes, a step known as hemifusion, and later the formation of a fusion pore by the complete fusion of both viral envelope and the plasma membrane. Through this fusion pore, MeV genome is released into the cytoplasm where replication occurs.

1.11.3.1 Attachment

As mentioned previously, the globular domain of H contains binding sites for its several receptors [293-296]. Vaccine strains of MeV that use CD46 as a receptor diverge from wild-type MeV H by accumulating several mutations in the globular head – most importantly the N481Y substitution, which was shown to be important for attachment and triggering of fusion in CD46-positive cells [297, 298]. When interacting with SLAMF1, MeV H binds to the V domain with three residues in SLAMF1 being particularly important for binding, I60, H61 and V63 [299, 300]. Complementarily, several residues in H have been identified to mediate binding to SLAMF1 [301] and fusion [293, 294].

Both mutagenic and crystallographic studies have been applied to elucidate the binding mechanism of MeV H to its receptors. A total of five crystal structures of MeV H have been resolved, most them in association with SLAMF1, CD46 or nectin-4. Initially, MeV H-CD46 complexes were resolved (**Fig.1-11**) [302, 303]. This structure showed that H is present as a dimer and interacts with two molecules of CD46 containing the SCR1 and SCR2 domains (**Fig.1-11A**). The main interaction site is on β-propeller 4, which contains an indentation that interacts with the SCR1 and SCR2 domains. A total of three contact sites between H and CD46 were identified: (1) region 1 is composed of a double proline motif (I37-P38-P39-L40), located at the N-

Fig.1-11 Structure of the MeV H receptor binding domains. A representation of the amino acids involved in binding to (A, in red) CD46, (B, in green) nectin 4 and (C, in blue) SLAMF1. The lower panel (D) reflects a superimposition of these three binding sites on the MeV H structure [192].

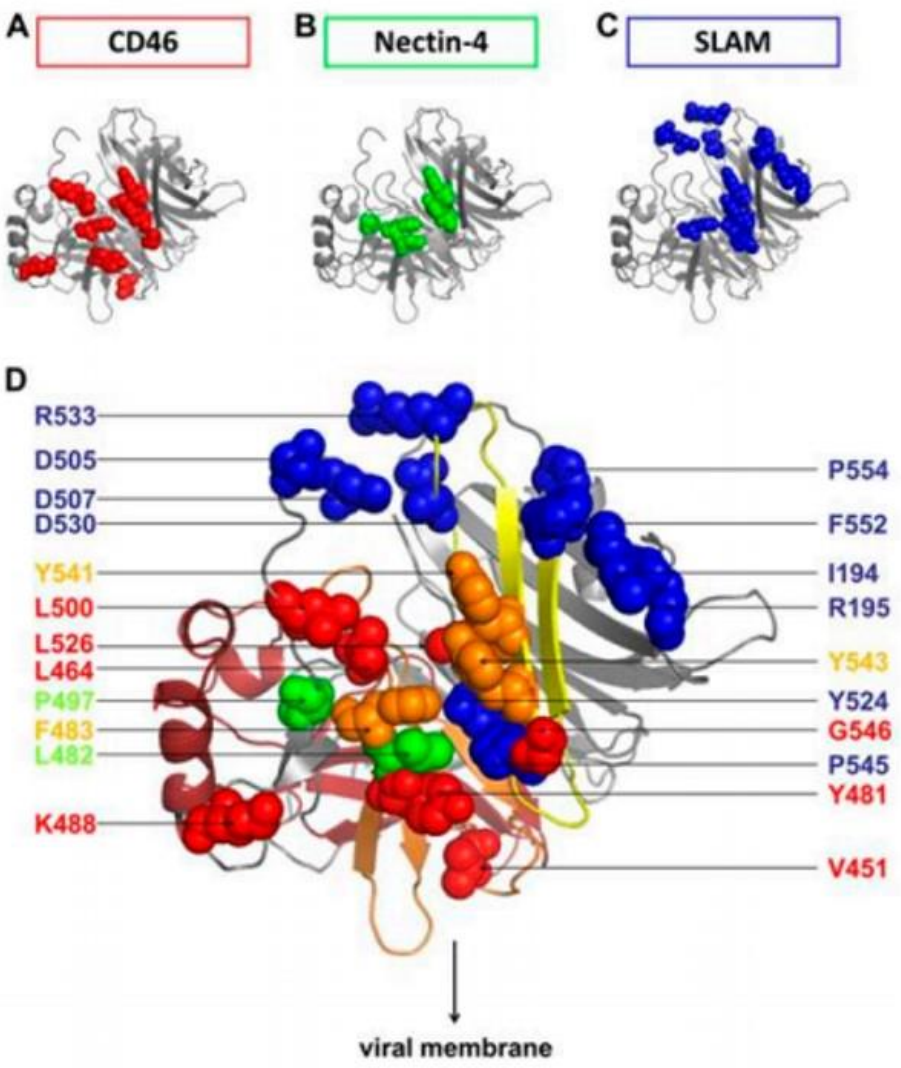
A
CD46
B
Nectin-4
C
SLAM
D
R533
D505
D507
D530
Y541
L500
L526
L464
P497
F483
L482
K488
P554
F552
I194
R195
Y543
Y524
G546
P545
Y481
V451
viral membrane

terminus of CD46 and the SCR1 domain, that inserts into a hydrophobic pocket in H located between the 4th and 5th β-propellers; (2) the second interaction site involves a hydrogen bond formed by Y481, a pivotal amino acid involved in CD46-tropism [297, 298], that interacts with C65 of CD46 that is located between the SCR1 and SCR2 domains; finally, (3) the third contact region is composed of Y67 and Y85 of CD46 that interacts with V451 and Y481 of H.

Similar studies have been performed for the SLAMF1-H interaction [180, 181]. MeV H interacts with the V domain of SLAMF1 via its 4th, 5th and 6th β-propellers (**Fig.1-11C**). Four binding sites are thought to govern SLAMF1-H interactions: (1) in site 1 two aspartic acid residues of H (505 and 507) interact with K77 and R90, respectively, of SLAMF1, (2) in site 2, two salt bridges established between the E123 of SLAMF1 and D530 and R533 of MeV H (which are known to contribute to the stabilisation of the interaction), (3) site 3 is composed of a planar interaction between five amino acids in the 6th β-propeller of H (P191-R195) and five other amino acids in the V domain of SLAMF1 (S127-F131); (4) lastly, at site 4, a patch of aromatic residues in H (Y541, Y524, Y543 and F552) interacts with F119, R130 and D75 of the SLAMF1.

Finally, the interaction of the MeV attachment protein with nectin-4 has also been described, again primarily with mutagenesis-based and crystallography approaches [296, 304]. The V domain of nectin-4 was shown to interact with an indentation formed between the 4th and 5th β-propeller blades, similar to the interaction of Edmonston strain MeV H with CD46 (**Fig.1-11B**). The Nectin-4-H interaction involves three binding sites: (1) in the first contact region, the H residues Y524, L526, Y541 and Y543 on the 5th β-propeller blade, which have previously been shown by

mutagenesis to be important for virus entry [295, 304], interact with seven amino acids in nectin-4 (S99-F106) while a stretch of amino acids in the β4 blade (P458, M459, L462-G465, L482 and F483) binds to F101-G104 in nectin-4; (2) the second site of interaction consists of a loop of amino acids in the interface between the 4th and 5th β-propeller blades (T498, Y499 and D505) that interacts with Q30, G32 and Q33 of nectin-4; while (3) the 3rd site of interaction is composed of the amino acids H52-Y55 in the nectin-4 V domain that interact with the loop located between the 4th and 5th β-blades (Y499 and L500) of H and amino acids in the β3 blade (K387-K389).

Biochemical studies that allowed the determination of the dissociation constant (K_d) for MeV H and its receptors identified the following, described here in ascending order: $K_{d\ nectin-4} = 20\ nM < K_{d\ CD46} = 75 - 100\ nM < K_{SLAMf1} = 80 - 500\ nM$ [204, 301, 305]. This suggests that MeV H binds with higher affinity to nectin-4, with some studies suggesting that ligand-receptor disengagement is mediated by other domains of nectin-4 not primarily involved in binding [306].

1.11.3.2 Fusion mechanism

The fusion mechanism of the H and F oligomeric complexes with their cellular receptors has been a topic of intense investigation with diverse studies, from mutagenesis to crystallography, allowing the development of a good understanding of how the process unfolds. Nevertheless, the exact transitional conformations and the overall process of membrane fusion still remain unknown. The F protein of MeV is a class I fusion protein, i.e. the conformational changes that F undergoes to mediate membrane fusion are irreversible [307]. A schematic representation of the fusion

process is depicted in **Fig.1-12**. The minimum unit for viral fusion is composed of a tetramer of H which interacts with a trimer of F, a macromolecular complex known as the fusion complex. The fusion complex is present at the surface of measles virions and the plasma membrane of MeV-infected cells (**Fig.1-12A**). After binding of H to its receptors (**Fig.1-12B**) – even when only one dimer of Hs is interacting with the receptor – H triggers a sequence of conformational changes in F (**Fig.1-12C**). This signal which induces the activation of F can be transferred across the interface of the two dimers, as the overall tetramer organisation of H is maintained during fusion [308]. Although MeV H is necessary to trigger F in the presence of the receptor, F can also be activated by exposure to high temperature in the absence of receptor or H [309]. This suggests that H might reduce the energy barrier required to trigger F. The important step during this process is understanding how the signal is transferred onto F upon coupling of H with the cellular receptor. The fourth and fifth blades of the β-propeller are involved in the interaction with the receptor while the stalk domain is involved in the triggering of the F protein [180]. Before triggering F, the H tetramer assumes a planar “heads-down” configuration; the interaction with the receptor possibly induces conformational changes in the tetramer, leading to the segregation of the stalks of the two dimers [180, 308]. Mutagenesis of the stalk of H interferes with its ability to trigger fusion, and it is believed that the detachment of H and F is required to induce fusion [310]. Two domains located to the upper central and lower central stalk sections are involved in triggering and modulating fusion: the lower domain is responsible for activating F and initiating fusion while the upper domain is required to promote fusion beyond the initial activation step [309, 311-313]. Activated F protein exposes the fusion peptide and inserts it into the membrane of the target

Fig.1-12 Schematic representation of the fusion mechanism of MeV. In its resting state, a tetramer of H assumes the “heads down” configuration, in which F strongly interacts with the stalk domain of H (A). Upon binding to SLAMF1, the tetramer of H undergoes a conformational change described as the “heads up” configuration (B). This will release F and trigger it, leading to the initiation of the fusion process (C). At this point, F unfolds exposing the fusion peptide that penetrates the target membrane (D). Further conformational modifications in the F, bring the two lipid bilayers to close proximity (E), where hydrophobic interactions between phospholipids lead to an intermediate stage called hemifusion (F). Finally, two membranes fuse completely leading to the release of the viral genome into the cytosol (G). Adapted from [308] and [317].

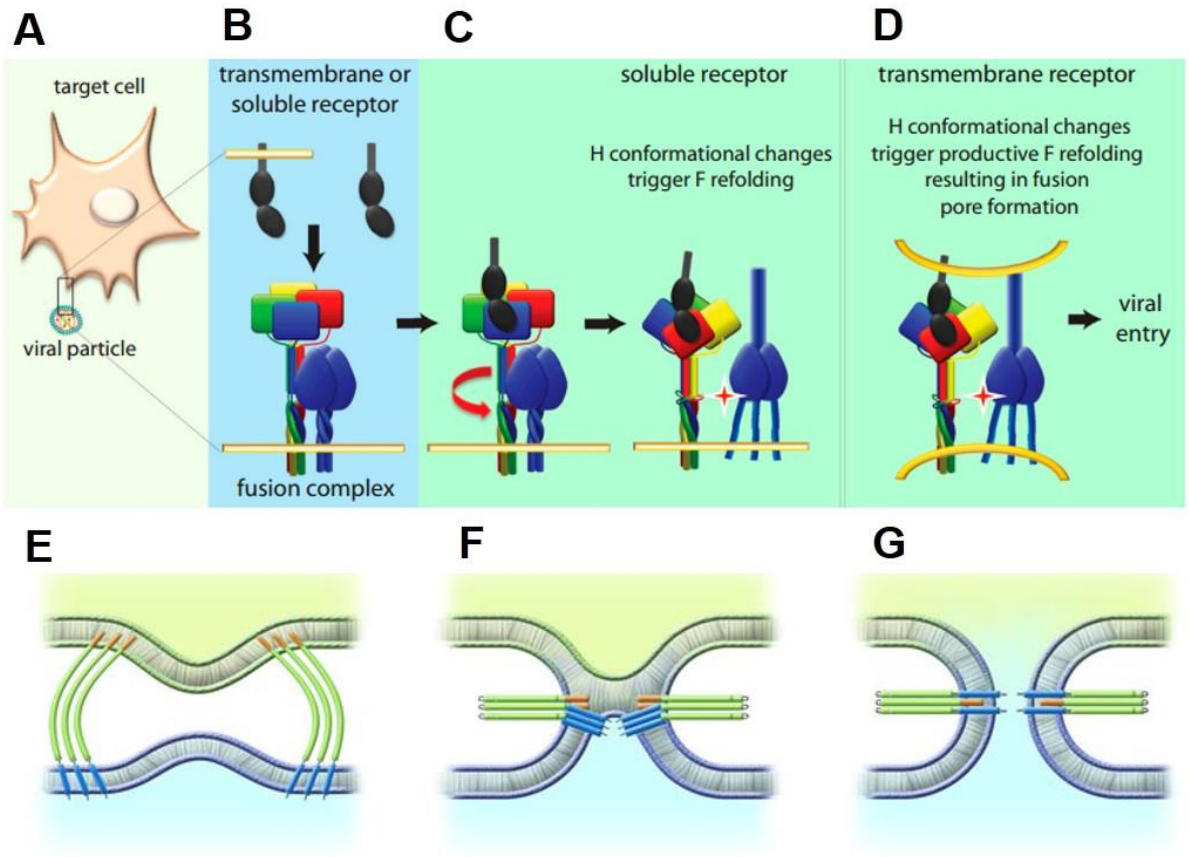
A
B
C
D
target cell
viral particle
transmembrane or
soluble receptor
fusion complex
soluble receptor
H conformational changes
trigger F refolding
transmembrane receptor
H conformational changes
trigger productive F refolding
resulting in fusion
pore formation
viral
entry
E
F
G

cell (**Fig.1-12D**). Predictably the distance of the binding domain of the receptor from the surface influences fusion efficiency of the virus, suggesting a limited reach for the fusion peptide with respects to the plasma membrane [314]. Further refolding of the F protein consists of the formation of a transient structure called “hairpin”, in which N-terminus of the F1 fragment, inserted into the plasma membrane of the host, moves closer to the C-terminus of the protein, located in the viral envelope - bringing the viral and host membranes to close proximity (**Fig.1-12E**). The outer leaflets of the plasma membrane and the viral envelope coalesce – this step is known as hemifusion (**Fig.1-12F**). When hemifusion is reached, the inner layers of phospholipids mix, culminating in the formation of the fusion pore where the contents of the virion are released into the cytosol (**Fig.1-12G**) [315, 316].

1.11.3.3 Endocytosis

The entry of paramyxo- and pneumoviruses has long been regarded as independent of endocytosis mechanisms as infection occurs by direct fusion of the viral envelope to the plasma membrane of the cell [318, 319]. This conclusion was drawn in recognition of two of the main phenotypes of infection: (1) the pH-independent activation of paramyxoviral fusion proteins and (2) the ability of several viruses to induce cell-cell fusion, suggesting that fusion is essentially mediated by receptor binding. Since the seminal work of Helenius and colleagues on the entry mechanism of Semiliki virus [320], clathrin- and caveolin-mediated endocytosis have been regarded as entry pathways that viruses hijack to establish infection – studies that were possible due to the use of lysosomotropic agents and electron microscopy. Unfortunately, the lack of suitable techniques to investigate other endocytosis

pathways, such as macropinocytosis, phagocytosis, flotillin-dependent endocytosis, etc., hindered research into the entry mechanisms of viruses that did not use clathrin- and caveolin-dependent endocytosis [321]. Recent advances in immunofluorescent tracking of viral particles, siRNA screens and a wide collection of pharmacological inhibitors have, however, allowed the dissection of several endocytosis pathways that remained previously uncharacterised. As a consequence, several paramyxoviruses and pneumoviruses have been shown to internalise by distinct pathways, such as RSV [195, 322], Sendai virus [323], Nipah virus [324, 325], Newcastle disease virus [326] and human metapneumovirus [327]. However, these entry pathways have not been assessed during morbillivirus infection. Nevertheless, a study using lentivirus pseudotyped with MeV glycoproteins showed endocytosis into lymphocytes [328] while soluble MeV H is internalised in CD46-positive cells via clathrin-mediated endocytosis or macropinocytosis [329]. These studies suggest that MeV might be endocytosed during the initial stages of infection.

1.11.3.4 Membrane interactions

In recent years, MeV has been shown to manipulate the cellular membrane impacting on viral spread. Particularly, work performed by the Schneider-Schaulies research group has convincingly shown the modulation of sphingomyelinases during viral entry. Sphingolipids are a group of lipids that contain a sphingosine side chain and are components of cellular membranes that play important roles in cell signalling [330]. Sphingomyelin, a type of sphingolipid that contains ceramide, is hydrolysed by sphingomyelinases generating important secondary messengers during molecular signalling and signal transduction after extracellular stimulus [331]. In 2011, Avota *et*

al. showed that upon binding of MeV to DC-SIGN, ceramides accumulate on the outer leaflet of the plasma membrane due to the activity of sphingomyelinases [332]. This concentration of ceramide at the entry site was demonstrated to be necessary for the recruitment of SLAMF1 and internalisation of MeV. Subsequent studies showed that MeV modulates the activation of T cells by controlling the activity of the neutral sphingomyelinase, impacting on the formation of the immunological synapse and suppression [333]. Other studies showed that altering the shingosine-1-phosphate levels – a component of the signalling pathway of sphingomyelin – impacted on MeV replication, highlighting the importance of sphingolipids in the virus lifecycle [334]. The accumulation of ceramide at the plasma membrane leads to the coalescence of lipid rafts into larger microdomains; such domains are known to entrap and concentrate several membrane proteins, including cellular receptors, where the virus can enter [335, 336]. Such ceramide-enriched domains have been implicated in the fusogenicity of cellular membranes but also in internalisation pathways such as phagocytosis [337, 338]. Together these data are evidence of a highly organised mechanism of entry for MeV that perhaps requires clustering of cellular receptors and intracellular signalling, in contrast with the current paradigm of viral envelope fusion at the plasma membrane.

1.11.4 Virus exit

The molecular details of MeV budding are not described yet, but limited evidence has suggested a mechanism similar to other paramyxovirus (see **Fig.1-13** for a schematic representation of MeV egress. Briefly, MeV glycoproteins interact in the endoplasmic reticulum where they form an inactive fusion complex. Hijacking the vesicular

Fig.1-13. Schematic diagram of MeV egress. (A) MeV F and H proteins interact in the endoplasmic reticulum (ER) after being synthesised, forming the fusion complex. This complex is transported to the surface in a ESCRT-independent manner. The M protein interacts with recently formed RNP complexes and mediates transport to the plasma membrane using Rab11-positive endosomes. At the cell surface, MeV M bridges the fusion complex with the RNP by interacting the cytoplasmic tail of MeV glycoproteins. This interaction leads to the formation of virions and subsequent release into the extracellular environment. Adapted from [353].

A

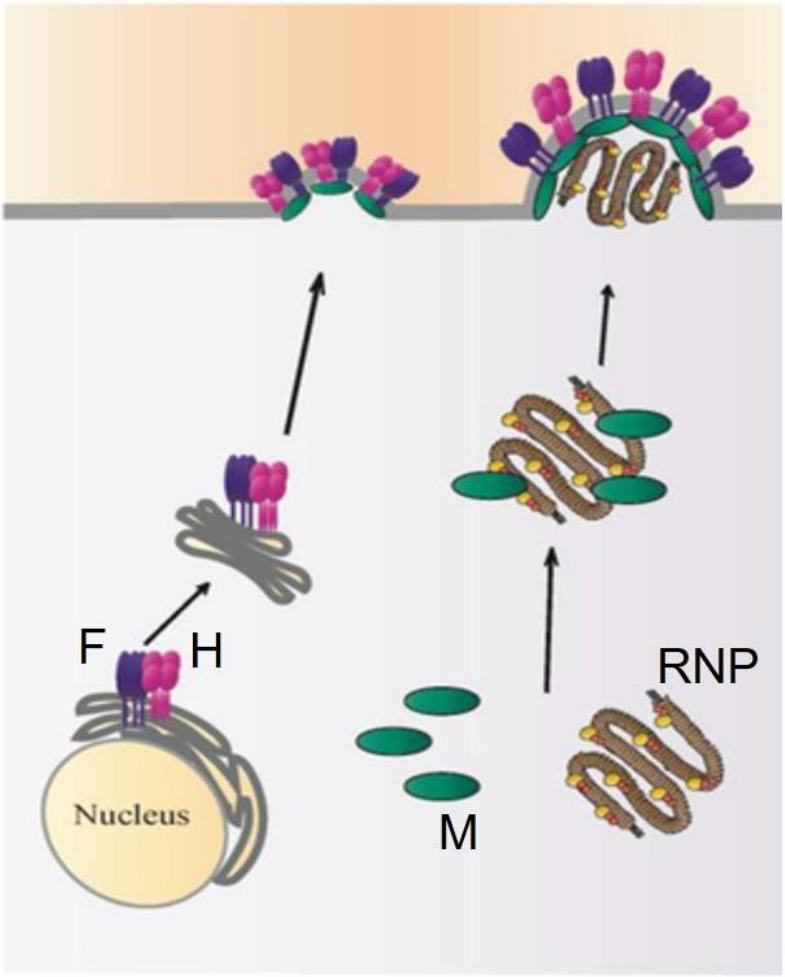

trafficking system, both glycoproteins are transported to the plasma membrane. The M protein may interact with the RNP which are co-transported to the cell surface by unknown mechanisms. It is commonly believed that M functions as a crosslinker between the cytoplasmic tails of MeV F and H and the RNP, initiating particle formation culminating in the release of the virion into the extracellular environment. Additionally, it has been suggested that cell fusion might be required for virus spread *in vivo* [339, 340]. Several studies have indicated that M modulates virus assembly and, interestingly, mutations in this protein change the balance of viral spread from particle to syncytia formation [341]. MeV enveloped proteins are expressed in the basolateral surface of polarised epithelial cells; however, when co-expressed with the M protein, they are re-directed to the apical surface, where the virus is naturally released [339, 342]. The underlying mechanism for this process is, only now, starting to be dissected. Firstly (1) M protein coats the RNP complex [99]; then (2) this complex associates with Rab11a positive recycling endosomes (Rab11a regulates exocytosis of recycling vesicles at the plasma membrane [343]) and is transported along the microtubules in the direction of the apical surface [344]. Lastly, (3) at the plasma membrane site, M protein interacts with the cytoplasmic tails of H and F proteins, combining the RNP with the envelope proteins and stabilizing the complex. This interaction is crucial for generating virus particles. Accordingly, mutations in either the M protein or glycoprotein cytoplasmic tails are thought to favour cell fusion over particle formation [345, 346]. One cellular protein that has been implicated in playing a role in modulating virus exit is actin, a component of the cytoskeleton which is known to contribute to the budding of other viruses [347]. Actin filaments have been identified in MeV particles and it has been shown that actin located to the

cortex of cells is required for the later stages of virus infection [348]. Other studies showed that actin competes with the cytoplasmic tails of viral GPs for interaction with M protein, promoting cell fusion [349]. Some paramyxoviruses take advantage of the endosomal sorting complex required for transport (ESCRT) proteins, a group of proteins that finish vesicle formation by inducing scission of the plasma membrane to complete budding [350]. However, MeV particle formation does not require proteins of the ESCRT pathway and its true budding mechanism is yet to be determined [346]. Nevertheless, viral budding in MeV infections is associated with cholesterol-rich microdomains (lipid rafts) [351] and CDV requires cholesterol in the viral envelope, but not in target cells, to allow infection [352], which suggests a substantial role for this molecule in virus maturation. In fact, MeV infection modifies the expression levels of two enzymes involved in the synthesis of cholesterol in cells (hydroxy-3methylglutaryl-conenzyme A reductase and squalene monooxygenase) [178].

1.12 General Aims

During infection, MeV infects a variety of cells that differ not only in their composition and nature, but also in the three-dimensional tissue architectures in which they reside. MeV has to overpass biological barriers, such as the extracellular matrix and mucus of the respiratory epithelium, to successfully infect target cells. When at last, MeV interacts with its cellular receptors, its genome must be transported into the cytoplasm so replication can start. As highlighted in this introduction, the mechanisms of MeV cellular spread are poorly characterised. Recent advances in

immunofluorescence microscopy, high-throughput screens and the expansion of well-characterised pharmacological inhibitors have been fundamental for unravelling these mechanisms for other viruses. Herein, I intend to explore two main questions related to viral spread:

1 – What are the molecular mechanisms governing the **entry of MeV** particles into the SLAMF1+ cells?

2 – What cellular components control **MeV exit** via cell-cell fusion and/or viral budding?

Specifically, I intend to use pseudotyped MeV particles and purified MeV particles in combination with pharmacological inhibitors, dominant negative mutants and microscopy to determine the entry route of MeV. A quantitative cell-cell fusion assay will also be used to study cellular requirements during early stages of MeV-induced cell fusion. Finally, to examine the later steps of MeV infection, particularly in relation to viral budding, I will take advantage of quantitative proteomic techniques to evaluate the membrane proteome of MeV infected cells.

Chapter 2

MATERIALS AND METHODS

2.1 Cell lines

All cell lines were maintained at 37°C with 5% CO_2. Human Embryonic Kidney 293T (HEK293T, kindly provided by Dr Maelle Lorvellec, University of Birmingham (UoB) [354]) cells, human lung adenocarcinoma epithelial cell line A549 (provided by Professor Jane McKeating, UoB [355]), human cervical cancer (HeLa) cells (kindly provided by Dr Magdalena Krzyzaniak, University of Basel [195]) and human osteosarcoma (U-2 OS, provided by Dr Jo Morris, UoB [356]) were cultured in Dulbecco's Modified Eagle Medium (DMEM, Sigma-Aldrich, USA) supplemented with 10% foetal bovine serum (FBS, Sigma-Aldrich, USA) and 1% ampicillin/streptomycin (Sigma-Aldrich, USA). African green monkey kidney (Vero) cells engineered to over-express human SLAM (Vero-SLAM, provided by Dr Kevin Brown, Public Health England/Health Protection Agency) were cultured in DMEM and 10% FBS under geneticin (G418) selection (0,4mg/mL, Sigma-Aldrich, USA). Epstein-Barr virus-immortalized peripheral B lymphocytes (LCLs, a kind gift from Dr Claire Shannon-Lowe, UoB [357]) were cultivated in RPMI-1640 (Sigma-Aldrich, USA) supplemented with 10% FBS and 1% penicillin/streptomycin.

HEK293T and A549 cell lines, engineered to over-express human SLAMf1 (from now on referred to as HEK293T-SLAM and A549-SLAM, respectively), were previously generated in our lab, as described previously [229]. These cells were maintained in DMEM with 10% FBS, supplemented with 1µg/mL puromycin (Sigma-Aldrich) as a selection marker. Briefly, the wild-type human SLAMF1 ORF was integrated via transduction into HEK293T or A549 cells, using a HIV backbone containing the Ψ

packaging signal, the long terminal repeat (LTR) 1 and 2 and the HIV-1 gag-pol protein.

2.2 Viruses

2.2.1 Recombinant viruses

Recombinant MeV strain IC323 carrying the enhanced green fluorescent protein (EGFP) ORF (p(+)MV323EGFP, a kind gift from Professor Yanagi, University of Tokyo, Japan) was generated as described previously [20]. Briefly, a plasmid containing the full genome of MeV strain IC323 with a 5' insertion of the EGFP gene, as a separate transcription unit, was transfected into HEK293T cells, previously infected with recombinant fowlpox virus encoding the T7 RNA polymerase, along with three plasmids encoding for MeV proteins N (pMeV-N-IC323), P (pMeV-P-IC323) and L (pMeV-L-IC323). After initial recovery, MeV was produced in Vero-SLAM cells. When infection was fully developed, cells were freeze-thawed once and centrifuged at 1000×g for 10min at 4°C. Supernatant was then collected and stored in aliquots at -80°C. Virus tissue culture infectious dose 50 (TCID-50) was calculated using the Reed-Müench method [358].

2.2.2 Virus Purification

Vero-SLAM cells, grown in eight T175 flasks to a confluence of approximately 40%, were infected with MeV (MOI~0.1) in 8mL of serum-free DMEM with 1% P/S for 1h at 37°C. This inoculum was then removed and replaced with 10mL of complete medium. Three to four days later, flasks were vigorously shaken and supernatants were collected and clarified as before. Supernatants were layered onto a 20%

sucrose cushion (weight/volume in Hank's balanced salt solution (HBSS)), 25mM HEPES NaOH, pH=7.4) and centrifuged at 125,000xg for 3h at 4°C in a SW32 Ti rotor (Beckman Coulter). The resultant pellets were resuspended in 1mL of HBSS-HEPES, pooled, layered onto a 30-45-60% stepped sucrose gradient and centrifuged at 154417xg for 3h at 4°C in a SW40 rotor (Beckman Coulter). Two opalescent bands were visualised under polarized light: one at the 60-45% interface (lower band) and the other below the 30-45% interface (upper band) (**Fig2-1A**). The lower band was extracted using a needle and dialysed separately overnight using 10 kDa molecular weight cut-off membrane tubing, against 1L of HBSS-HEPES. Purified virus was then aliquoted, stored at -80°C and titrated. Only the lower band was used in experiments since it had a higher virus titre. To analyse quality, purified MeV particles were resolved in an SDS-PAGE gel and protein bands were silver stained (**Fig2-1B** and **C**).

2.2.3 Spinoculation

LCLs (2×10^5 cells) were concentrated to a final volume of 300µL. Cells were then infected with MeV (as indicated) at 4ºC for 1h at 300×g. Cells were washed and resuspended in culture medium and incubated at 37ºC.

2.2.4 Virus growth curve

Vero-SLAM and LCLs were infected with MeV-EGFP IC323 strain at indicated MOIs. Vero-SLAM cells were incubated with a low volume of virus-containing solution at 37°C, for 1h, while LCLs were infected by spinoculation, as described above. After inoculation, the media was replaced and at 0, 12, 24, 48, 72, 96 and 120h post-

Fig.2-1 Purification of MeV particles. (**A**) Harvested supernatants of infected cells were pelleted and concentrated through a step-gradient sucrose cushion from 20 to 60% sucrose in HBSS. Virus was visualised under polarised light where two bands were identified. (**B/C**) Purified particles were resolved in SDS-PAGE gel and analysed by western blot (**B**) and silver stain (**C**).

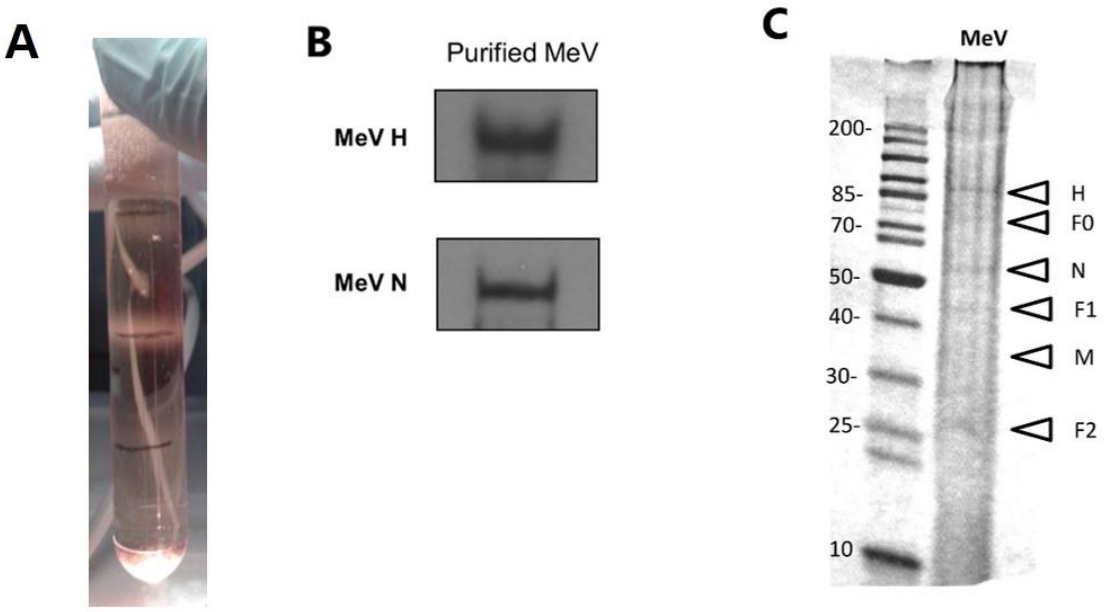
A
B
Purified MeV
MeV H
MeV N
C
MeV
200-
85-
70-
50-
40-
30-
25-
10
H
F0
N
F1
M
F2

infection, samples were frozen to -80°C. The TCID50 was then calculated in Vero-SLAM cells. At the same time points, whole cell lysates were generated using RIPA buffer (Life Technologies, Inc.) according to the manufacturer's guidelines and reduced in Reducing Sample Buffer (Thermo Fisher Scientific, USA) at 37°C for 30min.

2.3 Molecular Cloning

2.3.1 Plasmids

All the constructs mentioned and/or used in this project are listed in **Table 2-1**.

2.3.2 Polymerase Chain Reaction

All PCRs were performed using KOD polymerase (Toyobo Co, Ltd) according to the manufacturer's guidelines. KOD polymerase has strong proof-reading activity and was initially isolated from the hyperthermophilic archaea *Thermococcus kodakaraensis.* A typical PCR reaction contained 0.2mM of each dNTP, 1mM of $MgCl_2$, 0.15µM of each primer, 50ng of template DNA, 1U of KOD and water to a final volume of 50µL. A representative PCR reaction cycle is as follows:

$$95°C, 2'$$

$$25\ cycles \begin{bmatrix} T_D = 95°C, 10'' \\ T_A = 40°C, 30'' \\ T_E = 68°C, 1' \end{bmatrix}$$

Where T_D is denaturing temperature, T_A is the annealing temperature and T_E is extension temperature. T_A was modified accordingly to match the denaturation

Table 2-1. **List of plasmids used in this project**. All plasmids used and described in this thesis were either sourced from indicated labs, generated in our lab or bought from the biotechnology repository company Addgene.

Name	**Description (expressed protein)**	**Origin**
pDublin-H	MeV Dublin wildtype strain H	Our lab
pDublin-F	MeV Dublin wildtype strain F	
pDublin-HΔ24	MeV Dublin wildtype strain H with a truncated 24aa cytoplasmic tail	
pDublin-FΔ30	MeV Dublin wildtype strain F with a truncated 30aa cytoplasmic tail	
pIC323-H	MeV IC323 wildtype strain H	
pIC323-F	MeV IC323 wildtype strain F	
pIC323-HΔ24	MeV IC323 wildtype strain H with a truncated 24aa cytoplasmic tail	
pIC323-FΔ30	MeV IC323 wildtype strain F with a truncated 30aa cytoplasmic tail	
pPAK-1-WT	wild type p21-activated kinase 1	
pPAK-1-CA	Constitutively active p21-activated kinase 1 (T423E mutation)	
pVSV-G	Glycoprotein (G) of vesicular stomatitis virus (VSV)	Prof Jane McKeating [359]
pNL-4.3	Replication-defective, envelope-defective HIV-1 provirus expressing Firefly luciferase gene	
p8.91	HIV-1 gag-pro-pol	Dr Edward Wright [360]
pCSFLW	Replication-defective, envelope-	

	defective HIV-1 provirus carrying Firefly luciferase	
pEPS15-DN-RFP	Dominant negative Epidermal growth factor receptor pathway substrate 15 ΔEH2/EH3 fused with RFP	Dr Joshua Rappoport [361]
pCav-1-DN-GFP	Dominant negative Caveolin-1 (P132L mutation) fused with EGFP	
pDyn2-DN-RFP	Dominant negative Dynamin-2 (K44A mutation) fused to RFP	
pRhoA DN	Dominant negative RhoA -2 (T19N mutation) fused to GFP	Dr Patrick Caswell [362]
pRhoA CA	Constitutively active RhoA -2 (Q63L mutation) fused to GFP	
pRac1 DN	Dominant negative Rac1 -2 (T17N mutation) fused to GFP	
pRac1 CA	Constitutively active Rac1 (Q61L mutation) fused to GFP	
Cdc42 DN	Dominant negative Cdc42 (T17N mutation) fused to GFP	
Cdc42 CA	Constitutively active Cdc42 (Q61L mutation) fused to GFP	
pRLuc1-7	Split *Renilla luciferase* and *EGFP* reporter (lighter fragment)	Prof Zene Matsuda [363]

pRLuc18-11	Split *Renilla luciferase* and *EGFP* reporter (heavier fragment)	

temperatures of each set of primers. The length of T_E was modified to the size of each plasmid at a rate of approximately 1 min per 1kb.

The constructs pDublin-H, pDublin-F expressing the ORF of MeV strain H and F, respectively, and pDublin-HΔ24 and pDublin-FΔ30 expressing 24 and 30 amino acids deletion, respectively, of the cytoplasmic tail of the parental protein were generated as follows (See **Fig.2-2** for an overall representation of the cloning procedure). HΔ18 and HΔ24 were amplified from MeV Dublin strain H ORF using the forward primers 5'-AATTGGATCC ACCATGAACAGAGAACATCTTATGATT-3' and 5'-AATTGGATCCACCATGGGAAGTAGGATAGTTATACAGA-3', for Δ24 and Δ18 truncations, respectively, both containing a BamHI restriction site (underlined), and the reverse primer 5'-AATT-GATATC CTACTATCTGCGRTTGGTTCCAT-3' containing the EcoRV restriction site. Both inserts were digested with BamHI-HF and EcoRV-HF restriction enzymes (New England Bio Labs, Inc., USA) and ligated into the BamHI/EcoRV restriction sites of pcDNA3.1. Similarly, the construct Dublin FΔ30 encodes a truncated version of the MeV Dublin strain F protein lacking 30 amino acids at the C-terminus. This was amplified from pDublin-F, using the forward primer 5'-AATT-GCTAGCACCATGGGTCTCAAGGCGAG-3' and the reverse primer 5'-AATT-GATATCCTACTACGCCCCCTGCAGCAACATATT-3', containing the NheI and EcoRV restriction sites (underlined), respectively. The resultant PCR product was digested with NheI-HF and EcoRV-HF (New England Bio Labs, Inc., USA) and ligated into the NheI/EcoRV restriction sites of pcDNA3.1. The constructs IC323 H-WT, HΔ24 and HΔ18 encode the wild-type, N-terminal 24 and 18 amino acids truncations of the MeV IC323 strain H ORF, respectively. They were amplified from the p(+)MV323EGFP construct using the forward primers

Fig.2-2. Schematic representation of the cloning procedure. (A) Target genes were amplified by PCR using primers containing adequate restriction sites, as indicated. After amplification, amplicons were purified from the enzymatic reaction mix and digested using restriction enzymes at 37ºC for 1h. Digested DNA was further purified and incubated with digested and dephosphorylated plasmidic vector pcDNA3.1, in the presence of T4 ligase at 16ºC overnight. Successfully ligated plasmids were then transformed into competent cells.

A

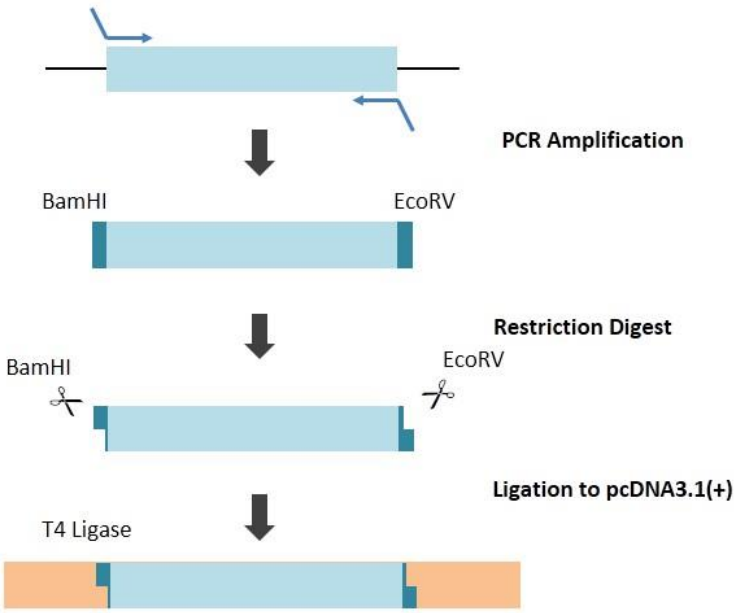
PCR Amplification
BamHI
EcoRV
Restriction Digest
BamHI
EcoRV
Ligation to pcDNA3.1(+)
T4 Ligase

5’-AATTGGATCCACCATGTCACCRCAACGAGACCR-3’, 5’-AATT-GGATCCACCATGaacagagaacatcttatgatt-3’ and 5’-AATTGGATCCACC ATGGGAAGTAGGATAGTTATyaacaga-3’, all of them containing the BamHI restriction site, and the reverse primer 5’-AATTGATATCCTACTA-TCTGCGRTTGGTTCCAT-3’ containing the EcoRV restriction site (underlined). Finally, the constructs IC323 F-WT and FΔ30 encode the wild-type and C-terminal 30 amino acid truncation, respectively of MeV IC323 strain F protein. Both were amplified from p(+)MV323EGFP using the forward primer 5’-AATTGCTAGCACCAGGGCCAAGGAACATACACAC-3’, containing the NheI restriction site, and the reverse primers 5’-AATT-GATATCCTATCAGAGTGACCTTACATATGA-3’ and 5’- AATT-GATATC CTACTACGCCCCCTGCAGCAACATATT-3’, both containing the EcoRV restriction site. Inserts were digested with NheI-HF and EcoRV-HF and ligated into the NheI/EcoRV restriction site of pcDNA3.1.

To generate the two constructs encoding PAK-1, mRNA was extracted from HEK293T cells using the GenElute^{TM} Mammalian Total RNA Miniprep Kit (Sigma) according to the manufacturer’s guidelines. A cDNA library was generated from the extracted mRNA using the Moloney Murine Leukaemia Virus Reverse Transcriptase (M-MLV RT, Promega) and a sequence of 15 thymine bases as a primer (OlidT). DNA encoding PAK-1 was amplified by PCR using the forward primer 5’-AATTGGATCCACCATGTCAAATAACGGCCTAGACA-3’ containing the *BamHI* restriction site (underlined) and the reverse primer 5’-AATTGCGGCCGCCTATTAGCTGCAGCAATCAGTG-3’ containing the NotI

restriction site. Digested cDNA was ligated into pcDNA3.1 and the point mutation T423E was introduced by site-directed mutagenesis using the primer 5'-AGCAAACGGAGCGAGATGGTAGGAACC-3' and its respective reverse complement.

The correct sequence of all plasmids was confirmed prior to use in experimentation.

2.3.3 Site-directed mutagenesis

Several constructs were generated by site-directed mutagenesis (SDM), as indicated. In summary, 300ng of template DNA was used in a 50µL PCR reaction, as before, containing 200nM of forward and reverse primers containing substituted codons for each desired mutation (See **appendix section A.1** for a complete list of primers used). The basic PCR reaction was set as follows:

$$95°C, 2\ min$$

$$18\ cycles \begin{bmatrix} T_D = 95°C, 10'' \\ T_A = 40°C, 30'' \\ T_E = 68°C, 3min\ 30'' \end{bmatrix}$$

T_A was modified accordingly to each set of primers. The length of T_E was modified to the size of each plasmid at a rate of approximately 1' per 1kb. Amplified DNA was then incubated with DpnI (New England Bio Labs), according to manufacturer's guidelines), for at least 2h at 37ºC to remove remaining template DNA. The resulting DNA was then transformed into competent cells, as described below.

2.3.4 Transformations

Ligations or plasmid stocks for transformation were mixed with 50µL of competent cells (Alpha-Select Bronze Efficiency, *E. coli* chemical competent cells, Bioline) on ice for 30 min before being heat-shocked for 45sec at 42°C. Heat-shocked bacteria were subsequently incubated on ice for a further 2min. Cells were then incubated with 200µL of super optimal broth with catabolite repression (SOC) medium (Sigma) at 37°C for 1h, with constant shaking, prior to streaking on LB agar (Sigma-Aldrich) plates containing relevant antibiotics. Of note, working concentrations of 100 µg/mL of carbenicillin (Sigma-Alrich) and 50µg/mL of kanamycin (Sigma-Alrich) were used. After overnight incubation at 37°C, a single colony of each transformation was picked from the plate and amplified by further incubation in Luria's Broth containing relevant antibiotics.

2.3.5 DNA extraction and purification

Depending on the experiment, plasmid DNA was purified using either GeneJET Plasmid Miniprep Kit (Thermo Scientific), GenEluteTM HP Plasmid Midiprep Kit (Sigma-Aldrich) or EndoFree® Maxiprep Kit (QIAGEN) according to the respective manufacturer's guidelines. Purification of DNA from enzymatic solutions, or agarose gels, was accomplished using illustra® GFX PCR DNA and Gel Band Purification Kit (GE Healthcare Life Sciences).

2.3.6 Gel electrophoresis of DNA

Gel electrophoresis of DNA was performed using 0.7%, 1% or 1.5% agarose gels in TBE (Trizma Base, boric acid and EDTA) buffer. DNA was mixed with Gel Loading

Dye (New England Biologicals) and run at 100-120V for 30 to 45 minutes. DNA bands were visualized using either intense blue light (if they were going to be used for downstream cloning) or ultraviolet (UV) light (in all other cases).

2.4 Transfections

2.4.1 DNA Transfections

All DNA transfections were performed by incubating purified DNA in Gibco™ Opti-MEM™ (200µL for 6-well plates, 50µL for 24-well plates) with either TransIT-X2™ Dynamic Delivery System (Mirus Bio LLC) – for fusion assays (see **chapter 2 section 2.5.6**) – or polyethylenimine (1mg/mL, Sigma-Aldrich) – for all other transfections. Mixtures were left for 20 min before being added dropwise to cells.

2.4.2 siRNA Transfections

A549-SLAM cells (7×10^5 cells 6-well plate) were transfected with 25nM of a pool of three target-specific short interfering RNA (siRNA), between 19 and 25 nucleotides long, targeting p21-activated kinase (PAK) proteins (including PAK-1, αPAK siRNA (m): sc-29701, Santa Cruz Biotechnology) using DharmaFECT™ 1 Transfection Reagent (Dharmacon™, GE Health Life Sciences) as per the manufacturer's instructions. As a control, scramble siRNAs purchased from Santa Cruz Biotechnology were transfected in a similar manner. The efficient knock-down of PAK-1 protein expression was confirmed 48 and 72h post-transfection by western blot.

2.5 Cell Biology

2.5.1 Pharmacological inhibitors

All of the pharmacological inhibitors used in this project are described in **Table 2-2**. These drugs were all tested in relevant cell lines for cytotoxicity using the reduction of 3-(4,5-dimethylthiazol-2-yl)-2,5-diphenyltetrazolium bromide (MTT) in living cells (see **chapter 2 section 2.5.2**). Drug concentrations that lowered viability beyond 87% of that seen in solvent-treated cells were not used.

2.5.2 MTT assay

To assess the level of cytotoxicity induced by the pharmacological inhibitors described previously, I used a cell viability assay based on the redox reaction of 3-(4,5-dimethylthiazol-2-yl)-2,5-diphenyltetrazolium (MTT) [364]. To begin MTT powder was dissolved in PBS to a final concentration of 5mg/mL. 15µL of this MTT solution was added to cells after treatment with pharmacological inhibitors at specific concentrations/times. This mixture was then incubated for 2h at 37ºC, the media removed and resultant formazan crystals dissolved using 50µL of isopropanol. Absorbance was then read at 600nm using a spectrophotometer.

2.5.3 Pseudotyped virus particles entry assay

Lentivirus-based viruses pseudotyped with MeV or VSV glycoproteins were used in this project. With the purpose of developing an efficient pseudotype assay for MeV, we used three distinct lentivirus-based backbones: (**1**) NL4.3-Fluc-Env-Rev- ([359], a first generation replication- and envelope-defective construct based on HIV-1, containing an extra ORF encoding the Firefly luciferase; (**2**) a combination of p8.91

Table 2-2. List of pharmacological inhibitors used in this project. All drugs used and described in this thesis were either sourced from indicated labs or purchased from indicated biotechnology companies.

Name	**Origin**
Chloroquine	Sigma-Aldrich
(-)-Blebbistatin	
Phorbol 12-myristate 13-acetate (PMA)	
Bafilomycin A1	
5-(N-Ethyl-N-isopropyl)amiloride (EIPA)	
IPA-3	
Chlorpromazine	
Cytochalasin D	Calbiochem® Merck Millipore
Jasplakinolide	
Taxol	
Wiskostatin	Enzo Life Sciences
ML141	Tocris
CK-666	
Glycyl-H1152	Cayman Chemical

(encoding for HIV-1 gag-pol) and CSFLW (HIV-1 provirus, lacking *env* and *gag-pol* genes and encoding for Firefly luciferase) ([360]; (**3**) and a combination of pCMVi (encoding Moloney Murine Leukaemia Virus gag-pol) and MLV-FLuc (MMLV provirus, lacking *env* and *gag-pol* genes, and containing an extra ORF encoding for Firefly luciferase) [360].

To generate PPs, 7×10^5 HEK293T cells were transfected with: (**1**) 3.5µg each of pDublin-FΔ30 and pDublin-H Δ24 (encoding cytoplasmic tail truncations of MeV protein F and H) or 1 µg of pVSV-G and (**2**) 1.5 µg of p8.91 and 1 µg of CSFLW or 1.5 µg of pCMVi and 1 µg of MLV-FLuc or 1.6 µg of NL4.3-Fluc. Supernatants containing viral pseudotyped particles (PPs) were collected 48 and 72h later, pooled and clarified by centrifugation $1000\times g$ at 4°C for 30min. Prior to transduction (infection) A549-SLAM or HEK293T-SLAM cells were seeded in a 96-well dish at 5×10^4 cells per well. After 24h these cells were pre-treated with pharmacological inhibitors, at the indicated concentrations, in FBS-free DMEM for 30 min at 37°C followed by the addition of 100µL of solution containing PPs. This mixture was then incubated for 5h. Alternatively, A549-SLAM or HEK293T-SLAM cells were transfected with 1µg of indicated constructs in 6-well dishes and 48h later these cells were transferred to 96-well plates. Cells were then incubated with 100µL of PPs for 5h. In all instances the media in PP infections was replaced after the 5h incubation. Following 72h of further incubation, lentiviral transduction efficiency was assessed by lysing the cells and measuring luciferase activity using the Luciferase Assay System (Promega), according to the manufacturer's instructions, on a Centro LB960 Microplate Luminometer (Berthold Technologies).

2.5.4 Virus entry assay

A549-SLAM cells were pre-treated or post-treated, in relation to virus infection, with pharmacological inhibitors. Pre-treated cells were incubated with the drug for 30 min prior to addition of virus (MOI~1) and incubated for an additional 1h at 37°C in the presence of a drug, while post-treated cells were inoculated for 1h, washed and incubated with a drug for 37°C for 90 min after infection. In both cases, cells were then trypsinised to remove non-internalized virus, replated and incubated for another 24h. Syncytia were counted under UV-light (to visualise GFP expressed by the virus) and whole cell lysates were generated using Laemmli buffer and analysed by western blotting. To assess glycoprotein sensitivity to trypsin, A549-SLAM were incubated with MeV (MOI=30) at 4°C for 1h. Inoculum was then removed and cells were washed in cold PBS and incubated at 37°C for 0, 15 or 30min. At these timepoints, cells were either trypsinised or detached with 2mM EDTA in PBS (untreated) for 7min at 37°C, pelleted and analysed by western blot. As a control, uninfected cells were treated in a similar way. To assess fusion upon entry mediated by the virus, we used a dual split reporter containing the *Renilla luciferase* gene[363]. HEK293T-SLAM cells were transfected with one part of the reporter, synchronously infected with purified MeV (MOI~30), washed and incubated at 37°C for 0, 15, 30 or 60 prior to co-culturing with HEK293T-SLAM expressing the complementary part of the reporter. When testing the effect of chlorpromazine (CPZ), cells were incubated for 30 min with 5µg/mL, prior to the adsorption of virus. The drug treatment was maintained throughout the short time-course of the experiment. At each timepoint, cells were incubated for 2h before luciferase activity was measured in a luminometer through the addition of 2µg/mL of cell-permeable coelenterazine 400A (Biotium).

2.5.5 Virus entry assay with pharmacological inhibitors

A549-SLAM cells were pre-incubated with 50µL of DMEM supplemented with inhibitors at the indicated concentrations for 30 min at 37°C. Virus was then added (MOI=1) and incubated at 37°C for 1h. Inoculum was removed and cells were trypsinised to remove non-internalized virus. Alternatively, cells were infected in the absence of drugs for 1h at 37°C, inoculum was then removed and drugs were added and incubated for 90min. Cells were trypsinised, replated and incubated for 24h. Foci of infection were counted under UV-light and whole cell lysates were generated using Laemmli buffer (Thermo Fisher Scientific, USA) and samples were analysed by Western blot.

2.5.6 Fusion assay

The quantitative fusion assay was adapted from Brindley *et al* [308]. Briefly, HEK293T cells were transfected with one part of a dual split reporter *Renilla reniformis* Luciferase-GFP together with 1µg of pDublin-H and pDublin-F (effector cells). Separately, HEK293T-SLAM cells were transfected with the complementary part of the split reporter (target cells). 48h post transfection, cells were detached from the plate and co-cultured at a 1:1 ratio to a final cell density of $1x10^5$ cells per well (in a white-bottomed 96 well dish). When indicated, pharmacological inhibitors at indicated concentration were added to the co-culture mix. Cultures were then incubated for a specific amount of time, as indicated in the relevant results section, at 37°C, before the medium was removed and 60µL of 2µg/mL of coelenterazine 400A (Biotium, USA) was added to each well. Luciferase activity was measured in a

luminometer, after 2min of incubation with coelenterazine; luminescence was recorded and integrated for a total of 10''. In addition, to see if the addition of the drug had an effect on the activity of the split reporter, cells were transfected with both parts of the dual split reporter and incubated in the presence of the drug. Luciferase activity was measured as described above. In subsequent experiments, other plasmids were added to either effector or target cells, as indicated. Total transfected DNA was always balanced with pcDNA3.1 and all cells were transfected with the same amount of plasmid DNA.

2.5.7 Fluid-phase uptake

A549 or A549-SLAM cells were plated onto poly-L-lysine treated glass coverslips and serum-starved for 16h. Prior to infection, cells were pre-chilled on ice and infected with MeV (MOI=10) or mock-infected (DMEM with 20% FBS) for 1h at 4°C with gentle agitation. Cells were then washed in cold PBS and incubated at 37°C in FBS-free medium containing 0.25µg/mL of Dextran-Alexa Fluor®488 10,000 MW (Molecular Probes Life Technologies^{TM}, UK) for 20min. Phorbol 12-myristate 13-acetate was used at a concentration of 200nM as a control. Cells were then moved to ice to stop internalisation and membrane-bound dextran was removed by incubation with cold bleach buffer (10mM sodium acetate, 50mM NaCl, pH 5.5) for 10 min followed by washing with PBS. Cells were then fixed with 4% PFA and prepared for Confocal Laser Scanning Microscopy (CSLM). To visualise the cells we used a Leiss LSM 510 Meta Confocal Microscope equipped with a Lasos 30mW (405-30) 405nm, a Lasos 30mM multiline Argon/2 458-514nm and a Lasos 2mW HeNe, 594nm confocal laser. Images were recorded using the LSM 510 Software.

2.6 Immunofluorescence Assays

Cells were plated onto glass coverslips and synchronously infected with MeV (at indicated MOIs) at 4°C for 1h with gentle rocking. As an uninfected control, cells were incubated with media containing 20% FBS. Cells were then washed and incubated in PBS at 37°C for the indicated lengths of time or, in the fluid uptake assay, incubated in PBS containing 0.25µg/mL of Dextran-Alexa Fluor®488 10,000 MW (Molecular Probes® 627 Life Technologies). Surface-bound dextran was removed by incubation with cold bleach buffer (10mM sodium acetate, 50mM NaCl, pH 5.5) for 10 min before being washed with PBS. In all cases, cells were fixed in 4% PFA for 10 min at room temperature, permeabilised with 0.1% TRITON® X-100 in PBS for 10 min and then blocked with 1% BSA in PBS for 30 min at room temperature. Cells were incubated with primary antibodies (**Table 2-3**) in 1% BSA at 4°C overnight, washed in PBS and incubated with secondary antibodies conjugated with AlexaFluor Dyes (Invitrogen) for 1h at room temperature. Slides were mounted using Hoechst 33342 in Mowiol 632 ® mounting medium (Merck Millipore). Cells were visualised by CLSM (see **chapter 2 section 2.9.3**).

2.6.1 Actin staining

A549-SLAM cells were plated onto a glass cover slip and serum-starved for 16h. Cells were then pre-chilled on ice for 5 min and infected with MeV-GFP (MOI=15) for 1h at 4°C with gentle agitation. Inoculum was removed and cells were washed with PBS. Cells were incubated at 37°C for 0, 10, 20 or 60 min prior to fixation with 4% PFA for 10 min at room temperature. Cells were then permeabilised with 0.01%

TRITON® X- 100 in PBS for 10min, washed and blocked with 1% BSA in PBS for 30min. A solution of 0.5µg/mL of the phalloidin conjugate tetramethylrhodamine B isocyanate (Phalloidin-TRITC, Sigma-Aldrich, USA) in PBS was added to the cells and incubated at room temperature for 30min. Cells were finally washed several times with PBS and analysed by CLSM as described in **chapter 2 section 2.9.6**.

2.7 Flow Cytometry of MeV-EGFP-infected cells

A549-SLAM cells were either pre- or post-treated with 25 or 50µM of EIPA for 30 min and infected for 1h at 37°C with recombinant MeV (MOI=1) that also expressed EGFP. After this period, cells were trypsinised, re-plated onto 6-well dishes and incubated at 37°C for 6.5h. Cells were then detached using a 2mM EDTA solution in PBS for 20min, washed and fixed in 4% PFA. Cells were resuspended in PBS and analysed for EGFP fluorescence by flow cytometry (CyAn 642 TM ADP analyser, Beckman Coulter).

2.8 Biochemistry

2.8.1 Protein quantification

To quantify total protein in solution, I used two methods: a bicinchoninic acid (BCA) assay [365], using Pierce BCA Protein Assay Kit (Thermo Scientific), and the Bradford assay [366], using Bradford Protein Assay Reagent (Bio-Rad), both according to the manufacturer's guidelines. When constituents of protein solvent interfere with the readout of the colorimetric assay, protein samples were diluted out in BCA/Bradford reagents until no background was observed and extrapolated to calculate actual concentrations.

2.8.2 Silver stain of protein gels

After SDS-PAGE, resolved protein gels were stained using the SilverQuest^{TM} Silver Staining Kit (Thermo Scientific), according to the manufacturer's guidelines. Stained gels were then photographed or scanned to calculate band densities. In case protein bands were extracted, as required for analysis by mass spectrometry, gel fragments were destained using the destaining reagents provided in the kit.

2.8.3 Antibodies

All antibodies used are listed in **Table 2-3**.

2.8.4 SDS-PAGE and Western Blotting

All protein samples were generated using radioimmunoprecipitation assay (RIPA) buffer (Cell Signalling Technology, USA), in the presence of Pierce Lane Marker Reducing Sample Buffer (Thermo Fisher Scientific, USA), or Laemmli buffer (120mM Tris-Base, 4% SDS, 20% glycerol, 0.02% bromophenol blue) as indicated, and reduced at 95°C or 37°C for 5 or 30min, respectively, as indicated. Samples were loaded into 7.5, 10 or 15% polyacrylamide gel, as indicated, and run by SDS-PAGE at a constant current of 40mA. Protein samples were then transferred to a methanol-activated polyvinylidene difluoride (PVDF) membrane by semi-dry transfer (at a constant voltage of 15V). Protein-transferred membranes were then blocked with a 5% skimmed milk solution in tris-buffered saline (TBS) containing 0.01% Tween20 (Bio-Rad Laboratories, Inc., USA). Primary antibodies, for blotting, were diluted at indicated concentrations in 5% skimmed milk in TBS with 0.01% Tween20. The

Table 2-3. List of antibodies used in this project. All antibodies used and described in this thesis were either sourced from indicated labs or purchased from indicated biotechnology companies.

Description	Species	Origin
Anti-cytoplasmic tail of Measles virus haemagglutinin	Rabbit	Prof. Roberto Cattaneo's lab
Anti-measles virus nucleocapsid 505	Rabbit	
Anti-glyceraldehyde 3-phosphate dehydrogenase (mAb 2118)	Rabbit	Cell Signalling Technology
Anti-phospho-Ezrin (Thr567)/Radixin(Thr564)/Moesin (Thr558) (41A3, mAb 5175)	Rabbit	
Anti-ezrin/radixin/moesin (mAb 3142)	Rabbit	
Anti-phospho-cofilin (Ser3, mAb 3313)	Rabbit	
Anti-cofilin (D3F9, mAb 5175)	Rabbit	
Anti-alpha-p21-acivated kinase (mAb 2602)	Rabbit	
Anti-Rabbit IgG1 coupled with horseradish peroxidase	Mouse	

following antibodies were purchased from Cell Signalling Technology, USA: Anti-GAPDH (1:1000), Anti-Ezrin/Radixin/Moesin (3142), Anti-Phospho-Ezrin (Thr567)/Radixin (Thr564)/Moesin (Thr558) (41A3, mAb 3149), Anti-Phospho-Cofilin (Ser3, mAb 3313), Anti-Cofilin (D3F9, mAb 5175). These antibodies are all of rabbit origin while Anti-Rabbit IgG1 coupled with horseradish peroxidase (HRPO) is of mouse origin. All primary antibodies were incubated with the membrane overnight at 4°C. Secondary antibodies were incubated for 90 min at room temperature. Membranes were exposed to Clarity Western ECL substrate (Bio-Rad Laboratories, USA) according to manufacturer's guidelines and exposed to autoradiographic film.

2.8.5 In vitro dephosphorylation of MeV H

HEK293T were transfected with MeV H-HA and MeV F as described previously. After 48h, cells were lysed in TNE buffer containing Protease Inhibitor Cocktail Mix (Pierce Thermo Scientific), scraped into suspension and subsequently resuspended again on ice using a gauge syringe. Lysates were pelleted and 20µL of supernatants were incubated with 200 units of λ Protein Phosphatase (λPP, New England Bio Labs) in the presence of $MnCl_2$ for 30 min at 30°C. As a control, 25mM of the λPP inhibitor Na_3VO_4 was added to final mix prior to incubation. The enzymatic reaction was stopped through addition of Laemmli buffer.

2.9 Microscopy

2.9.1 Morphological changes upon virus entry using phase-contrast microscopy

Serum starved A549-SLAM cells were pre-chilled on ice and MeV (MOI~45) bound to the cells at 4°C for 1h. Mock-infected cells were treated with DMEM with 20% FBS. After 1h the inoculum was removed and cells were washed in ice-cold PBS before being moved to 37°C for 10min. Cells were then fixed with a solution of 4% paraformaldehyde (PFA) in PBS and visualized by phase-contrast microscopy using an inverted UV microscope (Nikon Eclipse TE2000-5 microscope coupled with a Nikon HB-10101AF Super High Pressure Mercury Lamp) equipped with a camera (Hamamatsu Digital Camera C472-95). Ten micrographs of each condition were recorded and cells presenting membranous blebs were counted in relation to total cell count.

2.9.2 Scanning electron microscopy

Similarly to the phase-contrast studies, serum-starved A549-SLAM cells were pre-chilled on ice before MeV (MOI~45) was bound to the cells at 4°C for 1h (as a uninfected control, I have incubated cells DMEM with 20% FBS). The inoculum was then removed and the cells were washed in ice-cold PBS before being incubated at 37°C for 10min. Infected cells were then fixed with a solution of 4% PFA and 2.5% Glutaraldehyde overnight at 4°C. Fixed cells were washed in PBS, post-fixed in 2% Osmium tetroxide, dehydrated in acetone and critical-point dried for 2h. Finally, cells were coated with a 3nm layer of platinum and visualized by scanning electron microscopy (JSM-7000F (JEOL) SEM - Oxford Instruments INCA EDS system).

2.9.3 Confocal laser scanning microscopy

Immunofluorescence microscopy was performed using a Leiss LSM 510 Meta Confocal Microscope equipped with a Lasos 30mW (405-30) 405nm, a Lasos 30mM multiline Argon/2 458-514nm and a Lasos 2mW HeNe, 594nm confocal laser. Images were recorded using the LSM Software.

2.10 Proteomics

2.10.1 SILAC

LCLs were cultured in RPMI-1640 medium suitable for SILAC triple labelling, i.e. supplemented with either: (1) unlabelled arginine and lysine (**Light** R0K0, RMPI-19 Dundee Cell Products), (2) ^{13}C labelled arginine and ^{2}D labelled lysine (**Medium** R6K4, RPMI-22 Dundee Cell Products), or (3) ^{13}C and ^{15}N labelled arginine and ^{13}C and ^{15}N labelled lysine (**Heavy** R10K8, RPMI-21 Dundee Cell Products). All SILAC culture media was supplemented with penicillin/streptomycin, 10 kDa dialysed FBS (Dundee Cell Products) and MEM non-essential amino acids (Gibco®, Thermo Fisher). Cells were passaged in labelling media for 15 passages prior to subsequent experiments. Complete incorporation of labelled amino acids was confirmed by mass spectrometry.

LCLs labelled with heavy and light amino acids were infected with MeV (MOI~0.01), see **chapter 2 section 2.2.3**, and incubated for 64 or 96h. These infected cells were then pelleted and used for downstream protein and RNA extraction. As a control, medium-labelled LCLs were mock-infected and incubated for 96h prior to collection and subsequent protein and RNA extraction.

2.10.2 Enrichment of Membrane Proteins

Labelled LCLs (3×10^7 cells per label) were pelleted, washed in PBS and pelleted again. Membrane proteins were extracted using the ProteoExtract® Native Membrane Protein Extraction Kit (#444810, Merk Milipore) according to the manufacturer's guidelines. The total protein was then quantified (using both BCA and Bradford methods, see **chapter 2 section 2.8.1**) and the three samples (Light, Medium and Heavy) were mixed at equimolar ratio and subsequently analysed by mass spectrometry.

2.10.3 LC-MS/MS analysis

Protein samples containing three the differently labelled protein populations were resolved in a 10% SDS-PAGE gel. The running lane was fragmented into 10 slices and individual slices were tryptically digested using DigestPro (Intavis Ltd.). Peptides were then fractionated using 1% formic acid, injected onto an Ultimate 3000 nanoHPLC system equipped with an Acclaim PepMap C18 nano-trap column (Thermo Scientific), washed in 0.5% acetonitrile and 0.1% formic acid, and resolved in a reverse phase analytical column over a 150 min organic gradient using the following segments: 1-6% solvent V over 1 min; 6-15% B over 58 min; 32-40% B over 5min; 40-90% over 1 min; held at 90% B for 6 min and then reduced to 1% B over 1 min. Solvent A: 0.1% formic acid. Solvent B: aqueous 80% acetonitrile in 0.1% formic acid. Peptides ionised by nano-ectrospray at 2.0 kV using a stainless-steel emitter with a capillarity temperature of 275ºC. Mass spectra were acquired using an Orbitrap Fusion Tribid mass spectrometer controlled by Xcalibur 2.0 software

(Thermo Scientific). FTMS1 spectra were collected at a resolution of 120000 over a scan range (mass-to-charge) of 350-1550, gain control target of 300000 and a maximal time of injection of 100 milliseconds. Charge state was set to include charge states 2 to 6 and precursors were filtered with monoisotopic selection. Formerly interrogated precursors were excluded. Isolation of the MS2 precursors were accomplished using a quadrupole mass filter set to 1.4m/z. ITMS2 spectra were generated with an AGC target of 20 000, maximum injection time of 40 ms and 35% of collision induced dissociation (CID) collision energy. The generated raw files were analysed, processed and quantified using Proteome Discoverer software v1.4 (Thermo Scientific) and mined against a human protein database (UniProt Human database, 126385 entries) plus the MeV sequences Ichinose strain using the SEQUEST algorithm. Mass tolerance limit of peptide precursors was set at 10 parts per million (ppm) and MS/MS tolerance at 0.6 Da. The search criteria comprised of carbamidomethylation of cysteine (+57.0214) as a fixed modification and oxidation of methionine (+15.9949) and respective SILAC labels as variable modifications. Peptide mining was performed in an *in silico* tryptic digested peptide database, allowing a maximum of 1 missed cleavage. Additionally, reverse database search was performed and peptide data was filtered to verify a false discovery rate (FDR) of 5%.

2.11 Data Analysis

2.11.1 Image analysis using ImageJ

To evaluate the relative intensity of Western blot bands, films were scanned at maximum resolution (300dpi) and converted into unsaturated 8-bit images using

ImageJ (National Institute of Health, USA). Each lane was highlighted with a rectangular shape of equivalent size and pixel saturation was plotted onto a histogram. Peaks corresponding to each lane were selected in relation to basal levels of saturation and the area underneath the curve was measured using the same software. Densitometry values were then normalized to mock values. To calculate total cell fluorescence in the fluid-phase uptake experiment, micrographs recorded at 488nm were converted to 8-bit images. A total of 16 cells per sample were individually selected and the area and mean fluorescence intensity was calculated using ImageJ. To each cell, four different regions of the surrounding area were selected and the correspondent background mean fluorescence was subtracted from the cell intensity. The corrected total cell fluorescence was then averaged and plotted. Finally, to measure the average area of cells stained with the actin-specific phalloidin conjugate, the background of individual micrographs was brought to a level of threshold (overflow) that enabled clear distinction of the cell's edges from its surroundings. Each cell, or group of cells, was then individually selected and the area was calculated, summed and divided by the number of nuclei observed in the correspondent Hoechst stain micrograph. A total of 266 cells for mock, 222 cells for virus at 0 min post infection, 198 cell for virus 10min, 255 cells for virus 20 min and 175 cells for virus 60 min were used to calculate the mean cell area. The average cell area was then plotted in pixel units.

2.11.2 Matrix protein structure prediction and modulation

To generate a model of the 3D structure of the Matrix protein, we used the software SWISS-MODEL, developed and available through the ExPASy server of the Swiss

Institute of Bioinformatics, University of Basel. The MeV matrix protein sequence (UniProt entry #P06942) was compared against the Newcastle disease virus matrix protein structure (RSCB PDB entry #4G1L) with which it shares 21.45% identity at the amino acid level. The resultant model was calculated using ProMod Version 3.70 to have a Global Model Quality Estimate (GMQE) of 0.53 and a QMEAN4 of -6.34 [26]. Rendering of the 3D structure was achieved using the UCSF Chimera software.

2.11.3 Bioinformatics Analysis of LC-MS/MS Data

LC-MS/MS peptide data was analysed as described in Emmott *et al.*, 2014 [367]. Analysis was performed using Proteome Discovered v1.4 MS analysis software (Thermo Scientific) against an *in silico* protein database comprised of Uniprot Human database with 8 additional sequences corresponding to the protein sequences of the MeV Ichinose strain (N, P, C, V, M, F, H and L; see **appendix section A.2**). Low confidence peptides, i.e. peptides which FDR higher than 5%, were removed and SILAC ratios, i.e. light versus heavy, light versus medium and medium versus heavy, were calculated. These SILAC ratios (0.01 to 100) were then converted to log 2 values using Excel. Using graph pad, log2 SILAC ratios were plotted onto a histogram sorted by frequency distribution. After a Gaussian distribution curve was fitted onto the frequency distribution, mean and standard deviation of the Gaussian distribution were calculated and used to select a 95% confidence threshold using the formula:

$$threshold = 1.96 \times standard\ deviation + mean$$

2.11.4 Post-translation modifications discovery

Post-translation modifications discovery was performed using the raw data files obtained and described in **section 2.10.3** using the Proteome Discoverer v1.4, and against an *in silico* tryptically digested protein database consisting of the human protein database (UniProt Human database, 126385 entries) and the MeV sequences Ichinose strain. Search settings comprised the following peptide modifications: *N*-glycosylation of asparagines; ubiquitination of lysines; phosphorylation of tyrosines, serines and threonines; methylation of lysines; SUMOylation of lysines and α-acetylation of N-terminal amino acids. A FDR of 5% was set as threshold.

2.12 Statistical Analysis and Graphs

Statistical analysis was performed using GraphPad Prism 6 software where groups of two were analysed using the unpaired Student's t test. I have considered a *p*-value lower or equal to 0.05 (*) as a minimum threshold for significance. **, $p<0.01$, ***, $p<0.001$. n.s., non-significant

All graphs presented in this thesis were generated using either GraphPad Prism 7 or R programing console.

Chapter 3

Development of quantitative assays to study morbillivirus entry and exit

Measles virus spreads *in vivo* and *in vitro* via two main routes: cell-free and cell-to-cell virus transmission. In the first, a virion attaches to the cell's membrane where the viral protein H interacts with its receptor, e.g. SLAM. Subsequent triggering of the viral F protein allows release of the viral genome into the cytoplasm. Later on in infection, viral proteins concentrate at specific sites in the plasma membrane to form nascent virions which egress from the cell by budding; in particular, the matrix protein interacts with envelope glycoproteins and the RNP complex. Alternatively, MeV glycoproteins at the cell surface can interact, independently from virion genesis, with cognate receptors on a neighbouring cell, activating F and inducing the fusion of these two cells, defined as cell-cell fusion. In this instance, the cytosolic contents of the infected or viral glycoprotein expressing cell are mixed with the target cell and infection spreads. In this chapter, I describe the development of biochemical assays to quantify MeV cell-free and cell-cell transmission of the virus: (1) a pseudotyped virus entry assay based on a lentiviral backbone of HIV-1 genome that encodes a luciferase gene reporter and incorporates MeV encoded GPs; (2) a cell-cell fusion assay based on the expression of MeV glycoproteins, cellular receptors and a dual split reporter protein; and finally (3) a budding assay based on the egress of a viral matrix protein fused to luciferase. These assays are subsequently applied, in my other thesis chapters, to study measles virus transmission.

3.1 Development of a MeV GP-based cell-cell fusion assay

To study MeV-induced cell-cell fusion, I developed a MeV fusion assay based on a dual split reporter of EGFP and *Renilla reniformis* luciferase (RLuc) [308]. This split reporter is expressed from two constructs each encoding part of an EGFP and RLuc

fusion protein. These reporters are inactive when expressed individually, but become functional if the complementary parts interact [363]. A schematic illustrating the set-up a typical MeV fusion assay is represented in **Fig.3.1**. Of note, a cell line was chosen that is normally refractory to infection (e.g. HEK293T) as this was considered to express a low level of endogenous SLAM or Nectin-4 expression. These cells were transfected with MeV F and H and one part of the split reporter (becoming 'effector' cells) while a separate population, engineered to overexpress a cellular receptor, e.g. SLAM, was transfected with the complementary part of the split reporter (becoming 'target' cells). After 48h of incubation, cells were then detached from their plates, co-cultured at specific concentrations and incubated for a certain period of time. When these cells fused, their cytosolic contents mixed and the complementary parts of EGFP and RLuc interacted to form a functional dual reporter.

The expression of the MeV H protein in the cell membrane of HEK293T cells was first confirmed by fractionation and isolation of membrane, cytosolic and nuclear fractions of the cell, followed by western blot (**Fig.3.2**). Antibodies against human Na^+/K^+ATPase, an enzyme that exports Na^+ ions and imports K^+ ions to the cell and localizes at the plasma membrane, and the mitogen-activated protein kinase kinases 1 and 2 (MEK1/2), which is a cytosolic protein involved in certain signalling cascades, were used to evaluate the efficiency of fractionation and recovery of membrane and cytosolic proteins. MeV H co-fractionated with Na^+/K^+ATPase as shown by SDS-PAGE/western blot, suggesting that MeV H is present and in the membrane fraction of the cell.

Fig.3-1. Diagram of the quantitative cell-cell fusion assay. HEK293T cells were transfected with plasmids encoding MeV F, MeV H and half of a dual split reporter EGFP and Renilla luciferase (RLuc1), while HEK293T-SLAM cells were transfected with the complementary part of the dual split-reporter (RLuc2). When target cells, expressing SLAMF1, are co-cultured with effector cells, expressing MeV F and H, cell contact mediates attachment of H, culminating in the triggering and activation of F followed by the fusion of effector and target cells. After cytosolic mixing, the two complementary parts of the dual reporter assemble and become functional, allowing a fluorescence and luminescence read-out.

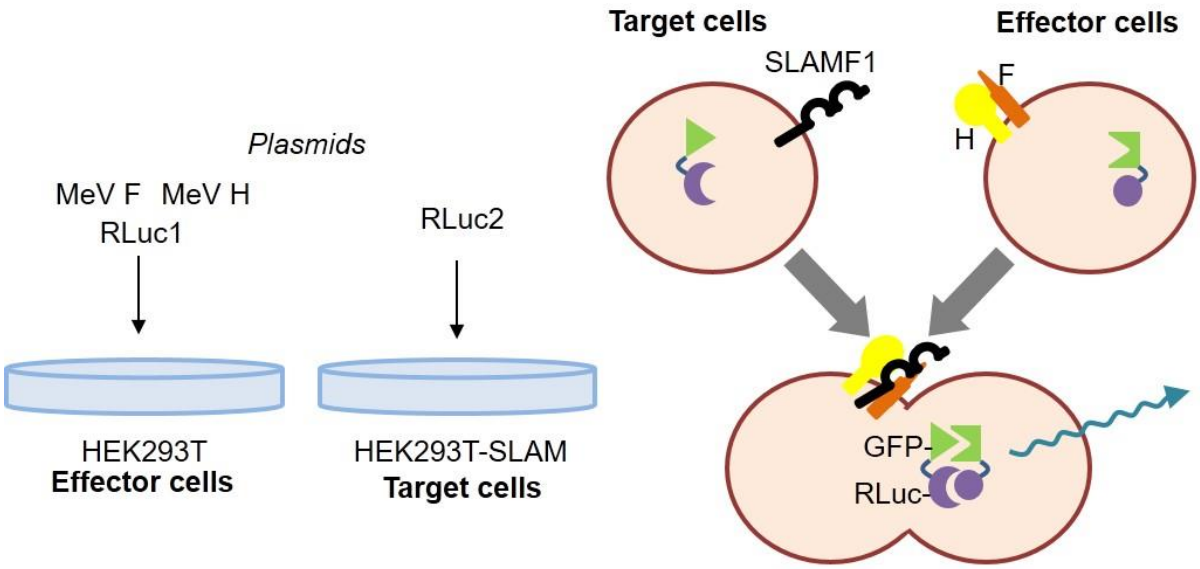
Plasmids
MeV F MeV H
RLuc1
RLuc2
HEK293T
Effector cells
HEK293T-SLAM
Target cells
Target cells
Effector cells
SLAMF1
F
H
GFP-
RLuc-

Fig.3-2. Development of MeV-glycoproteins-based cell-cell fusion assay. (**A**) HEK293T were transfected with MeV H. Forty-eight hours later, cells were lysed and membranes were fractionated as described in **chapter 2 section 2.10.2**. Cytosolic (soluble fraction) and membrane fractions were resolved on a 15% SDS-PAGE gel and MeV H, MEK1/2 and Na+/K+ ATPase were identified by western blot. (**B/C/D**) Effector and target cells were co-cultured at different ratios to a total concentration of $1x10^5$ cells per well, as indicated, before being observed by fluorescence microscopy (**B**). Luciferase activity was measured as described in **chapter 2 section 2.5.6** (**C/D**). (n=2 with 4 technical replicates). (**C**) Background levels of cell-fusion in HEK293Tlacking the expression of SLAMF1. (**E/F**) HEK293T transfected with part of the dual reporter were co-transfected with vesicular stomatitis glycoprotein (VSV-G) and co-cultured with target cells containing the complementary part of the dual-split reporter. After 24h, luciferase activity was measured before exposing the co-cultured cells to PBS solutions with adjusted pH as indicated. Cells were incubated for 4min prior to being observed by fluorescence microscopy (**F**) and the luminescence quantified as described previously (**E**) (n=1 with 4 technical replicates). Luciferase activity was plotted in relation to mock (RLU_{mock}=964,787±113,846). Statistical analysis was performing using Student's t test. *, p<0.05; **, p<0.01; ***, p<0.001; ****,p<0.0001, n.s., non-significant.

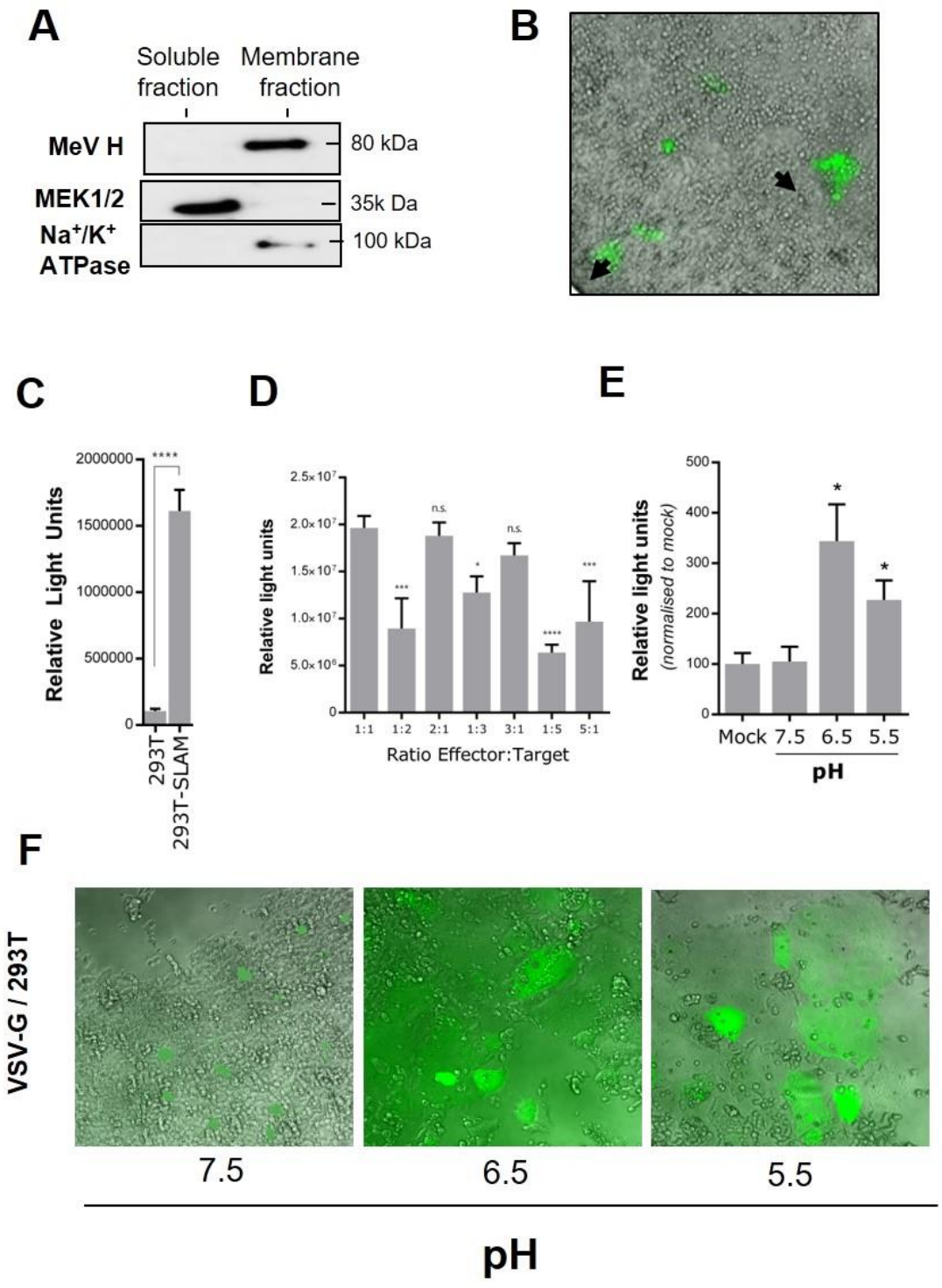
A
Soluble fraction
Membrane fraction
MeV H
80 kDa
MEK1/2
35k Da
Na+/K+ ATPase
100 kDa
B
C
Relative Light Units
2000000
1500000
1000000
500000
0
****
293T
293T-SLAM
D
Relative light units
2.5x10^7
2.0x10^7
1.5x10^7
1.0x10^7
5.0x10^6
0
n.s.
n.s.
*
***
***
****
1:1
1:2
2:1
1:3
3:1
1:5
5:1
Ratio Effector:Target
E
Relative light units
(normalised to mock)
500
400
300
200
100
0
*
*
Mock
7.5
6.5
5.5
pH
F
VSV-G / 293T
7.5
6.5
5.5
pH

To determine the optimum ratio for co-culturing effector and target cells, HEK293T cells were transfected with their respective plasmids, incubated for 24h, washed, resuspended and plated again for another 24h. This intermediate washing step was included in the protocol to remove extracellular plasmid DNA and avoid cross-contamination between the two cell populations. Cells were then resuspended and co-cultured overnight at different ratios (of note, cell densities were also optimised to maximise cell-cell contacts, data not shown). An example of EGFP-positive fused cells observed during this assay is presented in **Fig.3.2B** (black arrows). RLuc activity was measured by removing the media and adding 60µL of 2µg/mL of a cell-permeable luciferase substrate coelenterazine (**Fig.3.2C/D**). As a control, background levels obtained with co-culture with target cells lacking expression of SLAMF1 was performed (**Fig.3.2C**). The highest luciferase activity, proportional to the number of fused cells, was obtained at an equal ratio of target and effector cells (1:1). When comparing the different ratios of cell populations, co-cultures where effector cells were in greater abundance than target cells (e.g. ratios of 2:1 and 3:1) showed higher luciferase activity than the directly inverse ratio (1:2 and 1:3). A reduced number of GFP-positive cells and small syncytia were also observed in co-cultures containing HEK293T target cells that had not been transfected with the SLAM receptor, perhaps due to very low expression of human Nectin-4 on this cell line [221].

An issue that arises from the co-culture system is the putative cross-transfection of DNA encoding for the complementary parts of the luciferase, i.e. when effector and targets cells are detached from the well (in which they were transfected) and subsequently co-cultured, residual plasmid DNA may be also uptaken by the

complementary cells leading to a false positive reading of the luciferase activity that did not arise from the fusion of cells. To test if cross-DNA-contamination was an issue in this system, I have used the fusion protein of vesicular stomatitis virus (VSV), glycoprotein (G), which is activated by exposure to low pH [368]. VSV-G was transfected into effector cells, instead of MeV F and H, and co-cultured overnight. Co-cultures were then exposed to several PBS solutions containing differently buffered pH, namely 7.5, in which cell fusion induced by VSV should not occur, and two acidic pH 6.5 and 5.5, that should activate VSV-G and cell-cell fusion, for 3 min at 37°C before being washed and the reporter activity measured (**Fig.3.2E**). As a control, effector cells lacking any viral glycoproteins were incubated with target cells under similar conditions (mock). Indeed, co-cultures treated with pH 7.5 buffer had similar luciferase activity compared to mock, suggesting that cell fusion did not occur and this is the background levels observed. However, when co-cultures were treated with 6.5 or 5.5 buffers, luciferase activity was 300 and 200% of mock, suggesting the vast majority of luciferase activity. Of note, the slightly lower level of luciferase activity recorded in cells exposed to pH 5.5 may be due to detachment of cells from the surface of the well. Upon examination by UV-enabled microscopy large syncytia were observed in VSV-G expressing cells at the same pH ranges (**Fig.3.2F**). These observations are in accordance with the low pH dependency of VSV-G to induce fusion and demonstrate the activity of the dual reported is cell-intrinsic and specific for the fusion of neighbouring cells, and the luciferase readings observed are not due to cross-transfection with DNA upon co-culture. In summary, I demonstrated that this assay was capable of directly correlating MeV-induced cell-cell fusion to recorded luminescence and fluorescence from a quantitative, dual-reporter based readout and

could be used to study the molecular determinants of MeV cell-associated transmission.

3.2 Development of pseudoparticles using MeV GPs

The initial step of any viral infection is attachment to the cell, commonly via cellular receptor(s) such as proteins or sugar moieties. Entry to the cytosol and/or nucleus, sometimes also involves hijacking cellular endocytosis pathways such as clathrin-mediated endocytosis or macropinocytosis. It has been suggested that all paramyxovirus and pneumovirus entry, including MeV, occurs by direct fusion of the virus envelope with the plasma membrane. However, recent studies on various members of these families have shown that endocytic pathways are frequently involved in virus entry [195, 325]. To study the entry mechanism of MeV, I developed a quantitative entry assay based on pseudotyped virus particles (PPs) carrying MeV-GPs. In this system, illustrated in **Fig.3.3**, a defective self-limiting pro-lentivirus, based on HIV-1, containing the Ψ packing signal, the long terminal repeats (LTRs) and the firefly luciferase reporter gene, is transfected into HEK293Ts together with constructs encoding for the MeV-GPs. Components of the lentivirus particle assemble at the plasma membrane and MeV glycoproteins are incorporated into that particle, forming a replication incompetent chimera known as a PP. Recovered PPs can be used to transduce target cells, e.g. those expressing the MeV receptor SLAM. In this instance the luciferase activity in transduced cells serves as a direct correlate for MeV PP entry.

Previously, the intravirion tails of MeV GPs have been implicated in the correct assembly of MeV-PPs [369]. The mechanisms by which GPs are incorporated into

Fig.3-3. Schematic representation of the MeV pseudotype particle entry assay. To produce pseudotyped MeV particles, a plasmid encoding the HIV-1 gag-pol and another containing the pro-virus HIV-1 genome encoding the firefly luciferase (FLuc) were transfected into cells, alongside plasmids encoding MeV F and H lacking the 30 or 24 amino acids, respectively, at the cytoplasmic tails. Supernatants of cells transfected with these constructs were collected at 48 and 72h, clarified by centrifugation and used to transduce SLAMF1-positive cells. Luciferase activity was measured 72h post-transduction.

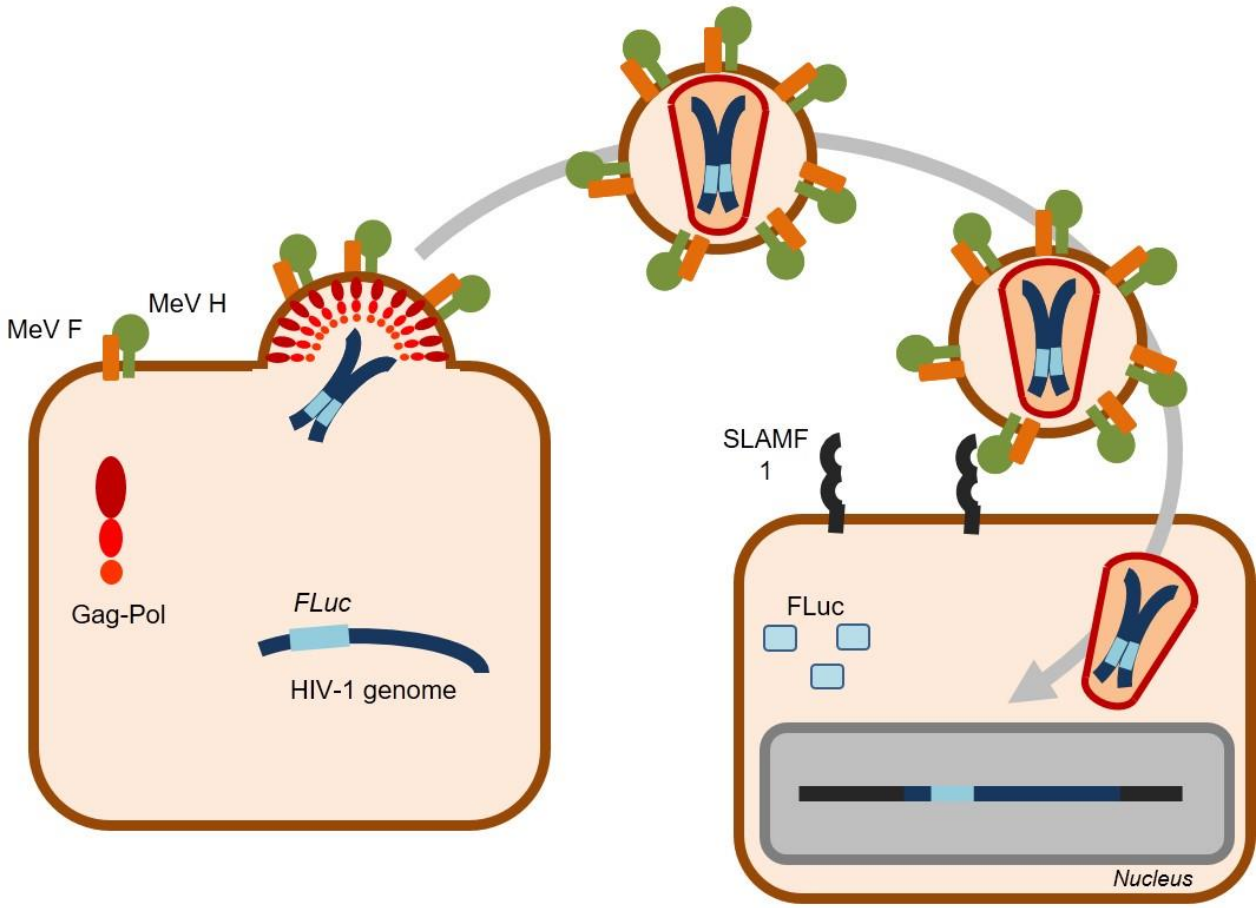
MeV F
MeV H
Gag-Pol
FLuc
HIV-1 genome
SLAMF
1
FLuc
Nucleus

PPs is not fully understood; however, the intravirion tails of MeV GPs might be interfering with the assembly machinery of the lentivirus, or perhaps differing localization between MeV GPs and lentivirus assembly sites may be responsible for hampering PP formation [370]. I hypothesised that variation in the efficiency of GP incorporation into PPs might be strain specific, therefore I examined the generation of PPs using the wild-type (WT) MeV F and H proteins from two different genotypes of MeV; Dublin (genotype D4) and IC323 (Ichinose-B95a, genotype D3), both of which are virulent strains, with 99.7% amino acid identity homology between the F proteins and 97.7% between the H proteins. To produce MeV-PP, HEK293T cells were transfected with plasmids encoding MeV F, MeV H and the pro-lentivirus construct pNL4.3-Luc-E^-R^- [359]. Extracellular secreted PPs were collected and clarified (for methods see **Chapter 2 Section 2.5.3**). As a negative control, parental plasmid (lacking any specific ORF for expression) was transfected along with the lentivirus backbone with the resultant pseudoparticles termed non-envelope (NE). As a positive control, VSV-G was transfected to generate VSV-PPs. VSV has a broad cellular tropism with several potential receptors for this virus [371], including the low density lipoprotein receptor family [372] and heparin sulphate [373].

I first examined the effect of co-expressing components of the pseudotype system. Expression of the MeV H protein at the cell surface did not appear to differ between strains under co-expression of the lentivirus vector, as suggested by western blot of the plasma membrane fraction of MeV H- and lentivirus-transfected cells (**Fig.3.4A**). Similarly, luciferase activity in PP-producing cells was not affected by co-expression of MeV GPs in comparison to VSV-G transfected cells (**Fig.3.4B**). When target cells (HEK293T-SLAM) were transduced with PPs, pseudotyped with Dublin or IC323

Fig.3-4. Generation of PPs using WT MeV glycoproteins. (**A**) HEK293T cells were transfected with plasmids encoding MeV H of Dublin or IC323 strains. At 48h post-transfections, cells were lysed and membrane proteins were extracted as described in **chapter 2 section 2.5.3**. Cytosolic and membrane fractions were resolved onto a 15% SDS-PAGE and MeV H, MEK1/2 and Na+/K+ ATPase were identified by western blot. (**B/C**) MeV-PP and VSV-PP were generated as previously described, using VSV-G or MeV H and F from MeV Dublin or IC323 strains. Cell lysates from producer cells were generated and luciferase activity was measured (**B**) (n=1 with 4 technical replicates). Produced PPs were then used to transduce HEK293T and HEK293T-SLAM cells. Seventy-two hours later, cell lysates were generated and luciferase activity was measured (**C**) (n=6 with 4 technical replicates).

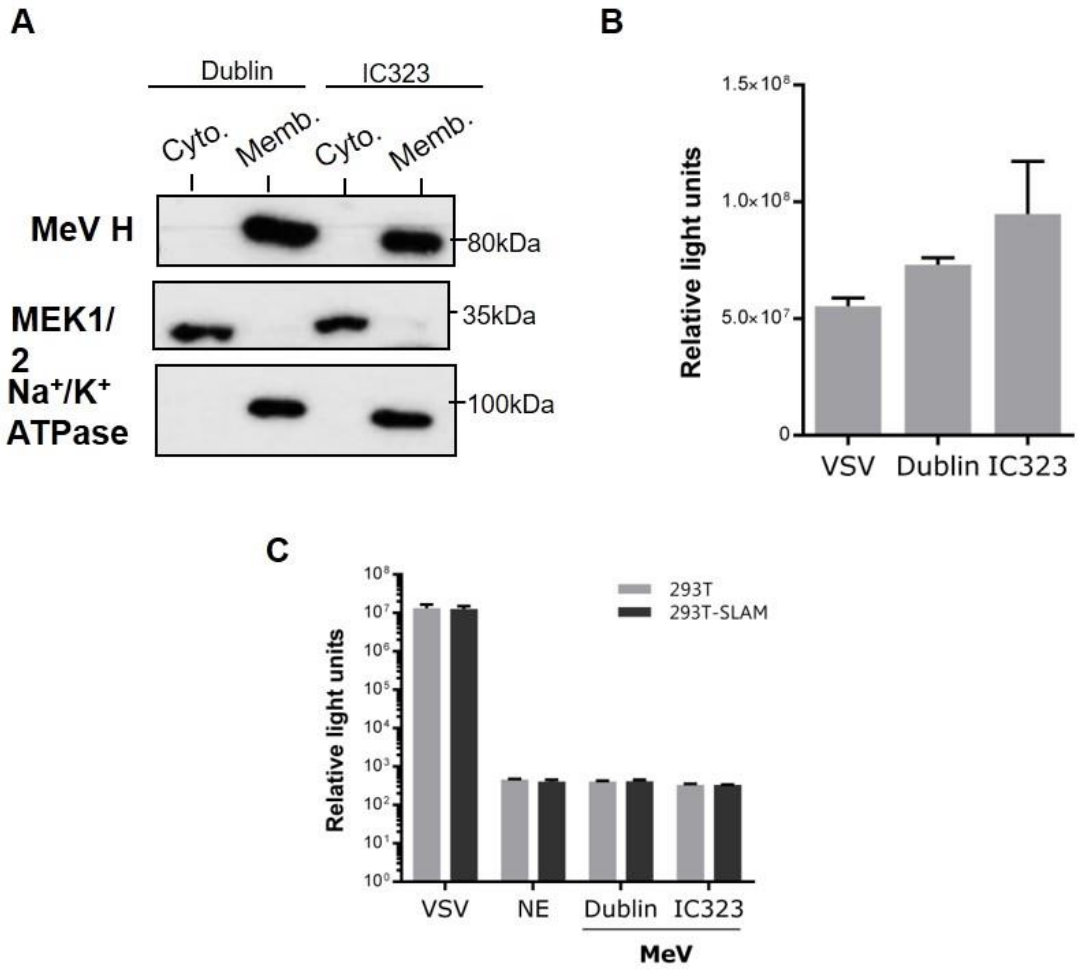
A
Dublin
IC323
Cyto.
Memb.
Cyto.
Memb.
MeV H
80kDa
MEK1/
2
35kDa
Na+/K+
ATPase
100kDa
B
Relative light units
1.5×10^8
1.0×10^8
5.0×10^7
0
VSV
Dublin
IC323
C
293T
293T-SLAM
Relative light units
VSV
NE
Dublin
IC323
MeV

strains MeV proteins, no significant activity could be detected, compared to NE-PPs (**Fig.3.4C**), while PPs carrying the VSV-G entered target cells with high efficiency. These data, in combination with the proven ability of MeV GPs to generate syncytia in SLAM-expressing cells (as shown previously), suggested that although GPs of several MeV strains can be expressed at the cell membrane, they do not incorporate into HIV-1 based PPs.

3.3 Truncation of MeV GP cytoplasmic tails facilitates pseudotyping

Several truncations of the intravirion tails of MeV GPs have been reported to be required for their efficient incorporation into PPs. In particular, deletion of 18, 19 and 24 amino acids in the H protein and 30 amino acids in the F protein have previously been shown to allow the generation of high titres of MeV-PPs, using both wild-type strains of MeV and the attenuated Edmonston strain, that uses CD46 as an additional receptor [369]. Therefore, I generated MeV H proteins lacking 24 or 18 amino acids from the N-terminal intravirion tail, and separately a MeV F protein with a 30 amino acid truncation from the C-terminal intravirion tail (**Fig.3.5A**). We first investigated whether these truncations affected the fusogenic potential of the MeV GPs in our cell-cell fusion assay, as described above (**Fig.3.5B**). HEK293T cells transfected with MeV GPs of the Dublin strain appeared to be more fusogenic than cells transfected with GPs belonging to the IC323 strain. With regards to their truncated variants, WT and HΔ24/FΔ30 truncated proteins exhibited demonstrably similar levels of fusion, whilst the HΔ18/FΔ30 proteins were significantly more fusogenic (**Fig.3.5B**). Nevertheless, since the antibody I had available to evaluate the

Fig.3-5. Truncation of MeV Glycoproteins' intravirion tails enables entry. (**A**) Cytoplasmic tail deletions of MeV H, lacking 24 or 18 amino acids, and MeV F lacking 30 amino acids. (**B**) A fusion assay was performed where effector cells were transfected with full-length (FL) MeV F and H, or mutants lacking 24, 18 or 30 amino acids of the cytoplasmic tails of MeV H and F, respectively (for both Dublin and IC323 strains). Readings of co-cultures with target cells lacking SLAMF1 (background) were subtracted to the respective effector+HEK293T-SLAM co-cultures. At 48h post-transfection, target and effector cells were co-cultured; luciferase activity was measured 24h later. (**C**) MeV-PP were generated using FL F and H, or mutants lacking 24, 18 or 30 amino acids of the cytoplasmic tails of MeV H and F, respectively (Dublin and IC323 strains). In addition PPs were generated with a combination of MeV H of Dublin or IC323 strains with Edmonston strain F protein. The generated PPs were then used to transfect HEK293T and HEK293T-SLAM cells. NE-PP entry values were subtracted to all MeV-PP RLUs. Statistical analysis was performed using Student's t tests, **$p<0.01$.

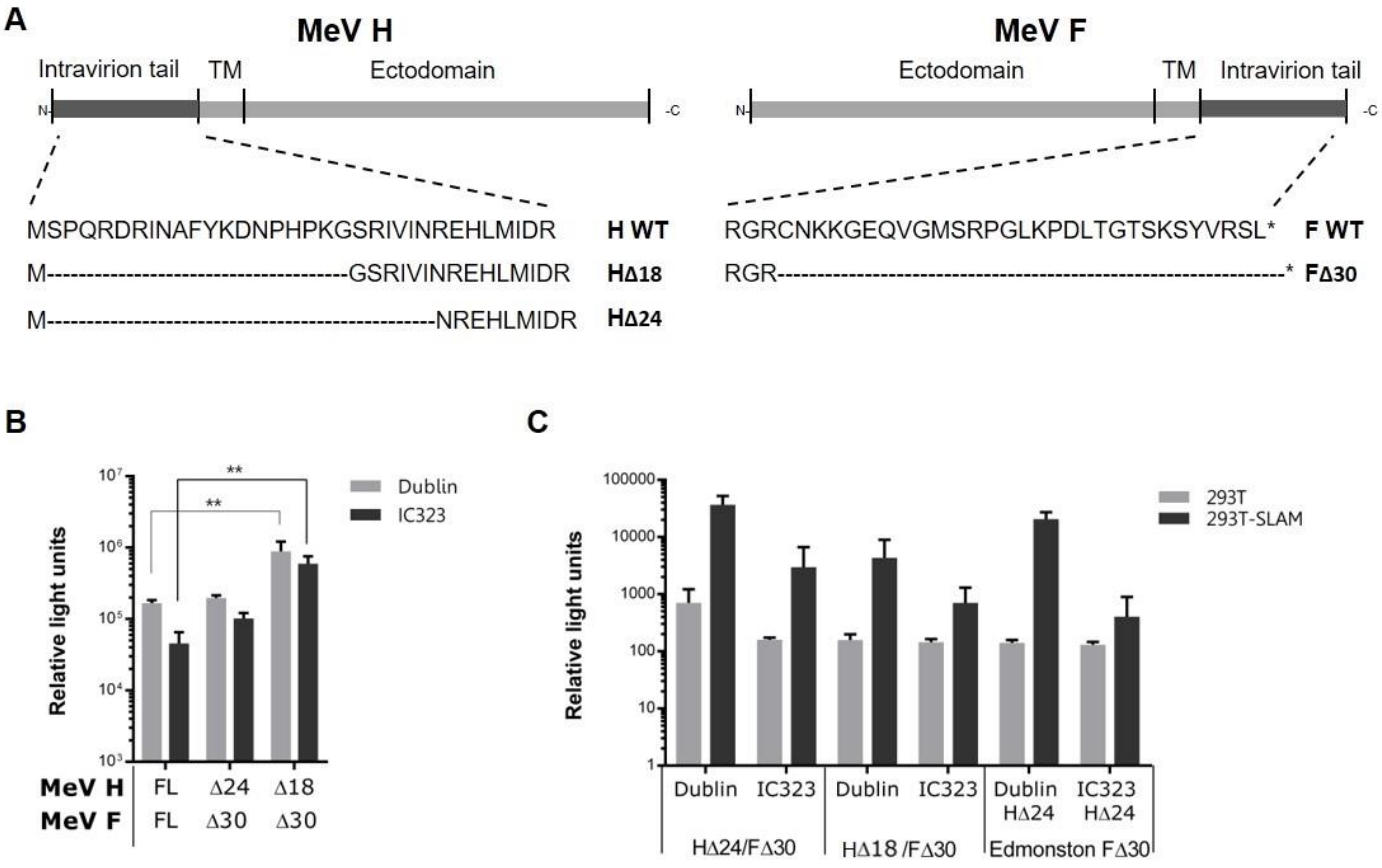
A
MeV H
Intravirion tail
TM
Ectodomain
N-
-C
MSPQRDRINAFYKDNPHPKGSRIVINREHLMIDR
H WT
M----------GSRIVINREHLMIDR
HΔ18
M----------NREHLMIDR
HΔ24
MeV F
Ectodomain
TM
Intravirion tail
N-
-C
RGRCNKKGEQVGMSRPGLKPDLTGTSKSYVRSL*
F WT
RGR----------*
FΔ30
B
Relative light units
Dublin
IC323
**
**
MeV H
FL
Δ24
Δ18
MeV F
FL
Δ30
Δ30
C
Relative light units
293T
293T-SLAM
Dublin
IC323
Dublin
IC323
Dublin
IC323
HΔ24
HΔ24
HΔ24/FΔ30
HΔ18 /FΔ30
Edmonston FΔ30

expression of MeV H was raised against the intravirion tail of this protein, fluctuation in MeV H mutant expression may also impact on cell-cell fusion.

We then assessed the pseudotyping potential of these truncation mutants. Using combinations of Dublin and IC323 HΔ24, HΔ18 and FΔ30, as well as Edmonston vaccine strain FΔ30, PPs were generated and used to infect HEK293T and HEK293T-SLAM cells (**Fig.3.5C**). PPs pseudotyped with H and F GPs with truncations had higher luciferase activity in SLAM-expressing cells compared to HEK293Ts, suggesting both successful pseudotyping and receptor specificity for these mutants. For both the Dublin and IC323 strains, PPs containing HΔ24 showed higher luciferase activity than PPs with HΔ18. Moreover, PPs generated with MeV Dublin strain GPs showed higher reporter values than their IC323 counterparts. Accordingly, PPs carrying Dublin HΔ24 and Edmonston FΔ30 had higher values than PPs carrying IC323 HΔ24 and Edmonston FΔ30. As mentioned before, due to the limitations in analysing the effect of such intravirion tail truncation in the expression of glycoprotein by western blot/flow cytometry, the mechanism behind the eventual pseudotyping of MeV-PP is not clear. Overall, PPs carrying the HΔ24/FΔ30 GP combination, and Dublin strain in particular, showed the highest signals in this assay suggesting the highest MeV-PP entry was achieved under these conditions. This combination was therefore used in all subsequent experiments, unless indicated otherwise.

3.4 The lentivirus system p8.91/pCSFLW generates high titres of MeV-PPs

Interestingly, using similar MeV GP truncations different titres of MeV-PPs are obtained, depending on the lentivirus system being applied and the research lab in

which they were produced [328, 369, 374]. To investigate whether different lentivirus systems could improve the titre of recovered MeV-PPs, I generated VSV-G and MeV PPs using (1) pNL4.3-Luc-E^-R^-, a first-generation provirus plasmid derived from HIV-1 encoding, in *cis*, the gag-pol ORF, Ψ signal peptide, HIV-1 LTRs and firefly luciferase reporter gene; (2) p8.91 and pCSFLW, a second-generation lentiviral system providing the gag-pol in *trans* (p.8.91), and HIV LTRs with the reporter gene, respectively; or (3) pCMVi and pMLV-Fluc, an equivalent second-generation lentivirus-system encoding the Moloney Murine Leukaemia Virus (MLV) gag-pol and LTRs with reporter gene, respectively. PPs were generated as described in **Chapter 2 Section 2.5.3** and luciferase activity values were plotted after subtracting NE-PP (background) values (**Fig.3.6B**). Particles pseudotyped with VSV-G demonstrated the highest luciferase signals with the p8.91+pCSFLW system, followed by the pNL4.3-Luc-E^-R^- (**Fig.3.6A**). Similarly, PPs bearing the MeV GPs generated with the p8.91+pCSFLW system yielded the highest luciferase activity. For both cases, PPs generated with the MLV-based system generated lower luciferase signals when compared to the HIV-based systems. Nevertheless, since the use of different lentiviral systems may impact on the number of particles produced, it is unknown if certain lentiviral constructs lead to the production of more particles or are more efficient in incorporating MeV GPs. As a result of these optimisation experiments further applications of MeV-PP in this project used the p8.91 and pCSFLW constructs.

Fig.3-6. PPs production using different lentivirus systems. (**A**) HEK293T were transfected with VSV-G or MeV FΔ30 and HΔ30 along with one of the following lentivirus-based constructs: NL4.3-Luc-E-R-, or p8.91 and pCSFLW, or pCMVi and MLV-FLuc. After 72h, supernatants were collected and clarified. HEK293T-SLAM cells were then incubated with PPs for 24h. Transduced cells were lysed at 72h post-transduction and luciferase activity was measured. (**B**) Transduction of NE-PP produced by three different lentiviral systems. Statistical analysis was performed using Student's t test. ***, $p<0.001$

A

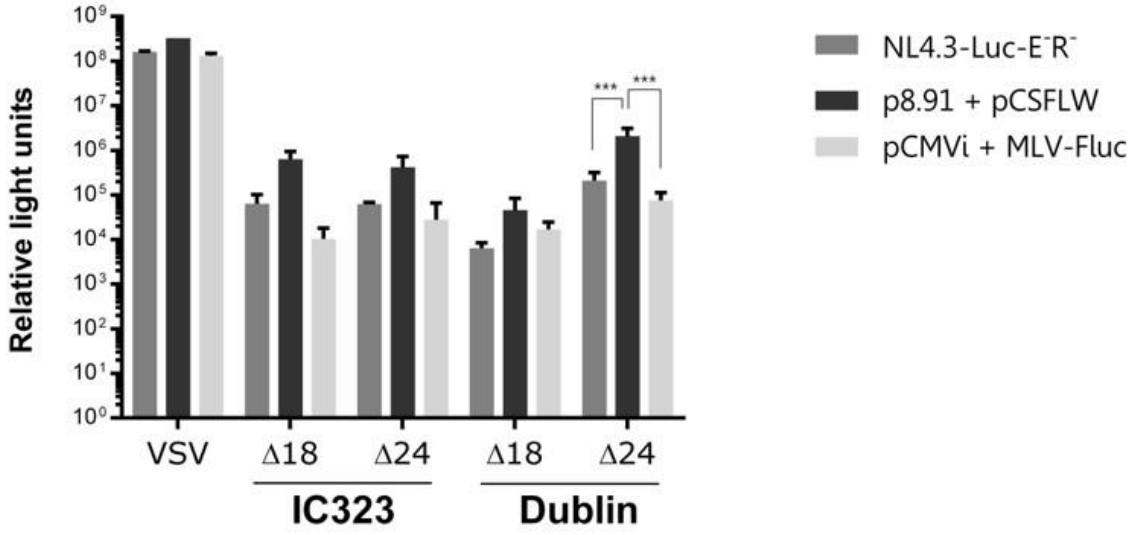
Relative light units
10^9
10^8
10^7
10^6
10^5
10^4
10^3
10^2
10^1
10^0
***
***
VSV
Δ18
Δ24
Δ18
Δ24
IC323
Dublin
NL4.3-Luc-E⁻R⁻
p8.91 + pCSFLW
pCMVi + MLV-Fluc

B

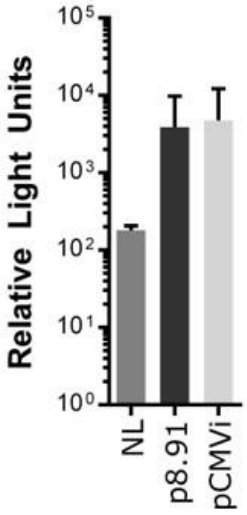
Relative Light Units
10^5
10^4
10^3
10^2
10^1
10^0
NL
p8.91
pCMVi

3.5 Development of a MeV matrix-based budding assay

The matrix protein of a wide range of enveloped viruses frequently functions as the driving force for viral budding and egress from the cell [375-377]. In MeV infection, the matrix (M) protein wraps the RNP complex [99] and interacts with Rab-11-positive endosomes to transport it to the plasma membrane [344]. At the plasma membrane, M is thought to oligomerise in lipid rafts to promote viral budding [351, 378]. Although the ESCRT system is a common exocytosis route hijacked by many viruses to escape the cell, MeV appears to use a different system to bud from cells [346]. To examine MeV egress in more detail, I developed a quantitative budding assay based on the activity of the M protein, i.e. its ability to generate virus-like particles (VLPs). To this effect, I generated a fusion protein comprising the MeV M protein fused to the firefly luciferase reporter, via a flexible linker (**Fig.3.7**). With the intention of assessing domains of the matrix protein that would better tolerate the insertion of the luciferase, I have generated a 3D model of the MeV M protein structure based on the related Newcastle disease virus Matrix protein structure. Details of protein modelling can be found in **section A.3 of the appendix**. According to the model, the N-terminus of M was located at the dimer interface while the C-terminal end was presented on the outside (**Fig.3.7A**). As dimer formation has been shown to impact on viral budding [379], I have fused the luciferase to the C-terminus of M, separated with a flexible linker (**Fig.3.7B**). This construct was transfected into HEK293T cells and incubated for 48h. Supernatants from these cells were collected, clarified by low speed centrifugation and overlaid onto a 20% sucrose cushion prior to high speed centrifugation. Resultant pellets were then lysed and the firefly luciferase activity measured using a luminometer (**Fig.3.7C**). Even though the evidence for the

Fig.3-7. Schematic representation of matrix-based quantitative budding assay. (**A**) 3D model of MeV M based on the crystal structure of the related Newcastle disease virus. The N-terminal end of a dimer of MeV (red and blue) is located at the dimer interface while the C-terminus is located on the side face of MeV M. (**B**) A fusion protein was generated carrying the N-terminal FLAG epitope, MeV Matrix, a flexible glycine-rich linker and the firefly luciferase gene. (**C**) After transfection into HEK293T, fusion proteins generate putative virus-like particles (VLPs). VLPs are then collected, purified and luciferase activity is measured.

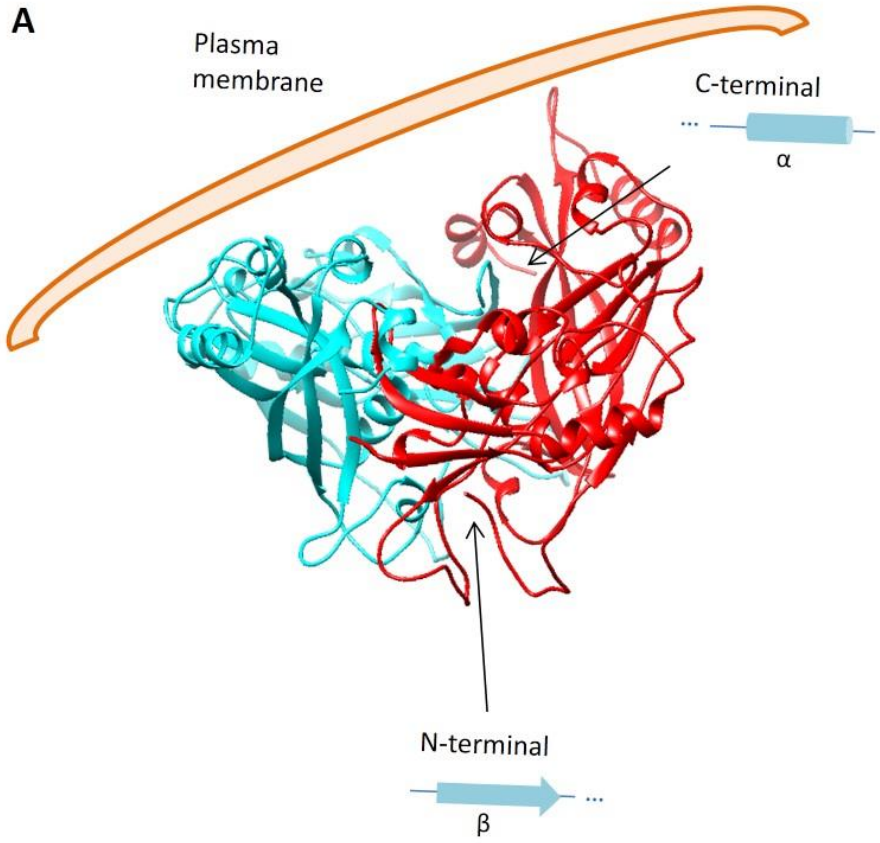
A
Plasma membrane
C-terminal
α
N-terminal
β

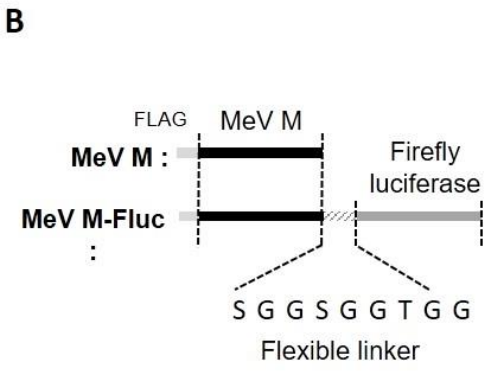
B
FLAG
MeV M
MeV M :
Firefly luciferase
MeV M-Fluc :
S G G S G G T G G
Flexible linker

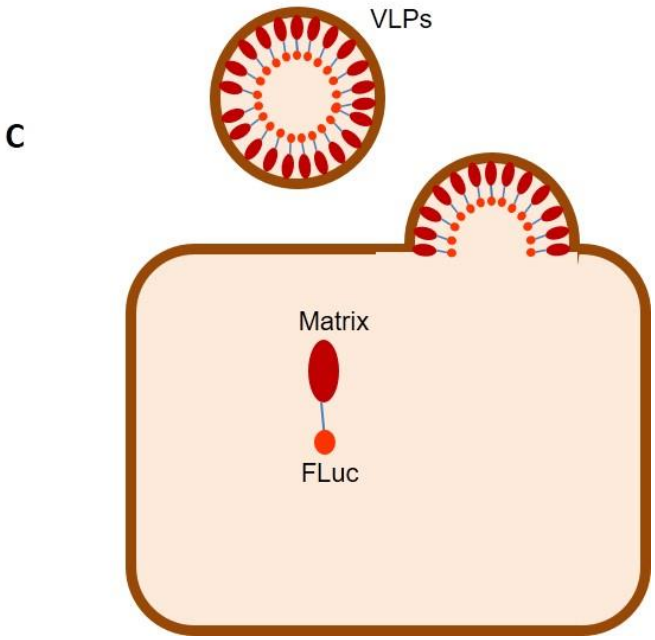
C
VLPs
Matrix
FLuc

formation of VLPs by expression of M herein is limited, a study using similar constructs and methodology demonstrated the isolation of M-derived VLPs by ultracentrifugation through a 20% sucrose cushion [346].

To assess the sensitivity of this VLP-assay HEK293T cells were transfected with various amounts of the M-FLuc plasmid. Luciferase activity in the supernatants and cell lysates from these cells was then measured (**Fig.3.8A**). Luminescence levels in both cell lysates and supernatants increased in relation to the total amount of transfected DNA. The minimum mass of transfected DNA required to detect luminescence signals, significantly different to background, was 73ng for cell lysates and 125ng for supernatants. The proportion between luciferase signals in cell lysates and supernatants was approximately 100-fold, suggesting that the majority of M remains inside the cell and does not form mature VLPs. Using an alternative approach, I subsequently compared the VLP formation efficiency of this fusion protein to wild-type MeV M. When transfecting cells with increasing amounts of M-FLuc or wild-type MeV M and harvesting supernatants as described before, I observed that only wild-type M could be efficiently detected by western blot (**Fig.3.8B**), even though both constructs contained the FLAG-epitope on their respective N-termini. Wild-type M was mainly detected around 35 kDa and detection limit by western blot in cell lysates and supernatants was in cells transfected with 250ng and 500ng, respectively. These results suggest that, even though the FLAG epitope could not be detected by western blot, the expression of this construct led to the efficient production of VLPs containing M-FLuc.

The generation of fusion proteins, especially with large additions such as the luciferase reporter, can disturb the function of the target protein. MeV M budding

Fig.3-8. M-FLuc produces VLPs containing luciferase. The matrix-luciferase (M-FLuc) fusion construct was transfected into HEK293T at the indicated concentrations and 48h later supernatants were collected, clarified and VLPs were pelleted through centrifugation. Luciferase activity was measured in whole cell lysates from producer cells or from pelleted VLP-containing supernatants (**A**) or resolved onto a 12.5% SDS-PAGE gel and M-FLuc (95 kDa) and M-FLAG (35 kDa) were visualised by western blot (**B/C**) (n=3 with 3 technical replicates). Short and long exposures of the same western blot probed with anti-FLAG.

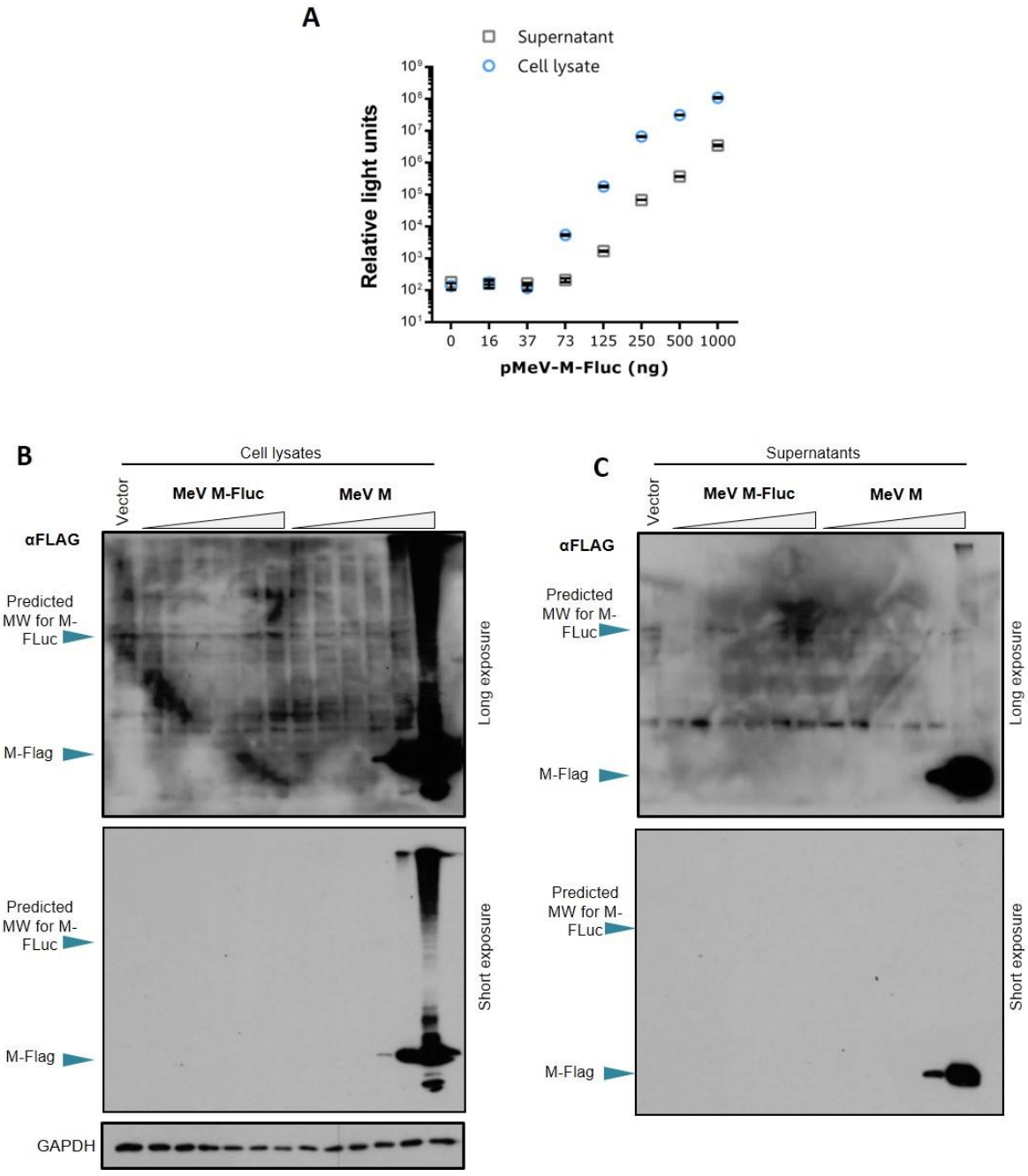
A
Supernatant
Cell lysate
Relative light units
pMeV-M-Fluc (ng)
0 16 37 73 125 250 500 1000
B
Cell lysates
Vector
MeV M-Fluc
MeV M
αFLAG
Predicted MW for M-FLuc
M-Flag
Long exposure
Short exposure
GAPDH
C
Supernatants

activity is dependent on oligomerization and interaction with several cellular and viral components. I hypothesised that M fusion with luciferase might impact on the general function of M, despite putative VLPs containing M-FLuc being detected. To minimise the impact of this fusion protein on VLP generation and M function, I supplemented M-FLuc transfection with wild-type M at different ratios to determine the optimal ratio and concentration for VLP generation (**Fig.3.9**). Co-transfection of wild-type MeV M had little impact on the activity of M-FLuc in cell lysates, implying a degree of saturation. However, in collected supernatants, a transfected DNA ratio of 1:3 (wild-type:M-Fluc) correlated with significantly higher luciferase activity, when compared to the expression of M-Fluc alone. This provides evidence that the expression of wild-type M at specific ratios improves luciferase-expressing VLP generation. This experimental set-up was therefore used in subsequent experiments.

3.6 Discussion

MeV spread requires the interaction of several viral proteins, most importantly H, F and M, with cellular components and it is likely that such interactions are highly complex and dependent on the context in which they are located. To overcome the complexity of a natural infection, I have isolated the functional units of viral spread, i.e. viral proteins involved in entry and exit, and incorporated them into quantitative assays, allowing the independent study of specific stages in the MeV lifecycle.

I have developed two assays that rely on the activity of MeV H and F proteins – the cell-cell fusion and MeV-PP entry assays. These are assayed in different contexts and can be used to distinguish the molecular requirements during MeV entry and fusion at the plasma membrane. It is frequently assumed that the entry of

Fig.3-9. Co-expression of wild-type M and M-FLuc increases viral release. To evaluate the effect of co-transfection of M-FLAG in M-FLuc release, HEK293T were transfected with a total 2ug of plasmid DNA encoding M-FLAG and M-Fluc at ratios 1:3, 1:1 and 3:1 or in isolation. After 48h, whole cell lysates were generated (**A**) and supernatants were collected, pelleted and lysed (**B**) prior to assessing luciferase activity (n=2 with 3 technical replicates). Student's t test, *p<0.05.

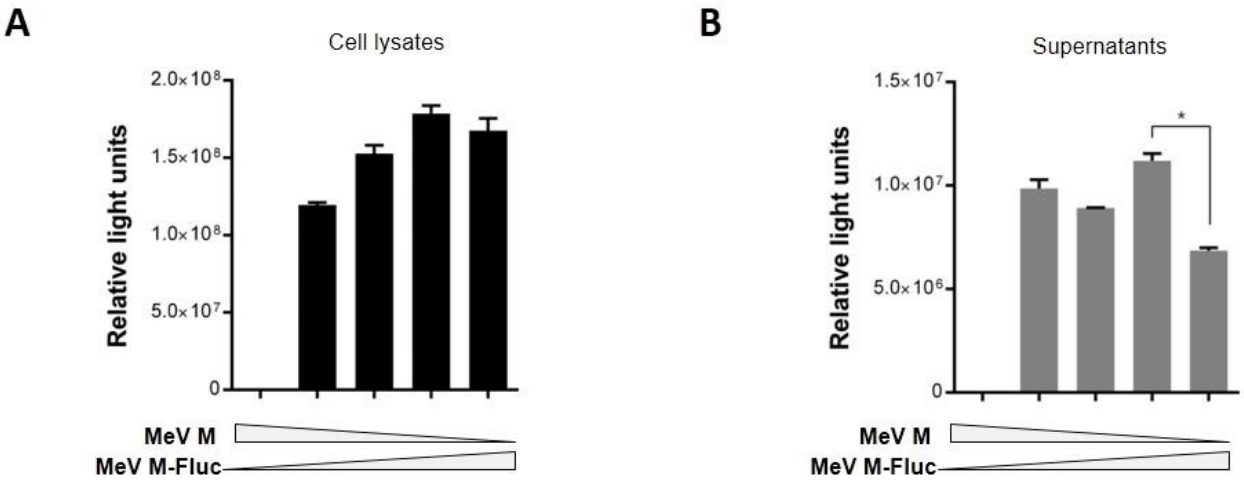
A
Cell lysates
Relative light units
2.0×10⁸
1.5×10⁸
1.0×10⁸
5.0×10⁷
0
MeV M
MeV M-Fluc
B
Supernatants
Relative light units
1.5×10⁷
1.0×10⁷
5.0×10⁶
0
*
MeV M
MeV M-Fluc

paramyxoviruses and pneumoviruses occurs at the plasma membrane, therefore forgoing the requirement to hijack endocytosis pathways. However, there is now growing evidence that several of these viruses are internalised [195, 325, 326, 374, 380]. Pseudotyped viruses have been instrumental tools for studying virus entry [359, 381, 382]. These systems take advantage of the genome packaging machinery of enveloped viruses, such as lentiviruses, to generate chimeric particles covered with unrelated viral envelope proteins. Previous studies have suggested that the intravirion tails of MeV GPs interfere with their correct incorporation into the lentiviral PP [369]. The data I have presented here supports this hypothesis. In addition, we have shown that the incorporation of GPs is not strain-specific; however, different strains can generate different PP titres. Since the expression of the H protein at the cell surface does not appear to vary extensively between strains by western blot analysis and Dublin strain GPs are more fusogenic than the IC323 strain, it is plausible that the higher entry levels observed with MeV Dublin PPs is due to a stronger interaction with MeV cellular receptors. Although predicted SLAM- and Nectin4-binding sites in the H proteins of MeV Dublin and IC323 are identical, substitutions in neighbouring areas may contribute to binding efficiency. Interestingly, the two strains also show different glycosylation patterns: the H protein of the Dublin strain has five potential N-glycosylation sites (N-X-S/T), while the IC323 strain has six; whilst the F protein of both strains have three and four, respectively. It has been reported that the N-glycosylation pattern of paramyxovirus GPs is involved in correct protein folding, virus replication and transport of the GPs to the cell surface [198, 383]. For instance, for MeV and CDV, it was demonstrated that glycosylation sites in the F protein are not only critical for protein folding but also modulate fusion [384].

This variance in these MeV GPs could explain their different properties *in vitro*. Other studies have shown that envelope protein glycosylation patterns in recent field isolates of MeV play a role in the evasion of pre-existing antibodies [385, 386]. These field isolates possess an addition N-glycosylation site that covers certain epitopes in the H protein. MeV H-specific antibodies circulating in the majority of human populations failed to inactivate MeV PPs when this glycosylation pattern was recreated, suggesting that certain post-translational modifications of H can cover epitopes involved in adaptive immune recognition. Since MeV PPs have many applications in gene therapy [328, 374], understanding how MeV glycoproteins affect evasion, entry and fusion can enable the development of better tools in this area.

The availability of cell receptors in tissue culture allied with the ability of F to be triggered in the absence of low pH has led to the belief that cell-cell fusion and fusion upon virion entry share the same mechanism. However, taking into consideration that the expression of MeV F and H at the plasma membrane precedes the translocation of the RNP complex to the plasma membrane [292, 344, 349, 387], that MeV M is dependent on dimerization to interact with lipid rafts [388] and that competitive interaction of F-actin filaments with the cytoplasmic tails of MeV F and H [349], it is likely that these two fusion mechanisms are different. Measles virions are densely covered by MeV glycoproteins [387, 389] while MeV F and H oligomers expressed at the cell surface (when cell fusion is possible) are very scattered (Roberto Cattaneo's lab scientific communication W45-10, Workshop 45, American Society for Virology Annual Conference, Blacksburg, VA 2016). The interactions with cellular receptors, and their availability, are also plausible mechanisms that may affect cell-cell fusion and viral entry. The fusion of lipid bilayers is regarded as a highly energetic process

and viral proteins, such as MeV F, might help to reduce the energy requirements [390]. Therefore, a cellular environment where either MeV GPs might not be expressed at great density (cell-cell fusion) or where the availability of receptors might be low (virus entry) is likely to impact on the progression of membrane fusion. Our separate assays can therefore help to clarify the mechanisms involved in each process.

MeV is thought to be the main driving force for viral budding. It is likely that the interaction of M with the viral GP cytoplasmic tails and lipid-rafts promotes the curvature of the plasma membrane culminating in the formation of the virion. Although several viruses hijack cellular exocytosis mechanisms to bud, MeV budding appears independent of this pathway [346]. Nevertheless, limited evidence suggests the involvement of the cytoskeleton in the budding process and formation of viral particles [348, 391]. A quantitative budding assay will be useful for screening the molecular requirements for virus budding and to understand any active dependence on the cytoskeleton. The matrix-luciferase fusion construct I have generated is the main component of this assay and is based on the concept that the independent expression of MeV M leads to the formation of VLPs [346]. To minimise the impact of the luciferase fusion protein I included a glycine-rich flexible linker between the two proteins. The expression of this construct in HEK293T yielded the formation of putative VLPs containing luciferase, i.e. VLPs containing the M-FLuc fusion protein that were able to cross a 20% sucrose cushion at 17000×g, while isolated proteins were likely retained on top of the cushion. The M protein of the related paramyxovirus NDV forms a lattice underneath the plasma membrane [392]. Although similar

phenotypes are hypothesised for MeV, MeV M has recently been shown to wrap the RNP complex in a helical configuration [99]. These supramolecular interactions of M monomers are possibly sensitive to the addition of extra domains such as a luciferase reporter. It is therefore unsurprising that the formation of VLPs is improved by the co-expression of wild-type M, as the co-ordinated interaction of several tagged M monomers might be alleviated by the expression of wild-type protein.

Although these assays are powerful and quantitative I understand their limitations, especially with regards to comparisons to natural infections. The abundance of these proteins, their localisation in the cell and the complexity and temporal nature of multiple interactions during infection impacts on the overall function of these proteins. Therefore any significant findings obtained with these assays were subsequently examined and validated in full MeV infections. In summary, these three assays are, in isolation, quantitative techniques to study the function of MeV F, H and M proteins and several stages of the MeV lifecycle. Throughout this thesis, these three assays are used to study MeV entry and exit.

Chapter 4

MEASLES VIRUS ENTERS SLAM^{+} CELLS VIA A MACROPINOCYTOSIS-LIKE PATHWAY

MeV is transmitted via aerosols and is thought to initially infect interstitial macrophages and dendritic cells of the lung [36]. Infection subsequently spreads to local draining lymph nodes and, after a viremia is established, the virus infects the airway epithelium releasing infectious viral particles into the lumen of the lung that are then expelled to the environment and transmitted to other hosts [36, 40]. Circulating field-isolates of MeV use two known proteinaceous receptors to invade different cell-types: SLAMF1 [203], is the immuno-tropic receptor for activated B and T cells, monocytes, dendritic cells and macrophages, while nectin-4 [204], a component of the adherens junctions found on the basolateral plane of polarised epithelium, is the epithelia-tropic receptor. These receptors are not thought to be expressed on the same cells, thus conferring a dual tropism to MeV that can explain both its immunosuppressive nature and the characteristic epithelial pathogenesis seen later in infection, especially in the lung. Functionally, SLAMF1 belongs to the immunoglobulin superfamily and acts as a self-ligand involved in the stimulation and activation of T and B cells [212].

MeV encodes six structural and two non-structural proteins. Two of these – the H and F proteins - are highly glycosylated proteins present on the virus envelope that direct virus attachment to the cell surface and formation of the fusion pore between viral and cellular membranes. During this process MeV H interacts with SLAM or Nectin-4 resulting in conformational changes that activate F [180, 296]. This induces the insertion of a highly hydrophobic peptide of F into the cell membrane, culminating in complete membrane fusion [202, 308]. Although this mechanism is integral to particle entry, it has also been observed, *in vitro* and *in vivo*, that MeV-infected cells can also induce cell-cell fusion of neighbouring cells resulting in multinucleated cells known as

syncytia [393]. This aspect of MeV dissemination is supported by the ability of MeV F and H glycoproteins to function at neutral pH.

It is commonly believed that the MeV genome enters cells after direct fusion of the viral envelope with the plasma membrane without endocytosis of the particle [380]. However, previously published research indicating that soluble measles H protein [329] and, more recently, pseudotyped MeV particles may be endocytosed [374] suggested a more complicated mechanism of entry divergent from simple fusion at the plasma membrane and immediate entry of the genome. Indeed other paramyxoviruses, such as respiratory syncytial virus (RSV), Newcastle disease virus (NDV), Nipah virus and Sendai virus, have also been reported to use endocytosis pathways to invade cells challenging the concept that these enveloped viruses deliver their genome simply by fusing at the plasma membrane [195, 325, 394]. Another important aspect to consider is distinguishing between molecular level interactions of MeV glycoproteins with cellular receptors and larger scale bio-physical interactions between the large incoming particle of MeV and the cellular membrane. These larger-scale interactions between virions and the cellular membrane have been shown to be critically important in the entry of Ebola virus particles [395]. In this study I have revisited the mechanism of entry of MeV into cells, particularly those expressing the immune-cell receptor SLAMF1, since these are considered the initial target during infection.

4.1 Internalisation of MeV particles

To evaluate if MeV particles are internalised I first examined the sensitivity of the viral H protein to trypsin during the initial stages of infection. I hypothesised that if MeV virions fuse directly at the plasma membrane its glycoproteins (F and H) would

remain at the cell surface and be sensitive to tryptic digestion. In contrast, if MeV particles were internalised, then extracellular trypsin could not cleave the viral glycoproteins and F and H would remain intact (**Fig.4-1A**). After confirming the sensitivity of H (found on MeV particles) to trypsin (**Fig.4-1B**), purified MeV particles were attached to A549-SLAM cells (MOI=30) at 4°C for 1h, washed in PBS before raising the temperature to 37°C for 0, 15 or 30 minutes (min, synchronous infection). At these time-points cells were either immediately trypsinised for 7 min, or detached with a solution of EDTA (2 mM in PBS) and whole cell protein lysates generated. These lysates were then analysed by western blotting using an antibody raised against the intra-virion tail of MeV H (**Fig.4-1C**). Full-length MeV H was detected in non-trypsinised cells around the 75 kDa mark (black arrow); however, when cells were trypsinised for 7 min after incubation at 37°C for 0 or 15 min post-infection (mpi) H was only detected at 24 and 20 kDa (blue and white arrows, respectively), indicating trypsin digestion. In contrast when cells were incubated for longer (30 min), H was detected both at its undigested size (75 kDa) as well as at 24 and 20 kDa, suggesting protection from trypsin. To assess the sensitivity of MeV to trypsin post attachment, I repeated the experiment, instead allowing infection to continue for 48h after the trypsin or EDTA treatment. At this time-point, yields of produced virus were calculated as an indicator of productive infection (**Fig.4-1D**). As expected virus yields were reduced after trypsin treatment, both at 0 and 10 mpi, relative to untreated controls. This reduction was, however, markedly less following incubation for 20 mpi at 37°C, again implying protection from trypsin.

In supporting experiments I addressed the same question using an adapted quantitative cell-to-cell fusion assay [308] in which target cells are transfected with

Fig. 4-1. Measles virions are resistant to tryptic digestion 30min post infection. (**A**) Diagram of experimental setup: purified MeV was attached to A549-SLAM cells (MOI=30) for 60min at 4°C, washed with PBS to remove unattached virus and incubated for 0, 15 or 30min at 37°C prior to trypsin treatment. (**B**) Sensitivity of MeV H to trypsin was confirmed by incubation of virions with trypsin for 7min at 37C, prior to SDS-PAGE/western blot analysis. (**C**) Total cells lysates were generated and resolved on a 15% SDS-PAGE gel prior to western blotting using a polyclonal antibody raised against the cytoplasmic tail of MeV H. Three H-specific bands were detected with the approximate size of 75 kDa (black arrow; full-length), 24 kDa (blue arrow) and 20 kDa (white arrow); the latter two only being detected after trypsin treatment. The results shown are representative of four individual experiments. (**D**) Similarly, cells were synchronously infected with MeV, incubated at indicated time-points (minutes post-infection, mpi) and trypsinised for 7min at 37°C. Cells were pelleted, resuspended in complete media, incubated for 48 h and the total virus was then titrated. Student's t test, n.s., non-significant.

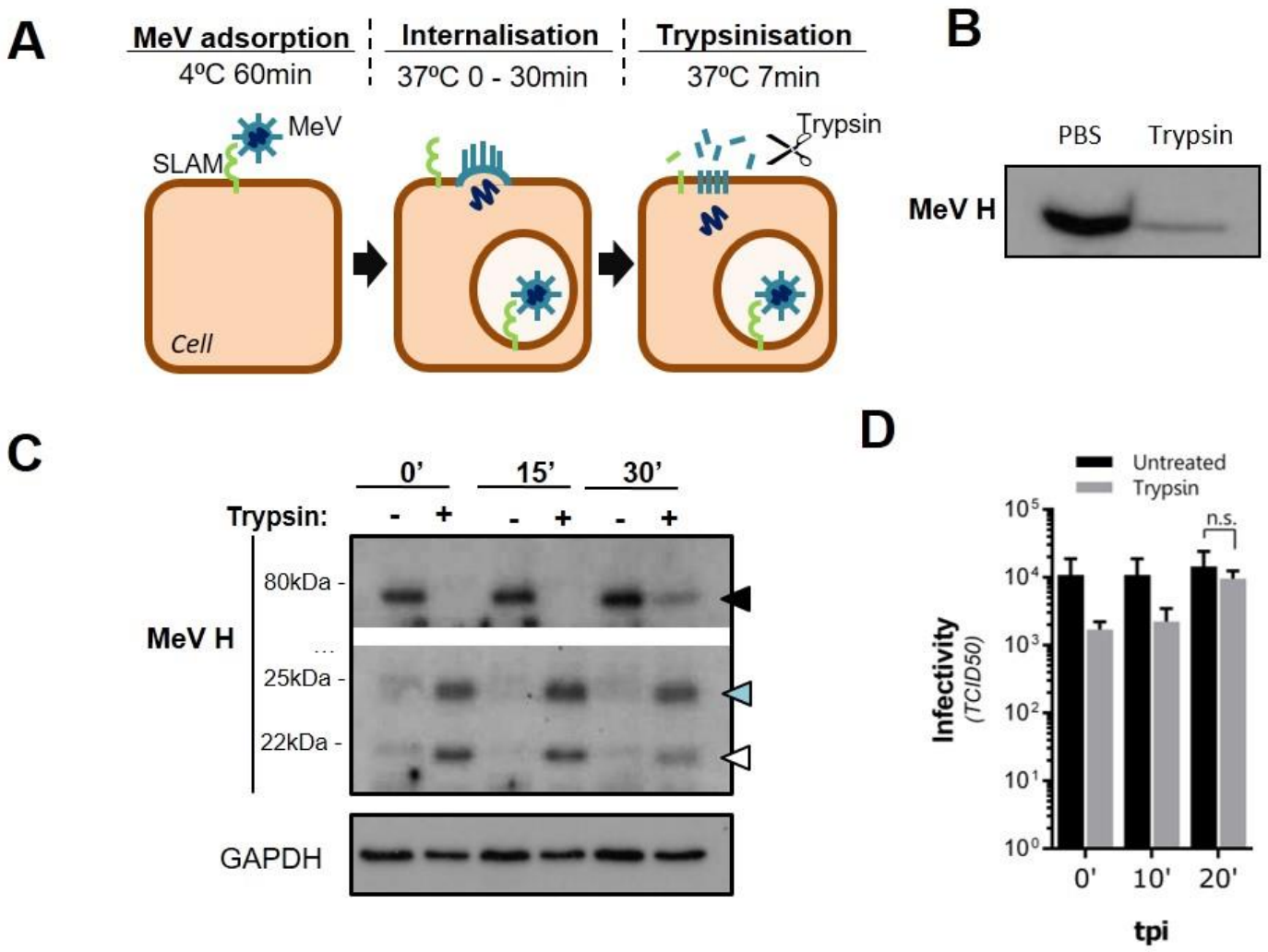
A
MeV adsorption
4ºC 60min
Internalisation
37ºC 0 - 30min
Trypsinisation
37ºC 7min
MeV
SLAM
Cell
Trypsin
B
PBS
Trypsin
MeV H
C
0'
15'
30'
Trypsin:
- + - + - +
80kDa -
MeV H
25kDa -
22kDa -
GAPDH
D
Untreated
Trypsin
n.s.
Infectivity
(TCID50)
0'
10'
20'
tpi

one half of a dual split-reporter, while effector cells are transfected with the complementary half. The dual reporter is only functional when target and effector cells fuse and cytosolic mixing takes place. I hypothesised that if MeV fuses at the plasma membrane, F and H would remain at the cell surface and induce cell-to-cell fusion when target cells are overlaid on top of MeV-infected cells. In contrast, if MeV particles are internalised, F and H would be removed from the cell surface and therefore be unable to interact with neighbouring cells to induce cell fusion (**Fig.4-2A**). To examine this, purified MeV particles were attached to effector cells (MOI=30) as stated previously. These cells were then washed and incubated at 37°C for 0, 15, 30 or 60 min prior to the addition of target cells for 90 min in the presence or absence of chlorpromazine (CPZ) (which blocks the formation of clathrin-coated pits), followed finally by the measurement of the luciferase activity in fused cells (**Fig.4-2B**). Cell-to-cell fusion decreased following extended incubation periods at 37°C even in the presence of the inhibitor of clathrin-mediated endocytosis, a common endocytosis pathway for sequestration of proteins at the plasma membrane [396]. These data suggest that the viral glycoproteins do not remain at the cell surface following viral attachment in a mechanism independent of receptor recycling pathways. Together, these results suggest a proportion of viral particles are internalised upon entry.

4.2 MeV entry is independent of low endosomal pH, dynamin, clathrin- and caveolin-mediated endocytosis.

To assess if the observed internalisation of viral particles was dependent on common endocytosis pathways, I used a combination of lentivirus-based pseudotyped MeV particles (MeV-PPs) or recombinant MeV engineered to express EGFP, together with pharmacological inhibitors of these pathways. Entry of MeV-PP into A549-SLAM cells

Fig. 4-2. MeV glycoproteins are removed from the surface soon after attachment. (**A/B**) Diagram of experimental setup: HEK293T-SLAM cells carrying a split form of Renilla luciferase were synchronously infected with purified MeV (MOI=30) for 60min at 4°C, washed with PBS and incubated for 0, 15, 30 or 60min at 37°C (in the presence or absence of 5µg/mL of chlorpromazine, CPZ) prior to the addition of HEK293T-SLAM cells carrying the complementary part of the luciferase. Cells were co-cultured for 90min before the addition of the luciferase substrate coelenterazine with produced light being measured using in a luminometer. Of note, values were normalised by subtracting the values from a negative control, i.e. cells to which virus was not attached and plotted as relative light units (n=3 with 4 technical replicates). Student's t test, **p<0.01 , ***p<0.001.

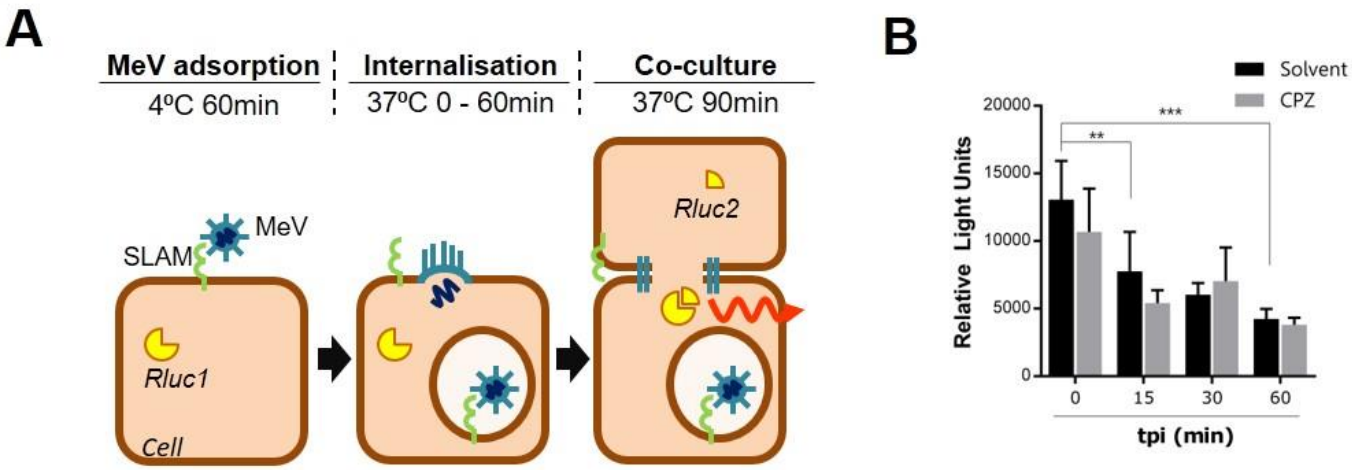
A
MeV adsorption
4ºC 60min
Internalisation
37ºC 0 - 60min
Co-culture
37ºC 90min
MeV
SLAM
Rluc1
Cell
Rluc2
B
Solvent
CPZ
Relative Light Units
20000
15000
10000
5000
0
**
***
0
15
30
60
tpi (min)

was unaffected by treatment with chloroquine (CQ) and bafilomycin A1 (BAF), two lysosomotropic agents that block endosomal acidification and caveolin-dependent endocytosis, however VSV-PP entry was significantly decreased (**Fig.4-3A**). Similarly, the dynamin-2 inhibitor dynasore (DYN) failed to block MeV-PP infection. When A459-SLAM cells were pre-treated with these drugs and infected with a recombinant MeV engineered to express EGFP (MOI=1), no difference was observed in the number of infected cells using UV-microscopy (**Fig.4-3B** and **3C**). To evaluate if cellular factors involved in clathrin-mediated endocytosis (such as the epidermal growth factor receptor substrate 15, EPS15), caveolin-mediated endocytosis (Cav-1) or dynamin-dependent endocytosis (Dyn2) were required for infection, cells were transfected with constructs encoding dominant negative (DN) mutants of these proteins and infected with MeV-PPs or VSV-PPs (**Fig.4-3D**). Unsurprisingly, none of these mutants had an appreciable effect on MeV-PP entry confirming dynamin-, clathrin- and caveolin-mediated endocytosis are not required for MeV entry via the SLAM receptor. To assess if internalised particles co-localize with clathrin-, caveolin- or dynamin2-positive vesicles, A549-SLAM cells were transfected with plasmids encoding GFP-fused clathrin heavy chain (CHC-GFP), caveolin-1 (Cav1-GFP) or synchronously infected with MeV and incubated for 30 min at 37ºC. Cells were then fixed, stained with anti-nucleocapsid (MeV N) antibody and prepared for confocal laser scanning microscopy (CLSM) (**Fig.4-4A**). Only a limited number of MeV N-positive puncta co-localized with CHC- and Cav1-positive vesicles while slightly more co-localized with dyn2-GFP-positive vesicles (**Fig.4-4B**). Despite the unexplained partial co-localisation of MeV particles with Dyn2- GFP, these data suggests that

Fig.4-3. MeV entry is insensitive to inhibitors and dominant negative mutants of clathrin- and dynamin-2-dependent endocytosis. (**A**) A549-SLAM cells were pre-treated with chloroquine (CQ, 50µg/mL), bafilomycin A1 (BAF, 50µg/mL), dynasore (DYN, 100µM) or solvent for 30min at 37°C. MeV- or VSV-PP encoding the firefly luciferase reporter were added to the cells and incubated for 3h. Media was then replaced and cells were incubated for 72h before lysis, addition of the luciferase substrate luciferin and measurement of produced light (n=5 with 4 technical replicates). (**B/C**) Equivalently, cells were pre-treated with indicated drugs at the same concentrations for 30min and infected with MeV (MOI=1) for 1h. Cells were trypsinised, pelleted and resuspended in complete media and after 24h of incubation at 37°C, visualized under UV light (**B**) and the number of GFP-positive infected cells counted (**C**) (n=2 with 1 technical replicate). (**B**) Representative images of the typical fields of view used for quantification are shown. (**D**) HEK293T-SLAM cells were transfected with plasmids expressing dominant negative (DN) mutants of EPS15, cav-1 and dyn2 and 48h post-transfection transduced with MeV- or VSV-PPs. As a control, cells were transfected with an empty plasmid (Vector). After 72h cells were lysed and the luciferase activity was measured (5 replicates per condition, error bars represent standard deviation). Student's t test, *$p<0.05$, **$p<0.01$, n.s. non-significant.

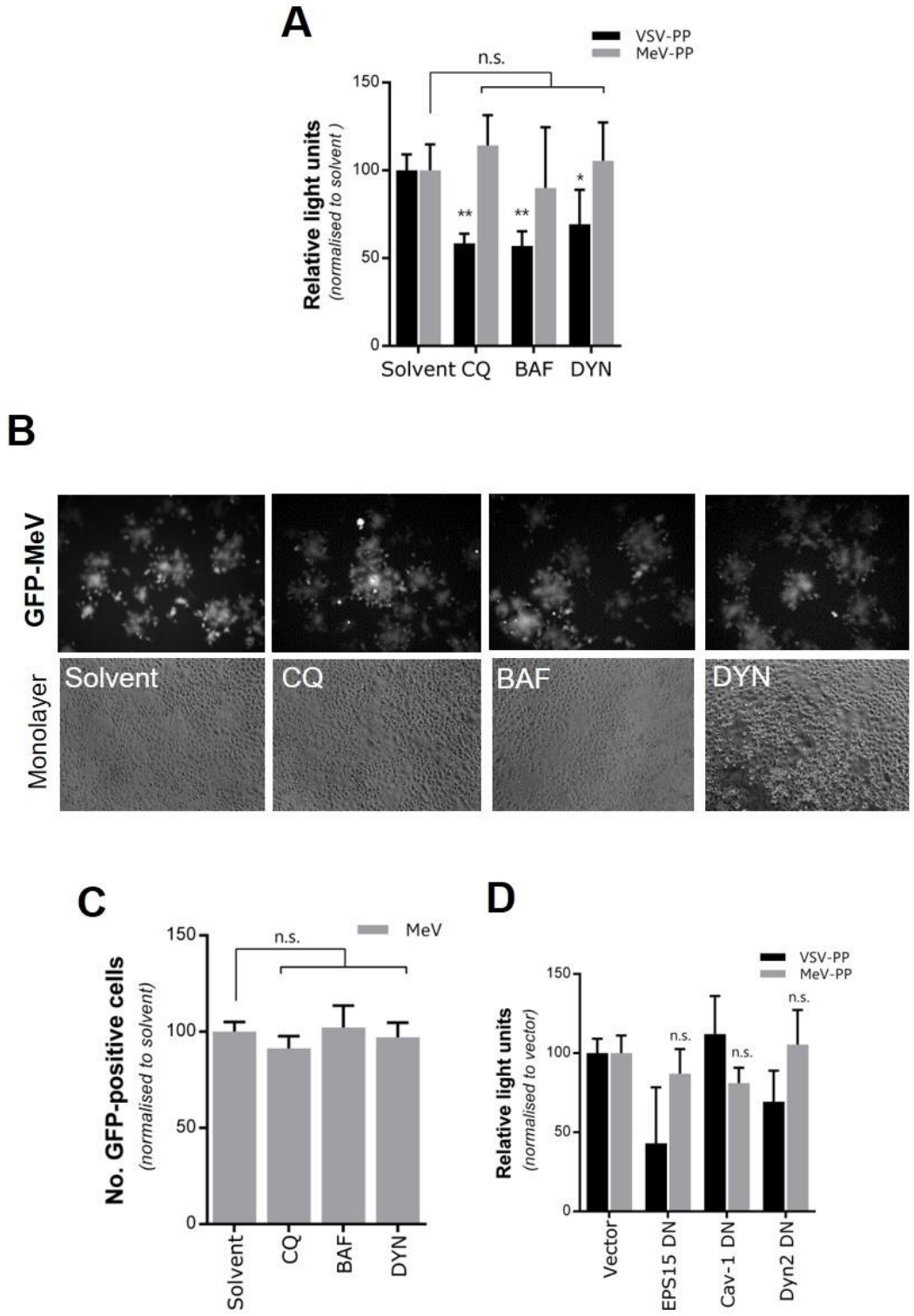
A
VSV-PP
MeV-PP
n.s.
150
100
50
0
Relative light units
(normalised to solvent)
**
**
*
Solvent CQ BAF DYN
B
GFP-MeV
Monolayer
Solvent
CQ
BAF
DYN
C
MeV
n.s.
150
100
50
0
No. GFP-positive cells
(normalised to solvent)
Solvent
CQ
BAF
DYN
D
VSV-PP
MeV-PP
150
100
50
0
Relative light units
(normalised to vector)
n.s.
n.s.
n.s.
Vector
EPS15 DN
Cav-1 DN
Dyn2 DN

MeV entry into SLAM-positive cells is independent of clathrin-, caveolin- and dynamin-2-mediated endocytosis.

4.3 MeV induces extensive membrane blebbing and is sensitive to blebbistatin.

Other mechanisms of entry into the cell, such as phagocytosis and macropinocytosis, involve a substantial rearrangement of the plasma membrane [397]. To examine if MeV was inducing similar rearrangements during entry, I synchronously infected cells with MeV (MOI~45) and, following fixation, observed their morphology by phase-contrast microscopy (**Fig.4-5A**). MeV-infected cells presented significantly more membrane blebs (arrows, **Fig.4-5A**) than uninfected cells (**Fig.4-5B**). To further investigate these membrane modifications I performed scanning electron microscopy (SEM) on cells synchronously infected with MeV (MOI=30) and incubated for 10, 30 or 60 min at 37°C prior to fixation and preparation for SEM (**Fig.4-5C**). Although uninfected cells showed a flat and well distributed morphology, MeV-infected cells at 10 and 30 mpi were visibly more contracted, also appearing partially detached from the coverslip (upper panel). Closer observation of the plasma membrane **(Fig.4-5C – see insets)** showed that while uninfected cells presented occasional small filopodia-like structures and an otherwise smooth plasma membrane (orange arrow, bottom left), the surfaces of MeV-infected cells at 10 and 30 mpi were almost exclusively covered with similar structures (orange arrow, bottom middle). In addition, only infected cells at 10 or 30 mpi presented membrane blebs, these being located predominantly at the cell's periphery dynamin2 (Dyn2-GFP) and 48h later (white arrows). Interestingly, infected cells incubated at 37°C for 60 min post viral attachment presented with a similar morphology to uninfected cells indicating that these morphological changes were transient (bottom right).

Fig.4-4. Internalised Measles virions do not colocalise with CHC, Cav-1 and only partially with Dyn-2. (**A**) A549-SLAM cells were transfected with plasmids encoding GFP (Green), Clathrin heavy chain 1 (CHC)-GFP, caveolin-1 (Cav1)-GFP or dynamin-2 (Dyn2)-GFP. Cells were then synchronously infected with MeV, incubated for 30min at 37ºC and prepared for and analysed by CSLM. Representative micrographs were taken (MeV nucleocapsid (**N**) is pseudocoloured in red) and (**B**) co-localisation of green- and red-channels was quantified. Scale bar represents 15µm.

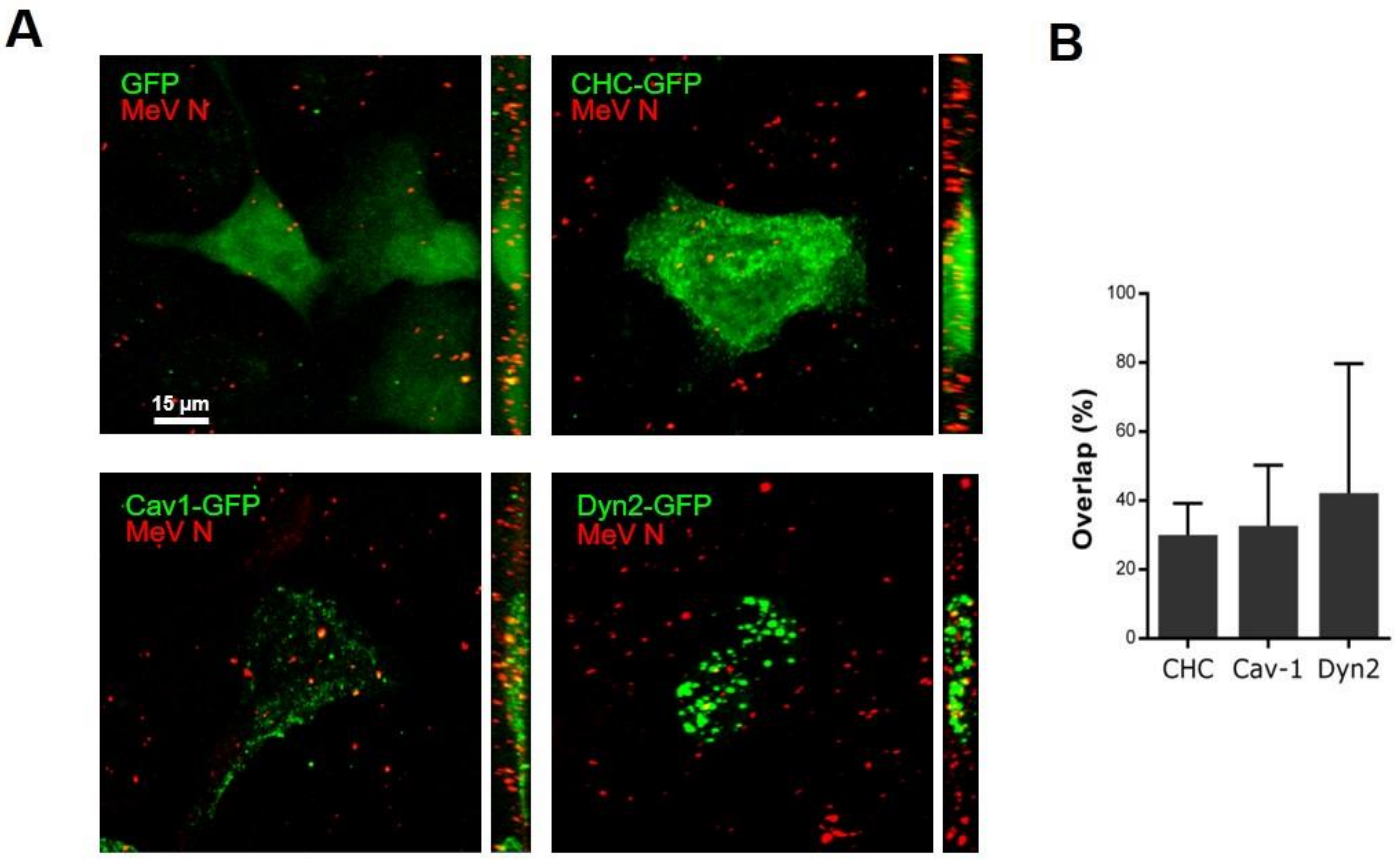
A
GFP
MeV N
15 µm
CHC-GFP
MeV N
Cav1-GFP
MeV N
Dyn2-GFP
MeV N
B
Overlap (%)
100
80
60
40
20
0
CHC
Cav-1
Dyn2

Fig.4-5. MeV induces extensive membrane blebbing. (**A**) A549-SLAMs were serum-starved overnight at 37°C and subsequently pre-chilled on ice for 5min. MeV (MOI=45) was then attached to cells for 1h at 4°C. As a control (uninfected) cells were exposed to media containing 20% FBS under the same conditions. Cells were washed with cold PBS and incubated for 30min at 37°C before fixation with 4% PFA and visualisation by phase-contrast microscopy. (**B**) The percentage of cells that presented membrane blebs (white arrows in A) per field of view was calculated for both samples. (**C**) Similarly, serum-starved A549-SLAM were synchronously infected with MeV (MOI=30) and incubated for 0, 10, 30 or 60min at 37°C before fixation and preparation for SEM. Both uninfected and infected cells presented small filopodia-like structures at the surface (orange arrows) but only infected cells presented membrane blebs (white arrows). Student's t test, **p<0.01

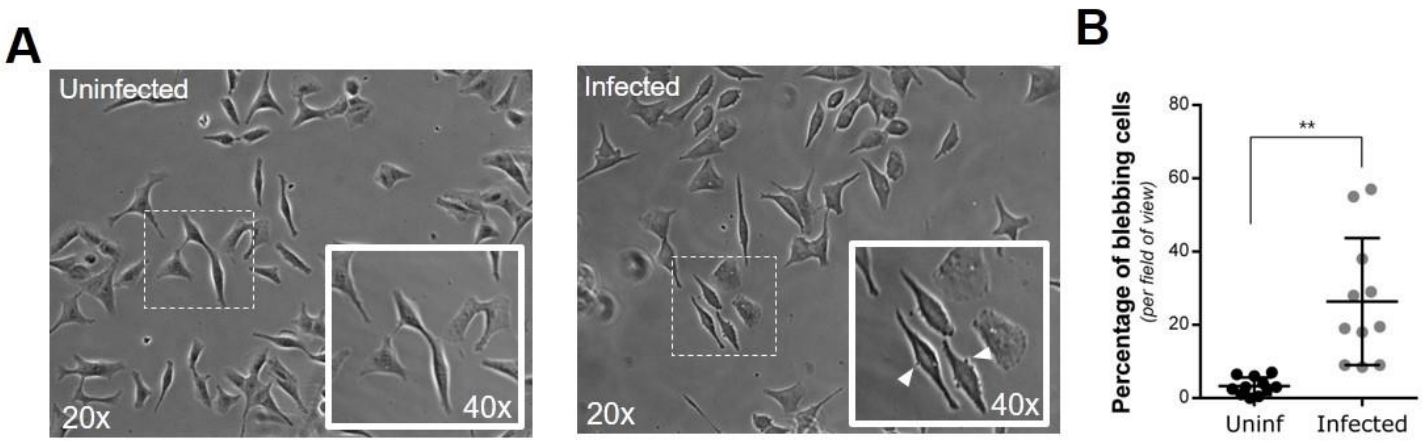

Figure continues on the next page

Continued from previous page

C

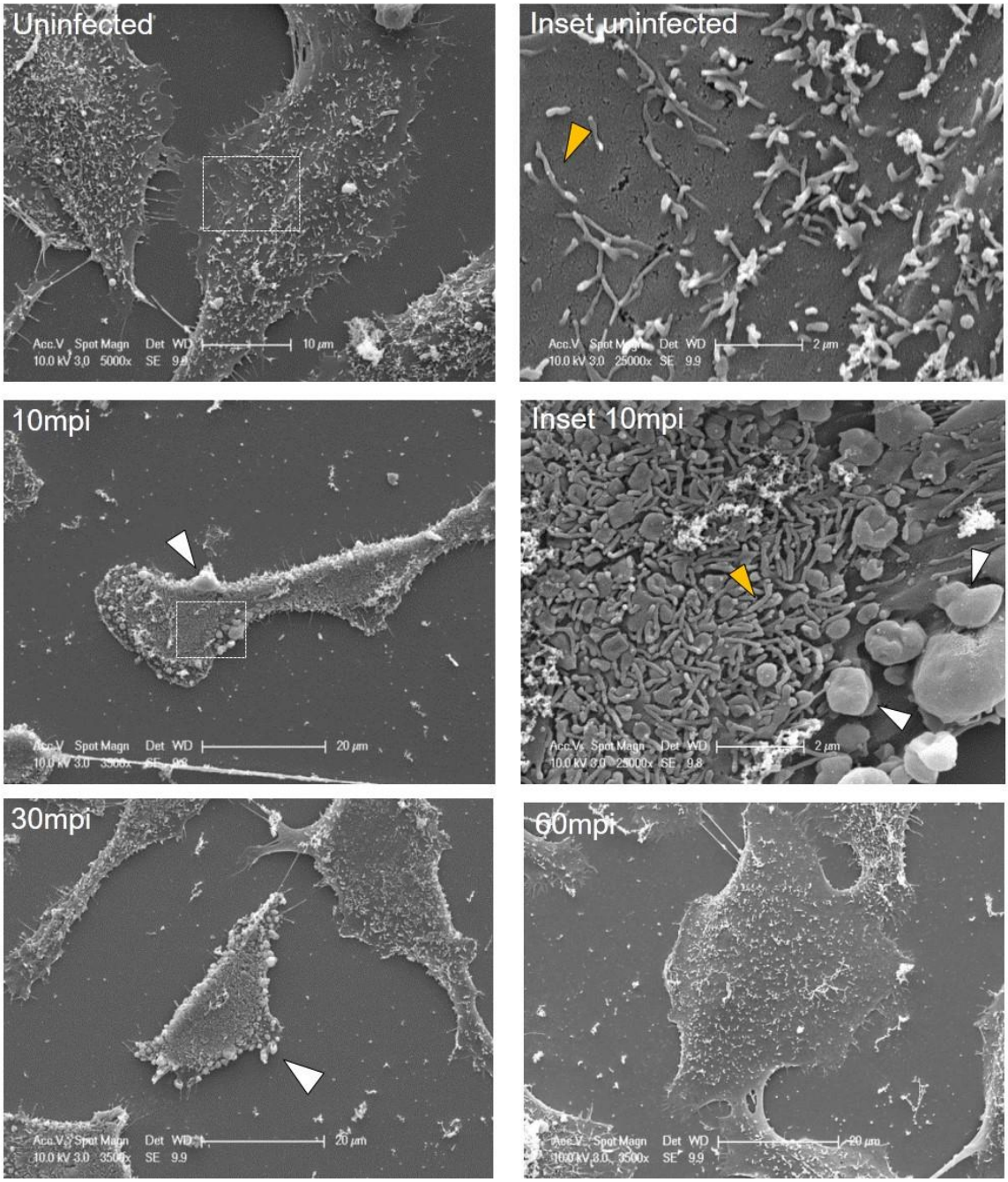

The formation of membrane blebs is largely governed by the activity of myosin-II, a protein involved in the rapid contractility of the cortical actin cytoskeleton [398]. To evaluate the role of membrane blebbing in MeV entry I therefore pre-treated cells with blebbistatin, an inhibitor of myosin-II, and infected these cells with MeV-PPs, VSV-PPs (**Fig.4-6A**) or MeV (**Fig.4-6B**). Efficiency of blebbistatin in blocking fluid-uptake was assessed prior to MeV infections (see **appendix section A-4**). Infection with both MeV-PP and MeV was reduced by this drug as was nascent MeV viral production in blebbistatin-treated cells (**Fig.4-6C**). In contrast blebbistatin had no effect on VSV-PP entry (**Fig.4-6A**). To assess the specificity of blebbistatin for MeV entry cells were infected with MeV and either, pre- or post-treated with a range of concentrations of this drug (**Fig.4-6D**). At all concentrations, the level of detected MeV H, after 24h of infection, was lower when cells were pre- rather than post-treated with the drug. These results highlight the essential importance of membrane blebbing during MeV entry and are indicative of early events in the macropinocytosis pathway.

4.4 MeV induces fluid-phase uptake and is sensitive to EIPA.

Underlying the definition of macropinocytosis is the uptake of fluid from extracellular medium [399]. I hypothesised that if MeV promotes macropinocytosis upon entry, it should also induce the internalization of extracellular fluid and the formation of macropinosomes. Using a cell-impermeable, soluble and fluorescent 10 kDa dextran (0.25 mg/mL in PBS), cells were synchronously infected with MeV (MOI=10) and then incubated at 37°C for 20 min. For controls, cells were pre-incubated with DMEM with 20% FBS (uninfected) or 200nM of the macropinocytosis-inducer phorbol 12-myristate 13-acetate (PMA) [400].

Fig.4-6. MeV infection is sensitive to treatment with blebbistatin. (**A**) A549-SLAM cells were pre-treated with blebbistatin (BLEB) or solvent for 30min before the addition of MeV- or VSV-PP. Cells were then incubated with PPs for 3h, washed with PBS and incubated for 72h in complete media prior to measurement of luciferase activity. (**B/C**) In a similar experiment, cells were pre-treated with 100µM of blebbistatin for 30min and infected with MeV (MOI=1) for 1h. Cells were then trypsinised and incubated for 24h before assessment of no. of GFP-positive cells and the total yield of virus. (**D**) To address if blebbistatin had a dose-dependent effect on MeV entry, A549-SLAM were either pre- or post-treated with the drug, in relation to the point of infection, at the indicated concentrations, trypsinised and subsequently incubated at 37°C for 24h. Total cells lysates were generated and resolved on a 15% SDS-PAGE gel prior to western blotting using a polyclonal antibody raised against the cytoplasmic tail of MeV H. Student's t test, *$p<0.05$, **$p<0.01$, n.s., non-significant

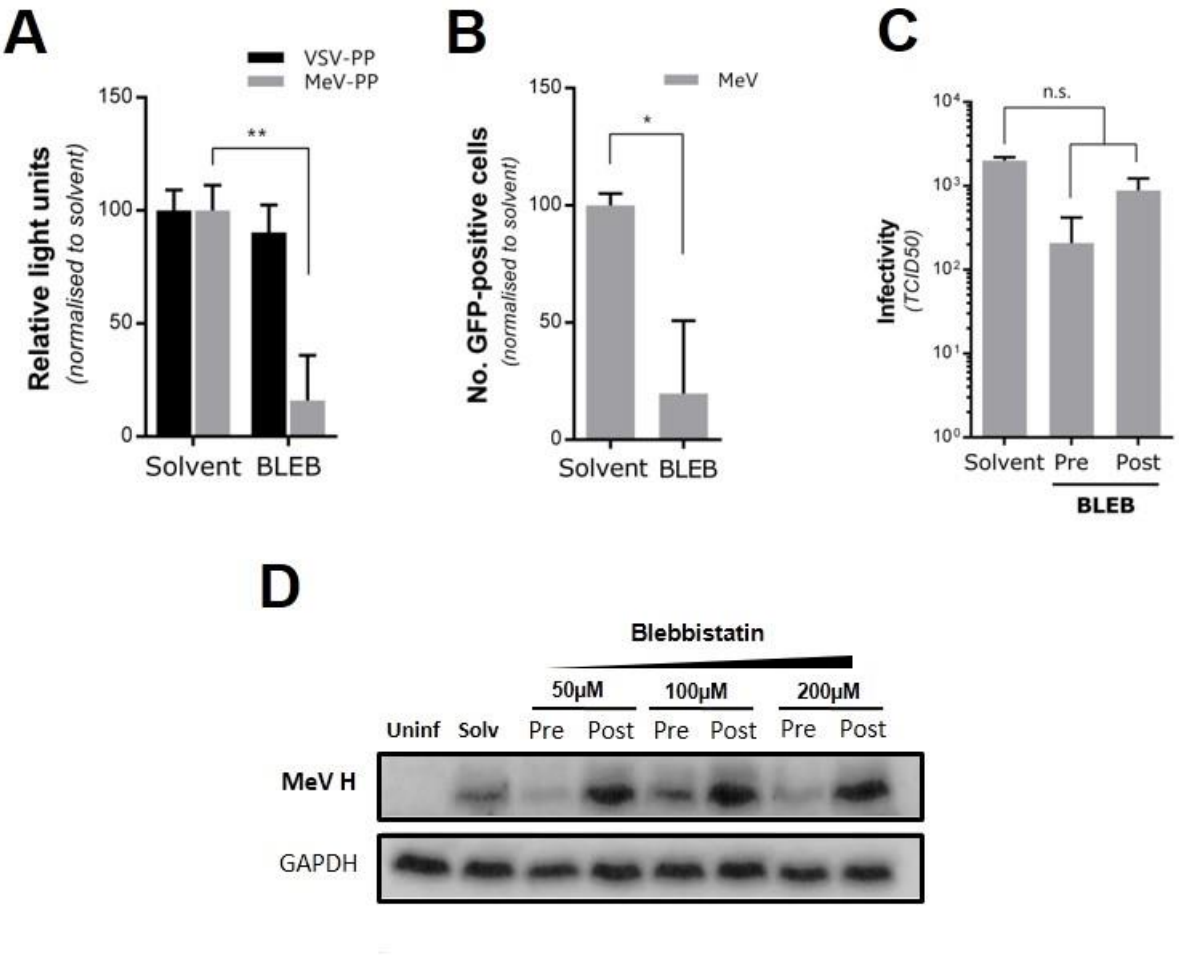
A
VSV-PP
MeV-PP
Relative light units
(normalised to solvent)
150
100
50
0
**
Solvent
BLEB
B
MeV
No. GFP-positive cells
(normalised to solvent)
150
100
50
0
*
Solvent
BLEB
C
n.s.
Infectivity
(TCID50)
10⁴
10³
10²
10¹
10⁰
Solvent
Pre
Post
BLEB
D
Blebbistatin
50μM
100μM
200μM
Uninf
Solv
Pre
Post
Pre
Post
Pre
Post
MeV H
GAPDH

After this period, surface bound dextran was removed by incubation with bleach buffer and cells were fixed and prepared for CLSM. MeV-infected cells were analysed by CSLM after fixation (**Fig.4-7A and B**) and showed a SLAM-specific increased uptake of the fluorescent dextran when compared to uninfected and PMA-treated cells (**Fig.4-7C** and **D**). In addition, the dextran's intracellular distribution was clearly more punctate, indicative of macropinosome formation (**Fig.4-7B;** white arrows). To assess the specific sub-cellular localization of internalised measles virus particles within dextran-positive vesicles, cells were synchronously infected with MeV (MOI=10), washed and incubated with dextran-containing medium at 37ºC for 15, 30, 45 and 60 min, prior to preparation for CLSM (**Fig.4-8A**). Internalized MeV N was shown to be associated with dextran-containing vesicles at 30 and 45 min, followed by a reduction in co-localisation at 60 mpi (**Fig.4-8B**). Furthermore, to specifically address the role of SLAM in inducing fluid-phase uptake during MeV infection, I synchronously infected parental A549 cells (lacking the MeV receptor SLAM) or A549-SLAM cells (engineered to overexpress SLAM) with MeV particles and incubated with dextran-containing medium for 45 min at 37ºC (**Fig.4-9**). Dextran-uptake was significantly higher in infected A549-SLAM cells confirming the SLAM-specificity of our observations (**Fig.4-9A and B**).

Fig.4-7. MeV induces fluid-phase uptake upon entry. (**A**) A549-SLAM cells were synchronously infected with MeV (MOI=10) for 1h at 4ºC, washed in cold PBS and incubated at 37°C for 20min with DMEM containing 0.25mg/mL of Dextran Alexa Fluor-488 conjugate. Cells were then moved to ice, washed, bleached and fixed in 4% PFA. Samples were prepared for and analysed by CLSM. Representative micrographs of uninfected cells treated with 20% FBS-containing DMEM and MeV-infected cells and cells treated were recorded. (**B**) Quantification of internalised Dextran (pseudo-coloured green) was performed by calculating corrected total cell fluorescence based on mean fluorescence intensity (MFI). Scale bars are representative of 20um. Statistical analysis was performed using Student's t-test, *$p<0.05$.

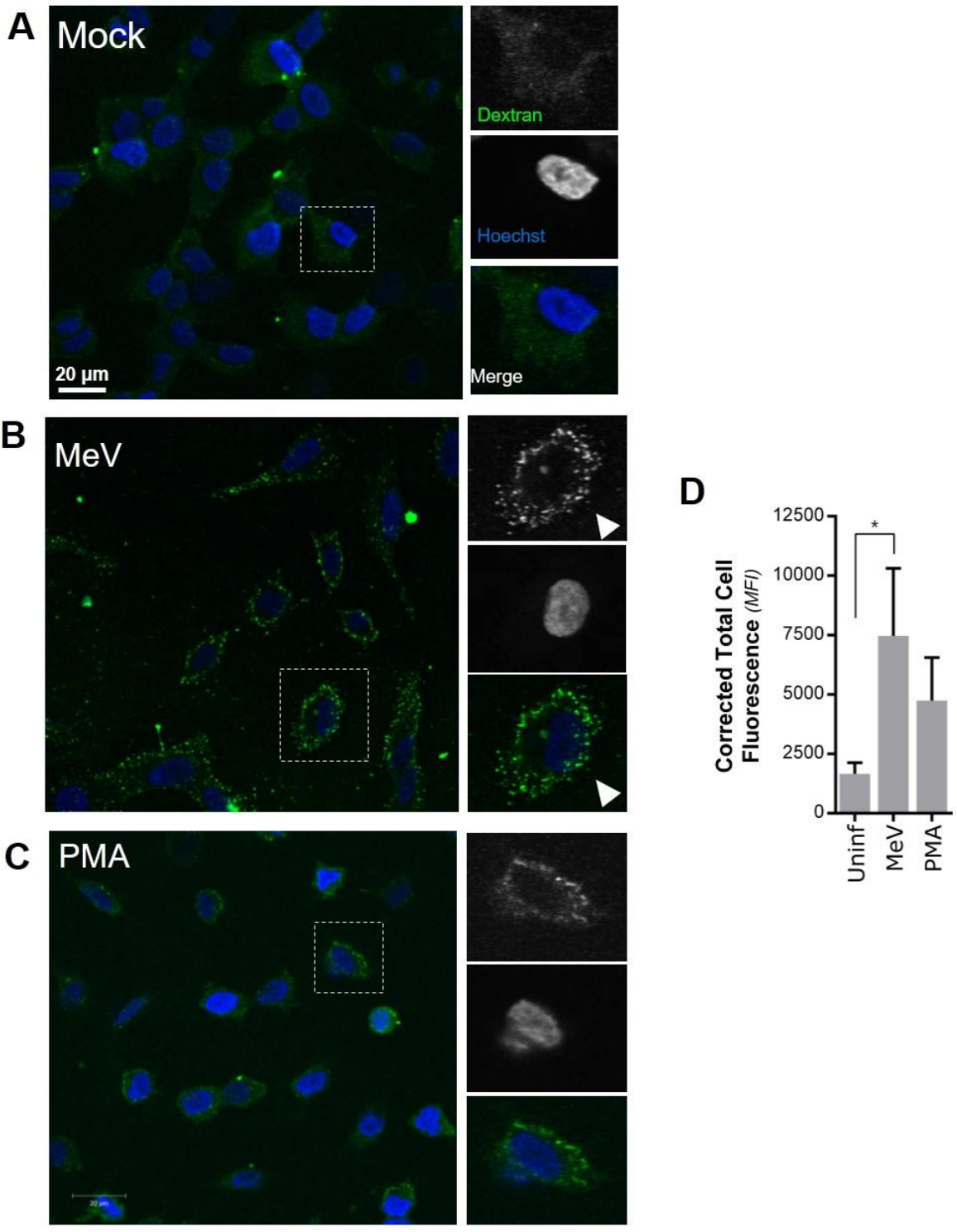
A
Mock
Dextran
Hoechst
Merge
20 µm
B
MeV
C
PMA
D
Corrected Total Cell Fluorescence (MFI)
12500
10000
7500
5000
2500
0
*
Uninf
MeV
PMA

Fig.4-8. Internalised MeV N colocalises with dextran-containing macropinosome-like structures. **(A)** In order to observed internalised MeV particles, A549-SLAM cells were synchronously infected with MeV (MOI=10), washed and incubated at 37ºC in dextran-containing PBS for the indicated time, fixed, prepared and analysed by CSLM. Dextran is showed in green while MeV N is pseudocoloured in red; arrows indicate co-localisation of N and dextran-positive vesicles, quantified in **(B)**. Scale bars are representative of 10um.

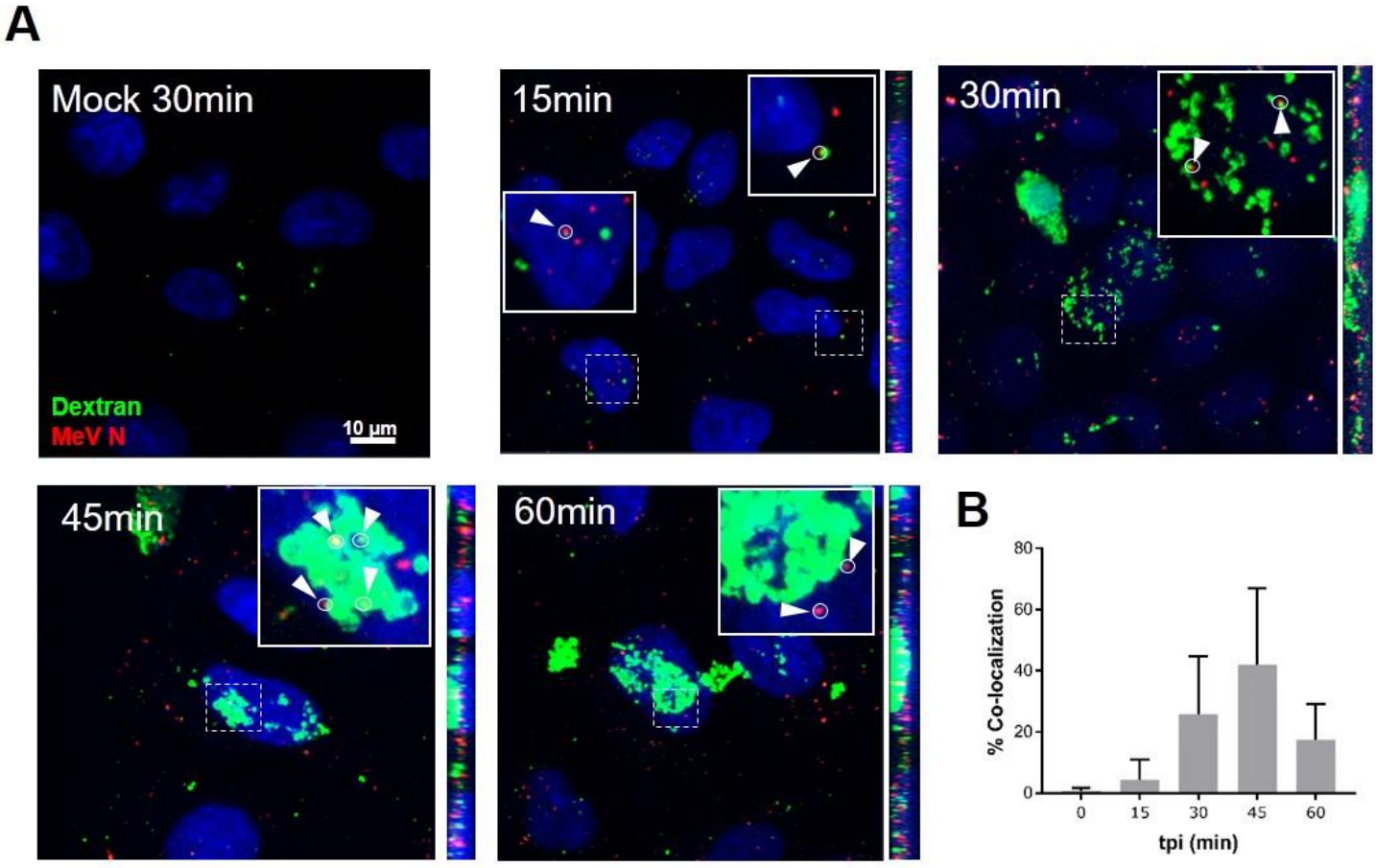
A
Mock 30min
Dextran
MeV N
10 µm
15min
30min
45min
60min
B
% Co-localization
0
20
40
60
80
0
15
30
45
60
tpi (min)

Fig.4-9. MeV-induced fluid-phase uptake is SLAM-specific. (**A**) To assess the role of SLAM in fluid-uptake during MeV-infection, A549 and A549-SLAM cell were synchronously mock- or MeV-infected (MOI=10), incubated with Dextran-containing PBS for 30min, fixed and analysed by CSLM. Bar represents 30µm. (**B**) Six representative micrographs of each condition was analysed and mean fluorescence intensity in the green channel was quantified and plotted. Student's t test *, $p<0.05$.

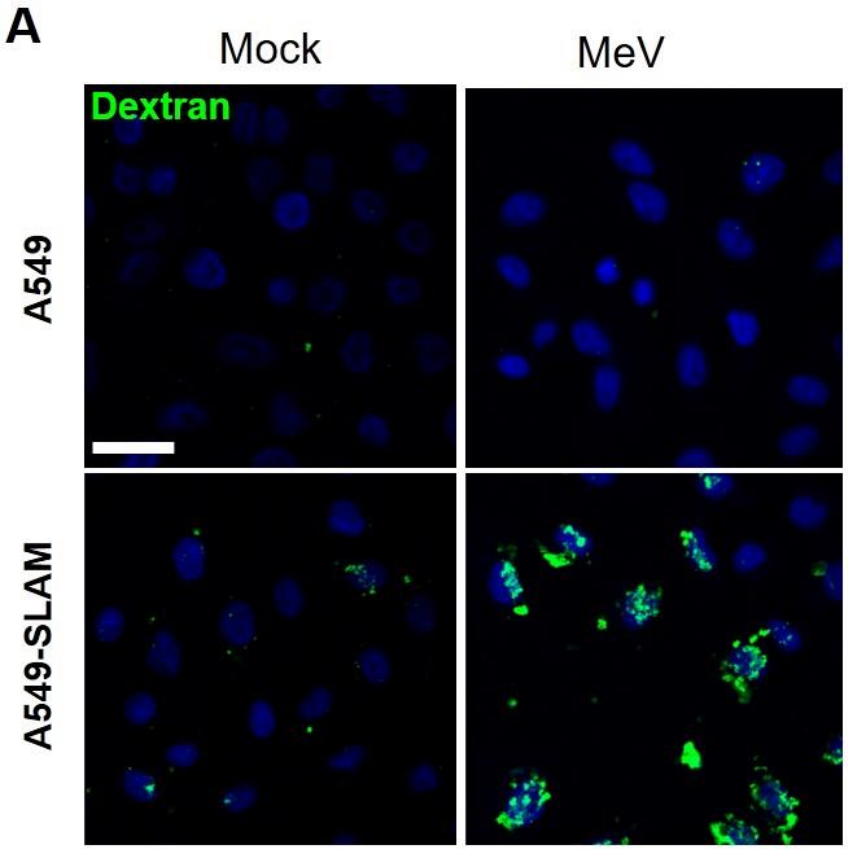
A
Mock
MeV
Dextran
A549
A549-SLAM

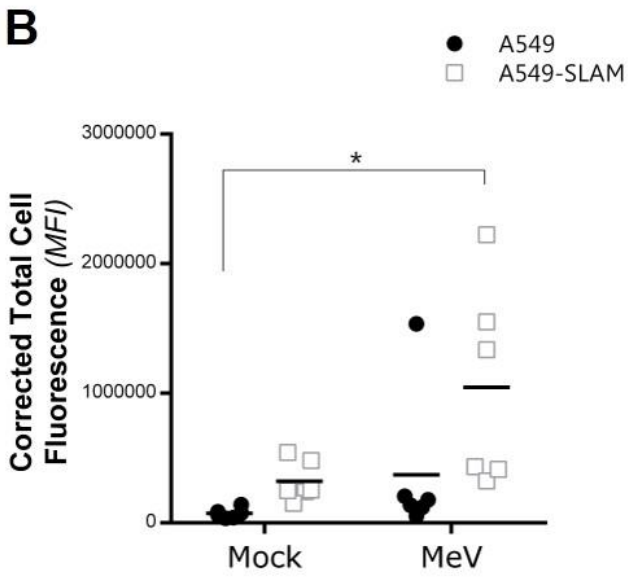
B
A549
A549-SLAM
3000000
2000000
1000000
0
*
Corrected Total Cell Fluorescence (MFI)
Mock
MeV

Treatment of cells with the amiloride analogue 5-(*N*-ethyl-*N*-isopropyl) amiloride (EIPA), a compound that selectively blocks the formation of macropinosomes [401], reduced

infection with MeV-PP (**Fig.4-10A**). Efficiency of EIPA in blocking fluid-uptake was assessed prior to MeV infections (see **appendix section A-4**). When cells were pre-treated with EIPA, infected with MeV and analysed by flow cytometry at 6.5h post-infection, MeV infection was reduced in a dose dependent manner (**Fig.4-10B**). Interestingly, when infected cells were analysed by western blot 24hpi, EIPA had an effect following both pre- and post-treatment, suggesting that its effect could be related not only to the immediate steps of MeV entry but possibly also on the stability of MeV H (**Fig.4-10C**). Nevertheless, our results highlight a critical role for the process of macropinocytosis in MeV-particle entry.

4.5 MeV induces actin rearrangements during entry.

Fundamental to the formation of membrane blebs and the capture of extracellular fluid via macropinocytosis is a dynamic actin network located at the cortex of the cell, on the inner face of the plasma membrane [402]. Using standard phalloidin-based actin staining techniques I examined the rearrangement of this cortical actin cytoskeleton during MeV entry. MeV (MOI=15) was bound to A549-SLAM cells at 4°C, washed and cells were incubated for 0, 20 or 60 min at 37°C prior to fixation and staining with phalloidin (**Fig.4-11A**). Cell contraction was observed, particularly at the cell periphery (**inset Fig.4-11A**) where partial loss of attachment led to the formation of multiple podosomes. Analysis of total cell area, based on measurement of the visible cell surface stained with actin, also demonstrated these cells were significantly

Fig.4-10. MeV infection is sensitive to EIPA. (**A**) MeV- or VSV-PPs were incubated for 3h with A549-SLAM cells pre-treated with 25µM of EIPA and incubated in complete medium. Luciferase activity was measured 72h later. (**B**) A549-SLAM cells were pre-treated with EIPA and infected with MeV (MOI=1) at the indicated concentrations, before being trypsinised and incubated for an additional 6.5h. Cells were then detached with 2mM EDTA solution and GFP-fluorescence was analysed by flow cytometry. (**C**) Cells were either pre- or post-treated with EIPA at indicated concentration, infected with MeV (MOI=1), trypsinised and incubated for 24h. After that period, whole cell lysates were generated and resolved on an SDS-PAGE gel prior to western blotting using a polyclonal antibody raised against the cytoplasmic tail of MeV H. Statistical analysis was performed using Student's t-test, *$p<0.05$, **$p<0.01$.

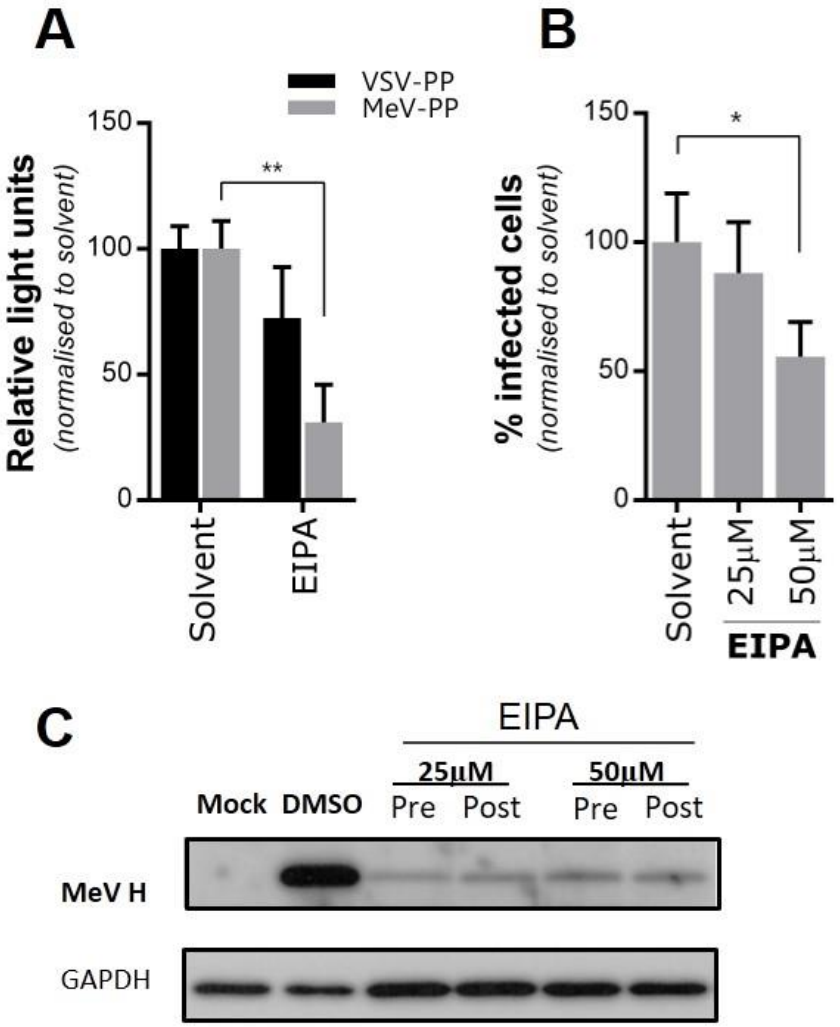
A
VSV-PP
MeV-PP
Relative light units
(normalised to solvent)
150
100
50
0
**
Solvent
EIPA
B
% infected cells
(normalised to solvent)
150
100
50
0
*
Solvent
25µM
50µM
EIPA
C
EIPA
25µM
50µM
Mock
DMSO
Pre
Post
Pre
Post
MeV H
GAPDH

Fig.4-11. MeV infection induces rapid but transient contraction of the cytoskeleton. (**A**) A549-SLAM cells were synchronously infected with MeV (MOI=15) for 1h at 4ºC or incubated with 20% FBS-DMEM under the same conditions (No virus). Cells were washed in cold PBS and incubated at 37ºC for 0, 10, 20 or 60min prior to fixation with 4% PFA, staining with phalloidin-TRITC (pseudocoloured in white) and analysis by CSLM. Details of the edge of cells are highlighted in selected area. (**B**) The average cell area (in pixel units) of individual cells was calculated based on representative micrographs of each condition using ImageJ (see **chapter 2 section 2.9.3**). Statistical analysis was performed using Student's t-test, *$p<0.05$.

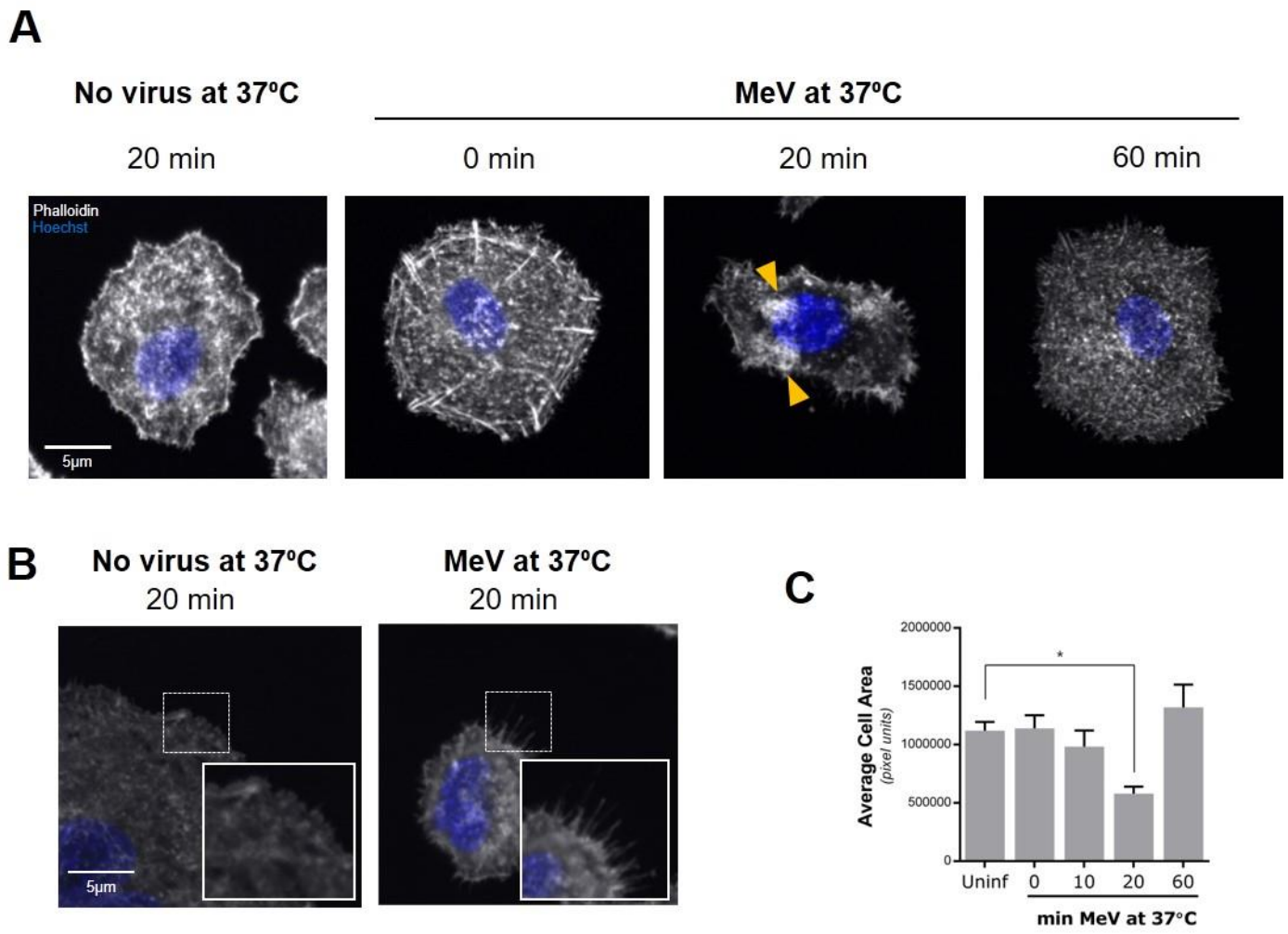
A
No virus at 37ºC
MeV at 37ºC
20 min
0 min
20 min
60 min
Phalloidin
Hoechst
5µm
B
No virus at 37ºC
20 min
MeV at 37ºC
20 min
5µm
C
Average Cell Area
(pixel units)
2000000
1500000
1000000
500000
0
*
Uninf
0
10
20
60
min MeV at 37°C

($p<0.05$; t-test) contracted relative to uninfected cells (**Fig.4-11B**). These modifications were transient and cells recovered normal morphology by 60 mpi (**Fig.4-11C**). As before, I assessed the specific role of SLAM in the MeV-induced actin cytoskeleton contraction. A549 and A549-SLAM cells were infected with MeV, incubated for 20 min at 37ºC and the surface area analysed as before (**Fig.4-12A and B**). Contraction of the actin cytoskeleton was significantly higher in infected A549-SLAM when compared to A549 cells. To evaluate the localisation of MeV particles within these cytoskeletal modifications, I synchronously infected A549-SLAM cells (MOI=10) and incubated at 37ºC for 0, 15, 30 or 60 mpi prior to preparation for CLSM (**Fig.4-13**). Interestingly, MeV N was shown to be associated with actin before internalisation (blue arrows, inset 0 min), presumably as actin is present inside the MeV particle, as reported previously [391]. At 15 min, MeV N was associated with actin enriched domains (blue arrow, 15 min) and at 30 min it was frequently found at the base of actin-enriched membrane structures resembling membrane blebs (blue arrows, inset 30 min). At 60 mpi, MeV N was no longer associated with actin and cells presented a cytoskeletal morphology similar to that of mock-infected cells (**Fig.4-13,** 60 min). Based on these findings I then evaluated whether a responsive and dynamic actin network is required for efficient viral entry, using a panel of well-characterised chemical inhibitors. MeV entry was shown to be sensitive to both cytochalasin D, an inhibitor of actin polymerization, and jasplakinolide, a promoter of actin polymerization (**Fig.4-14A**). Efficiency of these drugs in altering the cytoskeleton were confirmed by immunofluorescence prior to MeV infection (see **appendix section A.5**).

Fig.4-12. MeV induced cytoskeletal contraction is SLAM-specific. (**A**) To assess the role of SLAM in inducing the contraction of the cytoskeleton during MeV-infection, A549 and A549-SLAM cell were synchronously mock- or MeV-infected (MOI=10), incubated at 37ºC for 30min, fixed and analysed by CSLM. Bar represents 30µm. (**B**) Six representative micrographs of each condition were analysed and the average cell area was calculated and plotted. Statistical analysis was performed by applying Student's t tests. *, $p<0.05$; **, $p<0.01$.

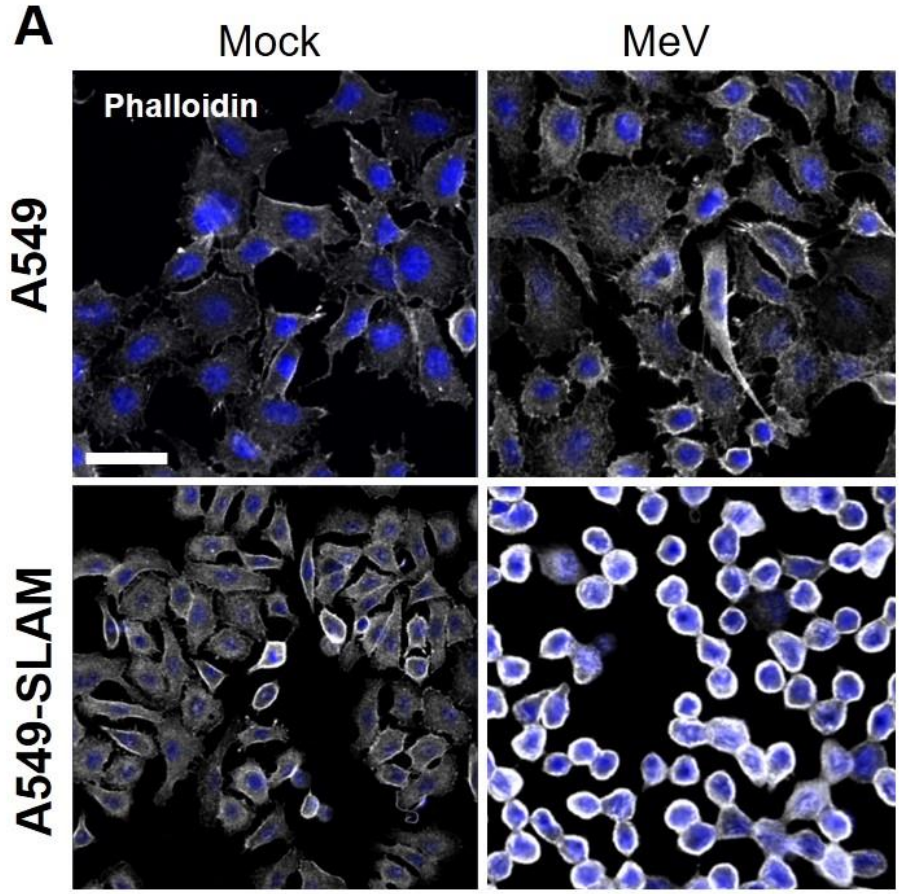
A
Mock
MeV
Phalloidin
A549
A549-SLAM

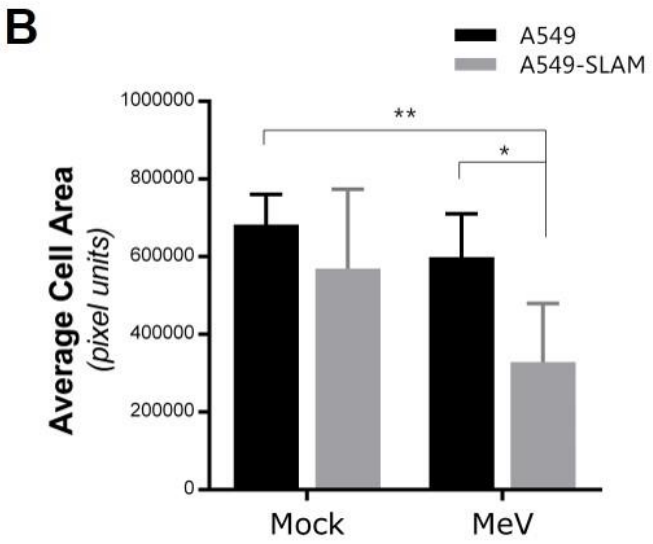
B
A549
A549-SLAM
Average Cell Area
(pixel units)
1000000
800000
600000
400000
200000
0
**
*
Mock
MeV

Fig.4-13. MeV N colocalises with actin-rich domains upon entry. A549-SLAM cells were synchronously infected with MeV (MOI), incubated at 37ºC for 0, 15, 30 or 60min, fixed and prepared for CSLM. Blue arrows represent co-localisation of MeV N (in red) and actin (white). Scale bars are representative of 10µm.

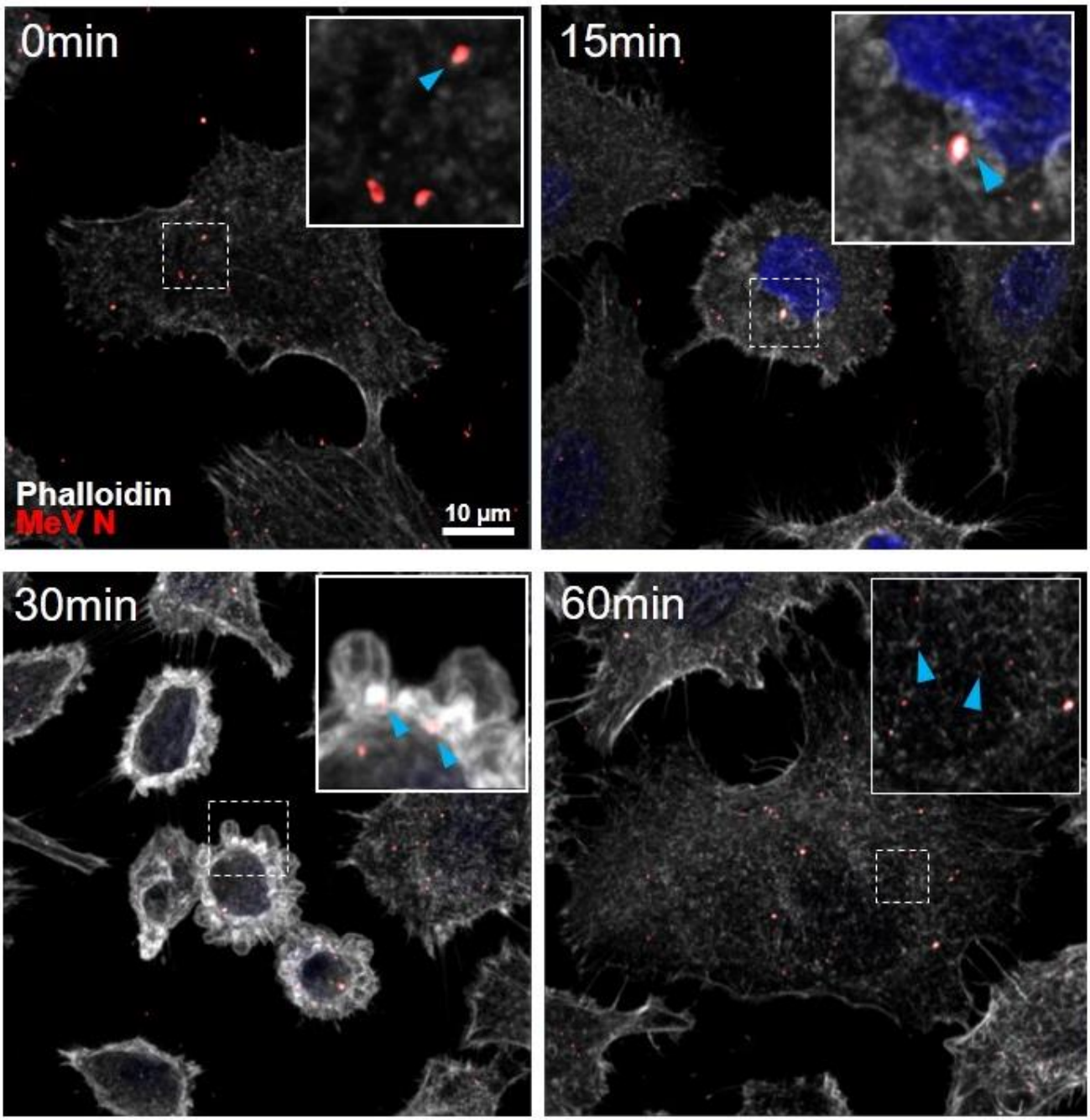
0min
15min
30min
60min
Phalloidin
MeV N
10 µm

Fig.4-14. MeV infection is sensitive to pharmacological inhibitors that target actin and microtubule dynamics. (**A/B**) A549-SLAM cells were pre- or post-treated with the indicated concentrations of cytochalasin D or jasplakinolide in relation to infection with MeV (MOI=1). Total cells lysates were generated 24h post infection and resolved on a 15% SDS-PAGE gel prior to western blotting using a polyclonal antibody raised against the cytoplasmic tail of MeV H. Densitometry analysis of western blot bands was performed and it represented in the figure. Ratio between area beneath peak of MeV H and GAPDH bands, normalised to DMSO. (**C**) In similar experiments A549-SLAM cells were pre-treated with 30μM of latrunculin A (LatA), 200μM of CK-666 Arp2/3 complex inhibitor, 5μM of wiskostatin (Wisk), 5μg/mL of nocodazole (Noco) or 5μM of taxol and infected with MeV (MOI=1). Total cells lysates were generated 24h post infection and resolved on a 15% SDS-PAGE gel prior to western blotting using a polyclonal antibody raised against the cytoplasmic tail of MeV H.

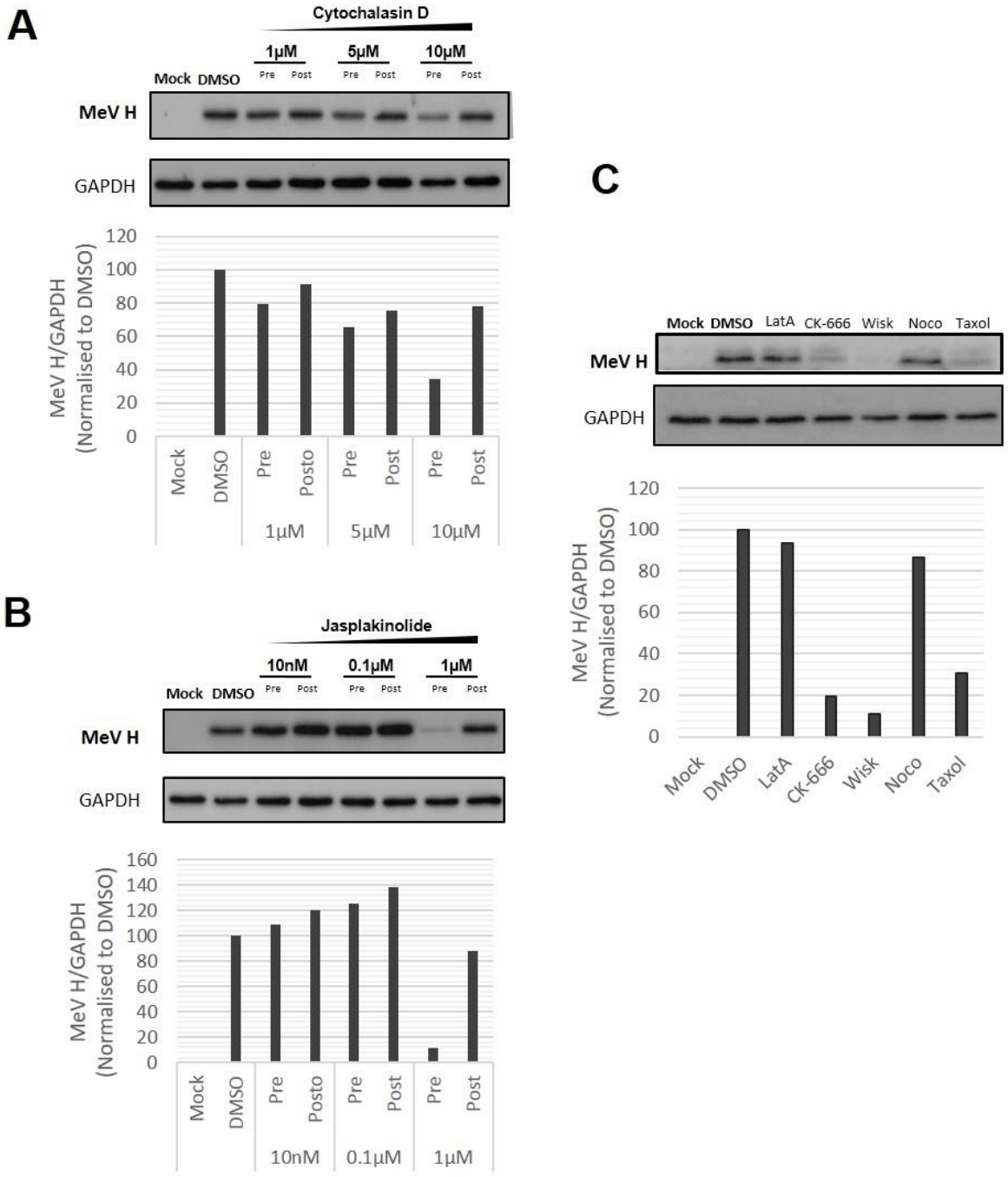
A
Cytochalasin D
1μM
5μM
10μM
Pre
Post
Mock
DMSO
MeV H
GAPDH
MeV H/GAPDH
(Normalised to DMSO)
120
100
80
60
40
20
0
Mock
DMSO
Pre
Posto
Pre
Post
Pre
Post
1μM
5μM
10μM
B
Jasplakinolide
10nM
0.1μM
1μM
Mock
DMSO
MeV H
GAPDH
MeV H/GAPDH
(Normalised to DMSO)
160
140
120
100
80
60
40
20
0
Mock
DMSO
Pre
Posto
Pre
Post
Pre
Post
10nM
0.1μM
1μM
C
Mock
DMSO
LatA
CK-666
Wisk
Noco
Taxol
MeV H
GAPDH
MeV H/GAPDH
(Normalised to DMSO)
120
100
80
60
40
20
0
Mock
DMSO
LatA
CK-666
Wisk
Noco
Taxol

Furthermore, MeV infection was also shown to be sensitive to inhibitors of related cytoskeletal components including CK-666, that inhibits the Arp2/3 complex, and wiskostatin, a Wiskott-Aldrich syndrome protein (WASP) inhibitor (**Fig.4-14B**). Both factors are involved in the branching of the actin cytoskeleton and contribute to the rigidity of plasma membrane structures [403]. In contrast, latrunculin A (LatA), an alternative inhibitor of actin polymerization, failed to block infection. Contrasting results were also observed when I analysed a role for microtubules in MeV entry. In these experiments treatment with nocodazole (noco) or taxol, which promotes or stabilizes microtubule formation, respectively, were shown to have opposed results. Together these results demonstrated that reorganization of the cytoskeleton was essential for establishing MeV infection; however, the exact dependence on specific components of the cytoskeleton and related regulatory pathways remains to be determined.

4.6 MeV entry is dependent on Rac1, RhoA, and, to a lesser extent, Cdc42 and PAK-1.

To identify specific pathways involved in MeV entry I therefore focused on the established cellular regulators of intracellular actin dynamics. Like many actin-dependent processes occurring at the plasma membrane macropinocytosis requires phosphatidylinositol-3-kinase (PI3K) and is orchestrated by the activation of small Rho GTPases, particularly Rac1 and Cdc42 [321]. I hypothesised that other GTPases including RhoA, not thought to be necessary for the induction of macropinocytosis, may also be involved as their presence mechanistically underpins the generation of membrane blebs [404].

To individually examine the roles of these factors I transfected cells with constructs expressing DN or constitutively active (CA) mutants of these proteins and subsequently infected them with MeV-PP or MeV. Entry of MeV-PPs in cells expressing DN forms of these Rho GTPases was significantly lower ($p<0.01$; t-test) when compared to cells transfected with an empty plasmid, but CA forms had no effect (**Fig.4-15A**). Similarly, MeV infection was reduced in cells expressing the same DN Rho GTPases (**Fig.4-15B**). In addition, when the Cdc42-specific inhibitor ML141 was used to pre-treat cells, infection was only modestly affected (**Fig.4-15C**); however, when using H-1152, an inhibitor of the Rho-associated protein kinase 1 (ROCK1), an effector of RhoA, MeV-PP entry was significantly ($p<0.01$; t-test) reduced (**Fig.4-15D**). In the context of MeV infection, H-1152 reduced measles virus infection when cells were treated pre-infection (**Fig.4-15E**). These results suggest that multiple Rho GTPases are required for MeV entry, particularly RhoA and Rac1 and to a lesser extent Cdc42. I also examined downstream effectors involved in macropinocytosis including p21-activated kinase-1 (PAK-1), a protein activated by Rac1 and Cdc42 and involved in macropinosome formation. Cells transfected with a CA form of PAK-1 were slightly more permissive to MeV PP and virus infection (**Fig.4-16A and B**). Similarly, siRNA knock-down of PAK-1 or inhibition via treatment with IPA-3 modestly affected MeV infection (**Fig.4-16C and D**), suggesting only a partial requirement for PAK-1 in MeV entry

Fig.4-15. MeV infection is dependent on the activities of Rac1 and RhoA. (**A**) A549-SLAM cells were transfected with constructs encoding myc-tagged dominant negative (DN) mutants (Rac1 N17, RhoA N19 and Cdc42 N17) or GFP-tagged constitutively (CA) active forms (Rac1 L61, RhoA L63 and Cdc42 L61) of the indicated RhoGTPases. Cells were then transduced with MeV-PP and the luciferase activity measured 72h later. (**B**) Similarly, cells were transfected with the same constructs, infected with MeV (MOI=1) and incubated for 24h. Infected cells were quantified under UV-microscopy. (**C/D**) A549-SLAM cells were pre-treated with the Cdc42 inhibitor ML141 or ROCK inhibitor H-1152 at the indicated concentrations for 5h before infection with MeV- or VSV-PP. Luciferase activity was measured 72h later. (**C**) A549-SLAM cells were pre- or post-treated with the indicated concentrations of H-1152 in relation to infection with MeV (MOI=1). Total cells lysates were generated 24h post infection and resolved on a 15% SDS-PAGE gel prior to western blotting using an antibody raised against MeV H. Student's t test, **, $p<0.01$, n.s. non-significant.

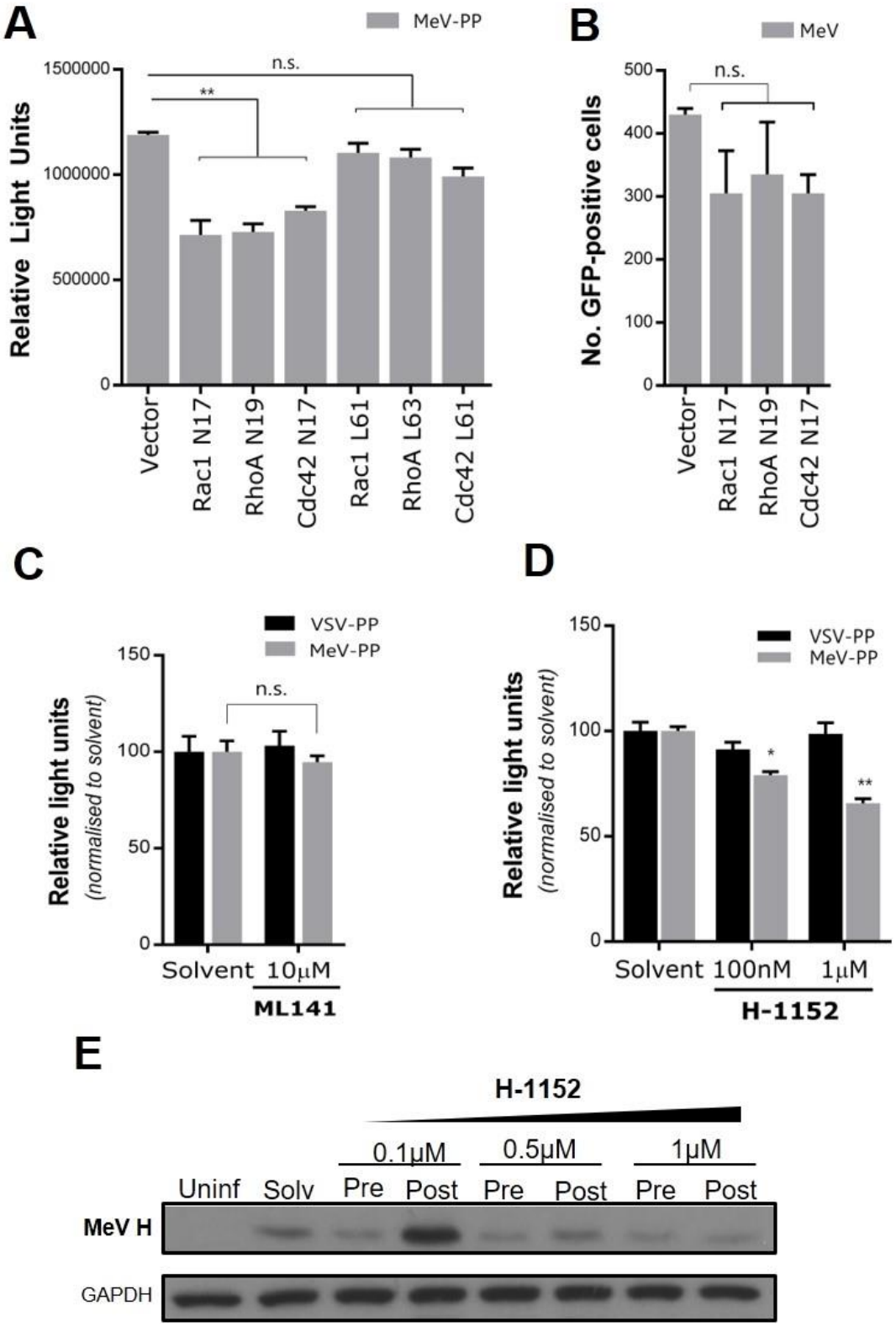
A
MeV-PP
Relative Light Units
1500000
1000000
500000
0
n.s.
**
Vector
Rac1 N17
RhoA N19
Cdc42 N17
Rac1 L61
RhoA L63
Cdc42 L61
B
MeV
No. GFP-positive cells
500
400
300
200
100
0
n.s.
Vector
Rac1 N17
RhoA N19
Cdc42 N17
C
VSV-PP
MeV-PP
Relative light units
(normalised to solvent)
150
100
50
0
n.s.
Solvent
10μM
ML141
D
VSV-PP
MeV-PP
Relative light units
(normalised to solvent)
150
100
50
0
*
**
Solvent
100nM
1μM
H-1152
E
H-1152
0.1μM
0.5μM
1μM
Uninf
Solv
Pre
Post
Pre
Post
Pre
Post
MeV H
GAPDH

Fig.4-16. MeV infection is not strictly dependent on PAK-1 activity. (**A/B**) Cells were transfected with plasmid constructs encoding wildtype (WT) or a CA mutant of PAK-1 and either transduced with MeV-PP (A) or infected with MeV (MOI=1, B) before quantification by luciferase assay or under UV microscopy. **(C)** A549-SLAM cells were transfected with either random siRNA (control), siRNA targeting PAK-1 or carrier. Seventy-two hours later, cells were infected with MeV (MOI=1), incubated for 24h and lysed for western blot analysis. **(D)** A549-SLAM cells were pre- or post-treated with the indicated concentrations of IPA-3 in relation to infection with MeV (MOI=1), incubated for 24h and analysed by western blot. Student's t test, **, $p<0.01$, n.s. non-significant.

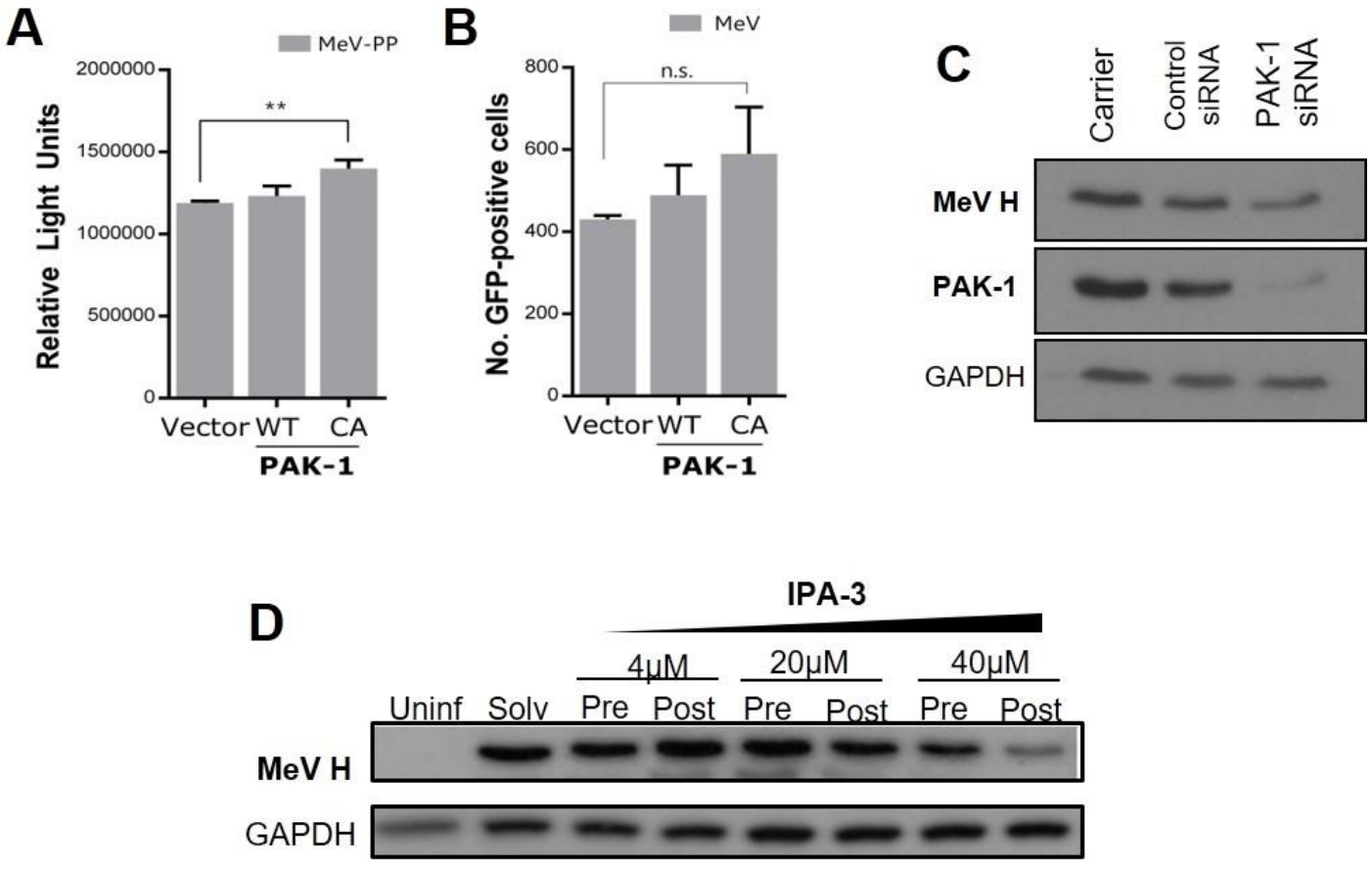
A
MeV-PP
Relative Light Units
2000000
1500000
1000000
500000
0
**
Vector
WT
CA
PAK-1
B
MeV
No. GFP-positive cells
800
600
400
200
0
n.s.
Vector
WT
CA
PAK-1
C
Carrier
Control siRNA
PAK-1 siRNA
MeV H
PAK-1
GAPDH
D
IPA-3
4μM
20μM
40μM
Uninf
Solv
Pre
Post
Pre
Post
Pre
Post
MeV H
GAPDH

4.7 MeV enters lymphocytes via a macropinocytosis-like mechanism.

SLAM/CD150-positive lymphocytes are key targets for MeV infection, particularly circulating and lymph-node resident B-cells [36]. A patient-derived immortalized lymphoblastoid B-cell line (LCLs) expressing endogenous levels of surface CD150 was identified from a selection of lymphocyte cell-lines by CD150 flow cytometry (a kind gift from Dr. Claire Shannon-Lowe; data not shown) and subsequently used as a physiologically relevant model for MeV entry. LCLs were synchronously infected with purified MeV (MOI~20) and observed under SEM (**Fig.4-17A**). Infected LCLs presented significantly more membrane blebs that uninfected cells ($p<0.005$; t-test); however, interestingly, no difference was observed in the proportion of cells with membrane ruffles, another common feature of macropinocytosis (**Fig.4-17B**). In subsequent experiments with the fluorescently labelled dextran I again observed that MeV-infected cells took up more extracellular fluid into large endosomal compartments when compared to uninfected cells (white arrows, **Fig.4-17C**). Finally, when LCLs were pre-treated with our previously established inhibitors of MeV entry, MeV infection was reduced by cytochalasin and blebbistatin and to a lesser extent EIPA (**Fig.4-17D**).

Fig.4-17 – MeV enters lymphocytes via macropinocytosis-like mechanism. (**A**) LCLs were synchronously infected with MeV (MOI~20) or uninfected with 20% FBS-containing DMEM, before fixation in 2.5% glutaraldehyde, preparation and visualisation by SEM. (**B**) Images were blinded and representative micrographs were subsequently used to quantify membrane blebs and membrane ruffles. Statistical analysis was performed using Student's t-test, ****p<0.001; n.s., non-significant. (**C**) LCLs were attached to a glass coverslip, synchronously infected with MeV (MOI~20) and incubated with DMEM containing 0.25mg/mL of Dextran Alexa Fluor-488 conjugate. Cells were moved to ice, washed, and fixed in 4%PFA before analysis by CLSM. (**D**) LCLs were pre-treated with 2.5µM of cytochalasin D (CytoD), 25µM of EIPA or 25µM of blebbistatin (Blebb) and infected with MeV (MOI=1). Total cells lysates were generated and resolved on a 15% SDS-PAGE gel prior to western blotting using a polyclonal antibody raised against the cytoplasmic tail of MeV H.

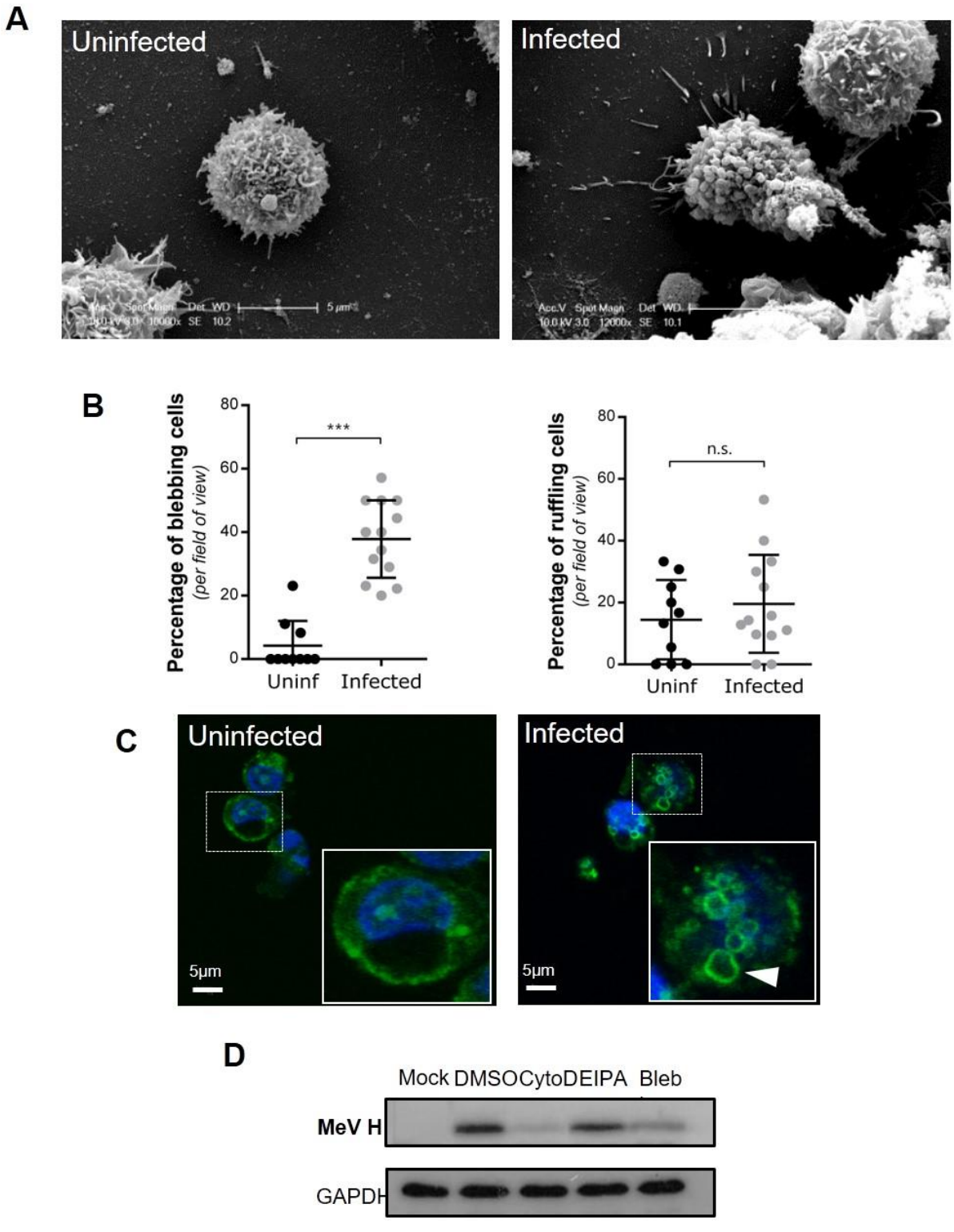
A
Uninfected
Infected
B
Percentage of blebbing cells
(per field of view)
***
Uninf
Infected
Percentage of ruffling cells
(per field of view)
n.s.
Uninf
Infected
C
Uninfected
Infected
5μm
5μm
D
Mock DMSO CytoD EIPA Bleb
MeV H
GAPDH

4.8 Discussion

My initial experiments characterising the sensitivity of incoming MeV glycoproteins to trypsin, together with my pseudoparticle data ruling out clathrin and caveolin-mediated endocytosis, led me to investigate macropinocytosis as a potential entry pathway for this virus. As such I investigated a number of characteristic features of this pathway including gross morphological changes, fluid uptake, cytoskeletal modification and Rho GTPase involvement.

The formation of membrane blebs, ruffles and filopodia at the plasma membrane are typical features of macropinocytosis. Our experiments demonstrated a SLAM- and MeV- specific activation of these features, particularly membrane blebs, upon virus attachment to cells; however, it remains unclear if collapse of these blebs leads to direct virus internalisation or alternatively if the virus “surfs” on these structures directing particles to the correct site of internalization [405]. A recent review on virus entry has highlighted the role of immunoglobulin-like domains, found in molecules such as SLAM, in driving pathogens to the correct site of entry [406], and although evidence is fairly limited, this could explain the extensive formation of filopodia-like structures I also observed.

Another critical characteristic of macropinocytosis is the uptake of large amounts of extracellular fluid into cells. Viruses that induce macropinocytosis are commonly found inside resulting macropinosomes, often remaining there until membrane penetration is triggered and the virus genome is released into the cytosol. Our experiments showed that MeV also induces a significant uptake of extracellular fluid and that incoming MeV particles associate with fluorescent-dextran positive macropinosomes. However, I observed that association with these labelled

endosomes is lost within 60 min, perhaps indicating the rapid escape of MeV genome into the cell, discussed in more detail below.

Actin rearrangements in the cell's cortical cytoskeleton are absolutely essential for efficient macropinocytosis [402, 407]. Our results showed that when actin dynamics were abrogated by a range of drugs, MeV entry was inhibited. In addition, I observed that MeV infection induced the profound rearrangement of the cytoskeleton and that particles directly associated with these arrangements. This was reflected in changes to the cell's overall morphology (cells contracted and became rounded) and the loss of adhesion sites. Similarly dramatic morphology changes were observed with Kaposi's sarcoma-associated herpesvirus (KSHV), Vaccinia and ASFV [408-410] and this is generally seen as a major feature of virus entry via macropinocytosis [321].

Macropinocytic rearrangements are controlled by a range of cellular factors. This requirement is highlighted by the sensitivity of macropinocytosis to blebbistatin and EIPA, two drugs that are commonly used to inhibit this pathway and were shown to inhibit MeV entry in our experiments. Blebbistatin blocks the action of the non-muscle myosin-II, a protein involved in the formation of ruffles and blebs [398, 411] while EIPA is a potent inhibitor of the Na^+/H^+ ATPases located at the plasma membrane. Accordingly, other viruses known to enter cells via macropinocytosis are inhibited by these drugs, e.g. RSV and Vaccinia virus [195, 408, 409].

The sensitivity of MeV, and other macropinocytosed viruses, to these chemical inhibitors is linked to key cellular regulators that coordinate the actin cytoskeleton during macropinocytosis, in particular Rho GTPases. For instance it is believed that changes in submembranous pH are the activation signal for Cdc42 and Rac1, and that EIPA prevents macropinosome formation by interfering with this process [401].

Interestingly, our results using a range of Rho GTPases mutants and inhibitors suggest a dependency on the activity of not only Rac1 and Cdc42, but also RhoA. RhoA is not generally perceived as being related to macropinocytosis; however, there is evidence for a role in the formation of membrane blebs [404].

The added requirement for RhoA and the observation that particle entry relies heavily on the formation of membrane blebs is an intriguing observation. These discrepancies build on the idea that macropinocytosis might not be just one single pathway, but rather an umbrella term for several endocytosis mechanisms for fluid internalization with distinct, yet overlapping, phenotypes and mechanisms [399, 412]. A RhoA/Rac1-dependent endocytosis mechanism was first described in the internalisation of the interleukin-2 receptor [413]; however, despite the observation that MeV particles co-localised with a small number of Dyn2 positive particles it would appear MeV entry is dynamin-independent, since it is insensitive to the specific inhibitor dynasore as well as dominant negative mutants. However, there are other viruses that enter via macropinocytosis where dynamin is also not required, for instance Vaccinia virus [414] and RSV [195]. In fact in some studies of the same virus, there is contradictory evidence for the role dynamin plays in entry [415-417]. Another interesting observation was the differing sensitivity of MeV entry to EIPA in A549-SLAM and LCL cells. This may indicate a degree of cell-type specificity within macropinocytosis and highlights MeV as a useful tool for future characterisation of this phenotype. It is also worth highlighting that the MeV cellular receptor I have investigated, SLAM (specifically SLAMF1), has recently been characterised as a microbial sensor that regulates phagocytosis in macrophages [210]. During this process it is thought that the cytoplasmic tail of SLAM interacts with Beclin-1,

recruiting a class III PI-3 kinase (PI3KC3) that generates phosphatidylinositol-3-phosphate (PI3P): a powerful signalling molecule involved in membrane rearrangement, cell motility and protein sorting [418]. This fits with the uptake of a range of pathogens (bacteria and viruses) that occur in a receptor-dependent manner [419-421]. To my knowledge the role of the cytoplasmic tail of SLAM in MeV entry has not yet been thoroughly investigated and it will be interesting to correlate how closely the atypical macropinocytosis of MeV particles correlates with SLAM-mediated bacterial phagocytosis.

Until recently, paramyxovirus genome entry into the cell was assumed to occur immediately after direct fusion of the virus particle envelope with the plasma membrane [380, 394]. The major argument for this theory is that triggering of the paramyxovirus fusion protein is pH-independent; a process that leads to extensive syncytia formation during *in vitro* passage of these viruses. In this model the particle remains at the cell surface without internalisation; however, in recent years several studies on paramyxovirus entry, i.e. RSV, NDV, Sendai virus and Nipah, have shown that these virions are actually endocytosed [195, 325, 394]. Our data now demonstrates that MeV particles are also internalised; however, it should be noted that the two processes are not necessarily mutually exclusive. It is possible that activation of the F protein is still initiated at the plasma membrane, but that this process is synchronous with particle endocytosis, unlike RSV where proteolytic activation of the F protein must take place in the macropinosome before the ribonucleocapsid can escape [195]. The changing environment of the maturing macropinosome could therefore play a role in pore expansion, rather than F activation allowing RNP escape into the cytoplasm. In this sense it was interesting to

observe that nucleocapsid co-localisation with fluorescent dextran was lost within 60 min of MeV-particle uptake. These discussions also highlight the difficulty in experimentally distinguishing a whole virus particle from a single oligomeric complex of F and H. MeV particles are large (up to 1 μm) and their size, shape and density of glycoprotein packaging may be a key additional factors in the stimulation of endocytic uptake.

In summary I have described a novel entry pathway for MeV that has major hallmarks of macropinocytosis. This adds MeV to the growing list of pathogens that are taken up by this pathway. Given their ubiquitous use of SLAM/CD150 as an entry receptor [16] these findings are also likely to apply to the other morbilliviruses, e.g. canine distemper and peste des petits ruminants viruses. This research therefore expands the potential for antiviral targeting of these viruses through the identification of novel pathways and host factors involved in infection.

Chapter 5

EARLY STAGES OF MEASLES VIRUS-INDUCED CELL-CELL FUSION ARE CONTROLLED BY RHO GTPASES AND MOESIN

Viruses have evolved a variety of ways to disseminate within the host. Viral spread centres on how virions, or infected cells, interact with uninfected, susceptible cells. Enveloped negative-stranded RNA viruses assemble into viral particles carrying one or more copies of the viral genome enclosed by a lipid envelope embedded with membrane proteins. These envelope proteins regulate particle entry via interaction with a variety of cellular plasma membrane proteins or ligands, known as cellular receptors. These glycoprotein-receptor interactions are key to establishing infection, since viruses have evolved several mechanisms to induce their uptake and internalisation by the host.

In the previous chapter, I demonstrated that MeV particles can be endocytosed by SLAMF1^{+} cells using a mechanism that resembles macropinocytosis, the internalisation of the IL-2 receptor and the mechanotransduction pathway. Alongside cell-free particle infection MeV can infect neighbouring cells by inducing cell-cell fusion that leads to the formation of multinucleated giant cells (known as syncytia); cells which are commonly observed both *in vitro* [95] and *in vivo* [295, 422]. This cell-associated transmission is an efficient and rapid mechanism to aid viral dissemination [423] and evade the adaptive humoral immune response [380]. Cell-cell fusion and syncytia formation may contribute to the exacerbation of pathogenesis *in vivo*. The eventual breakdown, detachment or death of these fused cells contributes to tissue damage and the severe pathological and inflammatory effects of viral infection [146, 424]. In addition persistent MeV infection in the brain and the expression of defective measles proteins leads to extensive cell-cell fusion and formation of plaques [46, 54, 425].

In tissue culture, the expression of MeV glycoproteins in permissive cell lines is sufficient to induce cell-cell fusion and formation of large syncytia. Indeed, this is a common feature among paramyxoviruses, which encode fusion proteins that promote the fusion of the plasma membranes of two cells. The fusion of membranes is a common process in the cell cycle, albeit occurring at a smaller scale, such as in the fusion of endosomes to lysosomes, or alternatively on a larger scale, with the fusion of myoblast in skeletal muscles, for example. Thermodynamically, the process of membrane fusion is associated with a high energy barrier and cells have evolved several families of proteins that reduce this energy barrier and assist membrane fusion [390, 426]. One such family are the SNARE proteins that promote the fusion of intracellular vesicles, such as endosomes, to other organelles like the Golgi apparatus or the plasma membrane [427]. The cellular interactions and molecular mechanisms underpinning physiological cell-cell fusion, e.g. the fusion of myoblasts, the generation of osteoclasts or trophoblasts, are not well understood [428]. Very few human cell proteins with fusogenic properties have been identified: the most striking example is employed during the formation of the placental syncytiotrophoblast. The formation of this layer of fused trophoblasts is dependent on the activity of endogenous retroviral fusion proteins called syncytin-1 and -2 [429-431].

As cell-cell fusion induced by MeV is likely to encounter a significant energy barrier at the point of membrane fusion, it is possible that MeV is hijacking previously unidentified membrane fusion cascades to overcome this energy barrier and promote viral spread by syncytia formation. An interesting observation that might be indicative of such manipulation is that viruses with defective cytoplasmic tails of H and F have enhanced cell-cell fusion activity [432]. The cytoplasmic tails of glycoproteins from

other paramyxoviruses have been implicated in the regulation of cell-cell fusion [433-436]. While paramyxovirus cell-cell fusion appears to be controlled, at some level, by the actin network [437], the involvement of the cytoskeleton in the establishment and expansion of the fusion pore has not been studied. Although MeV encoded N, M and L proteins are known to interact with the cytoskeleton [131, 132, 349], such interactions are not known for the two proteins that induce cell-cell fusion, MeV F and H. Understanding the early stages of MeV cell-cell fusion may impact on the design of new therapeutics and enhance our capacity to control disease progression in infected individuals. I will use my quantitative MeV F and H dependent cell-cell fusion assay to assess the role of several components of the cytoskeleton during stages of syncytia formation.

5.1 MeV-induced cell-cell fusion does not induce membrane blebbing

Previously I demonstrated that attachment of MeV to SLAMF1^{+} cells leads to extensive rearrangement of the plasma membrane, and the formation of membrane blebs. I speculated that this phenotype is dependent on the interaction of H with its receptor SLAMF1 via the myosin-II-RhoA-ROCKI axis, which is also involved in mechanotransduction processes. To evaluate if MeV-induced cell-cell fusion induce similar rearrangements of the plasma membrane, I infected A549-SLAM cells with recombinant MeV (MOI~1) expressing EGFP or, alternatively, mock-infected cells. After wide-spread virus-induced syncytia was observed, these monolayers were co-cultured with non-infected A549-SLAM cells (in suspension) for 30 min at 4ºC, washed in PBS and incubated for 30 or 60 min at 37ºC, prior to fixation and preparation for SEM (**Fig.5-1**). Monolayers of non-infected cells presented some

filopodia-like structures at the plasma membrane, as observed previously, but overall demonstrated a smooth cell surface (**Fig.5-1A**, non-infected, inset). In contrast, the surface of infected cells contained several additional structures, including small buds (**Fig.5-1A**, infected, blue arrows), possibly nascent MeV egressing from the cell. However, co-culture of uninfected A549-SLAM with MeV-infected cells did not induce observable membrane rearrangements in these cells after either 30 or 60 min of incubation (**Fig.5-1B**), contrasting with my previous findings with cell-free MeV entry into SLAMF1^{+} cells.

5.2 MeV-induced cell-cell fusion is restricted by the actin network

Since MeV-induced cell-cell fusion did not generate similar macropinocytosis-like plasma membrane structures in uninfected A549-SLAM cells, I investigated other cellular mechanisms that might potentially control cell-cell fusion. This was performed using the quantitative cell-fusion assay, described in **chapter 3, section 3.1**. In brief, plasmids encoding the MeV F and H proteins were transfected into HEK293T 'effector' cells expressing half of a dual-split reporter (an inactive form of *Renilla reniformis luciferase* and *EGFP*). A separate population of 'target' cells was generated expressing the MeV receptor SLAMF1 and the complementary part of the *RLuc* and *EGFP* reporter protein. Forty-eight hours post-transfection, target and effector cells were co-cultured. When the fusion processes started, the cytosolic content of these cells mixed, allowing the complementary parts of RLuc and EGFP to assemble and become functional (**Fig.5-2A**). Luciferase activity was then measured at several times following this initial point of co-culturing to monitor cell-cell fusion.

Fig.5-1. MeV-induced cell-cell fusion does not induce membrane blebbing. (**A/B**) A549-SLAM were infected with MeV (MOI~1) and incubated at 37°C for 48h, when large syncytia were observed (**A**). A549-SLAM cells were then co-cultured with infected or non-infected monolayers at 4°C for 30min, washed and further incubated at 37°C for 30 or 60min. Cells were then fixed and prepared for scanning electron microscopy (**B**) (n=1 with 1 technical replicate).

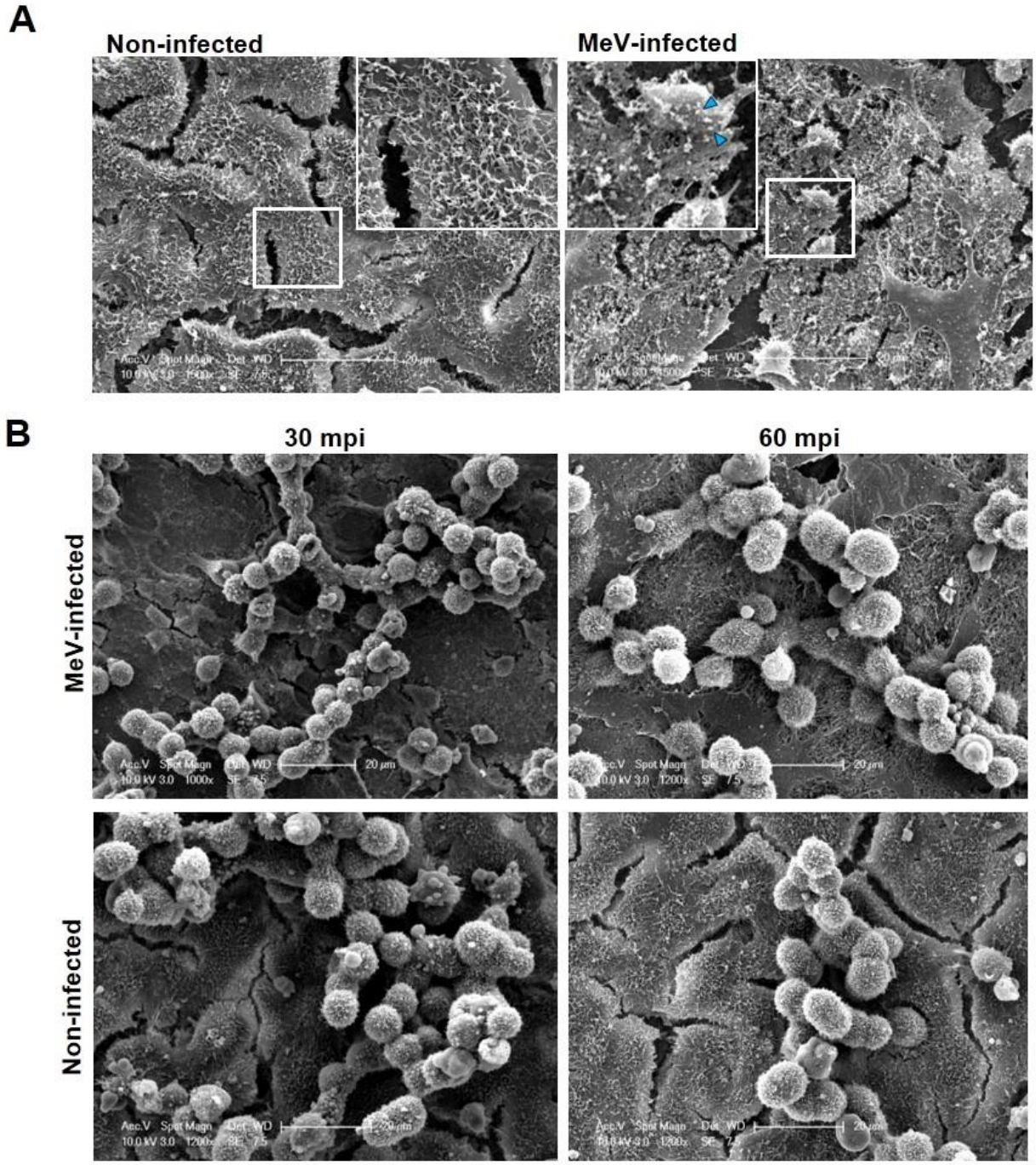
A
Non-infected
MeV-infected
B
30 mpi
60 mpi
MeV-infected
Non-infected

Fig.5-2. MeV-induced cell-cell fusion is restricted by the actin network. (**A**) Schematic representation of the fusion assay. Target cells, expressing SLAMF1, and effectors cells, expressing MeV F and H, each carrying a complementary part of the dual-split reporter EGFP-Renilla luciferase, are co-cultured. (**B**) Effector cells carrying full-length MeV F and H or cytoplasmic tail mutants (MeV FΔ30 and HΔ24) were co-cultured with SLAMF1-positive target cells. Luciferase activity was measured at the indicated times post co-culture (tpc) (n=2 with 4 technical replicates). As a control, effector cells were co-cultured with target cells lacking the expression of SLAMF1; luciferase activity was measured and subtracted to related SLAMF1-expressing co-cultures at indicated timepoints. (**C/D**) Effector cells carrying full-length MeV F and H were co-cultured with target cells and incubated for 90 min. At this time, cytochalasin D (5µM, CytoD), jasplakinolide (1µM, Jasp), wiskostatin (25µM, Wisk), griseofulvin (25µM, Griseo), nocodazole (10µg/mL, Noco) or taxol (1µM) were added and incubated for further 30 min prior to measurement of luminescence (n=3 with 5 technical replicates). All values were normalised to solvent (Solv, DMSO) treated cells which absolute RLUs were 9822±178 in **C** and 8662±449 in **D**, while negative control RLU was 838±102. Statistical analysis was performed using Student's t test; *,$p<0.05$; **,$p<0.01$, ***$p<0.001$.

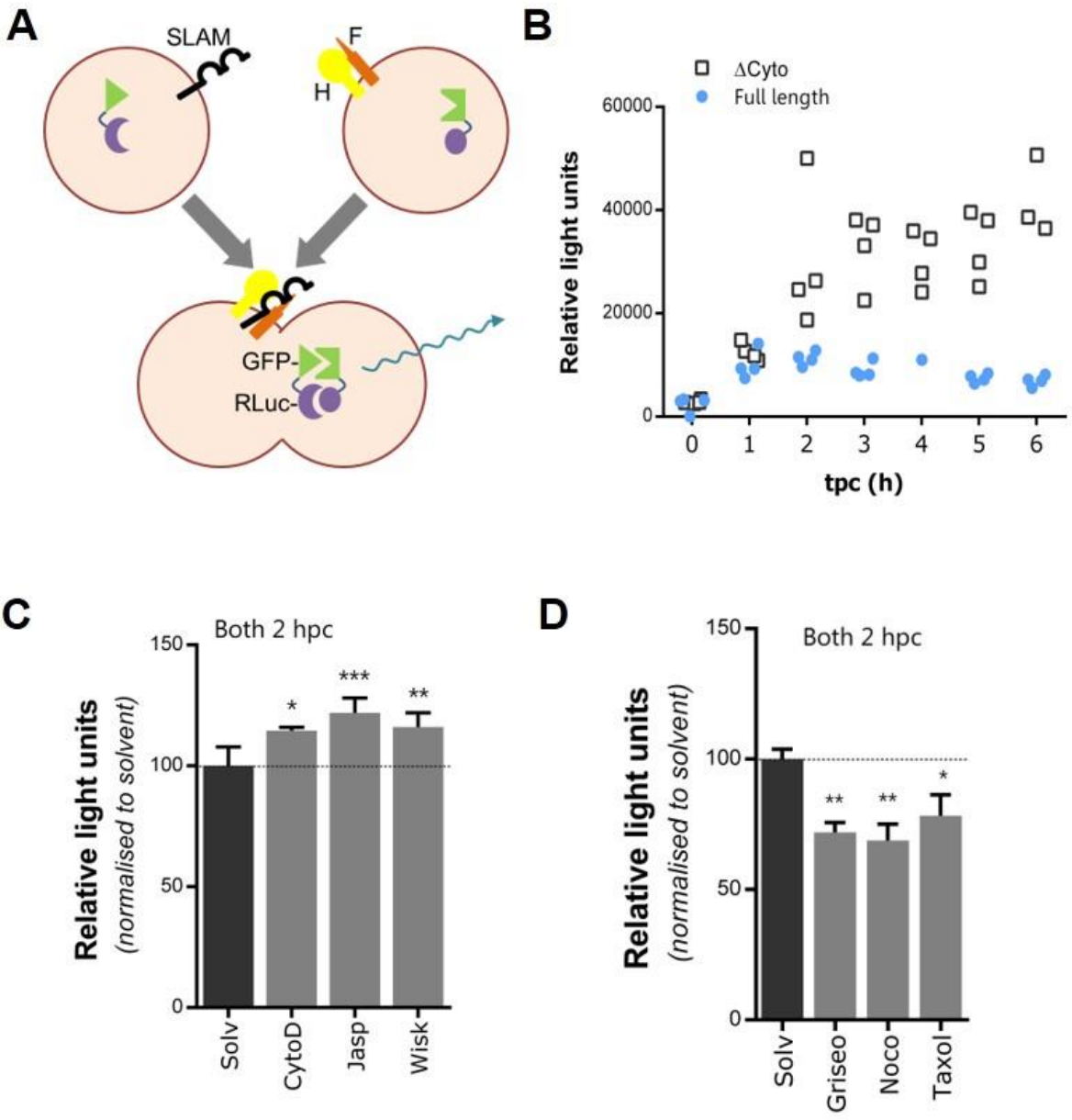
A
SLAM
F
H
GFP-
RLuc-
B
ΔCyto
Full length
Relative light units
60000
40000
20000
0
0
1
2
3
4
5
6
tpc (h)
C
Both 2 hpc
Relative light units
(normalised to solvent)
150
100
50
0
*
***
**
Solv
CytoD
Jasp
Wisk
D
Both 2 hpc
Relative light units
(normalised to solvent)
150
100
50
0
**
**
*
Solv
Griseo
Noco
Taxol

As mentioned previously, MeV glycoproteins with defective cytoplasmic tails have enhanced fusogenic activity [432], with some researchers suggesting a possible interaction of these tails with the cytoskeleton [433]. By quantifying fusion in the first six hours after co-culture (hpc), I was able to observe the overall kinetics of fusion including the initial steps of membrane pore formation and later stages of pore expansion (**Fig.5-2B**). Interestingly, I observed that when cells were transfected with wild-type (full-length) MeV F and H and co-cultured with target cells, cell-cell fusion peaked at 2hpc, followed by a slow decrease. However, when effector cells were transfected with plasmids expressing MeV F and H with 30 and 24 amino acid cytoplasmic tail truncations, respectively, cell-cell fusion increased steadily post co-culture (**Fig.5-2B**).

Since wild-type and truncated MeV F and H induced similar cell-cell fusion at 2hpc but developed differently afterwards, I hypothesised an equivalent level of pore formation (occurring prior to 2hpc), but varied expansion of the fusion pore, a feature dependent on the cytoplasmic tails of F and H. Building on my earlier hypothesis that the cytoskeleton restricts pore expansion co-cultured cells were treated with drugs that: promote actin filament depolymerisation (cytochalasin D [438]), polymerisation (jasplakinolide [439]), or target actin branching (wiskostatin [440]) (**Fig.5-2C**). These experiments showed that abrogation of cytoskeleton dynamics increases cell-cell fusion induced by wild-type MeV GPs, when compared to solvent treated cells at 2hpc. Using the same approach with drugs that target the microtubule network - nocodazole (which promotes the stabilisation of microtubules [441]), taxol (a microtubule destabiliser [442]) and griseofulvin (which disrupts centrosomes [443]) – I observed that all reduced cell-cell fusion (**Fig.5-2D**). This suggested that although

actin filaments may work as a restriction to pore expansion, microtubule dynamics may be important to initialise cell-cell contact and in formation of the membrane pore. These data support my previous observation that the cytoplasmic tail mutants of F and H show enhanced fusion activity, an effect that may be due to the expansion of the fusion pore and rapid mixing of cytosolic content. Due to time limitations, I was not able to evaluate the effect of such inhibitors in the context of cell-cell fusion induced by the mutants lacking the cytoplasmic tails. It is clear, however, that interfering with cytoskeletal dynamics impacts on cell-cell fusion, providing evidence that the actin network at the cell's cortex restricts the expansion of nascent MeV-induced fusion pores.

5.3 Dynamin-2 contributes to MeV-induced cell-cell fusion

The cell cortex is a highly dynamic region where components of the cytoskeleton concentrate to interact with membranous elements, such as membrane proteins and phospholipids. In particular, the cortical actin network has been implicated in a myriad of cellular process, such as motility, immune activation and endocytosis. As mentioned previously, dynamin-2 (dyn2) is a GTPase involved in the scission of endosomes from the plasma membrane and is regarded as an important factor in endocytosis. However, in recent years, dyn2 has been shown to interact with cortactin and actin filaments and also appears to be involved in cortical actin dynamics via interactions with Arp2/3 complex [444]. Following on from my observations that actin dynamics at the cell cortex are important during cell-cell fusion, I assessed the role of this protein in the initial stages of MeV-induced fusion. Using the cell-cell fusion assay, in combination with a pharmacological inhibitor of dyn2, dynasore [445], I observed that cell-cell fusion was significantly reduced at

2hpc following perturbation of dyn2 (**Fig.5.3A**). To further examine the role of dyn2, I co-transfected effector cells with plasmids expressing wild-type (WT) or dominant negative (DN) K44A dyn2. As a control, I compared cell-cell fusion in cells co-transfected with a plasmid encoding only EGFP, since both WT and DN-dyn2 constructs are EGFP-tagged. Expression was confirmed by visualisation under fluorescence microscopy where approximately 70% of the cells were GFP-positive. Interestingly, the co-expression of these plasmids in effector cells resulted in an increase in cell-cell fusion, particularly with the DN mutant (**Fig.5-3B**). I hypothesised that over-expression of dyn2 WT or DN may affect turnover of plasma membrane proteins, including MeV F and H, since this protein is also involved in several recycling processes, therefore impacting on the sequestration of MeV H into pathways targeted for degradation [446] . When the total amount of MeV H produced in the context of dyn2 co-expression was analysed, I observed elevated MeV H expression with dyn2 DN. This suggests that MeV H might have a high level of steady-state turnover mediated by dyn2 (**Fig.5-3C**). Since a dyn2 inhibitor decreased cell-cell fusion and overexpression of a DN mutant of dyn2 increased fusion (and MeV H expression), it is likely that dyn2 plays multiple roles in this process. As a result, further experiments are required to elucidate the specific role of this GTPase. Although this chapter focuses on is the early stages of cell-cell fusion, I also examined the effect of overexpression of the dyn2 DN mutant on both target and effector cells in the context of cell-cell fusion (**Fig.5-3D**). In this fusion assay, MeV-based target or effector cells were co-transfected with dyn2 DN and co-cultured overnight. Interestingly, in this experiment effector cells transfected with dyn2 DN showed reduced cell-cell fusion, when compared to cells transfected with EGFP,

Fig.5-3. Dynamin-2 contributes to pore-formation. (**A**) Effector cells carrying full-length MeV F and H were co-cultured with target cells and incubated for 90 min. At this time, co-cultures were incubated with Dynasore at indicated concentrations for a further 30 min prior to measurement of luminescence. RLUs were plotted in relation to solvent (DMSO) treated cells that had an absolute value of 9822±178. (**B**) Effector cells were co-transfected with plasmids encoding a wild-type (WT) or dominant negative (DN, K44A) mutant of dynamin-2 (Dyn2). Cells were then co-cultured with target cells, incubated for 2h at 37ºC prior to measurement of the luciferase activity. RLUs were plotted in relation to GFP expressing cells that had an absolute value of 8722±578. Negative control values were subtracted to Dyn2 WT and DN co-cultures and plotted. (**C**) The effect of co-transfecting Dyn2 WT and DN mutants on the expression of MeV H was assessed by lysing effector cells and analysing MeV H by SDS-PAGE/western blot. (**D**) Effector cells or target cells co-transfected with a plasmid encoding Dyn2 mutant or pcDNA3.1 were co-cultured for 24 prior to assessment of luciferase activity (n=3 with 5 technical replicates). RLUs are plotted in relation to vector-transfected cells with absolute value of 48334±3666. Statistical analysis was performed using Student's t test; **,$p<0.01$, hpc, hours post-co-culture.

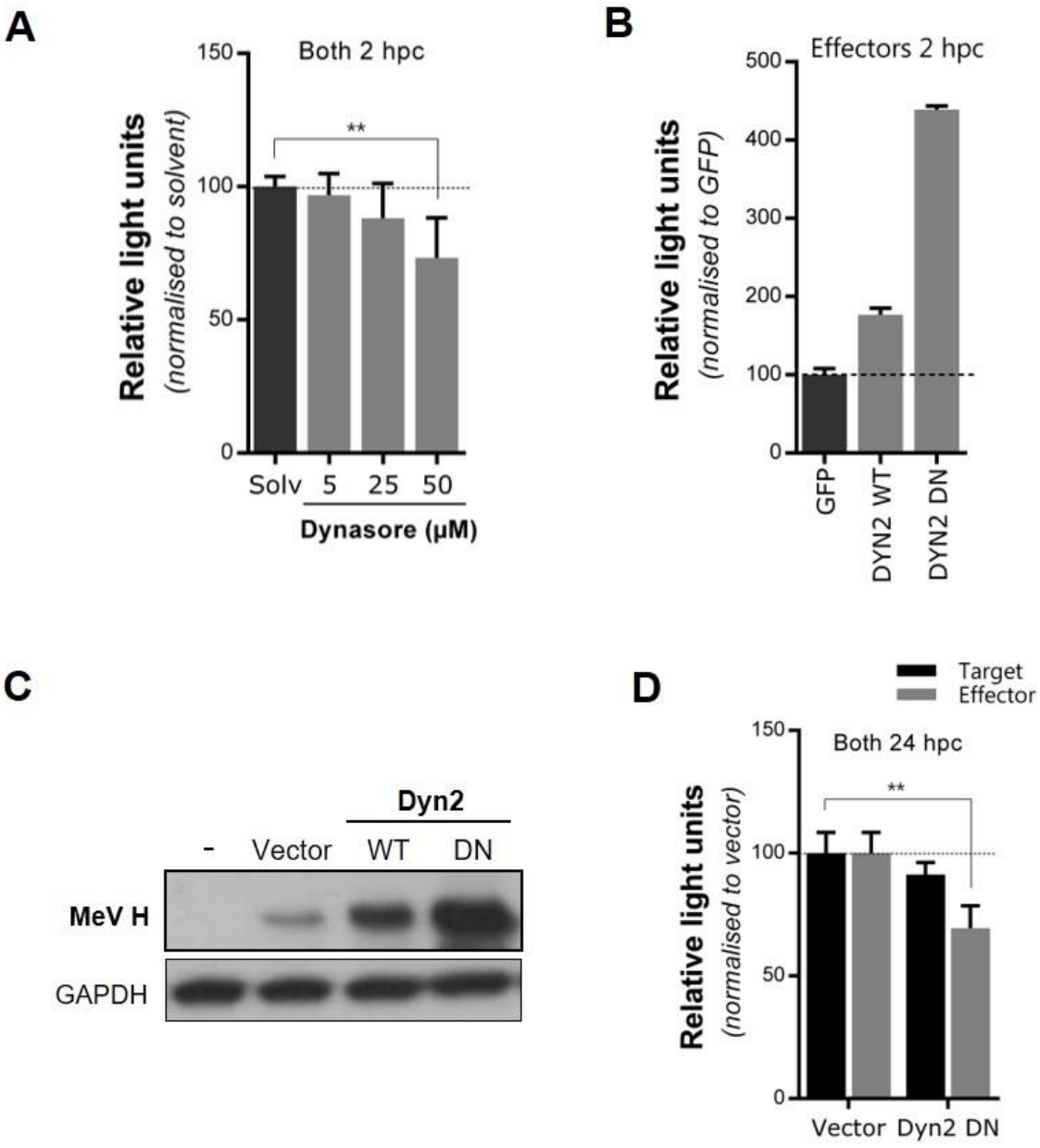
A
Both 2 hpc
Relative light units
(normalised to solvent)
150
100
50
0
**
Solv
5
25
50
Dynasore (μM)
B
Effectors 2 hpc
Relative light units
(normalised to GFP)
500
400
300
200
100
0
GFP
DYN2 WT
DYN2 DN
C
Dyn2
-
Vector
WT
DN
MeV H
GAPDH
D
Target
Effector
Both 24 hpc
Relative light units
(normalised to vector)
150
100
50
0
**
Vector
Dyn2 DN

while dyn2 appeared to have little effect on cell-cell fusion when transfected into target cells, suggesting a specific role of this protein in effector cells and not a general consequence of overexpression of these mutants in HEK293T. Altogether, these data provide evidence for a role for dyn2 in cell-cell fusion and MeV glycoprotein stability.

5.4 The activity of Rho GTPases modulate cell-cell fusion

The family of Rho GTPase proteins contains multiple members that mediate cytoskeleton organisation, impacting on cell motility, cell cycle progression and the vesicular trafficking system [447]. In particular, Rho GTPases tightly regulate the organisation of the cell cortex by orchestrating cytoskeletal rearrangement and the formation of specific micro-domains at the plasma membrane [448]. This family of proteins has also been implicated as being important in cell-cell fusion induced by other paramyxoviruses [449]. To assess the role of these proteins in the initial stages of MeV-mediated cell-cell fusion, effector cells were co-transfected with DN mutants of Rho GTPases, co-cultured with SLAMF1-expressing target cells and cell-cell fusion was assessed using a fusion assay (**Fig.5-4A**). The expression of DN mutants of RhoA, Rac1 and Cdc42 in MeV-effector cells dramatically increased cell-cell fusion in the two hours following co-culture, even though the total expression of MeV H remained relatively unaltered (**Fig.5-4B**). To further assess the role of these proteins in cell-cell fusion, we treated co-cultured cells with pharmacological inhibitors of Cdc42 (ML141) and the RhoA-associated kinase I (ROCKI), a downstream effector of RhoA (H1152) (**Fig.5-4C**). Interestingly, both inhibitors induced an increase in cell-cell fusion, particularly ML141 which targets Cdc42. As previously, I also evaluated

Fig.5-4. Rho GTPases are important in cell-cell fusion. (**A**) Effector cells were co-transfected with plasmids encoding dominant negative (DN) mutants of RhoA (N19), Rac1 (N17) and Cdc42 (N17). Cells were then co-cultured with target cells, incubated for 2h at 37ºC prior to the measurement of luciferase activity. RLUs were plotted in relation to GFP transfected cells which had an absolute value of 13124±836 (n=4 with 5 technical replicates). (**B**) The effect of co-transfecting these mutants on the expression of MeV H was assessed by lysing effector cells and analysing MeV H by SDS-PAGE/western blot. (**C**) Effector cells carrying full-length MeV F and H were co-cultured with target cells and incubated for 90 min. At this time, co-cultures were incubated with the ROCKI inhibitor H1152 or the Cdc42 inhibitor ML141 at the indicated concentration for a further 30 min prior to measurement of luminescence. RLUs were normalised to solvent (Solv, DMSO) treated cells that had an absolute value of 12282±422. (**D**) Effector cells or target cells co-transfected with plasmids encoding mutant Rho GTPases or pcDNA3.1 (vector) were co-cultured for 24 prior to assessment of luciferase activity. Statistical analysis was performed using Student's t test; **,$p<0.01$, ***,$p<0.001$, ****,$p<0.0001$ hpc, hours post-co-culture.

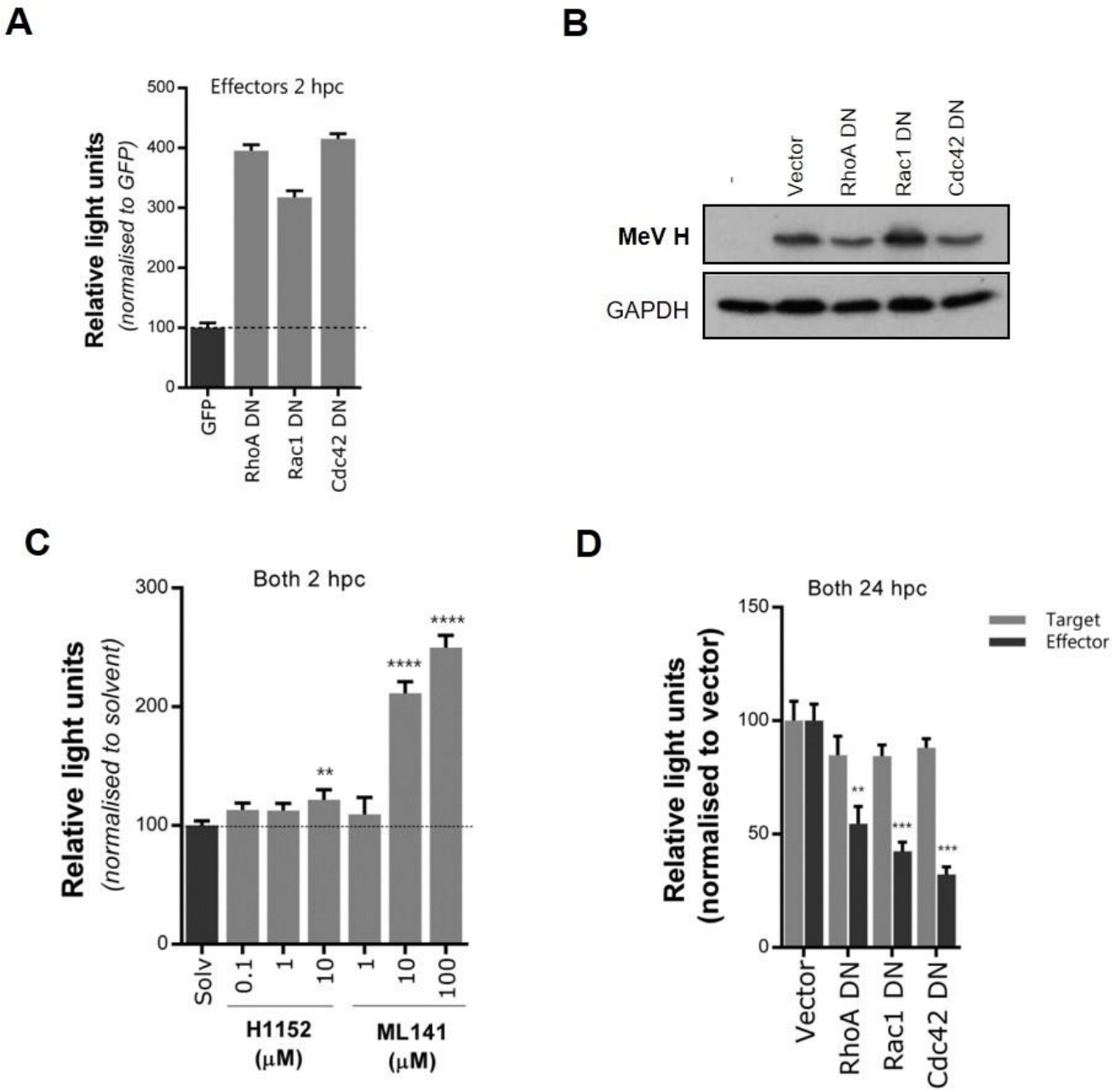
A
Effectors 2 hpc
Relative light units
(normalised to GFP)
500
400
300
200
100
0
GFP
RhoA DN
Rac1 DN
Cdc42 DN
B
Vector
RhoA DN
Rac1 DN
Cdc42 DN
MeV H
GAPDH
C
Both 2 hpc
Relative light units
(normalised to solvent)
300
200
100
0
**
****
****
Solv
0.1
1
10
1
10
100
H1152
(μM)
ML141
(μM)
D
Both 24 hpc
Target
Effector
Relative light units
(normalised to vector)
150
100
50
0
**
***
***
Vector
RhoA DN
Rac1 DN
Cdc42 DN

the effect of the DN Rho GTPase mutants (expressed in either target or effector cells) when cell-cell fusion was allowed to proceed for 24h post co-culture (**Fig.5-4D**). Although the DN mutants had little effect on fusion when expressed in target cells, these mutants significantly reduced cell-cell fusion when co-transfected with MeV glycoproteins, as observed elsewhere in similar assays with glycoproteins of Hendra and SV5 virus [449]. Altogether, these results suggest that inhibiting the activity of Rho GTPases impacts on the initial steps of cell-cell fusion.

5.5 Moesin regulates MeV-induced cell-cell fusion

Of particular importance to the organisation of microdomains within the plasma membrane is a family of proteins, known as the Ezrin/Radixin/Moesin (ERM(s)) family. ERMs function as cross-linkers between the plasma membrane and the actin cytoskeleton [450]. It has been observed previously that phosphorylated (activated) ERMs are components of the virological synapse between T lymphocytes and dendritic cells during MeV infection [266]. In a similar way, I hypothesised that ERMs might play role in the contextualization of the MeV fusion apparatus, i.e. in relation to the cytoskeleton and plasma membrane. I therefore examined the role of ezrin and moesin in the initial stages of cell-cell fusion. Initially, I observed that over-expression of MeV F and H in HeLa cells is sufficient to induce an increase in phosphorylated ERMs, particularly the lower molecular weight band that corresponds to the MSN protein (**Fig.5-5A**). In addition, phosphorylated ERMs also co-localised with MeV glycoproteins, when observed under confocal laser scanning microscopy (**Fig.5-5B**). A similar observation was made by Koethe *et al*. during MeV infection of immune cells. These data suggest that MeV glycoproteins can trigger the activation of ERMs and provide evidence for a role for these proteins in the MeV lifecycle. To further

Fig.5-5. Expression of MeV GPs promotes ERMs phosphorylation. (**A**) HEK293T cells were transfected with plasmids encoding wild-type MeV F and H or with pcDNA3.1 (vector). After 48h, cells were lysed and protein samples resolved in a SDS-PAGE gel; MeV H, ERMs or phosphorylated ERMs (P-ERMs) were subsequently analysed by western blot. (**B**) HeLa cells were transfected with HA-tagged MeV H and wild-type MeV F and incubated for 48h at 37ºC. Cells were then fixed, blocked in 1% BSA and incubated with antibodies specific for HA (Red) or phosphorylated ERMs (Green). Cells were then prepared for CLSM and observed by fluorescence microscopy. Scale bar is representative of 15µm.

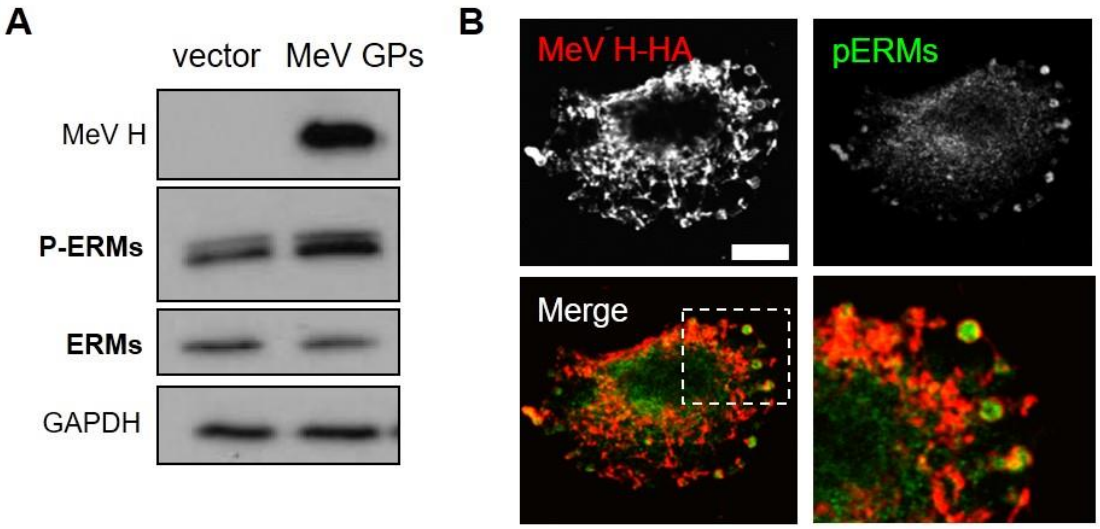
A
vector
MeV GPs
MeV H
P-ERMs
ERMs
GAPDH
B
MeV H-HA
pERMs
Merge

evaluate the involvement of ERMs in cell-cell fusion, constitutively active (CA) ezrin and moesin mutants were transfected into effector cells and their impact on MeV-induced cell-cell fusion was assessed as described previously (**Fig.5-6A**). Whilst the ezrin CA mutant had little effect on fusion, the moesin CA mutant significantly increased cell-cell fusion at 2hpc (**Fig.5-6A**). These constructs also impacted on the size of syncytia formed when co-transfected into Vero-SLAM cells with plasmids encoding the MeV glycoproteins (**Fig.5-6B**). These constructs did not, however, alter expression levels of MeV H (**Fig.5-6C**), suggesting the effect of MSN CA might perhaps be related to spatial organisation of MeV GPs at the plasma membrane. In reciprocal studies, I employed specific shRNA constructs to target EZR and MSN and knock-down endogenous expression of these proteins (**Fig.5-6E**). When these shRNAs were used to knock down EZR and MSN in effector cells, in the context of the fusion assay, MeV-induced cell-cell fusion was significantly increased in both cases (**Fig.5-6D**). Accordingly, MeV H expression in these effector cells was enhanced (**Fig.5-6F**). Since knockdown of ERMs has been implicated in the sequestration of plasma membrane proteins, such as the transferrin receptor [451], it is likely that ERMs, particularly moesin, are involved in controlling both turnover and organisation of MeV glycoproteins, ultimately impacting on the initial stages of cell-cell fusion.

5.6 MeV budding may be regulated by Rac1, ezrin and moesin

Canonical MeV exit is widely regarded to be through viral particle formation and budding from the cell, whilst cell-cell fusion has historically been considered an artefact of (1) receptor abundance on permissive cell lines used *in vitro* and (2) a

Fig.5-6. Moesin affects early stages of MeV-induced cell-cell fusion. (**A**) Effector cells were co-transfected with plasmids encoding constitutively active (CA) mutants of ezrin (EZR) or moesin (MSN). Cells were then co-cultured with target cells, incubated for 2h at 37ºC prior to the measurement of luciferase activity. (**B**) Vero-hSLAM cells were co-transfected with MeV F and H and EGFP, EZR CA-GFP or MSN CA-GFP. Cells were incubated for 48h at 37ºC, and prepared and observed by CLSM. The scale bar is representative of 20µm. (**C**) The effect of co-transfecting these mutants on the expression of MeV H was assessed by lysing effector cells at 48h post-transfection and analysing MeV H by SDS-PAGE/western blot. (**D**) Effector cells carrying full-length MeV F and H were transfected with shRNA constructs that target EZR and MSN mRNAs for degradation, incubated for 72h and co-cultured with target cells. Co-cultures were incubated for 2h prior to assessing luciferase activity. (**E**) Efficiency of EZR and MSN knock-down was confirmed by SDS-PAGE/western blot of lysed transfected cells. The white arrow indicates the predicted EZR and radixin (RDX) molecular weight, while the black arrow indicates MSN. (**F**) The effect of co-transfecting these shRNAs on the expression of MeV H was assessed by lysing effector cells at 72h post-transfection and analysing MeV H by SDS-PAGE/western blot. Statistical analysis was performed using Student's t test. *,$p<0.05$, **,$p<0.01$. hpc, hours post-co-culture.

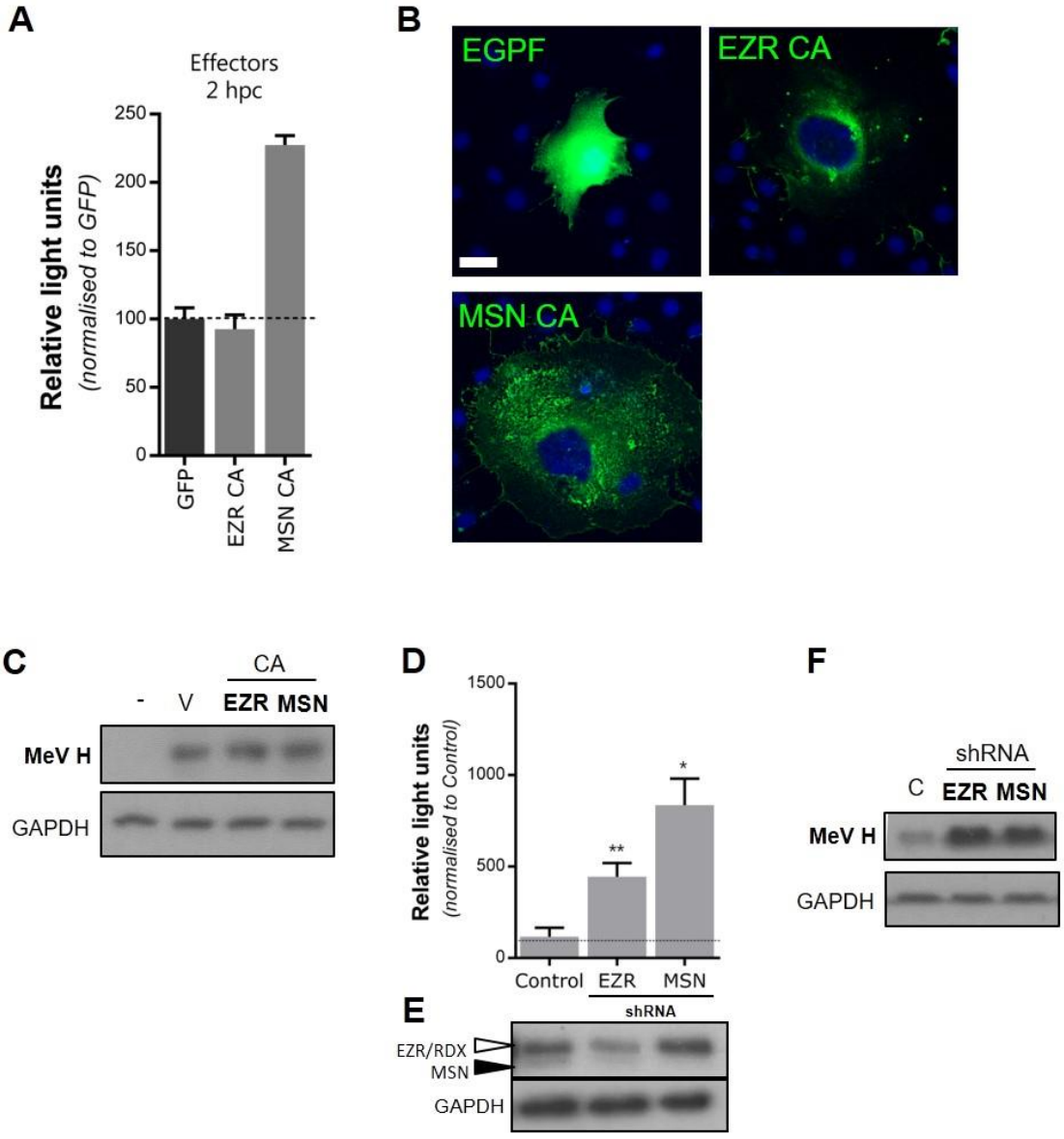
A
Effectors
2 hpc
Relative light units
(normalised to GFP)
250
200
150
100
50
0
GFP
EZR CA
MSN CA
B
EGPF
EZR CA
MSN CA
C
CA
-
V
EZR
MSN
MeV H
GAPDH
D
Relative light units
(normalised to Control)
1500
1000
500
0
**
*
Control
EZR
MSN
shRNA
E
EZR/RDX
MSN
GAPDH
F
shRNA
C
EZR
MSN
MeV H
GAPDH

result of the frequency of *in vitro* cell-cell contacts in a 2D monolayer of cells. In recent years, however, mounting evidence for MeV-induced syncytia *in vivo* [36, 295, 422] together with the elucidation of molecular mechanisms associated with cell-to-cell spread [423] has highlighted cell-cell fusion as a viable and important route in MeV transmission. Previously, I have demonstrated that certain cytoskeletal components impact upon cell-cell fusion induced by the viral glycoproteins, suggesting a complex mechanism underpinning this exit route. In particular the Rho GTPases and ERMs appear to be involved in the very early stages of MeV-induced cell-cell fusion. The immediate question that this raises is how the process of cell-cell fusion is distinguishable from MeV budding and how the virus balances the two processes. However, due to time-limitations, I was unable to thoroughly address this question. Nevertheless, using the budding assay developed in our laboratory and described in the **chapter 3, section 5**, I gathered some preliminary data on the impact of Rho GTPases and ERMs in MeV budding, mediated by the viral matrix (M) protein. Briefly, a plasmid expressing a fusion protein containing the MeV M protein and the firefly luciferase connected by a glycine-rich, flexible linker (M-Fluc) was transfected into HEK293T cells along with plasmids encoding DN mutants of Rho GTPases (**Fig.5-7A**), CA mutants of ezrin and moesin (**Fig.5-7B**) or ezrin- or moesin-specific shRNAs (**Fig.5C**). After 48h, supernatants were collected and M-Fluc-containing VLPs were pelleted by centrifugation through a 20% sucrose cushion. Respective pelleted lysates (SUP) and whole cell lysates (WCL) were generated from each transfection and the luciferase activity measured. Luciferase activity readings were then normalised to cells co-transfected with EGFP. The ratio between SUP values and WCL – that should reflect the amount of released VLPs in relation to total

Fig.5-7. MeV budding may be regulated by Rac1, ezrin and moesin. (**A/B/C**) HEK293T cells were co-transfected with a fusion construct described in **chapter 3 section 3.5** (M-Fluc) and plasmids encoding DN mutants of Rho GTPases (**A**), CA mutants of ezrin (EZR) and moesin (MSN) (**B**) or plasmids encoding shRNAs targeting EZR and MSN (**C**). Cells were then incubated for 48h at 37ºC, supernatants were collected, clarified by centrifugation and virus-like particles (VLPs) containing the fusion protein M-Fluc were pelleted through a 20% sucrose cushion in HBSS. Pellets were lysed and luciferase activity was measured. Statistical analysis was performed using Student's t test. *,$p<0.05$, ***, $p<0.001$, n.s., non-significant.

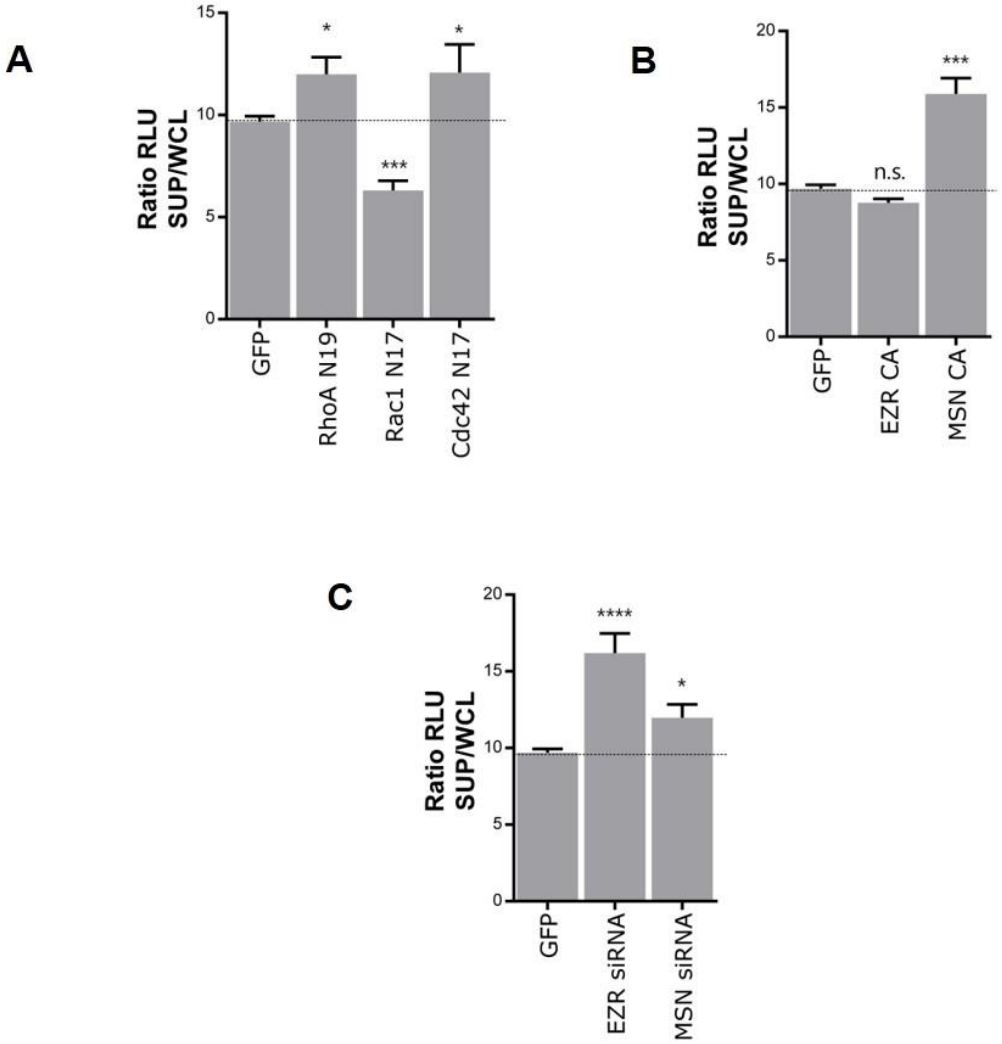
A
Ratio RLU SUP/WCL
15
10
5
0
*
*
***
GFP
RhoA N19
Rac1 N17
Cdc42 N17
B
Ratio RLU SUP/WCL
20
15
10
5
0
n.s.
***
GFP
EZR CA
MSN CA
C
Ratio RLU SUP/WCL
20
15
10
5
0
****
*
GFP
EZR siRNA
MSN siRNA

M-Fluc present in the cell – was significantly higher for co-expression of RhoA and Cdc42 DN mutants (**Fig.5-7A**). Interestingly, co-transfection with the Rac1 DN led to a substantial decrease in released VLPs and an increase in cell-associated or "retained" M-Fluc. This suggests that the activity of Rac1 might be important in MeV budding and directly contrasts with the observed increase in cell-cell fusion seen previously (**Fig.5-4A**). Moreover, when co-transfecting the M-Fluc construct with plasmids expressing ERMs CA mutants, expression of MSN CA led to an increase in released VLPs; however, no significant effect was observed after co-expression with EZR CA (**Fig.5-7B**). This observation is similar to the effect seen with MSN CA in the early stages of MeV-induced cell-cell fusion (**Fig.5-6A**). Finally, I assessed the specific role of endogenous ERMs by targeting ezrin and moesin with specific shRNA-encoding plasmids. The amount of released VLPs was substantially higher when ezrin in particular was knocked down (**Fig.5-7C**). MSN shRNA also increased the amount of released particles. To some degree these results mirror what was observed during MeV-induced cell-cell fusion (**Fig.5-5D**). Collectively these data suggest that although the activity of ezrin and moesin may play a role in MeV budding, the activity of Rac1 appears to be important in the release of MeV M-derived VLPs. Further experiments are required to confirm this dependence.

5.7 Discussion

Infection by MeV induces cell-cell fusion in various tissues, including lymph nodes, airway epithelia and the brain. This process relies on the interaction of MeV fusion machinery with cellular receptors, such as SLAMF1 and nectin-4. Since the activity of MeV F protein is independent of low pH, in contrast with other enveloped viruses

[452], it is commonly believed that fusion of the viral envelope with the plasma membrane at the moment of entry shares a common mechanism with the initial stages of cell-cell fusion. Nevertheless, the context in which these two events occur may differ.

My initial observation that the deletion of the cytoplasmic tails of F and H increases the kinetics of MeV-induced cell-cell fusion is evidence that MeV GPs-cytoskeleton interactions might restrict the progressive development of the fusion pore. It is unlikely that these differences in cell-cell fusion are due to altered protein expression since it has previously been shown that removing the cytoplasmic tail of morbillivirus F and H does not alter cell surface expression [453]. Previously it has been shown that MeV isolates recovered from patients suffering from SSPE, characterised by the formation of plaques of syncytiated cells in the brain, present mutations in their matrix protein and glycoprotein cytoplasmic tails, which impact on cell-cell fusion [425, 432]. It has been suggested that the increased fusogenicity of these viruses may be due to defective viral budding and the accumulation of viral glycoproteins at the plasma membrane, however, it is also possible that these mutations alter specific interactions with the cytoskeleton, therefore impacting on cell-cell fusion. Related viruses, such as PIV5 and RSV, have been shown to be sensitive to perturbation of cytoskeleton dynamics [437, 454]. My results show that abrogating actin dynamics with cytochalasin D and jasplakinolide very early in the fusion process, increases cell-cell fusion. This is in contrast with similar studies that looked at the effect of these drugs on long-term treatment and at later stages in cell-cell fusion [348]. Similarly, a restrictive role for the actin cytoskeleton in pore expansion was observed using exogenous fusogens, such as the baculovirus protein gp64 [455].

During physiological cell-cell fusion, such as the multinucleation of osteoclasts, an actin-enriched zipper-like structure is formed that regulates cell-cell fusion [456, 457]. Interestingly, this structure, and subsequent fusion of the two cells, has been shown to be sensitive to dynasore, a drug that targets dynamin GTPase [458]. My experiments show that short treatment with dynasore, during the initial stages of MeV-induced cell-cell fusion, reduced fusion suggesting a role for dyn2 in this process. In contrast, co-transfection of a DN dyn2 mutant into effector cells, increased cell fusion as well as the overall expression of MeV glycoproteins. Since this mutant has been show to impact on the sequestration and recycling of membrane receptors [459, 460], I hypothesised this increase in fusion might be due to the accumulation of viral glycoproteins, as a resulted of impaired turnover. Future experiments may examine the turnover or degradation of MeV F and H during a normal infection and its subsequent role in budding and fusion.

A role for Rho GTPases has been implicated in the cell-cell fusion induced by several viruses [449, 461, 462]. These studies support the theory that Rho GTPase activity promotes cell-cell fusion in the later stages of infection. Interestingly, the data presented here shows that the activity of Rho GTPases, particularly Cdc42, is deleterious to pore formation and expansion in the first moments of cell-cell fusion. It is plausible that interfering with Rho GTPase activity might result in the cortical actin network becoming less organised, alleviating the inherent restrictions to cell-cell fusion that this structure offers. Accordingly, a study has previously shown that inhibiting ROCKI in cancer cell lines increases MeV-induced syncytia [463]. One applicable theory is that Rho GTPases may impact on the activation and localisation of ERMs [464]. My results showed that shRNA knockdown of ezrin and moesin

dramatically increases cell-cell fusion. The knockdown of ezrin, in particular, has been shown to enhance cell-cell fusion induced by other viruses, such as HIV [465]. Since ezrin knock-down reduces the tension of the cell membrane [466], I hypothesise that targeting the ERMs might cause the cell membrane to become untethered from the cytoskeleton, perhaps promoting rapid pore expansion. Interestingly, moesin was initially thought to be a cellular receptor for MeV [259, 261]; however, over-expression of this molecule in non-permissive cells did not sustain MeV infection [262, 263]. Beside its ability to cross-link actin filaments to the plasma membrane, moesin has also been shown to interact with microtubules at the cell cortex and stabilise them to maintain cell shape [467]. In my results, disrupting microtubule dynamics reduced cell-cell fusion, however after overexpressing moesin, I observed an increase in cell-cell fusion. Although at first instance these data might appear contradictory, moesin is also known to antagonise the RhoA pathway [468]. Therefore, it is possible that the increase in cell-cell fusion induced by the overexpression of moesin might be due to diminished RhoA/ROCKI activity. Finally, I observed co-localisation of phosphorylated ERMs with MeV glycoproteins, a finding previously reported by another research group [266]. ERMs play a role during the budding process of some viruses and can sometimes be incorporated into virions [469-471]. They also function as organisers of the cell cortex [450]. Electron microscopy studies of MeV particles showed heavily decorated virions with H and F in organised arrays of proteins [292, 387, 389]. It is possible that ERMs might be organising and concentrating viral components, as suggested previously [266], promoting the formation of viral particles. Consequently, such organisation of MeV F

and H complexes may also impact, ultimately, on the activity of F and H and cell-cell fusion.

In conclusion, I have analysed the very early stages of MeV-induced cell-cell fusion and its dependence on the host cytoskeleton, in particular actin filaments, microtubules, dyn2, RhoGTPases and moesin. My results confirm that cell-cell fusion is likely to be a very complex process coordinated by several proteins with varying levels of interaction with the cellular cytoskeleton and plasma membrane. Future targeted research on how the MeV F and H glycoproteins specifically interact with the cellular cytoskeleton might help to elucidate this phenomenon.

Chapter 6

PHOSPHORYLATION OF MEASLES VIRUS HAEMAGGLUTININ CONTRIBUTES TO DIMERIZATION AND CELL-CELL FUSION

Viruses have evolved a myriad of ways to establish infection and generate progeny in the host cell. For instance, viruses are known to hijack several molecular mechanisms normally related to homeostatic processes of the cell cycle. Enveloped viruses hijack exocytosis pathways to accumulate viral components at the cell surface and to assemble new viral particles and egress. MeV relies on the expression of three viral proteins, F, H and M, to exit the cell via cell-cell fusion and/or viral budding. In the previous chapter of this thesis, I have demonstrated that several components of the cellular cytoskeleton are required for viral exit. However, the true complexity of host cell manipulation by MeV is far from being completely understood, since it is likely such process requires the interaction of multiple viral components and numerous host proteins.

Several envelope viruses are known to hijack the ESCRT pathway to facilitate particle egress [472-474]; a group of proteins involved in exocytosis of vesicles. However, MeV budding has been shown previously to be independent of this pathway [346]. What is known is that MeV M protein interacts with both the viral RNP complex and Rab11-containing endosomes to facilitate transport to the plasma membrane [344]. In addition, MeV glycoproteins assemble in the ER and traffic through the Golgi apparatus, wherein certain asparagine residues are *N*-glycosylated [475]. These glycosylated residues are known to impact on surface expression of viral glycoproteins and to stabilise the structure of MeV H [183, 196, 476], implicating a key role for post-translation modifications in the correct assembly and transport of envelope proteins to budding sites. Despite several efforts to elucidate this process, the finite budding mechanisms of morbilliviruses remain largely uncharacterised.

Next generation proteomics have helped to elucidate global changes in the cellular proteome during viral infection [477-479]. Allied to cellular fractionation, quantitative proteomics has been shown to be an effective systems-based approach to study how cellular components are manipulated by viruses. Advances in the field have allowed the simultaneous analysis of multiple samples using differently labelled proteins. One recent technology, known as stable isotope labelling of amino acids in cell culture (SILAC), takes advantage of isotopically labelled amino acids to distinguish peptide populations and therefore abundance of proteins within certain regions of the cell, i.e. under differing conditions [480]. This technology can also be used *in vivo* through labelling of multicellular organisms [481]. Briefly, the principle of SILAC relies on the differential incorporation of stable-isotope labelled amino acids through repeated culturing of cell lines in media containing these amino acids. Specifically, combinations of ^{13}C, ^{15}N and deuterium (D) of arginine and lysine residues are used as substrates to produce proteins with altered molecular weights. After protein extraction, labelled proteins are digested with trypsin, which cleaves at arginine and lysine residues, ensuring that each digested peptide will have at least one of these two labelled amino acids. These modifications are translated as small shifts in the detected mass-to-charge ratios during mass spectrometry analysis, allowing the relative quantification of protein abundance, specifically in lysates containing an equimolar ratio of protein lysate from two or more samples. The result is high-resolution characterisation of the proteome in certain organelles or whole cells. For virology researchers, this allows us to pinpoint the cellular pathways that may be hijacked by viruses. In this chapter, I summarise how I used SILAC to characterise the membrane proteome of MeV-infected LCLs with a focus on the identification of

cellular proteins involved in MeV budding. Initially I studied the growth kinetics of MeV in LCLs, in the context of a low MOI infection, to clarify the temporal nature of MeV infection and to identify when viral and cellular components concentrate to promote virus egress. Suitably SILAC-labelled LCLs were then infected and the membrane proteome extracted and analysed by quantitative mass spectrometry. Subsequently I used this SILAC data to identify post-translation modifications in several viral proteins and, focusing on the MeV H protein, I then evaluated their role in infection.

6.1 MeV growth in LCLs and Vero-hSLAM cells

During *in vivo* infection, lymphocytes are major targets for MeV, a tropism that greatly contributes to measles pathogenesis. Circulating human lymphocytes are naturally permissive to MeV due to expression of the cellular MeV receptor SLAMf1. When evaluating modifications in the cellular proteome induced by the virus, it was imperative that a physiologically relevant cell line be used, in order to capture changes of relevance to *in vivo* infections. I therefore employed human-derived LCLs, a cell line derived from circulating SLAMf1-positive human B lymphocytes. I initially investigated the kinetics of MeV replication in these cells and compared these to the well-established MeV-permissive cell line Vero-hSLAMs (see methods **chapter 2, section 2.2.4**). Cells were synchronously infected with recombinant EGFP-expressing MeV (MOI~0.01), washed and then incubated at 37°C. At the indicated time-points post infection, cells and supernatants were freeze-thawed and virus titres assessed by calculating individual TCID50s (**Fig.6-1A**). Graphical analysis of these growth

Fig.6-1. MeV growth in Vero-SLAM cells and LCLs. (**A/B/C**) LCLs or Vero-hSLAM cells were infected with MeV-EGFP (MOI~0.01), washed and incubated at 37ºC. Progression of infection in LCLs was followed by fluorescence microscopy (**C**). Foci of infection (red arrows) and multinucleated cells (white arrows) were observed. At each time point, cells and supernatants were freeze-thawed and virus titres were calculated (**A**) and MeV H expression in LCLs was confirmed by SDS-PAGE/western blot (B).

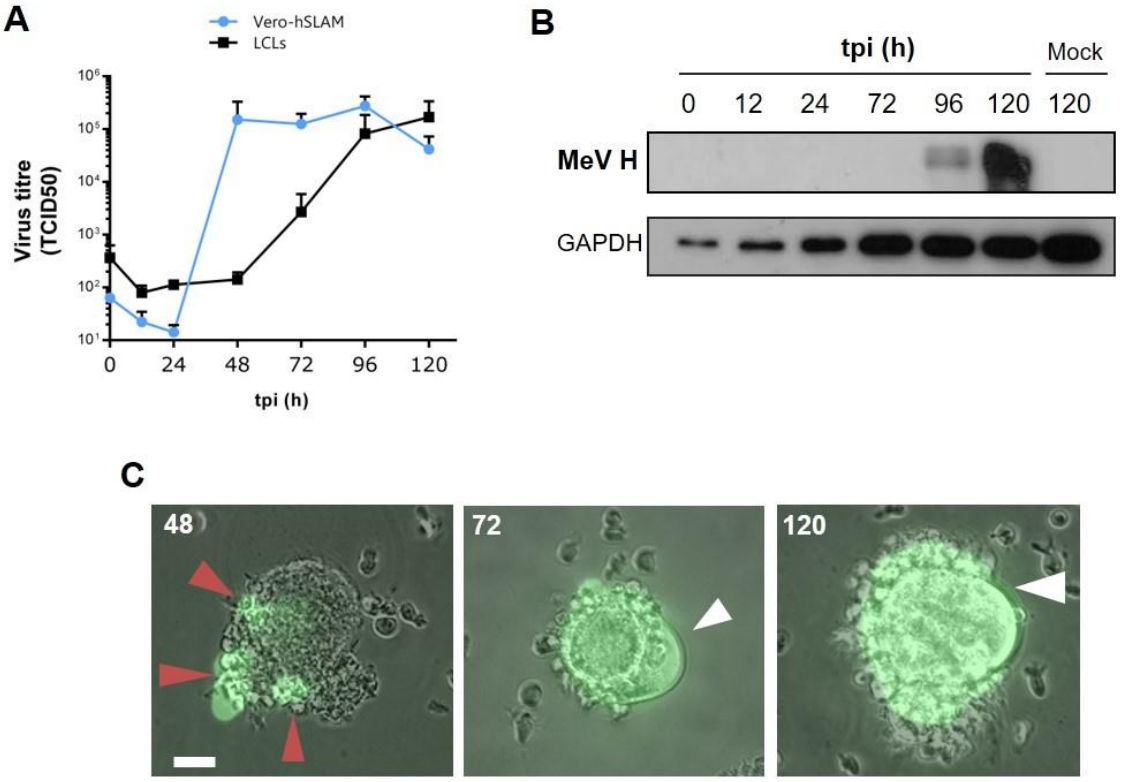
A
Vero-hSLAM
LCLs
Virus titre (TCID50)
tpi (h)
B
tpi (h)
Mock
0 12 24 72 96 120 120
MeV H
GAPDH
C
48
72
120

curves of infection, in Vero-hSLAM cells and LCLs, demonstrated a similar hyperbolic shape, with both infections producing similar viral titres at the later stages of infection. Infection in LCLs showed a prolonged eclipse phase of 48h (when compared to the 24h eclipse phase in Vero-hSLAM infection); however this was associated with higher viral titres – approximately 10-fold higher than in Vero-hSLAM cells at the same time-point. Although MeV titres in Vero-hSLAM cells plateaued at 48h, infection in LCLs only reached comparable levels at 96 and 120h post-infection. These delayed replication kinetics were also reflected in the amount of viral protein produced, with detectable levels of MeV H protein only observed after 96 and 120h post-infection by SDS-PAGE/western blot (**Fig.6-1B**). MeV infection led to enhanced aggregation of LCLs, as reported previously [482], possibly due to modulation of the leukocyte function-associated antigen-1 (LFA-1). During the time-course of this infection, and as soon as 48h post-infection, these large aggregates of LCLs were shown to contain multiple infected cells (red arrows, **Fig.6-1C**). MeV infection also induced the formation of multinucleated cells within these aggregates; often presenting with distended plasma membranes (white arrows, **Fig.6-1C**). Together, these data demonstrate that MeV can efficiently replicate in human-derived LCLs, leading to the formation of large fused cells and the production of high viral titres.

6.2 MeV replication is retarded in media containing 10 kDa-dialysed FBS

For efficient labelling of cellular proteins with stable isotope-labelled amino acids, external sources of protein, e.g. those found in the FBS used in tissue culture, must be eliminated or reduced [483]. These exogenous proteins carry naturally occurring amino acids and can be used as substrates to produce proteins. Quantitative SILAC

relies on homogenous populations of differentially labelled cells; hence contamination with other isotopes can mislead interpretation of any correlative proteomic study. To avoid these issues, LCLs were grown in media containing 10 kDa molecular weight-dialysed FBS and passaged for several weeks. MeV replication kinetics were then re-examined in these adapted cells and compared to LCLs cultured in standard FBS, by synchronously infecting LCLs (MOI~0.01), as before, and examining progeny virus production (**Fig.6-2A**). LCLs grown in dialysed FBS-containing media generally produced lower titres of MeV virus, with a significant difference between conditions seen at 96h post-infection. This discrepancy was also reflected in viral protein expression, since MeV H could be detected by western blot as early as 48h, in cells cultured in normal FBS, but only by 96h in LCLs cultured in dialysed FBS (**Fig.6-2B**). In summary, these data show that although MeV replication was retarded in LCLs grown in dialysed FBS, the infections still generated comparable virus titres by 120h post-infection.

6.3 Using SILAC to characterise the plasma membrane proteome of MeV-infected cells

Negative-stranded RNA viruses usually cause acute infections and rely on the rapid modulation of the host cell to replicate and assemble viral progeny. During the latter stages of the MeV life cycle viral components concentrate in the cytoplasm and are subsequently transported to the plasma membrane, where viral particles form and egress from the cell. Associated with this rapid takeover of the cell are the cytopathic effects commonly seen in tissue culture. These later stages of infection are associated with extensive cell death, as discussed in **chapter 1, section 1.10**. To capture the intact membrane protein profile of MeV- infected LCLs at the moment of

Fig.6-2. MeV growth is attenuated in media containing dialysed FBS. (**A/B**) LCLs cultured in media containing standard FBS or 10 kDa dialysed FBS were infected with MeV-EGFP (MOI~0.01), washed and incubated at 37ºC. At the indicated time-points, cells were freeze-thawed, virus titres were calculated (**A**) and MeV H expression was observed using SDS-PAGE/western blotting (**B**). Statistical Student's t test was performed between each time-point of differently grown cells, *,$p<0.05$

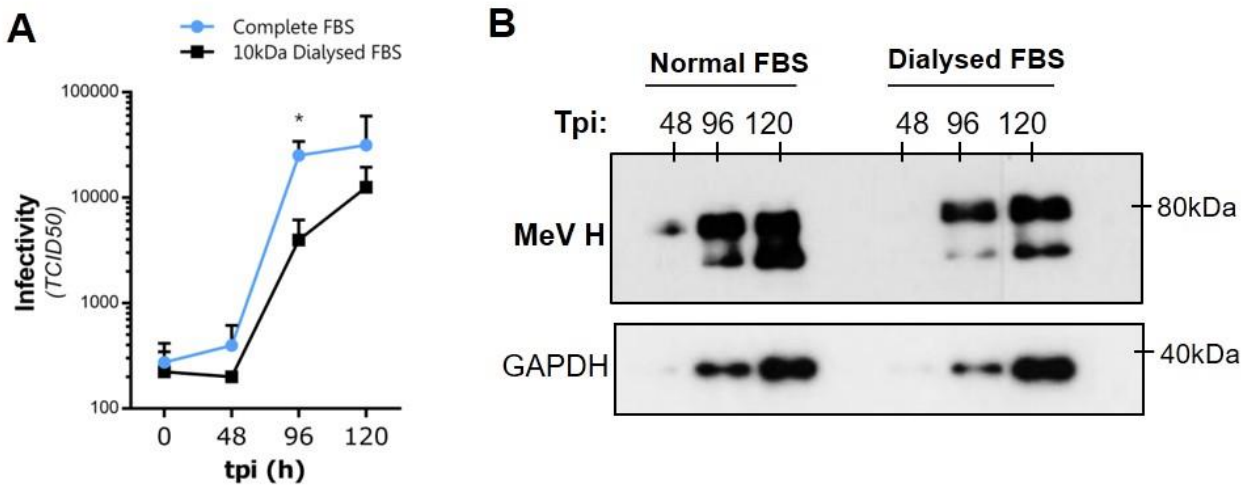
A
Complete FBS
10kDa Dialysed FBS
Infectivity
(TCID50)
100000
10000
1000
100
*
0
48
96
120
tpi (h)
B
Normal FBS
Dialysed FBS
Tpi:
48 96 120
48 96 120
MeV H
80kDa
GAPDH
40kDa

viral budding, and to avoid the consequences of extensive virus-induced apoptosis, I selected two time-points during MeV LCL-infections to analyse the cellular and viral proteome: 64 and 96h post-infection. Specifically, both time-points are located in the exponential phase of MeV growth, preceding production of peak virus titres in *in vitro* infections.

To analyse the membrane proteome of infected cells, I applied the workflow represented in **Fig.6-3A**. Using three RPMI-40-based cell culture medias, supplemented with unlabelled arginine and lysine (R0K0, light), ^{13}C-labelled arginine and ^{2}D-labelled lysine (R6K4, medium) or ^{13}C- and ^{15}N-labelled arginine and ^{13}C- and ^{15}N labelled lysine (R10K8, heavy) I labelled LCLs. Since cells can efficiently use labelled arginine as a substrate for proline production – thereby inferring with analysis of SILAC data - all cell culture medias were supplemented with non-essential amino acids, including proline [484]. Of note, to ensure total incorporation of the labelled amino acids, LCLs were cultured in SILAC media for at least 8 passages with efficient labelling being subsequently confirmed by mass spectrometry (data not shown). Cells cultured in light and heavy media were infected with MeV, while a mock-infection was performed in LCLs grown in the R6K4 medium (**Fig6-3A**). Importantly, late time-point infected cells were labelled with R0K0 medium, i.e. medium with naturally occurring amino acids, so post-translational modifications could be detected effectively. After 64h of incubation, the MeV-infected cells cultured in heavy medium were pelleted by centrifugation. Equivalent pelleting of the light- and medium-labelled cells was performed at 96h post-infection. At these time-points, total RNA and protein samples were collected. Membrane proteins were isolated as described in **chapter 2, section 2.10.2**, and resolved in a 10% SDS-PAGE gel which

Fig. 6-3. Diagram of experiment setup to determine the plasma membrane proteome of MeV-infected cells. (**A**) LCLs were cultured in three medias containing naturally occurring amino acids (L, light, R0K0), R6K4 (M, medium) or R10K8 (H, heavy) labelled arginines and lysines. LCLs grown in L and H media were infected with MeV-EGFP (MOI~0.01) while cells grown in M medium were mock-infected. At the indicated time-points, cells were collected and the membrane protein fraction was extracted. Protein samples from L, M, and H labelled cultures were analysed by SDS-PAGE/Silver stain (**B**) and mixed at an equimolar ratio before mass spectrometry analysis.

A

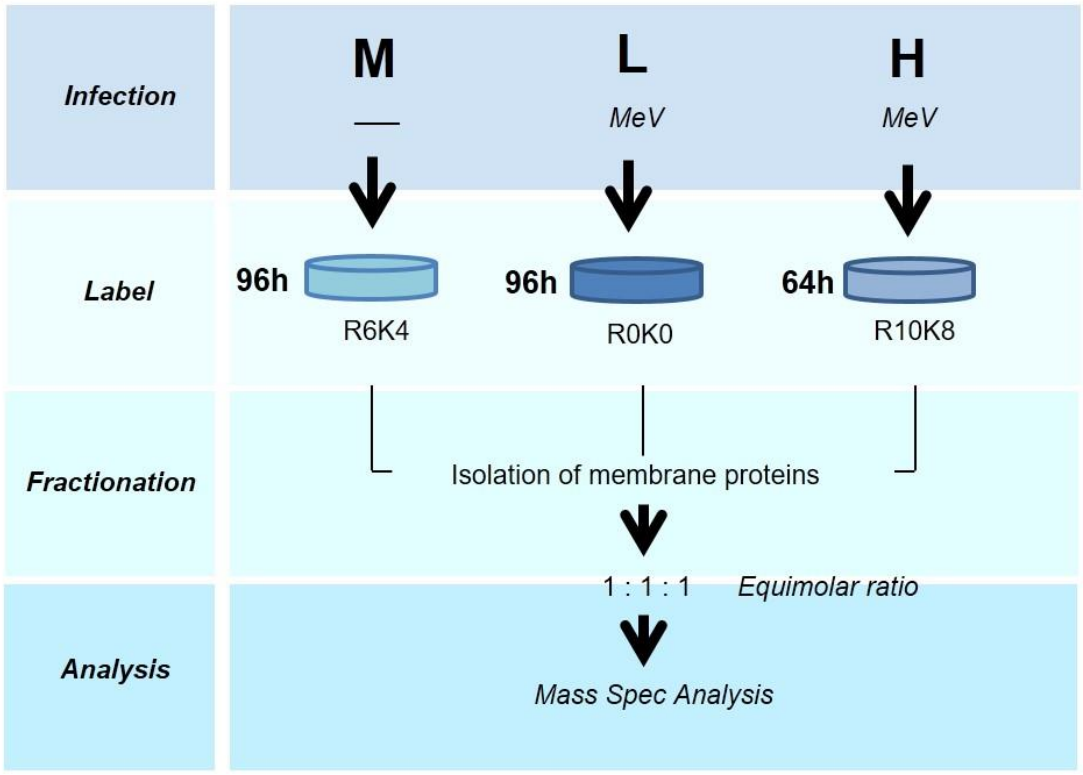
Infection
M
—
L
MeV
H
MeV
Label
96h
R6K4
96h
R0K0
64h
R10K8
Fractionation
Isolation of membrane proteins
1 : 1 : 1
Equimolar ratio
Analysis
Mass Spec Analysis

B

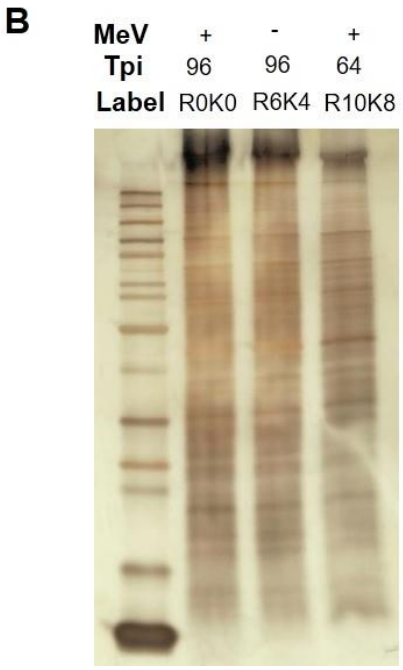
MeV + - +
Tpi 96 96 64
Label R0K0 R6K4 R10K8

was subsequently silver stained (**Fig.6-3B**). The protein concentration of these three lysates was determined using two independent protein quantification assays (BCA and Bradford methods, see **chapter 2, section 2.8.1**), before being mixed at an equimolar ratio to achieve a final mass of 45µg of protein. This sample was then analysed using mass spectrometry; performed by the Proteomics Facility at the University of Bristol. Briefly, the protein sample was resolved on an SDS-PAGE gel and the complete lane sliced into 10 fragments. Proteins were digested with trypsin and analysed on an Orbitrap Fusion Tribrid Mass Spectrometer equipped with electron transfer dissociation. Observed mass-to-charge ratios were compiled with Proteome Discoverer v1.4 Software (Thermo Scientific) and compared against an *in silico* database of human proteins as well as the 8 MeV proteins of the Ichinose strain. Further explanation of the methods employed can be found in **chapter 2, section 2.10.3**.

6.4 Analysis of the membrane proteome in MeV-infected LCLs

Proteomics approaches in virology often yield an extensive and complex dataset, where true viral targets or interaction partners are mixed with the dense background of the cellular proteome. In order to reduce the complexity of my dataset, I computationally filtered the data using a well-established protocol for SILAC, as described by Emmott and Goodfellow [367]. After comparison of mass spectrometry hits against an *in silico* protein database, the Proteome Discoverer software returns a list of proteins with specific SILAC ratios, i.e. quantifying the relative abundance of light/medium, light/heavy and medium/heavy proteins in the analysed sample. To determine significance within these relative peptide abundances, a threshold was

calculated based on the Gaussian distribution of the three SILAC ratios (**Fig.6-4**). Peptides with ratios above or below that threshold were considered up- or downregulated in the sample, respectively, with a 95% confidence interval. The distribution of detected proteins was then compared between samples, specifically 64h vs Mock and 96h vs Mock (**Fig.6-5A**). Global distribution followed a typical $y = x$ correlation, as seen in similar proteomic studies [367]. Although most of the detected peptides clustered around the mean of the two ratios (following an, as expected, Gaussian distribution), two distinct populations of peptides were observed: (1) a population that is underrepresented after analysis of both the 64h vs Mock and 96h vs Mock data sets (**Fig.6-5A**, orange circle) and (2) a population of proteins upregulated in the same analysis (**Fig.6-5A**, blue ellipse). Peptide counts, which often correlate well with the abundance and overall confidence of identified proteins, also followed a similar distribution (**Fig.6-5B**) with equivalent up- and downregulated populations being identified (**Fig.6-5B**, blue and orange shapes). Interestingly, peptides with particularly high numbers of counts clustered in the centre of the distribution (i.e. are equally abundant in both samples) and also in a specifically upregulated population (**Fig.6-5B**, black arrow). When defined, this cluster of highly abundant and well resolved proteins, upregulated in both samples, comprised the viral proteins (most prominently MeV H and F) as well as a small number of cellular proteins. These data are evidence for a significant alteration in the cellular membrane proteome induced after MeV infection. Selecting only significantly under- or overrepresented peptides, I subsequently determined the general composition of cellular components in these subsets, using pathway analysis software such

Fig.6-4. Analysis of the SILAC dataset: thresholds. Detected peptides were mined against an *in silico* library of human and MeV proteins. The abundance of a specific protein, which is related to the ratio of detected peptides in three differently labelled media, was calculated at 96h (**A**) or 64h (**B**) compared to mock, or 64h compared to 96h (**C**), and the frequency of each ratio was plotted. (**D**) Using linear normalisation of frequency distribution to Gaussian distribution, standard deviation and mean was calculated to each ratio.

A

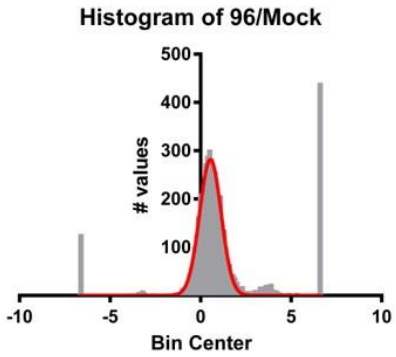

B

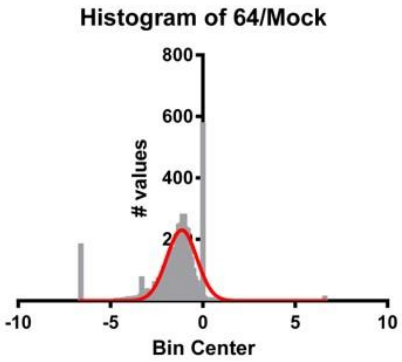

C

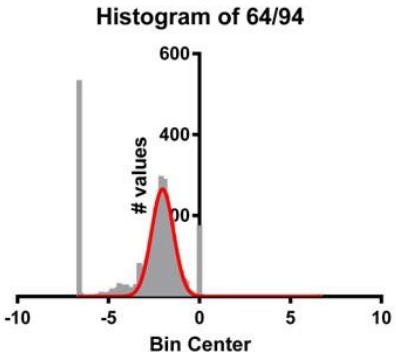

D

Ratio	96/Mock	64/Mock	64/96
Std. Deviation	0.5955	0.8146	0.6049
Mean	0.5422	-1.141	-2.025

Fig. 6-5. – Analysis of the SILAC dataset: distribution of peptides (**A**) Ratios were normalised in relation to individual means and plotted. Ratio distribution was correlated to a y=x linear regression (black line). (**B**) Total counts were sorted into class (light grey is peptides with low count numbers, while black is peptides with a high count number), and plotted onto a graph comparing 96h and 64h ratios. Under- and overrepresented peptides are highlighted in orange and blue shapes, respectively. Black arrow indicates viral peptides population.

A

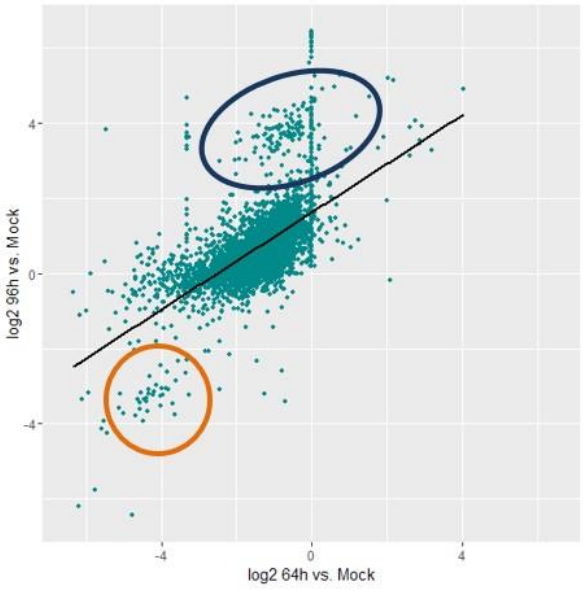
log2 96h vs. Mock
log2 64h vs. Mock
4
0
-4
-4
0
4

B

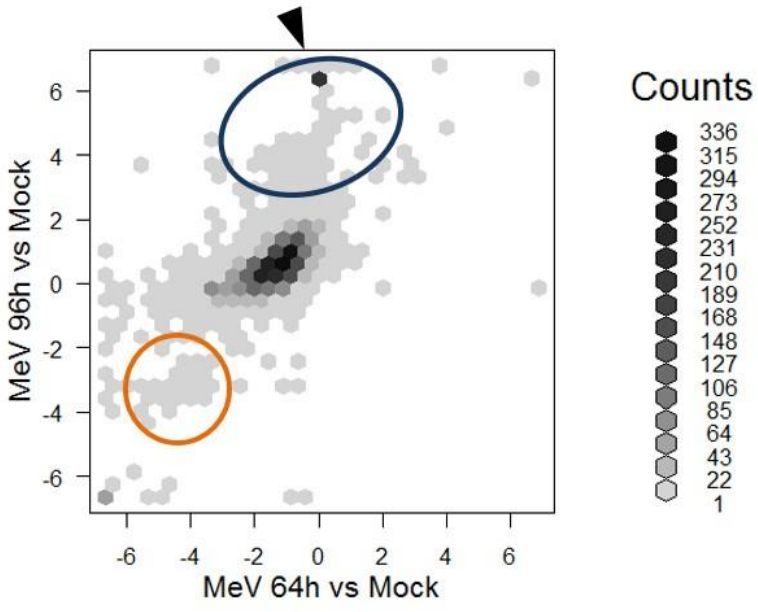
MeV 96h vs Mock
MeV 64h vs Mock
6
4
2
0
-2
-4
-6
-6
-4
-2
0
2
4
6
Counts
336
315
294
273
252
231
210
189
168
148
127
106
85
64
43
22
1

as STRING [485] and PANTHER [486] (**Fig.6-6A**). In both 64h vs Mock and 96h vs Mock comparisons, most proteins belonged to ‘organelles’ or ‘cell parts’, while isolated plasma membrane proteins represented approximately 10% of the population. Pathway analysis software such as STRING [485] and PANTHER [486] showed that upregulated proteins in the 96h vs Mock comparison contain components of extracellular vesicles and exomes with an associated false discovery rate (FDR) of 6.45×10^{-40} and 3.01×10^{-39}, respectively (**Fig.6-6B**). Many of the downregulated proteins in both 64h vs Mock and 96h vs Mock comparisons were part of ribosomal or nuclear components. Additionally, when studying the enrichment of specific biological processes, cellular, metabolic and locomotion processes were largely downregulated in both samples (**Fig.6-7B**). In particular, RNA processing was greatly underrepresented in these samples, when compared to mock infected cells (**Fig.6-7A**). On the contrary, the proteins upregulated in the membrane proteome of infected cells were shown to be involved in metabolic and cellular processes (**Fig.6-7A** and **B**). Together, these results suggest that within the membrane proteome MeV infection induces the modulation of the host’s translational machinery and upregulates exocytosis pathways and metabolic processes.

6.5 MeV proteins contain numerous post-translational modifications

Post-translation modification (PTMs) – a broad term to define modification to amino acids within a peptide or protein – can alter the function, localisation or abundance of a particular protein, both intra- and extracellularly [487]. The cell takes advantage of such PTMs to bypass information encoded in its genome and expand the overall

Fig.6-6. Analysis of the SILAC dataset: cellular components. (**A/B**) Upregulated or downregulated proteins at 96 and 64 hpi were analysed using the PANTHER Pathway Database. Enriched and depleted cellular components were plotted into pie charts (**A**) while specific components were arranged by lowest false discovery rate (FDR) (**B**).

A

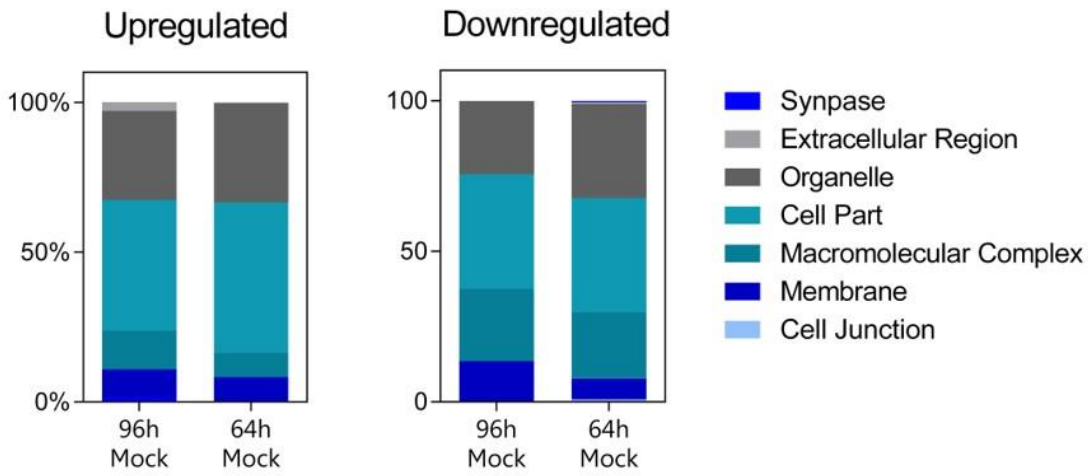

B

	Upregulated		Downregulated	
	Pathway	**FDR**	**Pathway**	**FDR**
96 vs Mock	Extracellular vesicle	6.54E-40	Preribosome	1.05E-11
	Extracellular exosome	3.01E-39	Small-subunit processome	1.06E-09
	Membrane-bounded vesicle	3.00E-37	Nucleolar part	1.93E-09
	Vesicle	1.76E-36	90S Preribosome	4.24E-09
	Pathway	**FDR**	**Pathway**	**FDR**
64 vs Mock	Intracellular organelle lumen	6.53E-04	Nuclear part	1.31E-98
	Nuclear part	1.67E-03	Nuclear lumen	2.15E-90
	Nucleoplasm	4.38E-03	Intracellular organelle part	2.61E-87
	Nuclear lumen	6.99E-03	Organelle part	8.79E-85

Fig.6-7. Analysis of the SILAC dataset: cellular pathways. (**A/B**) Upregulated or downregulated proteins at 96 and 64 hpi were analysed using PANTHER Pathway Database. Enriched and depleted cellular pathways were plotted into pie charts (**A**) while specific pathways were arranged by lowest false discovery rate (FDR) (**B**).

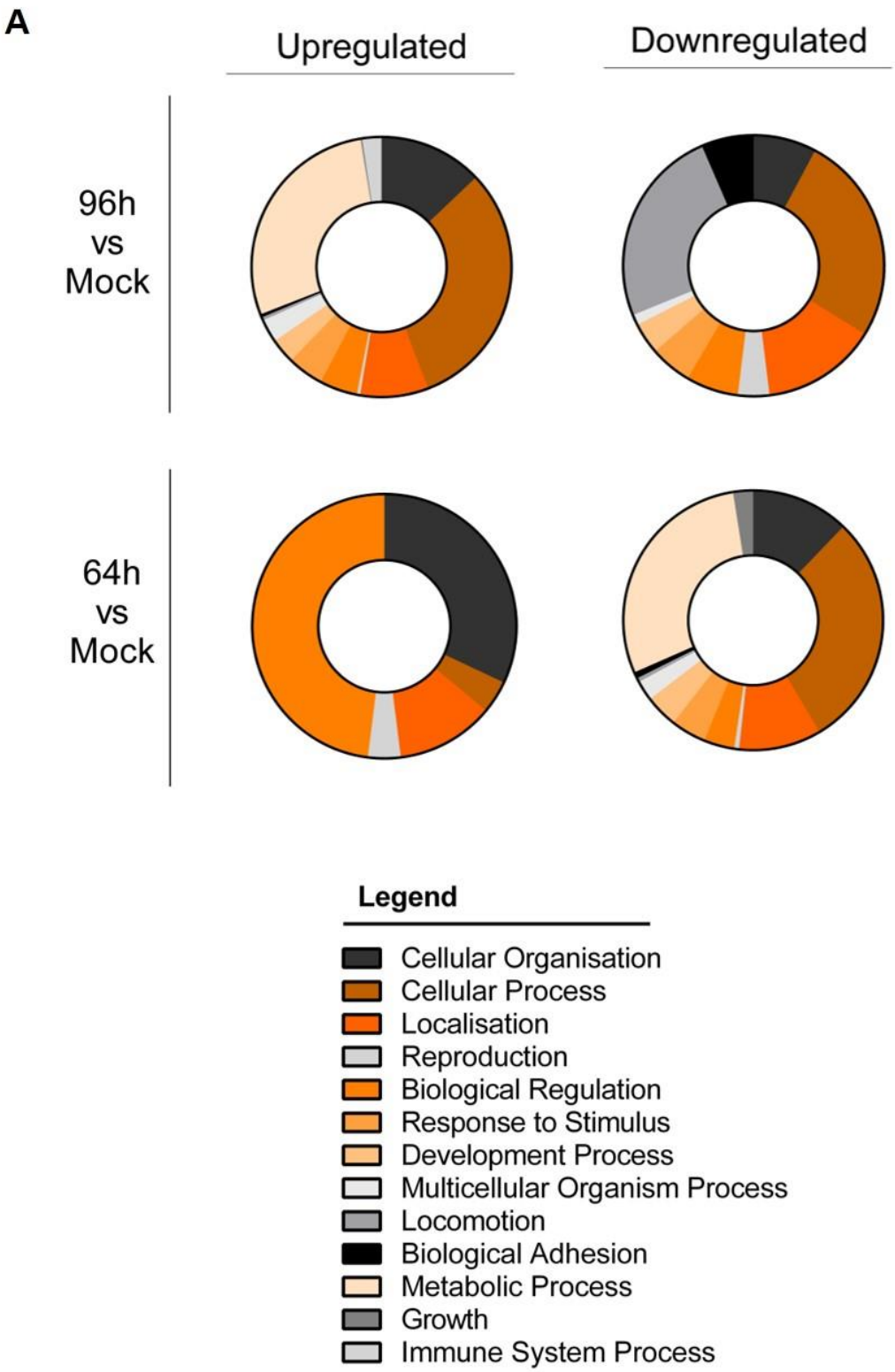
A
Upregulated
Downregulated
96h
vs
Mock
64h
vs
Mock
Legend
Cellular Organisation
Cellular Process
Localisation
Reproduction
Biological Regulation
Response to Stimulus
Development Process
Multicellular Organism Process
Locomotion
Biological Adhesion
Metabolic Process
Growth
Immune System Process

B

	Upregulated		Downregulated	
96 vs Mock	**Pathway**	**FDR**	**Pathway**	**FDR**
	Single-organism metabolic process	3.13E-09	rRNA processing	3.81E-10
	Small molecule metabolic process	4.13E-08	Ribosome biogenesis	4.69E-10
	Regulation of biological quality	1.20E-06	RNA processing	5.87E-09
	Catabolic process	8.35E-06	Ribonucleoprotein complex biogenesis	1.40E-08
64 vs Mock	**Pathway**	**FDR**	**Pathway**	**FDR**
	Arginine and proline metabolism	3.83E-02	RNA processing	1.54E-124
	Metabolic pathways	3.83E-02	mRNA metabolic process	2.49E-81
			Ribonucleoprotein complex biogenesis	8.76E-80
			mRNA processing	1.52E-79

phenotype of one particular protein. Several enveloped viruses take advantage of these PTMs to expand the functional repertoire of their encoded proteins. For instance MeV glycoproteins contain several sites for *N*-glycosylation of specific amino acids, which is important for the stability of the fusion complex and immune evasion by neutralising antibodies [181, 197, 311]. Additionally, MeV N and P proteins are phosphorylated at several key residues; PTMs that are important for genomic replication [488]. My analysis of the membrane proteome of MeV-infected LCLs also allowed me to map the virome (viral proteome) with great coverage and high confidence. In order to identify previously uncharacterised post-translation modifications in the MeV virome I reanalysed my mass spectrometry data set using another *in silico* mining approach, performed using the Proteome Discoverer software. In this search, mass/charge ratios of MeV peptides were compared to a library of *in silico* digested peptides of MeV proteins containing the following post-translation modifications: *N*-glycosylation of asparagines; ubiquitination of lysines; phosphorylation of tyrosines, serines and threonines; methylation of lysines; SUMOylation of lysines and α-acetylation of amino acids. Using this approach I identified a total 32 PTMs in several of the viral proteins, an overview of which can be found in **Fig.6-8**. Six of the identified PTMs have already been described elsewhere, namely the phosphorylation of residues S479, S510 and T279 of MeV N protein [489, 490] as well as the acetylation of its N-terminus [491]. In addition we identified phosphorylation of S86 and S151 in the MeV P protein [492]. In this experiment, however, no *N*-glycosylated asparagines were detected, as reported previously for the MeV F and H proteins [196, 384, 476]. Feasibly, this could be due to the protein/peptide fragmentation technique used in this experiment: collision-induced

Fig.6-8. Overview of MeV PTMs. A schematic representation of identified post-translation modifications in MeV proteins. The individual position of each coloured pin approximately refers to the number of the amino acid residue. Legend for each modification: orange, phosphorylated tyrosine, serines or threonine residues; dark blue, ubiquitinated lysines; grey, methylated lysines; purple, α-acetylation of amino acids; cyan, *N*-glycosylation of asparagines; and pink, SUMOylation of lysine residues. * indicates post-translation modifications that were previously reported.

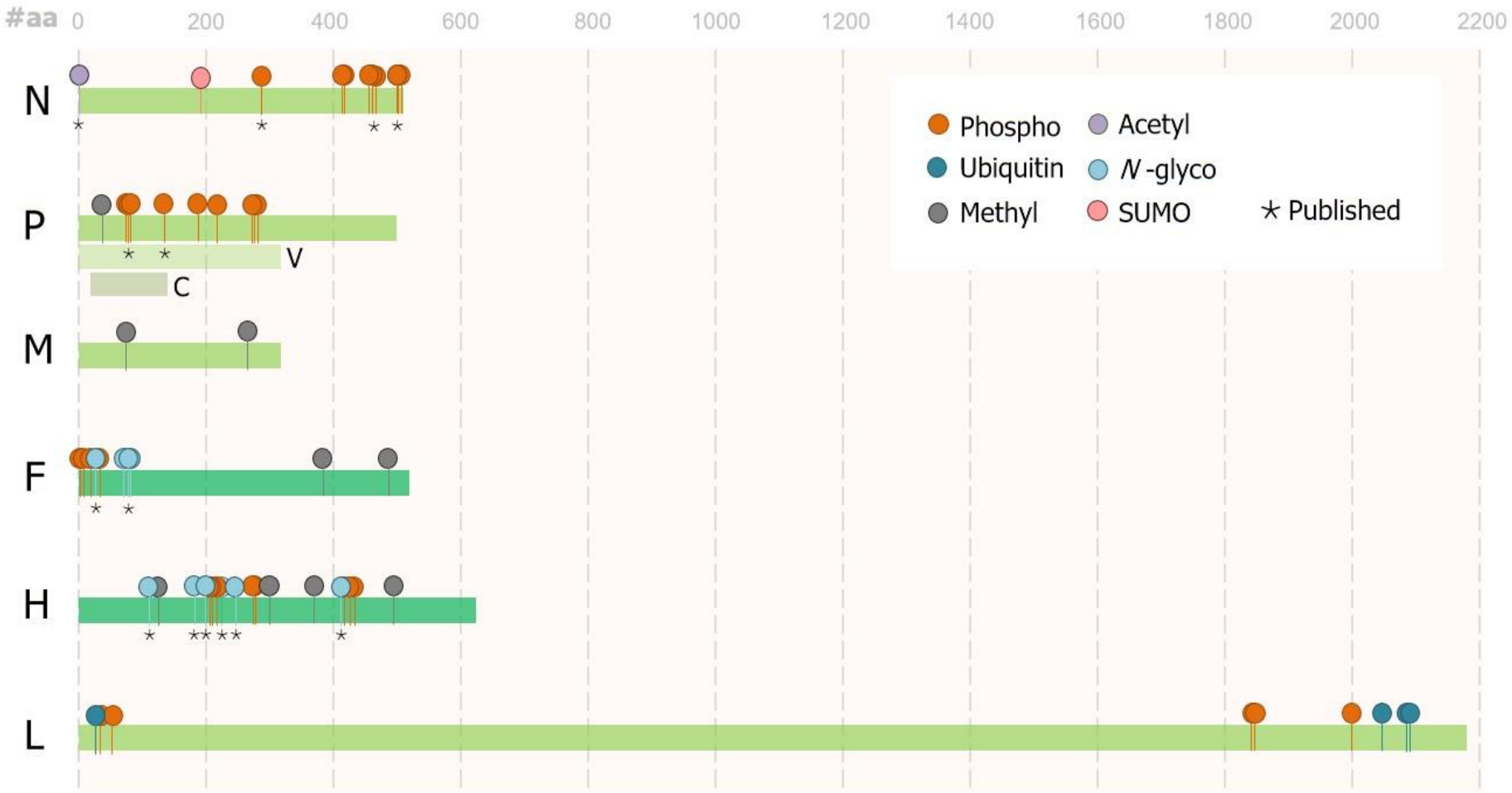
#aa
0
200
400
600
800
1000
1200
1400
1600
1800
2000
2200
N
P
V
C
M
F
H
L
Phospho
Acetyl
Ubiquitin
N-glyco
Methyl
SUMO
Published

dissociation (CID), which occurs through successive collisions between peptides. During this process, sugar moieties, such as the ones linked to asparagines during *N*-linked PTM glycosylation might be lost due to their high molecular weight and sterical hindrance. Accordingly, the PTMs identified in our experiment are considered more stable than *N*-glycosylated residues [493]. Interestingly, although we could not detect the expected glycosylation of MeV F and H proteins we did detect several phosphorylations and methylations, distributed mainly in the ectodomain of both proteins. Since the topic of this thesis lies mainly on the interaction of MeV H with its cellular receptor SLAMF1, I subsequently investigated the role of these putative phosphorylation sites in the activity of H.

Mapping the detected PTMs onto the crystal structure of H revealed these modified residues were distributed throughout the protein structure with no apparent pattern (**Fig.6-9A**). Exceptionally, a pocket of phosphorylated residues localised to the H dimer interface, three of which could be resolved in the structure (T221, T273, and Y275, **Fig.6-9B**), and another two (S240 and S241) which, feasibly, could be nearby matched to an unresolved part of the crystal (due to high instability). Building on the hypotheses that these PTMs are essential to the functionality of the MeV H protein we examined their conservation amongst other MeV H proteins and more broadly among other morbillivirus H proteins. Sequence analysis of several H proteins showed that certain residues are highly conserved (**Fig.6-9C**), in particular the threonine residues at positions 221 and 273 were absolutely conserved, while the tyrosine at position 275 was highly conserved, being variant in only one strain of PPRV which contains a histidine at this position (**Fig.6-9C**, red boxes). Of note,

Fig.6-9. Overview of MeV PTMs. (**A**) Phosphorylated (yellow) and methylated (red) residues identified in MeV H were mapped onto the crystal structure of MeV H bound to its receptor SLAMF1. Orange dotted boxes mark PTMs that map unresolved parts of the crystal. (**B**) Inset: a zoomed image of the dimer interface identifying the position of the relevant PTMs. (**C**) Alignment of MeV H protein sequences of several morbilliviruses. Yellow shading represents highly conserved amino acids.

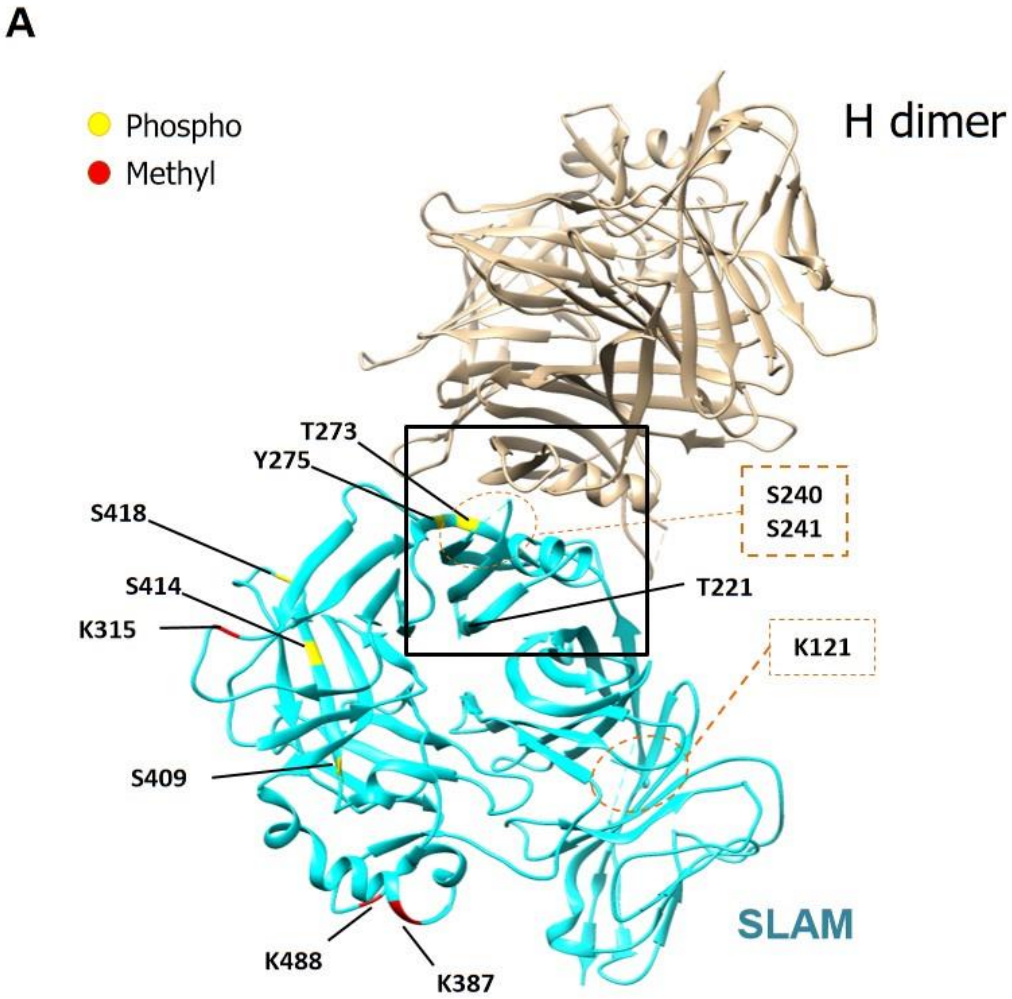
A
Phospho
Methyl
H dimer
T273
Y275
S418
S414
K315
S409
K488
K387
S240
S241
T221
K121
SLAM

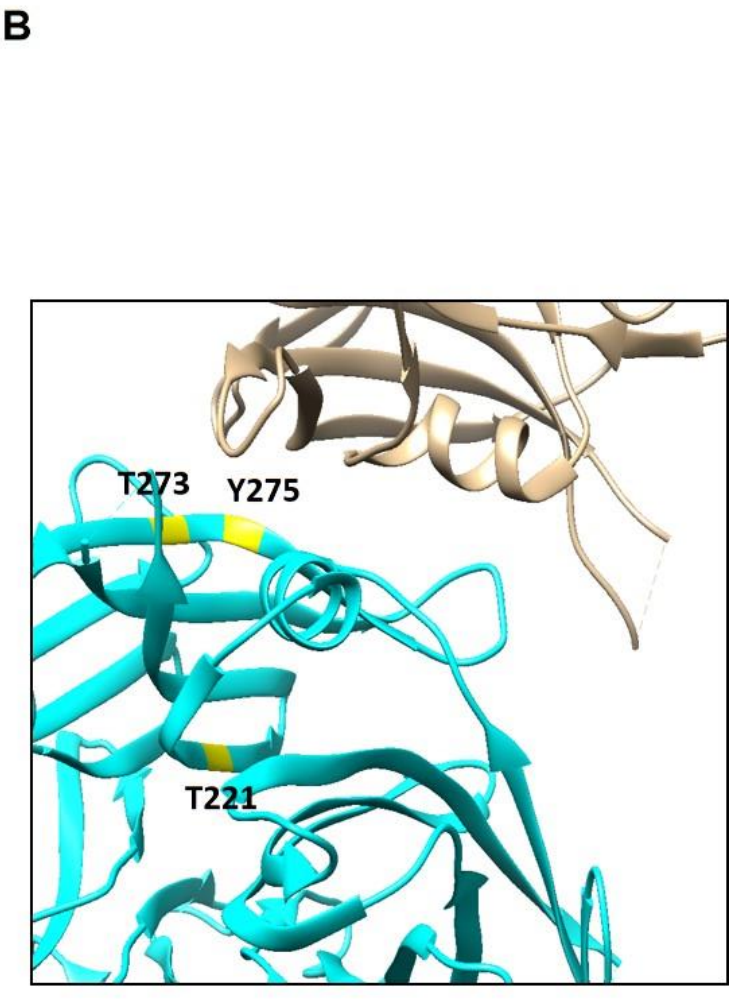
B
T273
Y275
T221

C

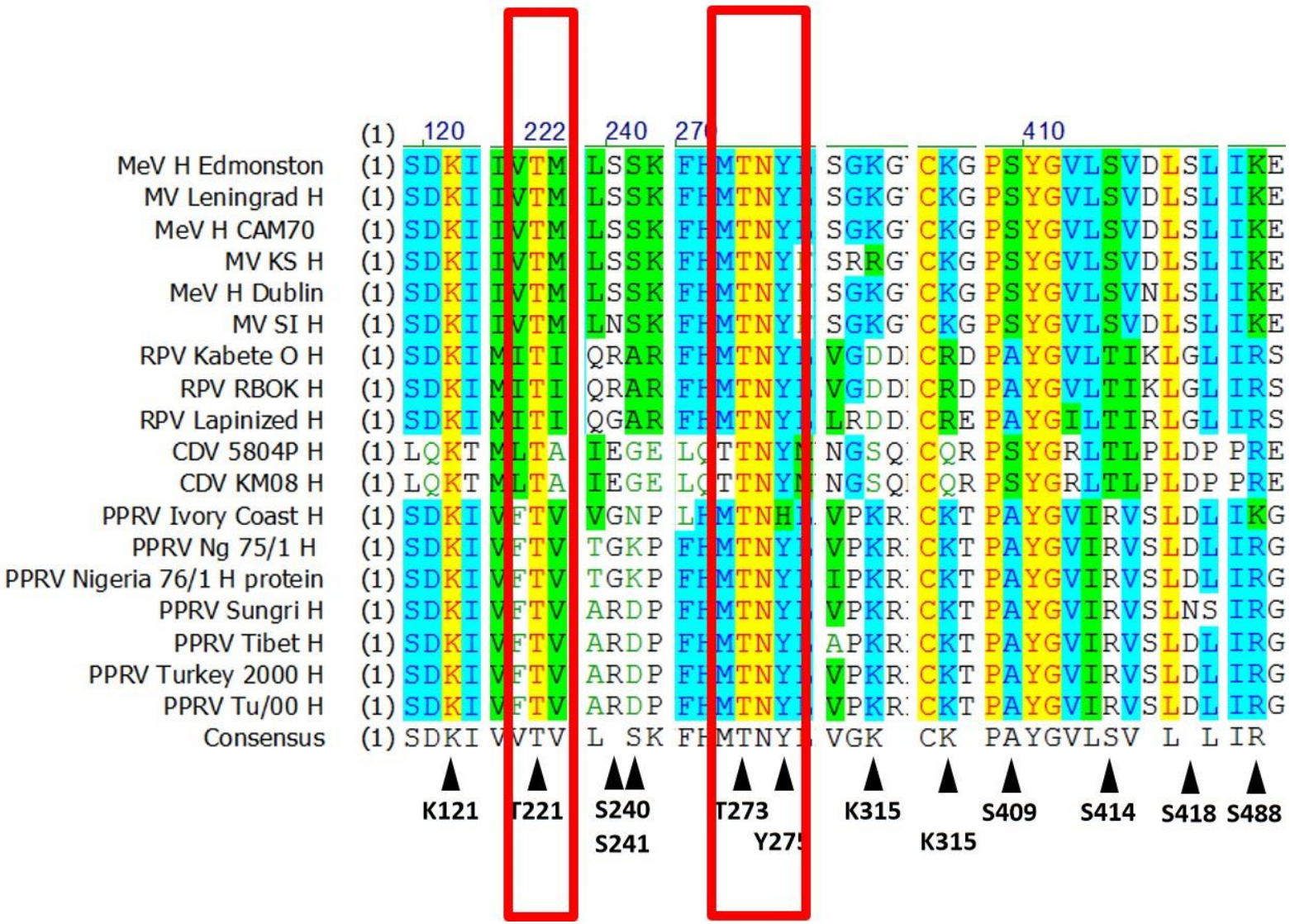
(1) 120 222 240 270 410
MeV H Edmonston
MV Leningrad H
MeV H CAM70
MV KS H
MeV H Dublin
MV SI H
RPV Kabete O H
RPV RBOK H
RPV Lapinized H
CDV 5804P H
CDV KM08 H
PPRV Ivory Coast H
PPRV Ng 75/1 H
PPRV Nigeria 76/1 H protein
PPRV Sungri H
PPRV Tibet H
PPRV Turkey 2000 H
PPRV Tu/00 H
Consensus
K121
T221
S240
S241
T273
Y275
K315
K315
S409
S414
S418
S488

histidine residues can function as substrates of histidine kinases that catalyse their phosphorylation [494]. Therefore, these data suggest a conserved patch of phosphorylated amino acids that localise to the H-H dimer interface of H monomers.

6.6 MeV H residues T221, T273 and Y275 are important for dimerization and cell-cell fusion

Since the residues T221, T273 and Y275 located at the dimer interface and were highly conserved across the morbillivirus genus, I hypothesised that they might be important for the formation of H-H dimers. To investigate this hypothesis, I initially examined the phosphorylation state of H using an *in vitro* dephosphorylation assay as described in **chapter 2 section 2.8.5** (**Fig.6-10**). In this experiment, cells expressing HA-tagged MeV H were lysed in a mild detergent solution, homogenised using a syringe and the protein fraction extracted. This lysate was then incubated with 100 units of λ Protein Phosphatase (λPP). As a control, λPP activity was blocked using 25mM of sodium orthovanadate. Dephosphorylation of proteins should induce mobility shifts in SDS-PAGE/western blot, since the removal of phosphate groups (PO_4^{3-}) alters the net charge of the protein and molecular weight. Accordingly, I observed a small shift in the migration of the MeV H when pre-incubated with λPP and analysed using a low density SDS-PAGE gel (**Fig.6-10**). This shift was not observed in the presence of sodium orthovanadate. As a positive control, to establish the dephosphorylation efficiency of the λPP, I used cofilin-specific antibodies that detect either total or phosphorylated forms of this protein. In this instance incubation with λPP reduced the amount of phosphorylated cofilin that

Fig.6-10. MeV H contains phosphorylated residues. HEK293T cells were transfected with a plasmid encoding MeV H with an N-terminal HA epitope tag. After 48h, cells were lysed and the protein fraction was incubated with or without λ protein phosphatase (λPP) in the presence or absence of its inhibitor sodium orthovanadate at 37ºC for 30min. Proteins were then resolved onto a 15% or 7.5% SDS-PAGE gel and MeV H-HA, cofilin and phospho-cofilin were visualised by western blot.

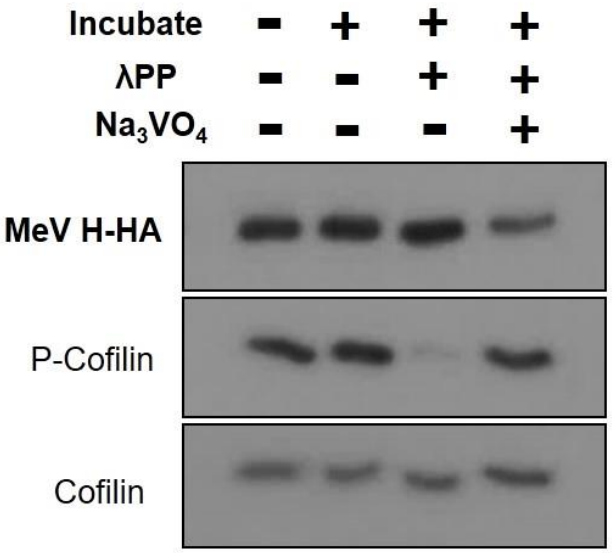
Incubate - + + +
λPP - - + +
Na3VO4 - - - +
MeV H-HA
P-Cofilin
Cofilin

Fig.6-11. Conserved phosphorylated residues may contribute to dimerization of H. (**A/B**) Several MeV H phospho-defective mutants were generated (T221A, T273A, Y275A and Y275F), transfected into HEK293T and cell-cell fusion assays were performed (**A**). HEK293T cells were transfected with constructs expressing the indicated mutants and 48h later cell lysates were generated and resolved in SDS-PAGE gels under reducing and non-reducing conditions, visualised by western blot (**B**). (**C/D**) Similarly, MeV H phospho-mimetic mutants were generated (T221D, T221E, T273D, T273E and Y275E), transfected into HEK293T and cell-cell fusion assays were performed (**A**). HEK293T cells were transfected with plasmids expressing the indicated mutants, and 48h later cell lysates were generated and resolved in SDS-PAGE gels under non-reducing conditions and visualised by western blot (**B**). Student's t test, **,$p<0.01$; ***, $p<0.001$.

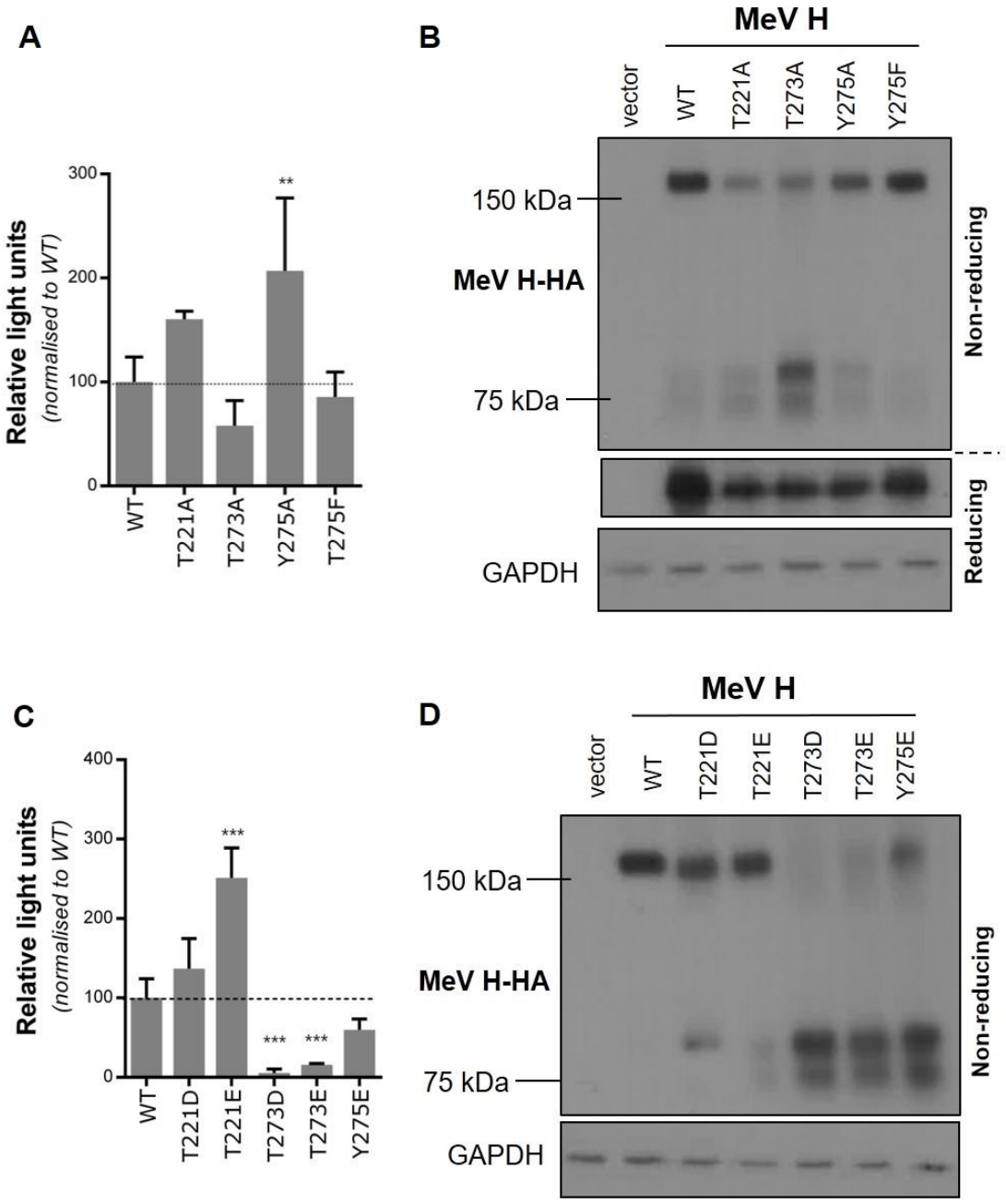
A
Relative light units
(normalised to WT)
300
200
100
0
**
WT
T221A
T273A
Y275A
T275F
B
MeV H
vector
WT
T221A
T273A
Y275A
Y275F
150 kDa
MeV H-HA
75 kDa
Non-reducing
Reducing
GAPDH
C
Relative light units
(normalised to WT)
400
300
200
100
0
***
***
***
WT
T221D
T221E
T273D
T273E
Y275E
D
MeV H
vector
WT
T221D
T221E
T273D
T273E
Y275E
150 kDa
MeV H-HA
75 kDa
Non-reducing
GAPDH

I could detect and I observed a small migration shift in the total protein. These data, together with the previous detection of PTMs by mass spectrometry, provide evidence of specific phosphorylation of amino acids in MeV H.

Analysing of the impact of phosphorylated residues on the activity of a protein can be hindered with biochemical studies due to the difficulties in interfering with phosphate groups. Common approaches include the mutagenesis of the phosphorylated residues with phospho-defective amino acids, i.e. residues that cannot be phosphorylated, such as alanine and phenylalanine, or phospho-mimetic amino acids, i.e. residues that resemble the negative charge of phosphorylated residues, such as aspartic or glutamic acids. Therefore, I have introduced alanine substitutions, which abrogate the addition of phosphate groups at these positions, since alanine residues are not substrates of kinases, or aspartic acid or glutamic acid substitutions – which mimic the negative charge of the phosphate group. To assess the role of the phosphorylated residues in H, I have generated MeV H constructs with phospho-defective substitutions and analysed the activity of H using a cell-cell fusion assay (**Fig.6-11A**). Interestingly, the substitution Y275A increased cell-cell fusion while T273A modestly decreased fusion, even though not significantly. As my initial hypothesis was that these residues might be involved in the dimerization of H, I looked at the abundance of dimeric and monomeric states of H using SDS-PAGE under reducing and non-reducing conditions (**Fig.6-11B**). Moreover, when mutating to phospho-mimetic residues, T221E increased cell-cell fusion, while substitutions in T273 and Y275 reduced cell-cell fusion (**Fig.6-11C**). In particular, replacing the threonine 273 to D or E residues completely abrogates cell-cell fusion. This might be greatly explained by the loss of the dimeric form of H, as shown by non-reducing

SDS-PAGE (**Fig.6-11D**). Although further investigation is required to determine the role of these phosphorylated residues, these data point to a particular sensitivity to the residue T273 to accommodate mutations, but also other residues in promoting dimer stability and cell-cell fusion.

6.7 Discussion

The complexity of virus-host interactions likely hinders our understanding of pathogenesis and virus biology, even in the case of small enveloped viruses, such as MeV. To address this problem, several high-throughput approaches have been applied in virology to better comprehend how viruses manipulate their hosts. In particular, and to this end, proteomics has become an important methodology in infectious disease research. In this chapter, I describe the use of SILAC technology to examine the membrane proteome of infected LCLs, with the intention being to investigate the egress mechanism of MeV. The dataset generated and presented herein demonstrates dramatic alteration of the cellular proteome following MeV infection of lymphocytes. Interestingly, infection in LCLs was shown to be slower than in Vero-hSLAMs. Since the parental Vero cell line is a primate cell line lacking expression of *IFNα* and *IFNβ*, it is possible that innate immunity in LCLs may be dampening MeV infection. Nevertheless, the growth curve I performed suggested that infection in both cell lines can generate equivalent titres of viral progeny. To this end, it was important to avoid cytopathic effects and, therefore, extensive protein degradation.

Analysis of the membrane proteome of infected cells showed that at both 64 and 96 hours post-infection the translation machinery was significantly downregulated. Particularly, proteins involved in RNA processing were highly affected by infection with FDRs of 1.54×10^{-124} and 3.81×10^{-9}, supporting previous evidence for host translational shut-off [137, 495]. Of note, FDRs were calculated based on multiple comparisons and enrichment analysis of cellular protein networks listed in PANTHER and STRING databases, as described previously [485, 486]. A very low FDR value for a particularly pathway (as the ones mentioned herein) suggests that pathway is significantly enriched or depleted when comparing two populations. Interestingly, proteins involved in metabolic pathways were significantly enriched in both samples, with associated FDRs ranging in order of magnitude from 10^{-9} at 96h and 10^{-2} at 64h. Using pathway analysis, I determined which cellular compartments (including the plasma membrane or organelles) were enriched in the SILAC dataset. Extracellular exosomes and vesicles were shown to be enriched in infected cells. Together, these observations suggest a possible upregulation of exocytosis pathways for metabolite secretion during infection. Although further investigation is required, it is plausible that MeV hijacks the exocytosis pathway to assemble at the plasma membrane and egress from the cell. MeV proteins have previously been shown to interact with $Rab11^{+}$ endosomes, culminating in the accumulation of viral components at the apical side of polarised cells [344]. The budding of other viruses, such as varicella-zoster virus and RSV, has been shown to be dependent on exocytosis pathways and interactions with Rab11 [496, 497]. Rab11 is a cellular GTPase that is involved in the trafficking of recycling endosomes [343] and the regulation, formation and secretion

of exosomes [498, 499]. Further analysis of the upregulated proteins belonging to these pathways might help to elucidate the budding mechanism for MeV.

Of particular interest was the identification of a myriad of post-translation modifications in the MeV proteome. Several phosphorylated residues in N and P have previously been identified and shown to have an impact on the activity of these proteins and, ultimately, viral replication and RNA synthesis [489, 490, 492]. Furthermore, PTMs in F and H, specifically glycosylated residues in the ectodomain, are known to modulate fusion activity and contribute to immune evasion. It is therefore clear that viruses, including MeV, have evolved to take advantage of the modification of proteins to expand their repertoire of functions during infection, such as the glycosylation of envelope proteins and the phosphorylation of residues involved in replication. Some suggest PTMs may play an important alternative role in viral evolution, in which additional ORFs can be replaced by protein modifications, bypassing the information contained in the genetic material [500]. Within my SILAC dataset, several PTMs were present in almost all viral proteins, most of which have not been reported yet. Another interesting observation is the diversity of amino acid modifications that I uncovered. The L and N proteins were associated with peptide-specific PTMs, respectively ubiquitin and the small ubiquitin-like modifier (SUMO). Ubiquitin is a small protein that, when covalently bound to a target protein, can trigger a signalling cascade impacting on its stability [501]. Other functions have also been attributed to ubiquitin conjugation, such as nuclear-cytosolic translocation and modification of the enzymatic activity of the target protein. Since the ubiquitin footprint after peptide fragmentation and mass spectrometry analysis – characterised by two remaining glycine residues of the ubiquitin peptide bound to a lysine – was

identified at both termini of the L protein, it is also possible that the ubiquitination that I identified might also be a sign that L is targeted for degradation. However, in other viruses, such as influenza A virus, ubiquitination of lysine residues within the polymerase polypeptide can lead to increased activity of the RNA polymerase without affecting protein expression levels [502]. Ubiquitination was shown to impact several steps of the virus lifecycle, contributing to the modulation of innate immunity, virus entry and egress from the cell [503]. In the study of Pentecost *et al*. several paramyxoviral matrix proteins are described to be ubiquitinated, with disruption of this ubiquitination impacting on nuclear translocation of this protein, including MeV M [504]. In contrast, my SILAC data identified no ubiquitin footprint on this protein. In the cited study MeV M protein was the least affected protein and the role of ubiquitin conjugation was inconclusive. It is also possible that transient expression of MeV M, rather than endogenous expression during a normal MeV infection, may alter the physiological background of M in these cells, explaining the observed ubiquitination. In support of this conclusion, my proteomics dataset was extracted from infected cells that more closely resemble natural infection in the host.

Interestingly, a small peptide related to ubiquitin, SUMO, was found associated with the N protein. The addition of SUMO molecules to proteins, often described as SUMOylation, can have a much broader impact on the protein than ubiquitin, such as the modulation of transcription and protein stability, nucleus-cytosol translocation, apoptosis, etc. [505]. Although this process might not be as well-characterised as ubiquitination cascades, some viruses have been shown to interfere with host SUMOylation upon infection [506-508]. Influenza A virus matrix 1 and nucleocapsid proteins have been shown to be SUMOylated, impacting on viral assembly,

trafficking and replication [509, 510]. Addition of SUMO molecules to paramyxoviral proteins has previously been reported [511]; in this study the P protein of PIV5 was shown to be SUMOylated, playing a role in virus replication. Although SUMO footprints were not identified in MeV P protein, my data supports the idea that this pathway might be involved in MeV infection. Network analysis of enriched pathways in SILAC samples showed that components of the protein polyubiquitination (FDR=0.98×10^{-2}) and ER-associated ubiquitin-dependent protein catabolic process (FDR=3.98×10^{-2}) were upregulated in infected cells. Nevertheless, since this experiment was designed to capture membrane proteins and SUMOylation and ubiquitination pathways are mainly cytosolic/nuclear, it is possible that the dataset does not reflect a putative subversion of these pathways.

Phosphorylation of virally encoded amino acid residues were among the most common post-translation modifications detected in the MeV proteome. Five of the eight viral proteins presented such modifications with additional phosphate groups attached to threonine, serine or tyrosine residues. Unsurprisingly, the N and P proteins were shown to be phosphorylated at different sites. It was previously demonstrated that phosphorylated MeV N is preferentially assembled into RNPs [512], a process which is also aided by P protein [513]. MeV P is thought to be a substrate for the cellular casein kinase II and has multiple phosphorylation sites [514]. Although the role of these phosphorylated residues is not fully understood, researchers believe that they are important in gene regulation [515] and the modulation of innate immune responses [488]. Similarly, phosphorylated residues in N have also been implicated in regulating gene expression and, by extension, modulating virus replication [490]. During my SILAC screen, additional

phosphorylated residues were identified in P and N, suggesting the existence of other active phosphorylation sites that might impact on the virus lifecycle. To my knowledge, no phosphorylated residues have been reported in the RNA-dependent RNA-polymerases of non-segmented negative-sense single-stranded RNA viruses. However, some positive strand RNA virus RNA polymerases were shown to be phosphorylated [516, 517], as well as certain subunits of the influenza A virus polymerase [518]. It is possible that the phosphorylated residues in L affect polymerase activity, as seen for other viruses, but further experiments are required to evaluate their role in the MeV lifecycle.

To my knowledge no previous report has shown phosphorylation of F and H either; however, my data also points to several phosphorylated residues within these proteins. In particular for H, although there are five crystal structures available; none of them show clear signs of phosphorylation [180, 181, 183, 296, 302]. In all these crystallisation studies, H is expressed as a truncated form, i.e. only the globular head is expressed, a process that is required for efficient secretion of a soluble form of H that can be subsequently purified and crystallised. It is possible that this soluble form of H might not function as a substrate for endogenous kinases, and may not be phosphorylated under these conditions. Additionally, these studies used insect cells [183, 296], Chinese hamster ovary cells [302] or HEK293 cells [180, 181] to produce the MeV H protein for crystallisation. None of these cells are naturally permissive for MeV; in addition none of these studies were performed in the context of viral infection. In contrast, my proteomics and PTM data was obtained from human derived-lymphocytes – a known target of virus infection *in vivo* and readily permissive to MeV – and infected with a wild-type strain of MeV. It is entirely possible that the

expression and isolation conditions in which these crystals were obtained interrupted the normal maturation pathways for MeV H. One argument to support this hypothesis is the limited detection of glycosylated sugar moieties attached to residues in these crystals: even though a total of five *N*-glycosylated residues have been identified biochemically, only two [181, 302] or three [296] were resolved within the protein structures, highlighting the limitation of crystallographic approaches in defining the complete structure of viral glycoproteins.

In preliminary studies I further investigated the phosphorylation of certain residues in H; in particular, focusing on three conserved amino acids located at the dimer interface of H (T221, T273 and Y275). Using site-directed mutagenesis, these residues were shown to be highly sensitive to certain amino acid changes, affecting both dimer formation and cell-cell fusion. The formation of H-dimers is not completely understood, with several studies suggesting that the globular head domain of H is, in solution, a monomer [183] or a dimer [181]. Two disulphide bridges located at the interface of the globular domain and the stalk domain are also implicated in dimer formation since these bridges are established between cysteines of different monomers [519]. As these cysteine residues are important for dimerization, induced reduction of these residues by β-mercaptoethanol and subsequently SDS-PAGE/western blot of these proteins shows the monomeric molecular weight of H around 75 kDa; however, if no reduction step is performed, the disulphide bounds remain intact and the detected MeV H band is located at 160 kDa (dimeric molecular weight). Alanine substitutions in all three residues decreased the total level of protein, while a phenylalanine mutation in Y275 maintained similar expression levels to wild-type H protein. Since phenylalanine residues are not kinase substrates, it is

possible that the phosphorylation of Y275 does not have an effect on cell-cell fusion and dimerization of H and might play other roles in MeV lifecycle that these assays cannot elucidate. In contrast, both phospho-defective and phospho-mimetic amino acid substitutions in the T273 severely affected dimer formation and cell-cell fusion, suggesting that this position is very sensitive to amino acid variation. Also, a caveat of using mutagenesis to evaluate the role of phosphorylated residues is the difficulty in accurately mimicking the phosphate groups bound to the original amino acid. It is possible that the E and D substitution at position T273 both cause steric hindrance, impacting on the formation of the dimer. Finally, an alanine substitution in T221 abrogated dimer formation while D or E substitutions maintained the dimer and increased cell-cell fusion. It is possible that this phosphorylated residue is affecting the overall stability of the protein, similar to what has been shown for *N*-glycosylated residues [181], thereby impacting on the ability of H to promote cell-cell fusion.

In summary, I have shown that MeV infection in LCLs induces a significant change in the membrane proteome with upregulation of cellular pathways involved in exocytosis. Additionally, PTMs in MeV H were shown to be important in the dimerization and function of this protein. Further experiments are required to determine the role of these phosphorylated residues in the MeV lifecycle.

Chapter 7
GENERAL DISCUSSION

7.1 Background and General Aims

MeV is one of the most contagious viral pathogens known to science. Like the other recognised members of the *Morbillivirus* genus, MeV interacts with SLAMF1 on immune cells of the lung to rapidly establish infection (see [41] for a review). These infected cells then drain to local lymph nodes, where several cell types become infected, including B- and T- lymphocytes, leading to the occasional formation of multinucleated cells. The virus then enters the bloodstream, mainly in association with circulating cells, and infection spreads to other parts of the body. The final stage of MeV infection occurs when infected circulating immune cells interact with the basolateral surface of polarised cells in the lung epithelium. Infection and spread within the airway epithelium can then occur by cell-cell fusion. At this point, nascent viral particles are preferentially released into the lumen of the lung and expelled to the environment.

For the virus to successfully complete this lifecycle in the host, it interacts with at least two cellular receptors, SLAMF1 and nectin-4. Both molecules grant cell's permissivity to MeV through direct interactions with viral particles but also by allowing cell-cell fusion. **Until now it has commonly been assumed that the fusion mechanism underpinning both processes are the same**. To be more specific, this fusion mechanism involves the initial interaction of H with either SLAMF1 and nectin-4, depending on the target cell type. This interaction induces conformational changes in H that trigger F. The F protein undergoes dramatic refolding leading to the insertion of the fusion peptide into the target cell's plasma membrane and fusion of both membranes. Although the structural rearrangements of these proteins during

this process is a topic of intense investigation, the cellular factors governing this process remain poorly defined.

Early evidence for specific differences between the cell-cell fusion process and the fusion occurring upon viral particle entry came from the François-Luic Cosset's lab: they showed that lentivirus particles pseudotyped with MeV glycoproteins were able to transduce quiescent human lymphocytes in a process that was sensitive to macropinocytosis inhibitors [328, 374, 385]. These reports provide evidence that more complex events are occurring at the moment of particle entry, processes that rely not only on the fusion of the viral envelope with the plasma membrane but also the involvement of other cellular factors, such as proteins involved in macropinocytosis. In addition, Stephen Russell's lab previously showed that soluble MeV H is internalised by cells via macropinocytosis or clathrin-mediated endocytosis [329]. The same lab showed that attachment of MeV to cells leads to the clustering of CD46 upon viral entry. Clustering of CD46 was observed upon infection with *Neisseria gonorrhoea*e and led to cytoskeletal rearrangements important for the entry of the pathogen [248, 253, 520]. These reports are evidence that MeV H interactions with its receptors might be more complex than previously thought, inducing cellular responses that might be important for the establishment of infection. Although these reports are specific for the CD46-MeV H interaction, recent findings from Cox Terhorst's lab have shown that SLAMF1 interacts with Gram-negative bacteria and controls the internalisation of the pathogen through the recruitment of autophagic machinery [210]. Interestingly, autophagy responses to MeV infection have been reported previously, where an early wave of autophagy was observed soon after MeV entry [172]. In addition, during MeV infection of DCs, attachment of the virus to

the cell surface leads to the clustering of SLAMF1 [332]. Based on these data and observations, I have revisited the entry mechanism of MeV entry into SLAMF1$^+$ cells.

7.2 Redefining MeV entry via SLAMF1

In chapter 4, I have shown that MeV and lentivirus pseudotyped with MeV glycoproteins are internalised by SLAMF1$^+$ cells via a pathway that resembles macropinocytosis. Evidence for this conclusion can be divided into two main observations: *i*) MeV entry required **the activity of certain cellular components**, such as myosin-2, ROCK-I and a dynamic actin cytoskeleton, and *ii*) attachment and **entry led to specific cellular responses**, including membrane blebbing, cytoskeleton contraction and fluid uptake. Before making any further conclusions on the entry pathway used by MeV particles, it is worth highlighting that these two observations are sufficient to disprove that MeV entry is an entirely unregulated process; moreover, it is likely to be far more complex than simple fusion of the viral envelope at the cell surface and subsequent release of the RNP complex into the cytosol. Firstly, one should consider the observed cellular responses to MeV entry as mentioned in *ii)*. One of the most striking observations described herein are the morphological rearrangements of the plasma membrane that led to the formation of membrane blebs. This was a rapid but transient phenomenon that occurred in the first 20 minutes of infection. As discussed previously, other viruses, such as vaccinia virus, were shown to induce similar membrane blebs upon entry [409, 521]. These structures are important in cellular homeostasis as membrane blebs play a role in locomotion and invasion [404] but also in phago- and macropinocytosis [195, 409]. Similarly, MeV attachment and entry led to other phenotypes related to the

macropinocytosis pathway, such as fluid-uptake and reorganisation of the actin cytoskeleton. Although the cellular proteins involved in the regulation of macropinocytosis are not fully described, it is plausible that this is modulated by molecular signalling from the plasma membrane, similarly to several receptor-mediated endocytosis pathways [420]. Macropinocytosis appears to be governed, at some level, by very mobile elements present at the plasma membrane, such as cholesterol-rich microdomains and phosphatidylinositol-3-phosphate[321]. I also performed experiments showing that certain macropinocytosis-related responses induced by MeV, namely the internalisation of fluid and the contraction of the cytoskeleton, are SLAMF1-specific. This observation shows that (1) MeV interaction with SLAMF1 is sufficient to induce these phenotypic responses and (2) the observed cell responses are not due to any contaminant present in the viral preparations, since the viral inoculum had little effect on cells lacking expression of SLAMF1. One plausible conclusion that can be drawn from the observations described in (1) is that the membrane blebbing, fluid-uptake and contraction of the cytoskeleton, brought about as a consequence of MeV-SLAMF1 interactions are related to signalling mediated by SLAMF1. As mentioned before, CD46-mediated signalling regulates the entry of the pathogen *Neisseria gonorrhoeae*, in a process that is dependent on the phosphorylation of the cytoplasmic tail of CD46 [520]. In our lab, we are currently investigating the role of the cytoplasmic tail of SLAMF1 in MeV entry. As mentioned in chapter 1, the cytoplasmic tail of SLAMF1 contains three SH2-binding motifs; motifs that are known to interact with several cellular proteins, each one starting with a tyrosine residue that it is phosphorylated by kinases located near the inner leaflet of the plasma membrane. We are developing SLAMF1 mutants in which these tyrosine

residues are substituted by phenylalanine residues as well as mutants with serial truncations of the cytoplasmic tail. The substitution mutants should have minimal impact on the overall folding of the protein, since the side chains of tyrosine and phenylalanine differ only in one hydroxyl group, however, importantly phosphorylation of this altered residue by cellular kinases can no longer occur. Although preliminary data suggests a specific role for a particular region of the cytoplasmic tail in MeV entry, further experiments are required to confirm downstream signalling mediated by SLAMF1 is directly involved in this process.

Secondly, one should reflect on the consequences of the observations listed in *i)* related to the requirement activity of certain cellular components. In chapter 4, I have shown that MeV entry is sensitive to inhibition of: myosin-II (a protein necessary for actin contraction and membrane blebbing), as well as certain Rho GTPases and actin dynamism (as demonstrated by the effects of cytochalasin D and jasplakinolide). Several of these components have been shown to be required for the formation of the macropinosome[321] and furthermore entry of other viruses that invade cells via macropinocytosis [195, 416, 521], supporting my hypothesis that MeV is entering cells using a pathway similar to this one. To my knowledge, this is the first time that cellular proteins were shown to be involved in MeV entry (either directly or indirectly) aside from the cellular receptors and co-entry factors previously identified. Indeed, actin, myosin-II and Rho GTPases are all cytosolic proteins; therefore, if they do indeed play a role in MeV entry, it is likely that there impact and role is in steps subsequent to MeV attachment.

Before continuing I provide a more detailed examination of the current dogma of entry for MeV; i.e. (1) the virus adsorbs to the cell surface; (2) attachment of MeV H

with SLAMF1 leads to conformational changes in H, triggering F; (3) activated F is sufficient to induced the fusion of the viral envelope to the plasma membrane and (4) the interior contents of the measles virion are released into the cytoplasm to initiate replication. This is assumed to be identical to the initial step of cell-cell fusion when a MeV-infected cell contacts with an uninfected SLAMF1^{+} cell. When looking at these two phenomena, i.e. entry of virions and cell-cell fusion, at approximately the same time point – i.e. the very early steps of infection – (see chapters 4 and 5), two very distinctive and opposite features were observed: (1) MeV entry was very sensitive to inhibitors of actin dynamism while the same drugs at the same concentration increased cell-cell fusion and (2) infection was shown to require the activity of Rho GTPases while blocking their activity led to an increase in cell-cell fusion. These contrasting findings, gathered and described in chapters 4 and 5, are evidence that indeed, even if MeV is entering cells at the plasma membrane, the fusion mechanism is not governed by the same cellular components nor in the same manner. Nevertheless, I am aware that the findings herein described are per se not sufficient to discern between the two fusion processes, but are indeed evidence of a more complex mechanism that involves other cellular proteins.

In conclusion, I believe that the current understanding of MeV entry should be re-assessed since my data and that of others suggest a more complex mechanism, than previously thought. Here I propose a new model for MeV entry, schematically represented in **Fig.7-1**, based on the current understanding of the fusion mechanism and the data collected during my doctorate. Upon binding of MeV to its receptor SLAMF1, extensive plasma membrane rearrangements lead to the formation of membrane blebs within 10min of viral attachment. It is likely that MeV binding to the

Fig.7-1. **Model of endocytic MeV entry into SLAMF1-positive cells**. (A) MeV binds to human SLAMF1 (CD150) via a specific protein-protein interaction between the viral haemagglutinin and SLAMF1. (B) Within 10 minutes the receptor interaction induces the formation of membrane blebs, governed in part by the RhoA-ROCK-myosin-II axis. Inhibition of this axis (with chemical inhibitors or dominant negative mutants) reduces MeV entry. (C) The formation of membranous blebs is followed by an acute retraction of the cell, orchestrated by the cortical cytoskeleton. Perturbation of this process with chemical inhibitors of actin modulation also reduces MeV entry. (D) The internalisation of MeV particles is concurrent with fluid uptake via a macropinocytosis-like pathway, a process that is sensitive to chemical inhibition with EIPA. Within 45 minutes infected cells begin to re-establish their characteristic morphology through specific phosphorylation of ERM proteins

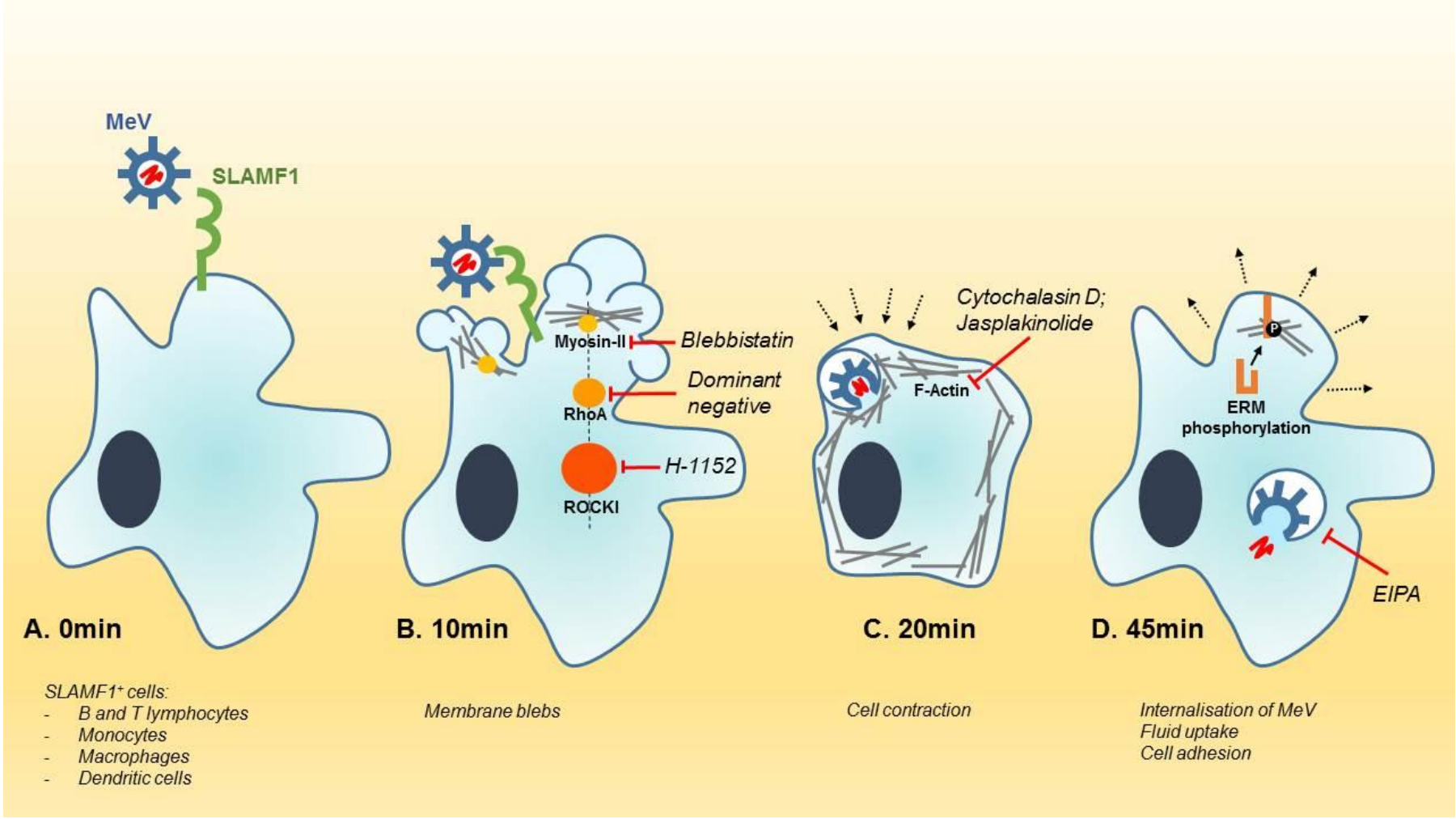
MeV
SLAMF1
Myosin-II
Blebbistatin
Dominant negative
RhoA
H-1152
ROCKI
Cytochalasin D;
Jasplakinolide
F-Actin
ERM phosphorylation
EIPA
A. 0min
B. 10min
C. 20min
D. 45min
SLAMF1+ cells:
- B and T lymphocytes
- Monocytes
- Macrophages
- Dendritic cells
Membrane blebs
Cell contraction
Internalisation of MeV
Fluid uptake
Cell adhesion

cell leads to clustering of SLAMF1, as observed previously [332], and SLAMF1-mediated signalling might activate the myosin-II-ROCKI-RhoA axis, as MeV entry was sensitive to mutants and drugs that target elements of this axis. It is also very likely that triggering of MeV F protein occurs at this point leading to hemifusion of the viral envelope with the plasma membrane or fusion pore formation, since binding to SLAMF1 is sufficient to activate the fusion complex in a pH-independent manner. Importantly, however, the expansion of the pore, and release of the viral genome into the cytosol, might be delayed until later stages. In the scenario where the RNP/genome is released directly into the cellular cortex, the RNP would immediately be presented with a dense cortical actin network that it must overcome before transport to the perinuclear region where replication starts. Hence it is plausible that MeV has evolved to exploit trafficking systems to reach this replication site. Accordingly, even 20min after infection, MeV colocalises with actin-enriched domains and vesicles containing extracellular fluid. This observation is in line with the entry pathways of other related viruses, such as RSV [195], in which the virus colocalises with macropinosomes upon entry. Disrupting actin dynamics and macropinosome formation blocked MeV entry, suggesting that the virus requires a macropinocytosis-like pathway to successfully establish infection. Finally, at 45 min post attachment, the viral RNP complex is released from the macropinosome and replication can start. This new model of MeV entry can certainly impact on the control of the disease, as we have identified several drugs that can block infection. Additionally, with the ongoing use of MeV as a therapeutic tool to treat certain types of cancer, this information can aid researchers in the design of better therapies, tuning MeV entry

into cancer cells by, for instance, the use of drugs that promote macropinocytic uptake of the virus.

7.3 The thermodynamics of disease: a hypothesis on MeV exit

MeV can exit cells via the formation of new virions, a process known as viral budding, or by inducing fusion of neighbouring cells, generating multinucleated cells known as syncytia. Several viruses are known to cause syncytia *in vitro*, including RSV, HIV-I, human metapneumovirus, Hendra and Nipah viruses, etc. Evidence for *in vivo* syncytia formation is also available, with MeV generating multinucleated fused cells in lymph nodes, airway epithelium and in the brain [422]. The relevance of such structures in viral spread has been largely neglected by the scientific community with several observations justifying this opinion in field. Historically, the most notorious example of cell-cell fusion induced by MeV is the formation of viral plaques in the brain during infection of the nervous system. Similarly to other pathogenic infections of the CNS, MeV infection of the brain is commonly seen as a “dead-end” infection, i.e. an infection that does not result in the transmission of virus to other hosts due to the anatomically isolated nature of the brain. MeV genomes isolated from patients suffering from SSPE accumulated several mutations in the *F* and *M* genes; some of these mutations were shown to impact on the ability of M to interact with the cytoplasmic tail of F, hampering the formation of viral particles and increasing the fusogenicity of F [134, 432, 522]. In other tissues, cell-cell fusion is unlikely to be the result of defective *M* or *F* genes, since infectious viral particles can be recovered from infected lymph nodes and lung epithelium where syncytia are normally observed. In recent years, studies on the mechanism of viral induced cell-cell fusion have shed a

new light on its relevance in viral spread. In particular, several reports from Roberto Cattaneo's lab have shown that MeV infection rapidly spreads through polarised lung epithelial cells where cell-cell fusion, induced by the virus, allows cytosolic content mixing and transmission of infection[423]. It is plausible that this mode of infection conveys certain advantages to the virus: by remaining intracellular, MeV escapes antibody neutralisation of virions while more resources for viral production and the release of particles are diverted from neighbouring cells. In our lab, we have been investigating the concept of "viral factories", i.e. infected multinucleated cells that concentrate molecules necessary for viral release leading to the focused production of viral particles. Early reports on the structure of MeV-induced syncytia *in vitro* show that human erythrocytes – that naturally bind MeV H – adsorb to the centre of the syncytium, where presumably MeV H is concentrated [523]. The same study showed that the area of attachment of erythrocytes expands with the maturation of the syncytium forming a ring. It is possible that MeV has evolved to compartmentalise the syncytium in order to maximise the production of viral particles, and perhaps the extensive subversion of the cytoskeleton by MeV, as summarised by Avota and colleagues [524], is evidence of such compartmentalisation. In chapter 5, I have explored the role of several cytoskeletal components in the early stages of MeV-induced cell-cell fusion. Particularly, cell-cell fusion was shown to be restricted by an intact actin cytoskeleton, as observed by other viruses [433, 437, 525]. I am aware, though, that the results presented in chapter 5 were not performed in the context of infection: MeV protein levels were modulated by the strength of the plasmid promoters and most likely certain elements of infection are being ignored or overlooked. However, for the sake of the argument, one should assume that MeV

has evolved to exploit any advantages of cell-cell fusion. One immediate question that emerges after accepting this concept is the balance between fusion and budding and the timing in which both processes occur. Gene expression precedes genome replication during the viral lifecycle, suggesting that MeV-induced cell-cell fusion happens first, as this is only reliant on viral protein expression. Additionally, in the *in vitro* model of infection of human-derived B lymphocyte cell line LCLs described in chapter 6, cell-cell fusion was observed very early in infection but infectious viral particles were only detected later. It was shown previously that interaction of MeV M with the cytoplasmic tails of F and H reduces cell-cell fusion by recruiting these glycoproteins to assembly sites [349, 524]. It is therefore evident that M may function as the molecular “switch” between cell-cell fusion and budding. Nevertheless, the M ORF precedes the *F* and *H* genes in MeV genomes, as described in chapter 1, which suggests that M is at least more transcriptionally abundant than F and H because of the morbillivirus transcriptional gradient. The untranslated region between M and F, present in their mRNAs, also appears to accentuate the difference in the expression of the two proteins, however the role of this region might be more complex than previously stated [124]. If the M protein is indeed more abundant than F and H, how can cell-cell fusion occur so profusely during infection? My prediction is that a putative switch from cell-cell fusion to viral budding is not solely governed by the overall ration of M/F+H but also on the inherent activity and localisation of M. Wakimoto *et al.* showed that actin competes with the cytoplasmic tail of H in the binding of M [349], while M has been shown to interact strongly with filamentous actin, and promote the formation of actin-rich viral-like buds[524]. My hypothesis is that interactions of M with the cytoskeleton impact on cell-cell fusion regardless of the

competitive interaction with cytoplasmic tails of F and H. Currently in our lab we are addressing the role of this protein in cell-cell fusion using our fusion assay. Preliminary data has shown that co-expression of MeV M increased cell-cell fusion induced by either full-length or cytoplasmic-tail-deletions of F and H. Further studies are required to determine the role of cytoskeleton components in cell-cell fusion, particularly in the context of infection.

To finalise, I would like to comment on the difficulties of relating observations *in vitro* to *in vivo* infection. For centuries, MeV has evolved together with the human population, tuning its molecular mechanisms of replication to optimise infection in the host. As shown in several studies [526, 527], *in vivo* infections present viruses with consecutive bottlenecks, as a result of the ever-changing environments that viruses face in the host. Taking MeV as an example, infection arguably starts in the lumen of the lung where the virus interacts with DCs and macrophages, and later infects highly organised tissues, such as those found in lymph nodes and the spleen. With the onset of the first symptoms, such as fever, the virus faces additional changes in the environment, followed by the emergence of IgM antibodies and specialised T cell populations. The complexity of this scenario is hard to reproduce *in vitro*. However, in my opinion, it is almost certain that such changes in environment may impact on the virus itself and the infection it causes. In 1987, Ogura and colleagues documented that the synthesis of the MeV M protein is blocked by exposure to high temperatures, i.e. 39ºC, although its transcript is as stable as the transcripts of other MeV proteins [118]. In the study, they argue that the high temperature blocks the interaction of M-encoding mRNA with polysomes. One can only speculate that the virus may have evolved to take advantage of the onset of fever, which can happen as early as nine

days after initial contact, to block the production of M protein. If so, the reduced expression of M may have certain implications for viral spread. In the future technological advances and a better understanding of the biology of viruses will certainly impact on how we perceive pathogen interactions with highly complex and dynamic organisms, such as humans.

Section 8 - References

1. Moss, W.J. and D.E. Griffin, *Global measles elimination.* Nat Rev Micro, 2006. **4**(12): p. 900-908.
2. Retief, F. and L. Cilliers, *Measles in antiquity and the middle ages.* SAMJ: South African Medical Journal, 2010. **100**: p. 216-217.
3. CASSEDY, J.H. and W.H. McNeill, *Plagues and People*. 1977, JSTOR.
4. Home, W.E., *Francis Home (1719-1813), First Professor of Materia Medica in Edinburgh.* Proceedings of the Royal Society of Medicine, 1928. **21**(6): p. 1013-1015.
5. Paterson, B.J., et al., *Historical data and modern methods reveal insights in measles epidemiology: a retrospective closed cohort study.* BMJ Open, 2013. **3**(1): p. e002033.
6. Katz, S.L., *The History of Measles Virus and the Development and Utilization of Measles Virus Vaccines*, in *History of Vaccine Development*, S.A. Plotkin, Editor. 2011, Springer New York: New York, NY. p. 199-206.
7. Njeumi, F., et al., *The long journey: a brief review of the eradication of rinderpest.* Rev Sci Tech, 2012. **31**(3): p. 729-46.
8. Banyard, A.C., M.D. Baron, and T. Barrett, *A role for virus promoters in determining the pathogenesis of Rinderpest virus in cattle.* J Gen Virol, 2005. **86**(Pt 4): p. 1083-92.
9. FAO, *Declaration of global freedom from rinderpest – Thirty-seventh Session of the FAO Conference, Rome 25 June-2 July 2011.* FAO Animal Production and Health Proceedings, 2013. **17**.
10. Kumar, N., et al., *Peste des petits ruminants virus infection of small ruminants: a comprehensive review.* Viruses, 2014. **6**(6): p. 2287-327.
11. Khan, H.A., et al., *The detection of antibody against peste des petits ruminants virus in sheep, goats, cattle and buffaloes.* Trop Anim Health Prod, 2008. **40**(7): p. 521-7.
12. Albina, E., et al., *Peste des Petits Ruminants, the next eradicated animal disease?* Vet Microbiol, 2013. **165**(1-2): p. 38-44.
13. Australia, A.H., *Disease strategy: Peste des petits ruminants (Version 3.0).* 3 ed. Australian Veterinary Emergency Plan (AUSVETPLAN). Canberra: Primary Industries Ministerial Council.
14. Munir, M., S. Zohari, and M. Berg, *Poverty Alleviation and Global Eradication of Peste des Petits Ruminants*, in *Molecular Biology and Pathogenesis of Peste des Petits Ruminants Virus*. 2013, Springer Berlin Heidelberg. p. 135-148.
15. Deem, S.L., et al., *Canine distemper in terrestrial carnivores: a review.* J Zoo Wildl Med, 2000. **31**(4): p. 441-51.
16. Beineke, A., et al., *Pathogenesis and immunopathology of systemic and nervous canine distemper.* Vet Immunol Immunopathol, 2009. **127**(1-2): p. 1-18.
17. Vandevelde, M., et al., *Demyelination in experimental canine distemper virus infection: immunological, pathologic, and immunohistological studies.* Acta Neuropathol, 1982. **56**(4): p. 285-93.
18. Rohowsky-Kochan, C., P.C. Dowling, and S.D. Cook, *Canine distemper virus-specific antibodies in multiple sclerosis.* Neurology, 1995. **45**(8): p. 1554-60.
19. Harder, T.C. and A.D. Osterhaus, *Canine distemper virus--a morbillivirus in search of new hosts?* Trends Microbiol, 1997. **5**(3): p. 120-4.
20. Otsuki, N., et al., *Canine distemper virus with the intact C protein has the potential to replicate in human epithelial cells by using human nectin4 as a receptor.* Virology, 2013. **435**(2): p. 485-92.

21. Sakai, K., et al., *Canine distemper virus associated with a lethal outbreak in monkeys can readily adapt to use human receptors.* J Virol, 2013. **87**(12): p. 7170-5.
22. Bieringer, M., et al., *Experimental adaptation of wild-type canine distemper virus (CDV) to the human entry receptor CD150.* PLoS One, 2013. **8**(3): p. e57488.
23. Hara, Y., et al., *Function of feline signaling lymphocyte activation molecule as a receptor of canine distemper virus.* J Vet Med Sci, 2013. **75**(8): p. 1085-9.
24. Woo, P.C., et al., *Feline morbillivirus, a previously undescribed paramyxovirus associated with tubulointerstitial nephritis in domestic cats.* Proc Natl Acad Sci U S A, 2012. **109**(14): p. 5435-40.
25. Furuya, T., et al., *Existence of feline morbillivirus infection in Japanese cat populations.* Arch Virol, 2014. **159**(2): p. 371-3.
26. Sakaguchi, S., et al., *Genetic diversity of feline morbilliviruses isolated in Japan.* J Gen Virol, 2014. **95**(Pt 7): p. 1464-8.
27. Muller, G., et al., *Phocine distemper in German seals, 2002.* Emerg Infect Dis, 2004. **10**(4): p. 723-5.
28. Harkonen, T., et al., *The 1988 and 2002 phocine distemper virus epidemics in European harbour seals.* Dis Aquat Organ, 2006. **68**(2): p. 115-30.
29. Sips, G.J., et al., *Involvement of morbilliviruses in the pathogenesis of demyelinating disease.* Rev Med Virol, 2007. **17**(4): p. 223-44.
30. McCarthy, A.J., et al., *Variation in European harbour seal immune response genes and susceptibility to phocine distemper virus (PDV).* Infect Genet Evol, 2011. **11**(7): p. 1616-23.
31. McCullough, S.J., et al., *Isolation and characterisation of a porpoise morbillivirus.* Arch Virol, 1991. **118**(3-4): p. 247-52.
32. Osterhaus, A., et al., *Morbillivirus in monk seal mass mortality.* Nature, 1997. **388**(6645): p. 838-9.
33. Van Bressem, M., et al., *An insight into the epidemiology of dolphin morbillivirus worldwide.* Vet Microbiol, 2001. **81**(4): p. 287-304.
34. Di Guardo, G., et al., *Morbillivirus infections in aquatic mammals: a brief overview.* J Vet Med A Physiol Pathol Clin Med, 2005. **52**(2): p. 88-93.
35. Drexler, J.F., et al., *Bats host major mammalian paramyxoviruses.* Nature Communications, 2012. **3**: p. 796.
36. Lemon, K., et al., *Early target cells of measles virus after aerosol infection of non-human primates.* PLoS Pathog, 2011. **7**(1): p. e1001263.
37. Wolfson, L.J., et al., *Estimates of measles case fatality ratios: a comprehensive review of community-based studies.* Int J Epidemiol, 2009. **38**(1): p. 192-205.
38. Tamashiro, V.G., H.H. Perez, and D.E. Griffin, *Prospective study of the magnitude and duration of changes in tuberculin reactivity during uncomplicated and complicated measles.* Pediatr Infect Dis J, 1987. **6**(5): p. 451-4.
39. Beckford, A.P., R.O. Kaschula, and C. Stephen, *Factors associated with fatal cases of measles. A retrospective autopsy study.* S Afr Med J, 1985. **68**(12): p. 858-63.
40. von Messling, V., D. Milosevic, and R. Cattaneo, *Tropism illuminated: lymphocyte-based pathways blazed by lethal morbillivirus through the host immune system.* Proc Natl Acad Sci U S A, 2004. **101**(39): p. 14216-21.
41. Takeda, M., et al., *Wild-Type Measles Virus is Intrinsically Dual-Tropic.* Front Microbiol, 2011. **2**: p. 279.
42. Zhang, Y., Y.S. Yu, and G.Q. Zang, *Maculopapular rash and Koplik's spots in adult measles.* Rev Soc Bras Med Trop, 2015. **48**(2): p. 231.
43. Lessler, J., et al., *Incubation periods of acute respiratory viral infections: a systematic review.* Lancet Infect Dis, 2009. **9**(5): p. 291-300.

44. Permar, S.R., et al., *Role of CD8(+) lymphocytes in control and clearance of measles virus infection of rhesus monkeys.* J Virol, 2003. **77**(7): p. 4396-400.
45. Enders, J.F., et al., *Isolation of measles virus at autopsy in cases of giant-cell pneumonia without rash.* N Engl J Med, 1959. **261**: p. 875-81.
46. Aicardi, J., et al., *Acute measles encephalitis in children with immunosuppression.* Pediatrics, 1977. **59**(2): p. 232-9.
47. Auwaerter, P.G., et al., *Measles virus infection in rhesus macaques: altered immune responses and comparison of the virulence of six different virus strains.* J Infect Dis, 1999. **180**(4): p. 950-8.
48. Permar, S.R., et al., *Prolonged measles virus shedding in human immunodeficiency virus-infected children, detected by reverse transcriptase-polymerase chain reaction.* J Infect Dis, 2001. **183**(4): p. 532-8.
49. van Binnendijk, R.S., et al., *Evaluation of serological and virological tests in the diagnosis of clinical and subclinical measles virus infections during an outbreak of measles in The Netherlands.* J Infect Dis, 2003. **188**(6): p. 898-903.
50. Lin, W.H., et al., *Prolonged persistence of measles virus RNA is characteristic of primary infection dynamics.* Proc Natl Acad Sci U S A, 2012. **109**(37): p. 14989-94.
51. Duke, T. and C.S. Mgone, *Measles: not just another viral exanthem.* Lancet, 2003. **361**(9359): p. 763-73.
52. Griffin, D.E., B.J. Ward, and L.M. Esolen, *Pathogenesis of measles virus infection: an hypothesis for altered immune responses.* J Infect Dis, 1994. **170 Suppl 1**: p. S24-31.
53. Garg, R.K., *Subacute sclerosing panencephalitis.* Postgrad Med J, 2002. **78**(916): p. 63-70.
54. Hardie, D.R., et al., *Molecular characterisation of virus in the brains of patients with measles inclusion body encephalitis (MIBE).* Virol J, 2013. **10**: p. 283.
55. WHO *Measles Case Distribution by Month and WHO Regions, 2008-2015*. Measles Data Surveillance, 2015.
56. WHO *Measles*. Immunization, Vaccines and Biologicals, 2015.
57. *Progress in global measles control and mortality reduction, 2000-2007.* Wkly Epidemiol Rec, 2008. **83**(49): p. 441-8.
58. Hall, R. and D. Jolley, *International Measles Incidence and Immunization Coverage.* Journal of Infectious Diseases, 2011. **204**(suppl 1): p. S158-S163.
59. *Measles vaccines: WHO position paper.* Wkly Epidemiol Rec, 2009. **84**(35): p. 349-60.
60. Moss, W.J. and P. Strebel, *Biological feasibility of measles eradication.* J Infect Dis, 2011. **204 Suppl 1**: p. S47-53.
61. Bhatt, P.N., et al., *Viral infections of monkeys in their natural habitat in southern India. I. Some properties of cytopathic agents isolated from Bonnet and Langur monkeys.* Am J Trop Med Hyg, 1966. **15**(4): p. 551-60.
62. Jones-Engel, L., et al., *Detection of antibodies to selected human pathogens among wild and pet macaques (Macaca tonkeana) in Sulawesi, Indonesia.* Am J Primatol, 2001. **54**(3): p. 171-8.
63. Hope, K., et al., *Measles transmission in health care waiting rooms: implications for public health response.* Western Pacific Surveillance and Response Journal : WPSAR, 2012. **3**(4): p. 33-38.
64. Edelson, P.J., *Patterns of measles transmission among airplane travelers.* Travel Med Infect Dis, 2012. **10**(5-6): p. 230-5.
65. White, S.J., et al., *Measles, Mumps, and Rubella.* Clinical Obstetrics and Gynecology, 2012. **55**(2): p. 550-559.
66. Rima, B.K., et al., *Temporal and geographical distribution of measles virus genotypes.* J Gen Virol, 1995. **76 (Pt 5)**: p. 1173-80.

67. Rota, P.A., et al., *Global distribution of measles genotypes and measles molecular epidemiology.* J Infect Dis, 2011. **204 Suppl 1**: p. S514-23.
68. Rota, J.S., et al., *Comparison of sequences of the H, F, and N coding genes of measles virus vaccine strains.* Virus Res, 1994. **31**(3): p. 317-30.
69. Rota, P.A., D.A. Featherstone, and W.J. Bellini, *Molecular epidemiology of measles virus.* Curr Top Microbiol Immunol, 2009. **330**: p. 129-50.
70. Griffin, D.E., *Measles virus-induced suppression of immune responses.* Immunological reviews, 2010. **236**: p. 176-189.
71. Mosquera, M.M., et al., *Evaluation of diagnostic markers for measles virus infection in the context of an outbreak in Spain.* J Clin Microbiol, 2005. **43**(10): p. 5117-21.
72. Nestibo, L., et al., *Differentiating the wild from the attenuated during a measles outbreak.* Paediatrics & Child Health, 2012. **17**(4): p. e32-e33.
73. Ikeno, S., et al., *Sensitive detection of measles virus infection in the blood and tissues of humanized mouse by one-step quantitative RT-PCR.* Front Microbiol, 2013. **4**: p. 298.
74. Kayikcioglu, O., et al., *Ocular findings in a measles epidemic among young adults.* Ocul Immunol Inflamm, 2000. **8**(1): p. 59-62.
75. Rota, P.A., et al., *Detection of measles virus RNA in urine specimens from vaccine recipients.* Journal of Clinical Microbiology, 1995. **33**(9): p. 2485-2488.
76. Enders, J.F. and T.C. Peebles, *Propagation in tissue cultures of cytopathogenic agents from patients with measles.* Proc Soc Exp Biol Med, 1954. **86**(2): p. 277-86.
77. Enders, J.F., et al., *Studies on an attenuated measles-virus vaccine. I. Development and preparations of the vaccine: technics for assay of effects of vaccination.* N Engl J Med, 1960. **263**: p. 153-9.
78. WHO *EURO Immunization Monitor.* WHO, Regional Office for Europe, 2009.
79. Muscat, M., et al., *Measles in Europe: an epidemiological assessment.* Lancet, 2009. **373**(9661): p. 383-9.
80. Muscat, M., *Who gets measles in Europe?* J Infect Dis, 2011. **204 Suppl 1**: p. S353-65.
81. Filia, A., et al., *Measles resurges in Italy: preliminary data from September 2007 to May 2008.* Euro Surveill, 2008. **13**(29).
82. Plattet, P., et al., *Measles Virus Fusion Protein: Structure, Function and Inhibition.* Viruses, 2016. **8**(4): p. 112.
83. D'Souza, R.M. and R. D'Souza, *Vitamin A for treating measles in children.* Cochrane Database Syst Rev, 2002(1): p. Cd001479.
84. Blumberg, B.M., et al., *Measles virus L protein evidences elements of ancestral RNA polymerase.* Virology, 1988. **164**(2): p. 487-497.
85. Bellini, W.J., et al., *Measles virus P gene codes for two proteins.* Journal of Virology, 1985. **53**(3): p. 908-919.
86. Cattaneo, R., et al., *Measles virus editing provides an additional cysteine-rich protein.* Cell, 1989. **56**(5): p. 759-64.
87. Andzhaparidze, O.G., et al., *Non-infectious morphologically altered nucleocapsids of measles virus from persistently infected cells.* Arch Virol, 1987. **95**(1-2): p. 17-28.
88. Anderson, D.E. and V. von Messling, *Region between the canine distemper virus M and F genes modulates virulence by controlling fusion protein expression.* J Virol, 2008. **82**(21): p. 10510-8.
89. Rima, B.K., et al., *Sequence divergence of measles virus haemagglutinin during natural evolution and adaptation to cell culture.* J Gen Virol, 1997. **78 (Pt 1)**: p. 97-106.
90. Jenkins, G.M., et al., *Rates of molecular evolution in RNA viruses: a quantitative phylogenetic analysis.* J Mol Evol, 2002. **54**(2): p. 156-65.
91. Pomeroy, L.W., O.N. Bjornstad, and E.C. Holmes, *The evolutionary and epidemiological dynamics of the paramyxoviridae.* J Mol Evol, 2008. **66**(2): p. 98-106.

92. Schrag, S.J., P.A. Rota, and W.J. Bellini, *Spontaneous Mutation Rate of Measles Virus: Direct Estimation Based on Mutations Conferring Monoclonal Antibody Resistance.* Journal of Virology, 1999. **73**(1): p. 51-54.
93. Zhang, X., et al., *Determination of spontaneous mutation frequencies in measles virus under nonselective conditions.* J Virol, 2013. **87**(5): p. 2686-92.
94. Fulton, B.O., et al., *Mutational Analysis of Measles Virus Suggests Constraints on Antigenic Variation of the Glycoproteins.* Cell Rep, 2015. **11**(9): p. 1331-8.
95. Duprex, W.P., et al., *Observation of measles virus cell-to-cell spread in astrocytoma cells by using a green fluorescent protein-expressing recombinant virus.* J Virol, 1999. **73**(11): p. 9568-75.
96. Gould, A.R., *Comparison of the deduced matrix and fusion protein sequences of equine morbillivirus with cognate genes of the Paramyxoviridae.* Virus Res, 1996. **43**(1): p. 17-31.
97. Casali, P., et al., *Purification of measles virus glycoproteins and their integration into artificial lipid membranes.* J Gen Virol, 1981. **54**(Pt 1): p. 161-71.
98. Armstrong, M.A., et al., *Immunoelectron microscopic studies on haemagglutinin and haemolysin of measles virus in infected HEp2 cells.* J Gen Virol, 1982. **59**(Pt 1): p. 187-92.
99. Liljeroos, L., et al., *Electron cryotomography of measles virus reveals how matrix protein coats the ribonucleocapsid within intact virions.* Proc Natl Acad Sci U S A, 2011. **108**(44): p. 18085-90.
100. Nakai, M. and D.T. Imagawa, *Electron microscopy of measles virus replication.* J Virol, 1969. **3**(2): p. 187-97.
101. Cox, R. and R.K. Plemper, *The paramyxovirus polymerase complex as a target for next-generation anti-paramyxovirus therapeutics.* Frontiers in Microbiology, 2015. **6**: p. 459.
102. Rager, M., et al., *Polyploid measles virus with hexameric genome length.* EMBO J, 2002. **21**(10): p. 2364-72.
103. Takeda, M., et al., *Generation of measles virus with a segmented RNA genome.* J Virol, 2006. **80**(9): p. 4242-8.
104. Waterson, A.P., *Two kinds of myxovirus.* Nature, 1962. **193**: p. 1163-4.
105. Thorne, H.V. and E. Dermott, *Y-forms as possible intermediates in the replication of measles virus nucleocapsids.* Nature, 1977. **268**(5618): p. 345-7.
106. Gutsche, I., et al., *Structural virology. Near-atomic cryo-EM structure of the helical measles virus nucleocapsid.* Science, 2015. **348**(6235): p. 704-7.
107. Stallcup, K.C., S.L. Wechsler, and B.N. Fields, *Purification of measles virus and characterization of subviral components.* J Virol, 1979. **30**(1): p. 166-76.
108. Calain, P. and L. Roux, *The rule of six, a basic feature for efficient replication of Sendai virus defective interfering RNA.* J Virol, 1993. **67**(8): p. 4822-30.
109. Portner, A., et al., *Antibodies against Sendai virus L protein: distribution of the protein in nucleocapsids revealed by immunoelectron microscopy.* Virology, 1988. **163**(1): p. 236-9.
110. Sidhu, M.S., et al., *Rescue of synthetic measles virus minireplicons: measles genomic termini direct efficient expression and propagation of a reporter gene.* Virology, 1995. **208**(2): p. 800-7.
111. Bhella, D., A. Ralph, and R.P. Yeo, *Conformational flexibility in recombinant measles virus nucleocapsids visualised by cryo-negative stain electron microscopy and real-space helical reconstruction.* J Mol Biol, 2004. **340**(2): p. 319-31.
112. Afzal, M.A., et al., *Comparative evaluation of measles virus-specific RT-PCR methods through an international collaborative study.* J Med Virol, 2003. **70**(1): p. 171-6.
113. Rima, B.K. and N.V. McFerran, *Dinucleotide and stop codon frequencies in single-stranded RNA viruses.* J Gen Virol, 1997. **78 (Pt 11)**: p. 2859-70.

114. Calain, P. and L. Roux, *Generation of measles virus defective interfering particles and their presence in a preparation of attenuated live-virus vaccine.* Journal of Virology, 1988. **62**(8): p. 2859-2866.
115. Hall, W.W. and V. ter Meulen, *The effects of actinomycin D on RNA synthesis in measles virus-infected cells.* J Gen Virol, 1977. **34**(2): p. 391-6.
116. Gotoh, B., et al., *Paramyxovirus accessory proteins as interferon antagonists.* Microbiology and immunology, 2001. **45**(12): p. 787-800.
117. Schneider-Schaulies, S., et al., *Expression of measles virus RNA in peripheral blood mononuclear cells of patients with measles, SSPE, and autoimmune diseases.* Virology, 1991. **182**(2): p. 703-11.
118. Ogura, H., et al., *Selective inhibition of translation of the mRNA coding for measles virus membrane protein at elevated temperatures.* J Virol, 1987. **61**(2): p. 472-9.
119. Cattaneo, R., et al., *Altered transcription of a defective measles virus genome derived from a diseased human brain.* The EMBO Journal, 1987. **6**(3): p. 681-688.
120. Plumet, S., W.P. Duprex, and D. Gerlier, *Dynamics of Viral RNA Synthesis during Measles Virus Infection.* Journal of Virology, 2005. **79**(11): p. 6900-6908.
121. Pfaller, C.K., et al., *Measles Virus Defective Interfering RNAs Are Generated Frequently and Early in the Absence of C Protein and Can Be Destabilized by Adenosine Deaminase Acting on RNA-1-Like Hypermutations.* Journal of Virology, 2015. **89**(15): p. 7735-7747.
122. Pfaller, C.K., et al., *Measles virus C protein impairs production of defective copyback double-stranded viral RNA and activation of protein kinase R.* J Virol, 2014. **88**(1): p. 456-68.
123. Nishie, T. and K. Nagata, *Measles virus C protein facilitates transcription by the control of N protein-viral genomic RNA interaction in early phases of infection.* Biochem Biophys Res Commun, 2015. **463**(4): p. 1262-6.
124. Anderson, D.E., et al., *Elements in the canine distemper virus M 3' UTR contribute to control of replication efficiency and virulence.* PLoS One, 2012. **7**(2): p. e31561.
125. Takeda, M., et al., *Long Untranslated Regions of the Measles Virus M and F Genes Control Virus Replication and Cytopathogenicity.* Journal of Virology, 2005. **79**(22): p. 14346-14354.
126. den Boon, J.A. and P. Ahlquist, *Organelle-like membrane compartmentalization of positive-strand RNA virus replication factories.* Annu Rev Microbiol, 2010. **64**: p. 241-56.
127. Follett, E.A., C.R. Pringle, and T.H. Pennington, *Events following the infections of enucleate cells with measles virus.* J Gen Virol, 1976. **32**(2): p. 163-75.
128. Ludlow, M., et al., *Measles virus superinfection immunity and receptor redistribution in persistently infected NT2 cells.* J Gen Virol, 2005. **86**(Pt 8): p. 2291-303.
129. Duprex, W.P., F.M. Collins, and B.K. Rima, *Modulating the Function of the Measles Virus RNA-Dependent RNA Polymerase by Insertion of Green Fluorescent Protein into the Open Reading Frame.* Journal of Virology, 2002. **76**(14): p. 7322-7328.
130. Bedows, E., K.M. Rao, and M.J. Welsh, *Fate of microfilaments in vero cells infected with measles virus and herpes simplex virus type 1.* Mol Cell Biol, 1983. **3**(4): p. 712-9.
131. Moyer, S.A., S.C. Baker, and S.M. Horikami, *Host cell proteins required for measles virus reproduction.* J Gen Virol, 1990. **71 (Pt 4)**: p. 775-83.
132. Koga, R., et al., *Actin-Modulating Protein Cofilin Is Involved in the Formation of Measles Virus Ribonucleoprotein Complex at the Perinuclear Region.* J Virol, 2015. **89**(20): p. 10524-31.
133. Rima, B.K. and W.P. Duprex, *The measles virus replication cycle.* Curr Top Microbiol Immunol, 2009. **329**: p. 77-102.
134. Cattaneo, R., et al., *Mutated and hypermutated genes of persistent measles viruses which caused lethal human brain diseases.* Virology, 1989. **173**(2): p. 415-25.
135. Irie, T., et al., *Sendai Virus C Proteins Regulate Viral Genome and Antigenome Synthesis To Dictate the Negative Genome Polarity.* Journal of Virology, 2014. **88**(1): p. 690-698.

136. Inoue, Y., et al., *Inhibition of host protein synthesis in B95a cells infected with the HL strain of measles virus.* Comp Immunol Microbiol Infect Dis, 2009. **32**(1): p. 29-41.
137. Sato, H., et al., *Measles virus N protein inhibits host translation by binding to eIF3-p40.* J Virol, 2007. **81**(21): p. 11569-76.
138. Inoue, Y., et al., *Selective Translation of the Measles Virus Nucleocapsid mRNA by La Protein.* Frontiers in Microbiology, 2011. **2**: p. 173.
139. Bartz, R., et al., *Differential receptor usage by measles virus strains.* J Gen Virol, 1998. **79 (Pt 5)**: p. 1015-25.
140. Condack, C., et al., *Measles virus vaccine attenuation: suboptimal infection of lymphatic tissue and tropism alteration.* J Infect Dis, 2007. **196**(4): p. 541-9.
141. Bitnun, A., et al., *Measles inclusion-body encephalitis caused by the vaccine strain of measles virus.* Clin Infect Dis, 1999. **29**(4): p. 855-61.
142. van Binnendijk, R.S., et al., *Viral replication and development of specific immunity in macaques after infection with different measles virus strains.* J Infect Dis, 1994. **170**(2): p. 443-8.
143. Sato, H., R. Miura, and C. Kai, *Measles virus infection induces interleukin-8 release in human pulmonary epithelial cells.* Comp Immunol Microbiol Infect Dis, 2005. **28**(4): p. 311-20.
144. Sato, H., et al., *Measles virus induces cell-type specific changes in gene expression.* Virology, 2008. **375**(2): p. 321-30.
145. Zilliox, M.J., W.J. Moss, and D.E. Griffin, *Gene expression changes in peripheral blood mononuclear cells during measles virus infection.* Clin Vaccine Immunol, 2007. **14**(7): p. 918-23.
146. Herschke, F., et al., *Cell-cell fusion induced by measles virus amplifies the type I interferon response.* J Virol, 2007. **81**(23): p. 12859-71.
147. Plumet, S., et al., *Cytosolic 5'-triphosphate ended viral leader transcript of measles virus as activator of the RIG I-mediated interferon response.* PLoS One, 2007. **2**(3): p. e279.
148. Ikegame, S., et al., *Both RIG-I and MDA5 RNA helicases contribute to the induction of alpha/beta interferon in measles virus-infected human cells.* J Virol, 2010. **84**(1): p. 372-9.
149. Bieback, K., et al., *Hemagglutinin protein of wild-type measles virus activates toll-like receptor 2 signaling.* J Virol, 2002. **76**(17): p. 8729-36.
150. Colombo, M., et al., *The interaction between the measles virus nucleoprotein and the Interferon Regulator Factor 3 relies on a specific cellular environment.* Virol J, 2009. **6**: p. 59.
151. tenOever, B.R., et al., *Recognition of the measles virus nucleocapsid as a mechanism of IRF-3 activation.* J Virol, 2002. **76**(8): p. 3659-69.
152. Ho, T.-H., et al., *PACT- and RIG-I-Dependent Activation of Type I Interferon Production by a Defective Interfering RNA Derived from Measles Virus Vaccine.* Journal of Virology, 2016. **90**(3): p. 1557-1568.
153. Naniche, D., et al., *Evasion of host defenses by measles virus: wild-type measles virus infection interferes with induction of Alpha/Beta interferon production.* J Virol, 2000. **74**(16): p. 7478-84.
154. Nakatsu, Y., et al., *A highly attenuated measles virus vaccine strain encodes a fully functional C protein.* J Virol, 2009. **83**(22): p. 11996-2001.
155. Bankamp, B., et al., *Adaptation to cell culture induces functional differences in measles virus proteins.* Virol J, 2008. **5**: p. 129.
156. Valsamakis, A., et al., *Recombinant measles viruses with mutations in the C, V, or F gene have altered growth phenotypes in vivo.* J Virol, 1998. **72**(10): p. 7754-61.
157. Patterson, J.B., et al., *V and C proteins of measles virus function as virulence factors in vivo.* Virology, 2000. **267**(1): p. 80-9.

158. Pfaller, C.K. and K.K. Conzelmann, *Measles virus V protein is a decoy substrate for IkappaB kinase alpha and prevents Toll-like receptor 7/9-mediated interferon induction.* J Virol, 2008. **82**(24): p. 12365-73.
159. Andrejeva, J., et al., *The V proteins of paramyxoviruses bind the IFN-inducible RNA helicase, mda-5, and inhibit its activation of the IFN-beta promoter.* Proc Natl Acad Sci U S A, 2004. **101**(49): p. 17264-9.
160. Parisien, J.P., et al., *A shared interface mediates paramyxovirus interference with antiviral RNA helicases MDA5 and LGP2.* J Virol, 2009. **83**(14): p. 7252-60.
161. Palosaari, H., et al., *STAT protein interference and suppression of cytokine signal transduction by measles virus V protein.* J Virol, 2003. **77**(13): p. 7635-44.
162. Takeuchi, K., et al., *Measles virus V protein blocks interferon (IFN)-alpha/beta but not IFN-gamma signaling by inhibiting STAT1 and STAT2 phosphorylation.* FEBS Lett, 2003. **545**(2-3): p. 177-82.
163. Tober, C., et al., *Expression of measles virus V protein is associated with pathogenicity and control of viral RNA synthesis.* J Virol, 1998. **72**(10): p. 8124-32.
164. Griffin, D.E., *Measles virus-induced suppression of immune responses.* Immunol Rev, 2010. **236**: p. 176-89.
165. Jaye, A., et al., *Vigorous but short-term gamma interferon T-cell responses against a dominant HLA-A*02-restricted measles virus epitope in patients with measles.* J Virol, 2003. **77**(8): p. 5014-6.
166. Griffin, D.E., et al., *Immune activation during measles: interferon-gamma and neopterin in plasma and cerebrospinal fluid in complicated and uncomplicated disease.* J Infect Dis, 1990. **161**(3): p. 449-53.
167. Ryon, J.J., et al., *Functional and phenotypic changes in circulating lymphocytes from hospitalized zambian children with measles.* Clin Diagn Lab Immunol, 2002. **9**(5): p. 994-1003.
168. Moss, W.J., et al., *Differential regulation of interleukin (IL)-4, IL-5, and IL-10 during measles in Zambian children.* J Infect Dis, 2002. **186**(7): p. 879-87.
169. Griffin, D.E. and B.J. Ward, *Differential CD4 T cell activation in measles.* J Infect Dis, 1993. **168**(2): p. 275-81.
170. Grégoire, I.P., et al., *IRGM Is a Common Target of RNA Viruses that Subvert the Autophagy Network.* PLoS Pathogens, 2011. **7**(12): p. e1002422.
171. Chauhan, S., M.A. Mandell, and V. Deretic, *IRGM governs the core autophagy machinery to conduct antimicrobial defense.* Molecular cell, 2015. **58**(3): p. 507-521.
172. Richetta, C., et al., *Sustained autophagy contributes to measles virus infectivity.* PLoS Pathog, 2013. **9**(9): p. e1003599.
173. Joubert, P.E., et al., *Autophagy induction by the pathogen receptor CD46.* Cell Host Microbe, 2009. **6**(4): p. 354-66.
174. Esolen, L.M., et al., *Apoptosis as a cause of death in measles virus-infected cells.* J Virol, 1995. **69**(6): p. 3955-8.
175. Yi, C., et al., *Hemagglutinin protein of measles virus induces apoptosis of HeLa cells via both extrinsic and intrinsic pathways.* Can J Microbiol, 2013. **59**(12): p. 814-24.
176. Sato, H., et al., *Measles Virus Infection Inactivates Cellular Protein Phosphatase 5 with Consequent Suppression of Sp1 and c-Myc Activities.* Journal of Virology, 2015. **89**(19): p. 9709-9718.
177. Takahashi, M., et al., *Suppression of virus replication via down-modulation of mitochondrial short chain enoyl-CoA hydratase in human glioblastoma cells.* Antiviral Res, 2007. **75**(2): p. 152-8.
178. Robinzon, S., et al., *Impaired cholesterol biosynthesis in a neuronal cell line persistently infected with measles virus.* J Virol, 2009. **83**(11): p. 5495-504.

179. Alkhatib, G. and D.J. Briedis, *The predicted primary structure of the measles virus hemagglutinin.* Virology, 1986. **150**(2): p. 479-90.
180. Hashiguchi, T., et al., *Structure of the measles virus hemagglutinin bound to its cellular receptor SLAM.* Nat Struct Mol Biol, 2011. **18**(2): p. 135-41.
181. Hashiguchi, T., et al., *Crystal structure of measles virus hemagglutinin provides insight into effective vaccines.* Proc Natl Acad Sci U S A, 2007. **104**(49): p. 19535-40.
182. Moll, M., H.D. Klenk, and A. Maisner, *Importance of the cytoplasmic tails of the measles virus glycoproteins for fusogenic activity and the generation of recombinant measles viruses.* J Virol, 2002. **76**(14): p. 7174-86.
183. Colf, L.A., Z.S. Juo, and K.C. Garcia, *Structure of the measles virus hemagglutinin.* Nat Struct Mol Biol, 2007. **14**(12): p. 1227-8.
184. Plemper, R.K., A.L. Hammond, and R. Cattaneo, *Characterization of a region of the measles virus hemagglutinin sufficient for its dimerization.* J Virol, 2000. **74**(14): p. 6485-93.
185. Richardson, C., et al., *The nucleotide sequence of the mRNA encoding the fusion protein of measles virus (Edmonston strain): a comparison of fusion proteins from several different paramyxoviruses.* Virology, 1986. **155**(2): p. 508-23.
186. Muhlebach, M.D., V.H. Leonard, and R. Cattaneo, *The measles virus fusion protein transmembrane region modulates availability of an active glycoprotein complex and fusion efficiency.* J Virol, 2008. **82**(22): p. 11437-45.
187. Caballero, M., et al., *Measles Virus Fusion Protein Is Palmitoylated on Transmembrane-Intracytoplasmic Cysteine Residues Which Participate in Cell Fusion.* Journal of Virology, 1998. **72**(10): p. 8198-8204.
188. Buckland, R., et al., *A leucine zipper structure present in the measles virus fusion protein is not required for its tetramerization but is essential for fusion.* J Gen Virol, 1992. **73 (Pt 7)**: p. 1703-7.
189. Plemper, R.K., A.L. Hammond, and R. Cattaneo, *Measles virus envelope glycoproteins hetero-oligomerize in the endoplasmic reticulum.* J Biol Chem, 2001. **276**(47): p. 44239-46.
190. Watanabe, M., et al., *Engineered serine protease inhibitor prevents furin-catalyzed activation of the fusion glycoprotein and production of infectious measles virus.* J Virol, 1995. **69**(5): p. 3206-10.
191. Bolt, G. and I.R. Pedersen, *The role of subtilisin-like proprotein convertases for cleavage of the measles virus fusion glycoprotein in different cell types.* Virology, 1998. **252**(2): p. 387-98.
192. Lin, L.-T. and C.D. Richardson, *The Host Cell Receptors for Measles Virus and Their Interaction with the Viral Hemagglutinin (H) Protein.* Viruses, 2016. **8**(9): p. 250.
193. Pager, C.T. and R.E. Dutch, *Cathepsin L is involved in proteolytic processing of the Hendra virus fusion protein.* J Virol, 2005. **79**(20): p. 12714-20.
194. Meulendyke, K.A., et al., *Endocytosis plays a critical role in proteolytic processing of the Hendra virus fusion protein.* J Virol, 2005. **79**(20): p. 12643-9.
195. Krzyzaniak, M.A., et al., *Host cell entry of respiratory syncytial virus involves macropinocytosis followed by proteolytic activation of the F protein.* PLoS Pathog, 2013. **9**(4): p. e1003309.
196. Hu, A., et al., *Influence of N-linked oligosaccharide chains on the processing, cell surface expression and function of the measles virus fusion protein.* J Gen Virol, 1995. **76 (Pt 3)**: p. 705-10.
197. Sawatsky, B. and V. von Messling, *Canine distemper viruses expressing a hemagglutinin without N-glycans lose virulence but retain immunosuppression.* J Virol, 2010. **84**(6): p. 2753-61.
198. Carter, J.R., et al., *Role of N-linked glycosylation of the Hendra virus fusion protein.* J Virol, 2005. **79**(12): p. 7922-5.
199. Stone, J.A., et al., *Multiple Novel Functions of Henipavirus O-glycans: The First O-glycan Functions Identified in the Paramyxovirus Family.* PLoS Pathog, 2016. **12**(2): p. e1005445.

200. Fournier, P., et al., *Antibodies to a new linear site at the topographical or functional interface between the haemagglutinin and fusion proteins protect against measles encephalitis.* J Gen Virol, 1997. **78 (Pt 6)**: p. 1295-302.
201. Xu, K., et al., *Crystal Structure of the Pre-fusion Nipah Virus Fusion Glycoprotein Reveals a Novel Hexamer-of-Trimers Assembly.* PLoS Pathog, 2015. **11**(12): p. e1005322.
202. Plattet, P. and R.K. Plemper, *Envelope protein dynamics in paramyxovirus entry.* MBio, 2013. **4**(4).
203. Tatsuo, H., N. Ono, and Y. Yanagi, *Morbilliviruses use signaling lymphocyte activation molecules (CD150) as cellular receptors.* J Virol, 2001. **75**(13): p. 5842-50.
204. Muhlebach, M.D., et al., *Adherens junction protein nectin-4 is the epithelial receptor for measles virus.* Nature, 2011. **480**(7378): p. 530-3.
205. Pratakpiriya, W., et al., *Nectin4 is an epithelial cell receptor for canine distemper virus and involved in neurovirulence.* J Virol, 2012. **86**(18): p. 10207-10.
206. Ono, N., et al., *Measles viruses on throat swabs from measles patients use signaling lymphocytic activation molecule (CDw150) but not CD46 as a cellular receptor.* J Virol, 2001. **75**(9): p. 4399-401.
207. Erlenhoefer, C., et al., *CD150 (SLAM) Is a Receptor for Measles Virus but Is Not Involved in Viral Contact-Mediated Proliferation Inhibition.* Journal of Virology, 2001. **75**(10): p. 4499-4505.
208. Tatsuo, H., et al., *SLAM (CDw150) is a cellular receptor for measles virus.* Nature, 2000. **406**(6798): p. 893-7.
209. van Driel, B.J., et al., *Responses to Microbial Challenges by SLAMF Receptors.* Front Immunol, 2016. **7**: p. 4.
210. Berger, S.B., et al., *SLAM is a microbial sensor that regulates bacterial phagosome functions in macrophages.* Nat Immunol, 2010. **11**(10): p. 920-7.
211. Baorto, D.M., et al., *Survival of FimH-expressing enterobacteria in macrophages relies on glycolipid traffic.* Nature, 1997. **389**(6651): p. 636-9.
212. Schwartzberg, P.L., et al., *SLAM receptors and SAP influence lymphocyte interactions, development and function.* Nat Rev Immunol, 2009. **9**(1): p. 39-46.
213. Veillette, A., *SLAM-family receptors: immune regulators with or without SAP-family adaptors.* Cold Spring Harb Perspect Biol, 2010. **2**(3): p. a002469.
214. Veillette, A., et al., *Importance and mechanism of 'switch' function of SAP family adapters.* Immunol Rev, 2009. **232**(1): p. 229-39.
215. Chan, B., et al., *SAP couples Fyn to SLAM immune receptors.* Nat Cell Biol, 2003. **5**(2): p. 155-60.
216. Sayos, J., et al., *The X-linked lymphoproliferative-disease gene product SAP regulates signals induced through the co-receptor SLAM.* Nature, 1998. **395**(6701): p. 462-469.
217. van Driel, B., et al., *The cell surface receptor Slamf6 modulates innate immune responses during Citrobacter rodentium-induced colitis.* Int Immunol, 2015. **27**(9): p. 447-57.
218. Llanes-Rodas, R. and C. Liu, *Rapid diagnosis of measles from urinary sediments stained with fluorescent antibody.* N Engl J Med, 1966. **275**(10): p. 516-23.
219. Moench, T.R., et al., *Acute measles in patients with and without neurological involvement: distribution of measles virus antigen and RNA.* J Infect Dis, 1988. **158**(2): p. 433-42.
220. Sakaguchi, M., et al., *Growth of measles virus in epithelial and lymphoid tissues of cynomolgus monkeys.* Microbiol Immunol, 1986. **30**(10): p. 1067-73.
221. Noyce, R.S., et al., *Tumor Cell Marker PVRL4 (Nectin 4) Is an Epithelial Cell Receptor for Measles Virus.* PLoS Pathog, 2011. **7**(8): p. e1002240.
222. Derycke, M.S., et al., *Nectin 4 overexpression in ovarian cancer tissues and serum: potential role as a serum biomarker.* Am J Clin Pathol, 2010. **134**(5): p. 835-45.

223. Takano, A., et al., *Identification of nectin-4 oncoprotein as a diagnostic and therapeutic target for lung cancer.* Cancer Res, 2009. **69**(16): p. 6694-703.
224. Fabre-Lafay, S., et al., *Nectin-4, a new serological breast cancer marker, is a substrate for tumor necrosis factor-alpha-converting enzyme (TACE)/ADAM-17.* J Biol Chem, 2005. **280**(20): p. 19543-50.
225. Reymond, N., et al., *Nectin4/PRR4, a new afadin-associated member of the nectin family that trans-interacts with nectin1/PRR1 through V domain interaction.* J Biol Chem, 2001. **276**(46): p. 43205-15.
226. Takai, Y., et al., *The immunoglobulin-like cell adhesion molecule nectin and its associated protein afadin.* Annu Rev Cell Dev Biol, 2008. **24**: p. 309-42.
227. Geraghty, R.J., et al., *Entry of alphaherpesviruses mediated by poliovirus receptor-related protein 1 and poliovirus receptor.* Science, 1998. **280**(5369): p. 1618-20.
228. Fan, Q., et al., *Herpes B virus utilizes human nectin-1 but not HVEM or PILRalpha for cell-cell fusion and virus entry.* J Virol, 2012. **86**(8): p. 4468-76.
229. Birch, J., et al., *Characterization of ovine Nectin-4, a novel peste des petits ruminants virus receptor.* J Virol, 2013. **87**(8): p. 4756-61.
230. Lan, N.T., et al., *The growth profiles of three types of canine distemper virus on Vero cells expressing canine signaling lymphocyte activation molecule.* J Vet Med Sci, 2005. **67**(5): p. 491-5.
231. Melia, M.M., et al., *Use of SLAM and PVRL4 and identification of pro-HB-EGF as cell entry receptors for wild type phocine distemper virus.* PLoS One, 2014. **9**(8): p. e106281.
232. Delpeut, S., R.S. Noyce, and C.D. Richardson, *The tumor-associated marker, PVRL4 (nectin-4), is the epithelial receptor for morbilliviruses.* Viruses, 2014. **6**(6): p. 2268-86.
233. Dorig, R.E., et al., *The human CD46 molecule is a receptor for measles virus (Edmonston strain).* Cell, 1993. **75**(2): p. 295-305.
234. Naniche, D., et al., *Human membrane cofactor protein (CD46) acts as a cellular receptor for measles virus.* Journal of Virology, 1993. **67**(10): p. 6025-6032.
235. Andrews, P.W., et al., *A human cell-surface antigen defined by a monoclonal antibody and controlled by a gene on human chromosome 1.* Ann Hum Genet, 1985. **49**(Pt 1): p. 31-9.
236. Sarma, J.V. and P.A. Ward, *The complement system.* Cell Tissue Res, 2011. **343**(1): p. 227-35.
237. Liszewski, M.K., T.W. Post, and J.P. Atkinson, *Membrane cofactor protein (MCP or CD46): newest member of the regulators of complement activation gene cluster.* Annu Rev Immunol, 1991. **9**: p. 431-55.
238. Barilla-LaBarca, M.L., et al., *Role of membrane cofactor protein (CD46) in regulation of C4b and C3b deposited on cells.* J Immunol, 2002. **168**(12): p. 6298-304.
239. Richards, A., et al., *Mutations in human complement regulator, membrane cofactor protein (CD46), predispose to development of familial hemolytic uremic syndrome.* Proceedings of the National Academy of Sciences of the United States of America, 2003. **100**(22): p. 12966-12971.
240. Kavanagh, D., A. Richards, and J. Atkinson, *Complement regulatory genes and hemolytic uremic syndromes.* Annu Rev Med, 2008. **59**: p. 293-309.
241. Rooney, I.A., T.J. Oglesby, and J.P. Atkinson, *Complement in human reproduction: activation and control.* Immunol Res, 1993. **12**(3): p. 276-94.
242. Riley, R.C., et al., *Characterization of human membrane cofactor protein (MCP; CD46) on spermatozoa.* Mol Reprod Dev, 2002. **62**(4): p. 534-46.
243. Kitamura, M., et al., *Possible association of infertility with sperm-specific abnormality of CD46.* J Reprod Immunol, 1997. **33**(1): p. 83-8.
244. Nomura, M., et al., *Genomic analysis of idiopathic infertile patients with sperm-specific depletion of CD46.* Exp Clin Immunogenet, 2001. **18**(1): p. 42-50.

245. Santoro, F., et al., *CD46 is a cellular receptor for human herpesvirus 6.* Cell, 1999. **99**(7): p. 817-27.
246. Gaggar, A., D.M. Shayakhmetov, and A. Lieber, *CD46 is a cellular receptor for group B adenoviruses.* Nat Med, 2003. **9**(11): p. 1408-12.
247. Maurer, K., et al., *CD46 is a cellular receptor for bovine viral diarrhea virus.* J Virol, 2004. **78**(4): p. 1792-9.
248. Kallstrom, H., et al., *Attachment of Neisseria gonorrhoeae to the cellular pilus receptor CD46: identification of domains important for bacterial adherence.* Cell Microbiol, 2001. **3**(3): p. 133-43.
249. Johansson, L., et al., *CD46 in meningococcal disease.* Science, 2003. **301**(5631): p. 373-5.
250. Feito, M.J., et al., *Membrane cofactor protein (MCP, CD46) binding to clinical isolates of Streptococcus pyogenes: binding to M type 18 strains is independent of Emm or Enn proteins.* Mol Immunol, 2007. **44**(14): p. 3571-9.
251. Yamamoto, H., et al., *CD46: the 'multitasker' of complement proteins.* Int J Biochem Cell Biol, 2013. **45**(12): p. 2808-20.
252. Reynaud, J.M. and B. Horvat, *Animal models for human herpesvirus 6 infection.* Front Microbiol, 2013. **4**: p. 174.
253. Merz, A.J., C.A. Enns, and M. So, *Type IV pili of pathogenic Neisseriae elicit cortical plaque formation in epithelial cells.* Mol Microbiol, 1999. **32**(6): p. 1316-32.
254. Heiska, L. and O. Carpen, *Src phosphorylates ezrin at tyrosine 477 and induces a phosphospecific association between ezrin and a kelch-repeat protein family member.* J Biol Chem, 2005. **280**(11): p. 10244-52.
255. Ludford-Menting, M.J., et al., *A functional interaction between CD46 and DLG4: a role for DLG4 in epithelial polarization.* J Biol Chem, 2002. **277**(6): p. 4477-84.
256. Cardone, J., et al., *Complement regulator CD46 temporally regulates cytokine production by conventional and unconventional T cells.* Nat Immunol, 2010. **11**(9): p. 862-71.
257. Yue, Z., et al., *A novel protein complex linking the delta 2 glutamate receptor and autophagy: implications for neurodegeneration in lurcher mice.* Neuron, 2002. **35**(5): p. 921-33.
258. Lankes, W.T. and H. Furthmayr, *Moesin: a member of the protein 4.1-talin-ezrin family of proteins.* Proceedings of the National Academy of Sciences of the United States of America, 1991. **88**(19): p. 8297-8301.
259. Dunster, L.M., et al., *Moesin: a cell membrane protein linked with susceptibility to measles virus infection.* Virology, 1994. **198**(1): p. 265-74.
260. Dunster, L.M., et al., *Moesin, and not the murine functional homologue (Crry/p65) of human membrane cofactor protein (CD46), is involved in the entry of measles virus (strain Edmonston) into susceptible murine cell lines.* J Gen Virol, 1995. **76 (Pt 8)**: p. 2085-9.
261. Schneider-Schaulies, J., et al., *Physical association of moesin and CD46 as a receptor complex for measles virus.* J Virol, 1995. **69**(4): p. 2248-56.
262. Doi, Y., et al., *Moesin is not a receptor for measles virus entry into mouse embryonic stem cells.* J Virol, 1998. **72**(2): p. 1586-92.
263. Devaux, P. and D. Gerlier, *Antibody cross-reactivity with CD46 and lack of cell surface expression suggest that moesin might not mediate measles virus binding.* J Virol, 1997. **71**(2): p. 1679-82.
264. Matsuyama, A., et al., *Cell surface-expressed moesin-like HDL/apoA-I binding protein promotes cholesterol efflux from human macrophages.* J Lipid Res, 2006. **47**(1): p. 78-86.
265. Tohme, Z.N., S. Amar, and T.E. Van Dyke, *Moesin functions as a lipopolysaccharide receptor on human monocytes.* Infect Immun, 1999. **67**(7): p. 3215-20.
266. Koethe, S., E. Avota, and S. Schneider-Schaulies, *Measles virus transmission from dendritic cells to T cells: formation of synapse-like interfaces concentrating viral and cellular components.* J Virol, 2012. **86**(18): p. 9773-81.

267. O'Connor, T.M., et al., *The role of substance P in inflammatory disease.* J Cell Physiol, 2004. **201**(2): p. 167-80.
268. Mantyh, P.W., *Neurobiology of substance P and the NK1 receptor.* J Clin Psychiatry, 2002. **63 Suppl 11**: p. 6-10.
269. Harrowe, G., M. Mitsuhashi, and D.G. Payan, *Measles virus-substance P receptor interactions. Possible novel mechanism of viral fusion.* J Clin Invest, 1990. **85**(4): p. 1324-7.
270. Rall, G.F., et al., *A transgenic mouse model for measles virus infection of the brain.* Proc Natl Acad Sci U S A, 1997. **94**(9): p. 4659-63.
271. Oldstone, M.B., et al., *Measles virus infection in a transgenic model: virus-induced immunosuppression and central nervous system disease.* Cell, 1999. **98**(5): p. 629-40.
272. Lawrence, D.M., et al., *Measles virus spread between neurons requires cell contact but not CD46 expression, syncytium formation, or extracellular virus production.* J Virol, 2000. **74**(4): p. 1908-18.
273. Makhortova, N., et al., *Neurokinin-1 enables measles virus trans-synaptic spread in neurons.* Virology, 2007. **362**(1): p. 235-244.
274. Alves, L., et al., *SLAM- and nectin-4-independent noncytolytic spread of canine distemper virus in astrocytes.* J Virol, 2015. **89**(10): p. 5724-33.
275. Takeuchi, O. and S. Akira, *Pattern Recognition Receptors and Inflammation.* Cell, 2010. **140**(6): p. 805-820.
276. Kawai, T. and S. Akira, *The role of pattern-recognition receptors in innate immunity: update on Toll-like receptors.* Nat Immunol, 2010. **11**(5): p. 373-84.
277. West, X.Z., et al., *Oxidative stress induces angiogenesis by activating TLR2 with novel endogenous ligands.* Nature, 2010. **467**(7318): p. 972-6.
278. Brandt, K.J., et al., *TLR2 ligands induce NF-kappaB activation from endosomal compartments of human monocytes.* PLoS One, 2013. **8**(12): p. e80743.
279. Vasselon, T., et al., *Toll-like receptor 2 (TLR2) mediates activation of stress-activated MAP kinase p38.* J Leukoc Biol, 2002. **71**(3): p. 503-10.
280. de Witte, L., et al., *Measles virus targets DC-SIGN to enhance dendritic cell infection.* J Virol, 2006. **80**(7): p. 3477-86.
281. van Kooyk, Y. and T.B. Geijtenbeek, *A novel adhesion pathway that regulates dendritic cell trafficking and T cell interactions.* Immunol Rev, 2002. **186**: p. 47-56.
282. Geijtenbeek, T.B., et al., *Identification of DC-SIGN, a novel dendritic cell-specific ICAM-3 receptor that supports primary immune responses.* Cell, 2000. **100**(5): p. 575-85.
283. McGreal, E.P., J.L. Miller, and S. Gordon, *Ligand recognition by antigen-presenting cell C-type lectin receptors.* Curr Opin Immunol, 2005. **17**(1): p. 18-24.
284. van Kooyk, Y. and T.B. Geijtenbeek, *DC-SIGN: escape mechanism for pathogens.* Nat Rev Immunol, 2003. **3**(9): p. 697-709.
285. de Witte, L., et al., *DC-SIGN and CD150 have distinct roles in transmission of measles virus from dendritic cells to T-lymphocytes.* PLoS Pathog, 2008. **4**(4): p. e1000049.
286. Mesman, A.W., et al., *A prominent role for DC-SIGN+ dendritic cells in initiation and dissemination of measles virus infection in non-human primates.* PLoS One, 2012. **7**(12): p. e49573.
287. Johnson, T.R., J.S. McLellan, and B.S. Graham, *Respiratory syncytial virus glycoprotein G interacts with DC-SIGN and L-SIGN to activate ERK1 and ERK2.* J Virol, 2012. **86**(3): p. 1339-47.
288. Lin, G., et al., *Differential N-linked glycosylation of human immunodeficiency virus and Ebola virus envelope glycoproteins modulates interactions with DC-SIGN and DC-SIGNR.* J Virol, 2003. **77**(2): p. 1337-46.
289. Londrigan, S.L., et al., *N-linked glycosylation facilitates sialic acid-independent attachment and entry of influenza A viruses into cells expressing DC-SIGN or L-SIGN.* J Virol, 2011. **85**(6): p. 2990-3000.

290. de Jong, M.A., et al., *Dendritic cells mediate herpes simplex virus infection and transmission through the C-type lectin DC-SIGN.* J Gen Virol, 2008. **89**(Pt 10): p. 2398-409.
291. Geijtenbeek, T.B.H., et al., *Identification of Different Binding Sites in the Dendritic Cell-specific Receptor DC-SIGN for Intercellular Adhesion Molecule 3 and HIV-1.* Journal of Biological Chemistry, 2002. **277**(13): p. 11314-11320.
292. Herndon, R.M. and L.J. Rubinstein, *Light and electron microscopy observations on the development of viral particles in the inclusions of Dawson's encephalitis (subacute sclerosing panencephalitis).* Neurology, 1968. **18**(1 Pt 2): p. 8-20.
293. Masse, N., et al., *Measles virus (MV) hemagglutinin: evidence that attachment sites for MV receptors SLAM and CD46 overlap on the globular head.* J Virol, 2004. **78**(17): p. 9051-63.
294. Vongpunsawad, S., et al., *Selectively receptor-blind measles viruses: Identification of residues necessary for SLAM- or CD46-induced fusion and their localization on a new hemagglutinin structural model.* J Virol, 2004. **78**(1): p. 302-13.
295. Leonard, V.H., et al., *Measles virus blind to its epithelial cell receptor remains virulent in rhesus monkeys but cannot cross the airway epithelium and is not shed.* J Clin Invest, 2008. **118**(7): p. 2448-58.
296. Zhang, X., et al., *Structure of measles virus hemagglutinin bound to its epithelial receptor nectin-4.* Nat Struct Mol Biol, 2013. **20**(1): p. 67-72.
297. Bartz, R., et al., *Mapping amino acids of the measles virus hemagglutinin responsible for receptor (CD46) downregulation.* Virology, 1996. **224**(1): p. 334-7.
298. Lecouturier, V., et al., *Identification of two amino acids in the hemagglutinin glycoprotein of measles virus (MV) that govern hemadsorption, HeLa cell fusion, and CD46 downregulation: phenotypic markers that differentiate vaccine and wild-type MV strains.* J Virol, 1996. **70**(7): p. 4200-4.
299. Ono, N., et al., *V domain of human SLAM (CDw150) is essential for its function as a measles virus receptor.* J Virol, 2001. **75**(4): p. 1594-600.
300. Ohno, S., et al., *Histidine at position 61 and its adjacent amino acid residues are critical for the ability of SLAM (CD150) to act as a cellular receptor for measles virus.* J Gen Virol, 2003. **84**(Pt 9): p. 2381-8.
301. Navaratnarajah, C.K., et al., *Dynamic interaction of the measles virus hemagglutinin with its receptor signaling lymphocytic activation molecule (SLAM, CD150).* J Biol Chem, 2008. **283**(17): p. 11763-71.
302. Santiago, C., et al., *Structure of the measles virus hemagglutinin bound to the CD46 receptor.* Nat Struct Mol Biol, 2010. **17**(1): p. 124-9.
303. Santiago, C., et al., *Crystallization and preliminary crystallographic analysis of the measles virus hemagglutinin in complex with the CD46 receptor.* Acta Crystallographica Section F: Structural Biology and Crystallization Communications, 2010. **66**(Pt 1): p. 91-94.
304. Tahara, M., et al., *Measles virus infects both polarized epithelial and immune cells by using distinctive receptor-binding sites on its hemagglutinin.* J Virol, 2008. **82**(9): p. 4630-7.
305. Santiago, C., et al., *Distinct kinetics for binding of the CD46 and SLAM receptors to overlapping sites in the measles virus hemagglutinin protein.* J Biol Chem, 2002. **277**(35): p. 32294-301.
306. Mateo, M., et al., *Different roles of the three loops forming the adhesive interface of nectin-4 in measles virus binding and cell entry, nectin-4 homodimerization, and heterodimerization with nectin-1.* J Virol, 2014. **88**(24): p. 14161-71.
307. Kielian, M. and F.A. Rey, *Virus membrane-fusion proteins: more than one way to make a hairpin.* Nat Rev Microbiol, 2006. **4**(1): p. 67-76.
308. Brindley, M.A., et al., *Triggering the measles virus membrane fusion machinery.* Proc Natl Acad Sci U S A, 2012. **109**(44): p. E3018-27.

309. Ader, N., et al., *Mechanism for active membrane fusion triggering by morbillivirus attachment protein.* J Virol, 2013. **87**(1): p. 314-26.
310. Ennis, M.K., et al., *Mutations in the stalk region of the measles virus hemagglutinin inhibit syncytium formation but not virus entry.* J Virol, 2010. **84**(20): p. 10913-7.
311. Paal, T., et al., *Probing the spatial organization of measles virus fusion complexes.* J Virol, 2009. **83**(20): p. 10480-93.
312. Porotto, M., et al., *Spring-loaded model revisited: paramyxovirus fusion requires engagement of a receptor binding protein beyond initial triggering of the fusion protein.* J Virol, 2011. **85**(24): p. 12867-80.
313. Talekar, A., A. Moscona, and M. Porotto, *Measles virus fusion machinery activated by sialic Acid binding globular domain.* J Virol, 2013. **87**(24): p. 13619-27.
314. Buchholz, C.J., et al., *Cell entry by measles virus: long hybrid receptors uncouple binding from membrane fusion.* J Virol, 1996. **70**(6): p. 3716-23.
315. Russell, C.J., T.S. Jardetzky, and R.A. Lamb, *Membrane fusion machines of paramyxoviruses: capture of intermediates of fusion.* EMBO J, 2001. **20**(15): p. 4024-34.
316. Russell, C.J., et al., *A dual-functional paramyxovirus F protein regulatory switch segment: activation and membrane fusion.* J Cell Biol, 2003. **163**(2): p. 363-74.
317. Moscona, A., *Entry of parainfluenza virus into cells as a target for interrupting childhood respiratory disease.* J Clin Invest, 2005. **115**(7): p. 1688-98.
318. Lamb, R.A., R.G. Paterson, and T.S. Jardetzky, *Paramyxovirus membrane fusion: lessons from the F and HN atomic structures.* Virology, 2006. **344**(1): p. 30-7.
319. Chang, A. and R.E. Dutch, *Paramyxovirus Fusion and Entry: Multiple Paths to a Common End.* Viruses, 2012. **4**(4): p. 613-636.
320. Helenius, A., et al., *On the entry of semliki forest virus into BHK-21 cells.* The Journal of Cell Biology, 1980. **84**(2): p. 404-420.
321. Mercer, J. and A. Helenius, *Virus entry by macropinocytosis.* Nat Cell Biol, 2009. **11**(5): p. 510-20.
322. Kolokoltsov, A.A., et al., *Small interfering RNA profiling reveals key role of clathrin-mediated endocytosis and early endosome formation for infection by respiratory syncytial virus.* J Virol, 2007. **81**(14): p. 7786-800.
323. Rasmusson, B.J., et al., *Fusion of Sendai virus and individual host cells and inhibition of fusion by lipophosphoglycan measured with image correlation spectroscopy.* Biochim Biophys Acta, 1998. **1404**(3): p. 338-52.
324. Diederich, S., L. Thiel, and A. Maisner, *Role of endocytosis and cathepsin-mediated activation in Nipah virus entry.* Virology, 2008. **375**(2): p. 391-400.
325. Pernet, O., et al., *Nipah virus entry can occur by macropinocytosis.* Virology, 2009. **395**(2): p. 298-311.
326. Cantin, C., et al., *Newcastle disease virus may enter cells by caveolae-mediated endocytosis.* J Gen Virol, 2007. **88**(Pt 2): p. 559-69.
327. Cox, R.G., et al., *Human Metapneumovirus Is Capable of Entering Cells by Fusion with Endosomal Membranes.* PLoS Pathog, 2015. **11**(12): p. e1005303.
328. Frecha, C., et al., *Stable transduction of quiescent T cells without induction of cycle progression by a novel lentiviral vector pseudotyped with measles virus glycoproteins.* Blood, 2008. **112**(13): p. 4843-52.
329. Crimeen-Irwin, B., et al., *Ligand binding determines whether CD46 is internalized by clathrin-coated pits or macropinocytosis.* J Biol Chem, 2003. **278**(47): p. 46927-37.
330. Hannun, Y.A. and L.M. Obeid, *Principles of bioactive lipid signalling: lessons from sphingolipids.* Nat Rev Mol Cell Biol, 2008. **9**(2): p. 139-50.
331. Marchesini, N. and Y.A. Hannun, *Acid and neutral sphingomyelinases: roles and mechanisms of regulation.* Biochem Cell Biol, 2004. **82**(1): p. 27-44.

332. Avota, E., E. Gulbins, and S. Schneider-Schaulies, *DC-SIGN mediated sphingomyelinase-activation and ceramide generation is essential for enhancement of viral uptake in dendritic cells.* PLoS Pathog, 2011. **7**(2): p. e1001290.
333. Mueller, N., et al., *Neutral sphingomyelinase in physiological and measles virus induced T cell suppression.* PLoS Pathog, 2014. **10**(12): p. e1004574.
334. Vijayan, M., et al., *Sphingosine kinase 1 regulates measles virus replication.* Virology, 2014. **450-451**: p. 55-63.
335. Gulbins, E. and R. Kolesnick, *Raft ceramide in molecular medicine.* Oncogene, 2003. **22**(45): p. 7070-7.
336. Riethmuller, J., et al., *Membrane rafts in host-pathogen interactions.* Biochim Biophys Acta, 2006. **1758**(12): p. 2139-47.
337. Utermohlen, O., et al., *Fusogenicity of membranes: the impact of acid sphingomyelinase on innate immune responses.* Immunobiology, 2008. **213**(3-4): p. 307-14.
338. Bollinger, C.R., V. Teichgräber, and E. Gulbins, *Ceramide-enriched membrane domains.* Biochimica et Biophysica Acta (BBA) - Molecular Cell Research, 2005. **1746**(3): p. 284-294.
339. Moll, M., et al., *Polarized glycoprotein targeting affects the spread of measles virus in vitro and in vivo.* J Gen Virol, 2004. **85**(Pt 4): p. 1019-27.
340. Kobune, F., H. Sakata, and A. Sugiura, *Marmoset lymphoblastoid cells as a sensitive host for isolation of measles virus.* J Virol, 1990. **64**(2): p. 700-5.
341. Cathomen, T., et al., *A matrix-less measles virus is infectious and elicits extensive cell fusion: consequences for propagation in the brain.* Embo j, 1998. **17**(14): p. 3899-908.
342. Naim, H.Y., E. Ehler, and M.A. Billeter, *Measles virus matrix protein specifies apical virus release and glycoprotein sorting in epithelial cells.* EMBO J, 2000. **19**(14): p. 3576-85.
343. Takahashi, S., et al., *Rab11 regulates exocytosis of recycling vesicles at the plasma membrane.* J Cell Sci, 2012. **125**(Pt 17): p. 4049-57.
344. Nakatsu, Y., et al., *Intracellular transport of the measles virus ribonucleoprotein complex is mediated by Rab11A-positive recycling endosomes and drives virus release from the apical membrane of polarized epithelial cells.* J Virol, 2013. **87**(8): p. 4683-93.
345. Tahara, M., M. Takeda, and Y. Yanagi, *Altered interaction of the matrix protein with the cytoplasmic tail of hemagglutinin modulates measles virus growth by affecting virus assembly and cell-cell fusion.* J Virol, 2007. **81**(13): p. 6827-36.
346. Salditt, A., et al., *Measles virus M protein-driven particle production does not involve the endosomal sorting complex required for transport (ESCRT) system.* J Gen Virol, 2010. **91**(Pt 6): p. 1464-72.
347. Taylor, M.P., O.O. Koyuncu, and L.W. Enquist, *Subversion of the actin cytoskeleton during viral infection.* Nat Rev Microbiol, 2011. **9**(6): p. 427-39.
348. Dietzel, E., L. Kolesnikova, and A. Maisner, *Actin filaments disruption and stabilization affect measles virus maturation by different mechanisms.* Virol J, 2013. **10**: p. 249.
349. Wakimoto, H., et al., *F-actin modulates measles virus cell-cell fusion and assembly by altering the interaction between the matrix protein and the cytoplasmic tail of hemagglutinin.* J Virol, 2013. **87**(4): p. 1974-84.
350. Shaikh, F.Y. and J.E. Crowe, Jr., *Molecular mechanisms driving respiratory syncytial virus assembly.* Future Microbiol, 2013. **8**(1): p. 123-31.
351. Manie, S.N., et al., *Measles virus structural components are enriched into lipid raft microdomains: a potential cellular location for virus assembly.* J Virol, 2000. **74**(1): p. 305-11.
352. Imhoff, H., et al., *Canine distemper virus infection requires cholesterol in the viral envelope.* J Virol, 2007. **81**(8): p. 4158-65.
353. El Najjar, F., A.P. Schmitt, and R.E. Dutch, *Paramyxovirus glycoprotein incorporation, assembly and budding: a three way dance for infectious particle production.* Viruses, 2014. **6**(8): p. 3019-54.

354. Lorvellec, M., et al., *B-Myb is critical for proper DNA duplication during an unperturbed S phase in mouse embryonic stem cells.* Stem Cells, 2010. **28**(10): p. 1751-9.
355. Mee, C.J., et al., *Polarization Restricts Hepatitis C Virus Entry into HepG2 Hepatoma Cells.* Journal of Virology, 2009. **83**(12): p. 6211-6221.
356. Garvin, A.J., et al., *The deSUMOylase SENP7 promotes chromatin relaxation for homologous recombination DNA repair.* EMBO Rep, 2013. **14**(11): p. 975-83.
357. Heath, E., et al., *Epstein-Barr virus infection of naive B cells in vitro frequently selects clones with mutated immunoglobulin genotypes: implications for virus biology.* PLoS Pathog, 2012. **8**(5): p. e1002697.
358. Reed, L.J.M., H., *A SIMPLE METHOD OF ESTIMATING FIFTY PER CENT ENDPOINTS.* Am. J. Epidemiol., 1938. **27**(3): p. 493-497.
359. Hsu, M., et al., *Hepatitis C virus glycoproteins mediate pH-dependent cell entry of pseudotyped retroviral particles.* Proc Natl Acad Sci U S A, 2003. **100**(12): p. 7271-6.
360. Wright, E., et al., *Investigating antibody neutralization of lyssaviruses using lentiviral pseudotypes: a cross-species comparison.* J Gen Virol, 2008. **89**(Pt 9): p. 2204-13.
361. Mutch, L.J., et al., *Polarised clathrin-mediated endocytosis of EGFR during chemotactic invasion.* Traffic, 2014. **15**(6): p. 648-64.
362. Jacquemet, G., et al., *RCP-driven alpha5beta1 recycling suppresses Rac and promotes RhoA activity via the RacGAP1-IQGAP1 complex.* J Cell Biol, 2013. **202**(6): p. 917-35.
363. Ishikawa, H., et al., *Generation of a dual-functional split-reporter protein for monitoring membrane fusion using self-associating split GFP.* Protein Eng Des Sel, 2012. **25**(12): p. 813-20.
364. Vega, M.V., et al., *Adaptation of a colorimetric microtitration assay for quantifying Pasteurella haemolytica A1 leukotoxin and antileukotoxin.* Am J Vet Res, 1987. **48**(11): p. 1559-64.
365. Smith, P.K., et al., *Measurement of protein using bicinchoninic acid.* Anal Biochem, 1985. **150**(1): p. 76-85.
366. Bradford, M.M., *A rapid and sensitive method for the quantitation of microgram quantities of protein utilizing the principle of protein-dye binding.* Anal Biochem, 1976. **72**: p. 248-54.
367. Emmott, E. and I. Goodfellow, *Identification of Protein Interaction Partners in Mammalian Cells Using SILAC-immunoprecipitation Quantitative Proteomics.* Journal of Visualized Experiments : JoVE, 2014(89): p. 51656.
368. Roberts, P.C., T. Kipperman, and R.W. Compans, *Vesicular stomatitis virus G protein acquires pH-independent fusion activity during transport in a polarized endometrial cell line.* J Virol, 1999. **73**(12): p. 10447-57.
369. Funke, S., et al., *Targeted Cell Entry of Lentiviral Vectors.* Mol Ther, 2008. **16**(8): p. 1427-1436.
370. Christodoulopoulos, I. and P.M. Cannon, *Sequences in the cytoplasmic tail of the gibbon ape leukemia virus envelope protein that prevent its incorporation into lentivirus vectors.* J Virol, 2001. **75**(9): p. 4129-38.
371. Yee, J.K., T. Friedmann, and J.C. Burns, *Generation of high-titer pseudotyped retroviral vectors with very broad host range.* Methods Cell Biol, 1994. **43 Pt A**: p. 99-112.
372. Finkelshtein, D., et al., *LDL receptor and its family members serve as the cellular receptors for vesicular stomatitis virus.* Proc Natl Acad Sci U S A, 2013. **110**(18): p. 7306-11.
373. Guibinga, G.H., et al., *Cell surface heparan sulfate is a receptor for attachment of envelope protein-free retrovirus-like particles and VSV-G pseudotyped MLV-derived retrovirus vectors to target cells.* Mol Ther, 2002. **5**(5 Pt 1): p. 538-46.
374. Frecha, C., et al., *Measles virus glycoprotein-pseudotyped lentiviral vector-mediated gene transfer into quiescent lymphocytes requires binding to both SLAM and CD46 entry receptors.* J Virol, 2011. **85**(12): p. 5975-85.

375. Oda, S., et al., *Crystal Structure of Marburg Virus VP40 Reveals a Broad, Basic Patch for Matrix Assembly and a Requirement of the N-Terminal Domain for Immunosuppression.* J Virol, 2016. **90**(4): p. 1839-48.
376. Forster, A., et al., *Dimerization of matrix protein is required for budding of respiratory syncytial virus.* J Virol, 2015. **89**(8): p. 4624-35.
377. Raux, H., et al., *The matrix protein of vesicular stomatitis virus binds dynamin for efficient viral assembly.* J Virol, 2010. **84**(24): p. 12609-18.
378. Vincent, S., D. Gerlier, and S.N. Manie, *Measles virus assembly within membrane rafts.* J Virol, 2000. **74**(21): p. 9911-5.
379. Runkler, N., et al., *Measles virus nucleocapsid transport to the plasma membrane requires stable expression and surface accumulation of the viral matrix protein.* Cell Microbiol, 2007. **9**(5): p. 1203-14.
380. Chang, A. and R.E. Dutch, *Paramyxovirus fusion and entry: multiple paths to a common end.* Viruses, 2012. **4**(4): p. 613-36.
381. Wool-Lewis, R.J. and P. Bates, *Characterization of Ebola virus entry by using pseudotyped viruses: identification of receptor-deficient cell lines.* J Virol, 1998. **72**(4): p. 3155-60.
382. Wang, Z., et al., *Characterization of classical swine fever virus entry by using pseudotyped viruses: E1 and E2 are sufficient to mediate viral entry.* Virology, 2004. **330**(1): p. 332-41.
383. Zhang, J., et al., *Effects of N-linked glycosylation of the fusion protein on replication of human metapneumovirus in vitro and in mouse lungs.* J Gen Virol, 2011. **92**(Pt 7): p. 1666-75.
384. von Messling, V. and R. Cattaneo, *N-linked glycans with similar location in the fusion protein head modulate paramyxovirus fusion.* J Virol, 2003. **77**(19): p. 10202-12.
385. Levy, C., et al., *Lentiviral vectors displaying modified measles virus gp overcome pre-existing immunity in in vivo-like transduction of human T and B cells.* Mol Ther, 2012. **20**(9): p. 1699-712.
386. Lech, P.J., et al., *Epitope dampening monotypic measles virus hemagglutinin glycoprotein results in resistance to cocktail of monoclonal antibodies.* PLoS One, 2013. **8**(1): p. e52306.
387. Raine, C.S., et al., *Ultrastructure of measles virus in cultures of hamster cerebellum.* J Virol, 1969. **4**(2): p. 169-81.
388. Pohl, C., et al., *Measles virus M and F proteins associate with detergent-resistant membrane fractions and promote formation of virus-like particles.* J Gen Virol, 2007. **88**(Pt 4): p. 1243-50.
389. Raine, C.S., et al., *Ultrastructural study of long-term measles infection in cultures of hamster dorsal-root ganglion.* J Virol, 1971. **8**(3): p. 318-29.
390. Chernomordik, L.V. and M.M. Kozlov, *Mechanics of membrane fusion.* Nat Struct Mol Biol, 2008. **15**(7): p. 675-83.
391. Bohn, W., et al., *Involvement of actin filaments in budding of measles virus: Studies on cytoskeletons of infected cells.* Virology, 1986. **149**(1): p. 91-106.
392. Battisti, A.J., et al., *Structure and assembly of a paramyxovirus matrix protein.* Proc Natl Acad Sci U S A, 2012. **109**(35): p. 13996-4000.
393. Takeuchi, K., et al., *Wild-type measles virus induces large syncytium formation in primary human small airway epithelial cells by a SLAM(CD150)-independent mechanism.* Virus Res, 2003. **94**(1): p. 11-6.
394. Smith, E.C., et al., *Viral entry mechanisms: the increasing diversity of paramyxovirus entry.* FEBS J, 2009. **276**(24): p. 7217-27.
395. Aleksandrowicz, P., et al., *Ebola virus enters host cells by macropinocytosis and clathrin-mediated endocytosis.* J Infect Dis, 2011. **204 Suppl 3**: p. S957-67.
396. Grant, B.D. and J.G. Donaldson, *Pathways and mechanisms of endocytic recycling.* Nature reviews. Molecular cell biology, 2009. **10**(9): p. 597-608.

397. Swanson, J.A., *Shaping cups into phagosomes and macropinosomes.* Nat Rev Mol Cell Biol, 2008. **9**(8): p. 639-49.
398. Jiang, J., A.L. Kolpak, and Z.Z. Bao, *Myosin IIB isoform plays an essential role in the formation of two distinct types of macropinosomes.* Cytoskeleton (Hoboken), 2010. **67**(1): p. 32-42.
399. Lim, J.P. and P.A. Gleeson, *Macropinocytosis: an endocytic pathway for internalising large gulps.* Immunol Cell Biol, 2011. **89**(8): p. 836-43.
400. Swanson, J.A., *Phorbol esters stimulate macropinocytosis and solute flow through macrophages.* J Cell Sci, 1989. **94 (Pt 1)**: p. 135-42.
401. Koivusalo, M., et al., *Amiloride inhibits macropinocytosis by lowering submembranous pH and preventing Rac1 and Cdc42 signaling.* J Cell Biol, 2010. **188**(4): p. 547-63.
402. Lee, E. and D.A. Knecht, *Visualization of actin dynamics during macropinocytosis and exocytosis.* Traffic, 2002. **3**(3): p. 186-92.
403. Smith, B.A., et al., *Pathway of actin filament branch formation by Arp2/3 complex revealed by single-molecule imaging.* Proceedings of the National Academy of Sciences, 2013. **110**(4): p. 1285-1290.
404. Charras, G.T., et al., *Reassembly of contractile actin cortex in cell blebs.* J Cell Biol, 2006. **175**(3): p. 477-90.
405. Lehmann, M.J., et al., *Actin- and myosin-driven movement of viruses along filopodia precedes their entry into cells.* J Cell Biol, 2005. **170**(2): p. 317-25.
406. Bhella, D., *The role of cellular adhesion molecules in virus attachment and entry.* Philos Trans R Soc Lond B Biol Sci, 2015. **370**(1661): p. 20140035.
407. Yamamoto, K., et al., *Deregulation of the actin cytoskeleton and macropinocytosis in response to phorbol ester by the mutant protein kinase C gamma that causes spinocerebellar ataxia type 14.* Front Physiol, 2014. **5**: p. 126.
408. Sanchez, E.G., et al., *African swine fever virus uses macropinocytosis to enter host cells.* PLoS Pathog, 2012. **8**(6): p. e1002754.
409. Mercer, J. and A. Helenius, *Vaccinia virus uses macropinocytosis and apoptotic mimicry to enter host cells.* Science, 2008. **320**(5875): p. 531-5.
410. Valiya Veettil, M., et al., *Interaction of c-Cbl with myosin IIA regulates Bleb associated macropinocytosis of Kaposi's sarcoma-associated herpesvirus.* PLoS Pathog, 2010. **6**(12): p. e1001238.
411. Kovacs, M., et al., *Mechanism of blebbistatin inhibition of myosin II.* J Biol Chem, 2004. **279**(34): p. 35557-63.
412. Jones, A.T., *Macropinocytosis: searching for an endocytic identity and role in the uptake of cell penetrating peptides.* Journal of Cellular and Molecular Medicine, 2007. **11**(4): p. 670-684.
413. Lamaze, C., et al., *Interleukin 2 receptors and detergent-resistant membrane domains define a clathrin-independent endocytic pathway.* Mol Cell, 2001. **7**(3): p. 661-71.
414. Sandgren, K.J., et al., *A differential role for macropinocytosis in mediating entry of the two forms of vaccinia virus into dendritic cells.* PLoS Pathog, 2010. **6**(4): p. e1000866.
415. Mulherkar, N., et al., *The Ebola virus glycoprotein mediates entry via a non-classical dynamin-dependent macropinocytic pathway.* Virology, 2011. **419**(2): p. 72-83.
416. Saeed, M.F., et al., *Cellular entry of ebola virus involves uptake by a macropinocytosis-like mechanism and subsequent trafficking through early and late endosomes.* PLoS Pathog, 2010. **6**(9): p. e1001110.
417. Nanbo, A., et al., *Ebolavirus is internalized into host cells via macropinocytosis in a viral glycoprotein-dependent manner.* PLoS Pathog, 2010. **6**(9): p. e1001121.
418. Ma, C., et al., *Receptor signaling lymphocyte-activation molecule family 1 (Slamf1) regulates membrane fusion and NADPH oxidase 2 (NOX2) activity by recruiting a Beclin-*

1/Vps34/ultraviolet radiation resistance-associated gene (UVRAG) complex. J Biol Chem, 2012. **287**(22): p. 18359-65.
419. Kang, B.K. and L.S. Schlesinger, *Characterization of mannose receptor-dependent phagocytosis mediated by Mycobacterium tuberculosis lipoarabinomannan.* Infect Immun, 1998. **66**(6): p. 2769-77.
420. Grove, J. and M. Marsh, *The cell biology of receptor-mediated virus entry.* J Cell Biol, 2011. **195**(7): p. 1071-82.
421. Fujimoto, I., et al., *Virus clearance through apoptosis-dependent phagocytosis of influenza A virus-infected cells by macrophages.* J Virol, 2000. **74**(7): p. 3399-403.
422. Ohno, S., et al., *Measles virus infection of SLAM (CD150) knockin mice reproduces tropism and immunosuppression in human infection.* J Virol, 2007. **81**(4): p. 1650-9.
423. Singh, B.K., et al., *The Nectin-4/Afadin Protein Complex and Intercellular Membrane Pores Contribute to Rapid Spread of Measles Virus in Primary Human Airway Epithelia.* Journal of Virology, 2015. **89**(14): p. 7089-7096.
424. Nozawa, Y., et al., *An immunohistochemical study of Warthin-Finkeldey cells in measles.* Pathol Int, 1994. **44**(6): p. 442-7.
425. Watanabe, S., et al., *Mutant Fusion Proteins with Enhanced Fusion Activity Promote Measles Virus Spread in Human Neuronal Cells and Brains of Suckling Hamsters.* J Virol, 2013. **87**(5): p. 2648-59.
426. Chernomordik, L.V., J. Zimmerberg, and M.M. Kozlov, *Membranes of the world unite!* The Journal of Cell Biology, 2006. **175**(2): p. 201-207.
427. Chen, Y.A. and R.H. Scheller, *SNARE-mediated membrane fusion.* Nat Rev Mol Cell Biol, 2001. **2**(2): p. 98-106.
428. Ogle, B.M., M. Cascalho, and J.L. Platt, *Biological implications of cell fusion.* Nat Rev Mol Cell Biol, 2005. **6**(7): p. 567-575.
429. Potgens, A.J., et al., *Syncytin: the major regulator of trophoblast fusion? Recent developments and hypotheses on its action.* Hum Reprod Update, 2004. **10**(6): p. 487-96.
430. Mi, S., et al., *Syncytin is a captive retroviral envelope protein involved in human placental morphogenesis.* Nature, 2000. **403**(6771): p. 785-789.
431. Vargas, A., et al., *Syncytin-2 plays an important role in the fusion of human trophoblast cells.* J Mol Biol, 2009. **392**(2): p. 301-18.
432. Cathomen, T., H.Y. Naim, and R. Cattaneo, *Measles viruses with altered envelope protein cytoplasmic tails gain cell fusion competence.* J Virol, 1998. **72**(2): p. 1224-34.
433. Dutch, R.E. and R.A. Lamb, *Deletion of the cytoplasmic tail of the fusion protein of the paramyxovirus simian virus 5 affects fusion pore enlargement.* J Virol, 2001. **75**(11): p. 5363-9.
434. Popa, A., C.T. Pager, and R.E. Dutch, *C-terminal tyrosine residues modulate the fusion activity of the Hendra virus fusion protein.* Biochemistry, 2011. **50**(6): p. 945-52.
435. Aguilar, H.C., et al., *Polybasic KKR motif in the cytoplasmic tail of Nipah virus fusion protein modulates membrane fusion by inside-out signaling.* J Virol, 2007. **81**(9): p. 4520-32.
436. Seth, S., A. Vincent, and R.W. Compans, *Mutations in the cytoplasmic domain of a paramyxovirus fusion glycoprotein rescue syncytium formation and eliminate the hemagglutinin-neuraminidase protein requirement for membrane fusion.* J Virol, 2003. **77**(1): p. 167-78.
437. Wurth, M.A., et al., *The actin cytoskeleton inhibits pore expansion during PIV5 fusion protein-promoted cell-cell fusion.* Virology, 2010. **404**(1): p. 117-26.
438. Casella, J.F., M.D. Flanagan, and S. Lin, *Cytochalasin D inhibits actin polymerization and induces depolymerization of actin filaments formed during platelet shape change.* Nature, 1981. **293**(5830): p. 302-5.

439. Bubb, M.R., et al., *Jasplakinolide, a cytotoxic natural product, induces actin polymerization and competitively inhibits the binding of phalloidin to F-actin.* J Biol Chem, 1994. **269**(21): p. 14869-71.
440. Peterson, J.R., et al., *Chemical inhibition of N-WASP by stabilization of a native autoinhibited conformation.* Nat Struct Mol Biol, 2004. **11**(8): p. 747-55.
441. Vasquez, R.J., et al., *Nanomolar concentrations of nocodazole alter microtubule dynamic instability in vivo and in vitro.* Mol Biol Cell, 1997. **8**(6): p. 973-85.
442. Horwitz, S.B., *Taxol (paclitaxel): mechanisms of action.* Ann Oncol, 1994. **5 Suppl 6**: p. S3-6.
443. Rebacz, B., et al., *Identification of griseofulvin as an inhibitor of centrosomal clustering in a phenotype-based screen.* Cancer Res, 2007. **67**(13): p. 6342-50.
444. Ferguson, S.M. and P. De Camilli, *Dynamin, a membrane-remodelling GTPase.* Nat Rev Mol Cell Biol, 2012. **13**(2): p. 75-88.
445. Macia, E., et al., *Dynasore, a Cell-Permeable Inhibitor of Dynamin.* Developmental Cell, 2006. **10**(6): p. 839-850.
446. Maxfield, F.R. and T.E. McGraw, *Endocytic recycling.* Nat Rev Mol Cell Biol, 2004. **5**(2): p. 121-132.
447. Heasman, S.J. and A.J. Ridley, *Mammalian Rho GTPases: new insights into their functions from in vivo studies.* Nat Rev Mol Cell Biol, 2008. **9**(9): p. 690-701.
448. Sit, S.T. and E. Manser, *Rho GTPases and their role in organizing the actin cytoskeleton.* J Cell Sci, 2011. **124**(Pt 5): p. 679-83.
449. Schowalter, R.M., et al., *Rho GTPase activity modulates paramyxovirus fusion protein-mediated cell-cell fusion.* Virology, 2006. **350**(2): p. 323-34.
450. Fehon, R.G., A.I. McClatchey, and A. Bretscher, *Organizing the cell cortex: the role of ERM proteins.* Nat Rev Mol Cell Biol, 2010. **11**(4): p. 276-87.
451. Barroso-Gonzalez, J., et al., *Moesin regulates the trafficking of nascent clathrin-coated vesicles.* J Biol Chem, 2009. **284**(4): p. 2419-34.
452. Sun, X., et al., *Role of clathrin-mediated endocytosis during vesicular stomatitis virus entry into host cells.* Virology, 2005. **338**(1): p. 53-60.
453. Sawatsky, B., et al., *Morbillivirus and henipavirus attachment protein cytoplasmic domains differently affect protein expression, fusion support and particle assembly.* J Gen Virol, 2016. **97**(5): p. 1066-76.
454. Kallewaard, N.L., A.L. Bowen, and J.E. Crowe, Jr., *Cooperativity of actin and microtubule elements during replication of respiratory syncytial virus.* Virology, 2005. **331**(1): p. 73-81.
455. Chen, A., et al., *Fusion-pore expansion during syncytium formation is restricted by an actin network.* Journal of cell science, 2008. **121**(Pt 21): p. 3619-3628.
456. Takito, J. and M. Nakamura, *Precursors linked via the zipper-like structure or the filopodium during the secondary fusion of osteoclasts.* Communicative & Integrative Biology, 2012. **5**(5): p. 453-457.
457. Takito, J., et al., *The transient appearance of zipper-like actin superstructures during the fusion of osteoclasts.* J Cell Sci, 2012. **125**(Pt 3): p. 662-72.
458. Shin, N.Y., et al., *Dynamin and endocytosis are required for the fusion of osteoclasts and myoblasts.* J Cell Biol, 2014. **207**(1): p. 73-89.
459. Clifford, R.J., E.B. Maryon, and J.H. Kaplan, *Dynamic internalization and recycling of a metal ion transporter: Cu homeostasis and CTR1, the human Cu(+) uptake system.* J Cell Sci, 2016. **129**(8): p. 1711-21.
460. van Dam, E.M., et al., *Endocytosed transferrin receptors recycle via distinct dynamin and phosphatidylinositol 3-kinase-dependent pathways.* J Biol Chem, 2002. **277**(50): p. 48876-83.
461. Gower, T.L., et al., *RhoA signaling is required for respiratory syncytial virus-induced syncytium formation and filamentous virion morphology.* J Virol, 2005. **79**(9): p. 5326-36.

462. Tsurudome, M., et al., *Effects of hemagglutinin-neuraminidase protein mutations on cell-cell fusion mediated by human parainfluenza type 2 virus.* J Virol, 2008. **82**(17): p. 8283-95.
463. Opyrchal, M., et al., *Inhibition of Rho associated coiled-coil forming kinase increases efficacy of measles virus infection in vitro and in vivo.* Cancer gene therapy, 2013. **20**(11): p. 630-637.
464. Niggli, V. and J. Rossy, *Ezrin/radixin/moesin: versatile controllers of signaling molecules and of the cortical cytoskeleton.* Int J Biochem Cell Biol, 2008. **40**(3): p. 344-9.
465. Roy, N.H., et al., *Ezrin is a component of the HIV-1 virological presynapse and contributes to the inhibition of cell-cell fusion.* J Virol, 2014. **88**(13): p. 7645-58.
466. Rouven Brückner, B., et al., *Ezrin is a Major Regulator of Membrane Tension in Epithelial Cells.* Scientific Reports, 2015. **5**: p. 14700.
467. Solinet, S., et al., *The actin-binding ERM protein Moesin binds to and stabilizes microtubules at the cell cortex.* The Journal of Cell Biology, 2013. **202**(2): p. 251-260.
468. Speck, O., et al., *Moesin functions antagonistically to the Rho pathway to maintain epithelial integrity.* Nature, 2003. **421**(6918): p. 83-7.
469. Sagara, J., et al., *Cellular actin-binding ezrin-radixin-moesin (ERM) family proteins are incorporated into the rabies virion and closely associated with viral envelope proteins in the cell.* Virology, 1995. **206**(1): p. 485-94.
470. Ott, D.E., et al., *Cytoskeletal proteins inside human immunodeficiency virus type 1 virions.* J Virol, 1996. **70**(11): p. 7734-43.
471. Ren, X., et al., *Proteomic analysis of purified Newcastle disease virus particles.* Proteome Sci, 2012. **10**(1): p. 32.
472. McDonald, B. and J. Martin-Serrano, *No strings attached: the ESCRT machinery in viral budding and cytokinesis.* J Cell Sci, 2009. **122**(Pt 13): p. 2167-77.
473. Usami, Y., et al., *The ESCRT pathway and HIV-1 budding.* Biochem Soc Trans, 2009. **37**(Pt 1): p. 181-4.
474. Silvestri, L.S., et al., *Involvement of vacuolar protein sorting pathway in Ebola virus release independent of TSG101 interaction.* J Infect Dis, 2007. **196 Suppl 2**: p. S264-70.
475. Ogura, H., et al., *Glycosylation of measles virus haemagglutinin protein in infected cells.* J Gen Virol, 1991. **72 (Pt 11)**: p. 2679-84.
476. Alkhatib, G., et al., *Functional analysis of N-linked glycosylation mutants of the measles virus fusion protein synthesized by recombinant vaccinia virus vectors.* Journal of Virology, 1994. **68**(3): p. 1522-1531.
477. Matheson, N.J., et al., *Cell Surface Proteomic Map of HIV Infection Reveals Antagonism of Amino Acid Metabolism by Vpu and Nef.* Cell Host Microbe, 2015. **18**(4): p. 409-23.
478. Kummer, S., et al., *Alteration of Protein Levels during Influenza Virus H1N1 Infection in Host Cells: A Proteomic Survey of Host and Virus Reveals Differential Dynamics.* PLoS ONE, 2014. **9**(4): p. e94257.
479. Jacobs, J.M., et al., *Proteome analysis of liver cells expressing a full-length hepatitis C virus (HCV) replicon and biopsy specimens of posttransplantation liver from HCV-infected patients.* J Virol, 2005. **79**(12): p. 7558-69.
480. Ong, S.E. and M. Mann, *A practical recipe for stable isotope labeling by amino acids in cell culture (SILAC).* Nat Protoc, 2006. **1**(6): p. 2650-60.
481. Zanivan, S., M. Krueger, and M. Mann, *In vivo quantitative proteomics: the SILAC mouse.* Methods Mol Biol, 2012. **757**: p. 435-50.
482. Hummel, K.B., W.J. Bellini, and M.K. Offermann, *Strain-Specific Differences in LFA-1 Induction on Measles Virus-Infected Monocytes and Adhesion and Viral Transmission to Endothelial Cells.* Journal of Virology, 1998. **72**(10): p. 8403-8407.
483. Gauthier, N.P., et al., *Cell-selective labeling using amino acid precursors for proteomic studies of multicellular environments.* Nat Methods, 2013. **10**(8): p. 768-73.

484. Bendall, S.C., et al., *Prevention of Amino Acid Conversion in SILAC Experiments with Embryonic Stem Cells.* Molecular & Cellular Proteomics : MCP, 2008. **7**(9): p. 1587-1597.
485. Franceschini, A., et al., *STRING v9.1: protein-protein interaction networks, with increased coverage and integration.* Nucleic Acids Research, 2013. **41**(Database issue): p. D808-D815.
486. Thomas, P.D., et al., *PANTHER: a library of protein families and subfamilies indexed by function.* Genome Res, 2003. **13**(9): p. 2129-41.
487. Lothrop, A.P., M.P. Torres, and S.M. Fuchs, *Deciphering post-translational modification codes.* FEBS Lett, 2013. **587**(8): p. 1247-57.
488. Devaux, P., et al., *Tyrosine 110 in the measles virus phosphoprotein is required to block STAT1 phosphorylation.* Virology, 2007. **360**(1): p. 72-83.
489. Sugai, A., et al., *Newly identified minor phosphorylation site threonine-279 of measles virus nucleoprotein is a prerequisite for nucleocapsid formation.* J Virol, 2014. **88**(2): p. 1140-9.
490. Sugai, A., et al., *Phosphorylation of measles virus nucleoprotein affects viral growth by changing gene expression and genomic RNA stability.* J Virol, 2013. **87**(21): p. 11684-92.
491. Prodhomme, E.J., et al., *Extensive phosphorylation flanking the C-terminal functional domains of the measles virus nucleoprotein.* J Proteome Res, 2010. **9**(11): p. 5598-609.
492. Sugai, A., et al., *Phosphorylation of measles virus phosphoprotein at S86 and/or S151 downregulates viral transcriptional activity.* FEBS Lett, 2012. **586**(21): p. 3900-7.
493. Mechref, Y., *Use of CID/ETD Mass Spectrometry to Analyze Glycopeptides.* Current protocols in protein science / editorial board, John E. Coligan ... [et al.], 2012. **0 12**: p. Unit-12.1111.
494. Puttick, J., E.N. Baker, and L.T. Delbaere, *Histidine phosphorylation in biological systems.* Biochim Biophys Acta, 2008. **1784**(1): p. 100-5.
495. Gainey, M.D., et al., *Paramyxovirus-Induced Shutoff of Host and Viral Protein Synthesis: Role of the P and V Proteins in Limiting PKR Activation.* Journal of Virology, 2008. **82**(2): p. 828-839.
496. Buckingham, E.M., et al., *Exocytosis of Varicella-Zoster Virus Virions Involves a Convergence of Endosomal and Autophagy Pathways.* J Virol, 2016. **90**(19): p. 8673-85.
497. Utley, T.J., et al., *Respiratory syncytial virus uses a Vps4-independent budding mechanism controlled by Rab11-FIP2.* Proc Natl Acad Sci U S A, 2008. **105**(29): p. 10209-14.
498. Raposo, G. and W. Stoorvogel, *Extracellular vesicles: Exosomes, microvesicles, and friends.* The Journal of Cell Biology, 2013. **200**(4): p. 373.
499. Savina, A., M. Vidal, and M.I. Colombo, *The exosome pathway in K562 cells is regulated by Rab11.* Journal of Cell Science, 2002. **115**(12): p. 2505.
500. Prabakaran, S., et al., *Post-translational modification: nature's escape from genetic imprisonment and the basis for dynamic information encoding.* Wiley Interdiscip Rev Syst Biol Med, 2012. **4**(6): p. 565-83.
501. Komander, D. and M. Rape, *The ubiquitin code.* Annu Rev Biochem, 2012. **81**: p. 203-29.
502. Kirui, J., A. Mondal, and A. Mehle, *Ubiquitination up-regulates influenza virus polymerase function.* Journal of Virology, 2016.
503. Luo, H., *Interplay between the virus and the ubiquitin-proteasome system: molecular mechanism of viral pathogenesis.* Curr Opin Virol, 2016. **17**: p. 1-10.
504. Pentecost, M., et al., *Evidence for ubiquitin-regulated nuclear and subnuclear trafficking among Paramyxovirinae matrix proteins.* PLoS Pathog, 2015. **11**(3): p. e1004739.
505. Flotho, A. and F. Melchior, *Sumoylation: A Regulatory Protein Modification in Health and Disease.* Annual Review of Biochemistry, 2013. **82**(1): p. 357-385.
506. Wimmer, P., S. Schreiner, and T. Dobner, *Human pathogens and the host cell SUMOylation system.* J Virol, 2012. **86**(2): p. 642-54.
507. Domingues, P., et al., *Global Reprogramming of Host SUMOylation during Influenza Virus Infection.* Cell Rep, 2015. **13**(7): p. 1467-80.

508. Pal, S., et al., *Influenza A virus interacts extensively with the cellular SUMOylation system during infection.* Virus Res, 2011. **158**(1-2): p. 12-27.
509. Wu, C.Y., K.S. Jeng, and M.M. Lai, *The SUMOylation of matrix protein M1 modulates the assembly and morphogenesis of influenza A virus.* J Virol, 2011. **85**(13): p. 6618-28.
510. Han, Q., et al., *Sumoylation of influenza A virus nucleoprotein is essential for intracellular trafficking and virus growth.* J Virol, 2014. **88**(16): p. 9379-90.
511. Sun, D., P. Xu, and B. He, *Sumoylation of the P Protein at K254 Plays an Important Role in Growth of Parainfluenza Virus 5.* Journal of Virology, 2011. **85**(19): p. 10261-10268.
512. Gombart, A.F., A. Hirano, and T.C. Wong, *Nucleoprotein phosphorylated on both serine and threonine is preferentially assembled into the nucleocapsids of measles virus.* Virus Res, 1995. **37**(1): p. 63-73.
513. Spehner, D., R. Drillien, and P.M. Howley, *The assembly of the measles virus nucleoprotein into nucleocapsid-like particles is modulated by the phosphoprotein.* Virology, 1997. **232**(2): p. 260-8.
514. Das, T., et al., *Involvement of cellular casein kinase II in the phosphorylation of measles virus P protein: identification of phosphorylation sites.* Virology, 1995. **211**(1): p. 218-26.
515. Fuentes, S.M., et al., *Phosphorylation of paramyxovirus phosphoprotein and its role in viral gene expression.* Future Microbiol, 2010. **5**(1): p. 9-13.
516. Jakubiec, A., et al., *Phosphorylation of viral RNA-dependent RNA polymerase and its role in replication of a plus-strand RNA virus.* J Biol Chem, 2006. **281**(30): p. 21236-49.
517. Eden, J.S., et al., *Norovirus RNA-dependent RNA polymerase is phosphorylated by an important survival kinase, Akt.* J Virol, 2011. **85**(20): p. 10894-8.
518. Hutchinson, E.C., et al., *Mapping the phosphoproteome of influenza A and B viruses by mass spectrometry.* PLoS Pathog, 2012. **8**(11): p. e1002993.
519. Brindley, M.A. and R.K. Plemper, *Blue Native PAGE and Biomolecular Complementation Reveal a Tetrameric or Higher-Order Oligomer Organization of the Physiological Measles Virus Attachment Protein H.* Journal of Virology, 2010. **84**(23): p. 12174-12184.
520. Lee, S.W., et al., *CD46 is phosphorylated at tyrosine 354 upon infection of epithelial cells by Neisseria gonorrhoeae.* J Cell Biol, 2002. **156**(6): p. 951-7.
521. Schmidt, F.I., et al., *Vaccinia extracellular virions enter cells by macropinocytosis and acid-activated membrane rupture.* The EMBO Journal, 2011. **30**(17): p. 3647-3661.
522. Cattaneo, R. and J.K. Rose, *Cell fusion by the envelope glycoproteins of persistent measles viruses which caused lethal human brain disease.* J Virol, 1993. **67**(3): p. 1493-502.
523. Rentier, B., E.L. Hooghe-Peters, and M. Dubois-Dalcq, *Electron microscopic study of measles virus infection: cell fusion and hemadsorption.* J Virol, 1978. **28**(2): p. 567-77.
524. Avota, E., E. Gassert, and S. Schneider-Schaulies, *Cytoskeletal dynamics: concepts in measles virus replication and immunomodulation.* Viruses, 2011. **3**(2): p. 102-17.
525. Eitzen, G., *Actin remodeling to facilitate membrane fusion.* Biochim Biophys Acta, 2003. **1641**(2-3): p. 175-81.
526. Gutiérrez, S., Y. Michalakis, and S. Blanc, *Virus population bottlenecks during within-host progression and host-to-host transmission.* Current Opinion in Virology, 2012. **2**(5): p. 546-555.
527. Zwart, M.P. and S.F. Elena, *Matters of Size: Genetic Bottlenecks in Virus Infection and Their Potential Impact on Evolution.* Annual Review of Virology, 2015. **2**(1): p. 161-179.

APPENDIX

The following data supports some of the findings mentioned previously in this document.

A.1 – Primers used for SDM

All primers used in SDM are listed in **Table A-1**.

Description	Sequence
MeV H T221A	5′-TCTATAGTC**GCT**ATGACATCC
MeV H T221D	5′-TCTATAGTC**GAC**ATGACATCC
MeV H T221E	5′-TCTATAGTC**GAG**ATGACATCC
MeV H T273A	5′-TTCCATATG**GCA**AACTATTTT
MeV H T273D	5′-TTCCATATG**GAC**AACTATTTT
MeV H T273E	5′-TTCCATATG**GAA**AACTATTTT
MeV H Y275A	5′-ATGACAAAC**GCT**TTTGAGCAA
MeV H Y275F	5′-ATGACAAAC**TTC**TTTGAGCAA
MeV H Y275E	5′-ATGACAAAC**GAA**TTTGAGCAA

A.2 – Protein sequences of MeV Ichinose-B95a strain proteins

All protein sequences of Ichinose-B95a strain proteins used for bioinformatics purposes in this these are presented below.

>sp|Q9WMB5|NCAP_MEASC **Nucleoprotein** OS=Measles virus (strain Ichinose-B95a) GN=N PE=3 SV=1

MATLLRSLALFKRNKDKPPITSGSGGAIRGIKHIIIVPIPGDSSITTRSRLLDRLVRLIG
NPDVSGPKLTGALIGILSLFVESPGQLIQRITDDPDVSIRLLEVVQSDQSQSGLTFASRG
TNMEDEADQYFSHDDPSSSDQSRSGWFENKEISDIEVQDPEGFNMILGTILAQIWVLLAKAV
TAPDTAADSELRRWIKYTQQRRVVGEFRLERKWLDVVRNRIAEDLSLRRFMVALILDIKRTP
GNKPRIAEMICDIDTYIVEAGLASFILTIKFGIETMYPALGLHEFAGELSTLESLMNLYQQMGET
APYMVILENSIQNKFSAGSYPLLWSYAMGVGVELENSMGGLNFGRSYFDPAYFRLGQEMV
RRSAGKVSSTLASELGITAEDARLVSEIAMHTTEDRISRAVGPRQAQVSFLHGDQSENELPG
LGGKEDRRVKQGRGEARESYRETGSSRASDARAAHPPTSMPLDIDTASESGQDPQDSRR
SADALLRLQAMAGILEEQGSDTDTPRVYNDRDLLD

>sp|Q9WMB4|PHOSP_MEASC **Phosphoprotein** OS=Measles virus (strain Ichinose-B95a) GN=P/V PE=3 SV=1

MAEEQARHVKNGLECIRALKAEPIGSLAVEEAMAAWSEISDNPGQDRATCKEEEAGSSGLS
KPCLSAIGSTEGGAPRIRGQGSGESDDDAETLGIPSRNLQASSTGLQCYHVYDHSGEAVKG

IQDADSIMVQSGLDGDSTLSGGDDESENSDVDIGEPDTEGYAITDRGSAPISMGFRASDVET
AEGGEIHELLKLQSRGNNFPKLGKTLNVPPPPNPSRASTSETPIKKGTDARLASFGTEIASLL
TGGATQCARKSPSEPSGPGAPAGNVPECVSNAALIQEWTPESGTTISPRSQNNEEGGDYY
DDELFSDVQDIKTALAKIHEDNQKIISKLESLLLLKGEVESIKKQINRQNISISTLEGHLSSIMIAI
PGLGKDPNDPTADVELNPDLKPIIGRDSGRALAEVLKKPVASRQLQGMTNGRTSSRGQLLK
EFQLKPIGKKVSSAVGFVPDTGPASRSVIRSIIKSSRLEEDRKRYLMTLLDDIKGANDLAKFH
QMLMKIIMK

>sp|Q9W850|MATRX_MEASC **Matrix** protein OS=Measles virus (strain Ichinose-B95a) GN=M PE=3 SV=1

MTEIYDFDKSAWDIKGSIAPIQPTTYSDGRLVPQVRVIDPGLGDRKDECFMYMFLLGVVEDS
DPLGPPIGRAFGSLPLGVGRSTAKPEELLKEATELDIVVRRTAGLNEKLVFYNNTPLTLLTPW
RKVLTTGSVFNANQVCNAVNLIPLDTPQRFRVVYMSITRLSDNGYYTVPRRMLEFRSVNAVA
FNLLVTLRIDKAIGPGKIIDNAEQLPEATFMVHIGNFRRKKSEVYSADYCKMKIEKMGLVFALG
GIGGTSLHIRSTGKMSKTLHAQLGFKKTLCYPLMDINEDLNRLLWRSRCKIVRIQAVLQPSVP
QEFRIYDDVIINDDQGLFKVL

>sp|Q786F3|FUS_MEASC **Fusion glycoprotein F0** OS=Measles virus (strain Ichinose-B95a) GN=F PE=3 SV=1

MGLKVNVSAIFMAVLLTLQTPTGQIHWGNLSKIGVVGIGSASYKVMTRSSHQSLVIKLMPNIT
LLNNCTRVEIAEYRRLLRTVLEPIRDALNAMTQNIRPVQSVASSRRHKRFAGVVLAGAALGV
ATAAQITAGIALHQSMLNSQAIDNLRASLETTNQAIEAIRQAGQEMILAVQGVQDYINNELIPS
MNQLSCDLIGQKLGLKLLRYYTEILSLFGPSLRDPISAEISIQALSYALGGDINKVLEKLGYSG
GDLLGILESRGIKARITHVDTESYFIVLSIAYPTLSEIKGVIVHRLE
GVSYNIGSQEWYTTVPKYVATQGYLISNFDESSCTFMPEGTVCSQNALYPMSPLLQECLRG
STKSCARTLVSGSFGNRFILSQGNLIANCASILCKCYTTGTIINQDPDKILTYIAADHCPVVEVN
GVTIQVGSRRYPDAVYLHRIDLGPPISLERLDVGTNLGNAIAKLEDAKELLESSDQILRSMKG
LSSTSIVYILIAVCLGGLIGIPALICCCRGRCNKKGEQVGMSRPGLKPDLTGTSKSYVRSL

>sp|Q786F2|HEMA_MEASC **Hemagglutinin glycoprotein** OS=Measles virus (strain Ichinose-B95a) GN=H PE=1 SV=1

MSPQRDRINAFYKDNPHPKGSRIVINREHLMIDRPYVLLAVLFVMFLSLIGLLAIAGIRL
HRAAIYTAEIHKSLSTNLDVTNSIEHQVKDVLTPLFKIIGDEVGLRTPQRFTDLVKFISD
KIKFLNPDREYDFRDLTWCINPPERIKLDYDQYCADVAAEELMNALVNSTLLEARATNQFLA
VSKGNCSGPTTIRGQFSNMSLSLLDLYLSRGYNVSSIVTMTSQGMYGGTYLVGKPNLSSKG
SELSQLSMHRVFEVGVIRNPGLGAPVFHMTNYFEQPVSNDFSNCMVALGELKFAALCHRED
SITIPYQGSGKGVSFQLVKLGVWKSPTDMRSWVPLSTDDPVIDRLYLSSHRGVIADNQAKW
AVPTTRTDDKLRMETCFQQACKGKNQALCENPEWAPLKDNRIPSYGVLSVNLSLTVELKIKI
ASGFGPLITHGSGMDLYKTNHNNVYWLTIPPMKNLALGVINTLEWIPRFKVSPNLFTVPIKEA
GEDCHAPTYLPAEVDGDVKLSSNLVILPGQDLQYVLATYDTSRVEHAVVYYVYSPSRSFSYF
YPFRLPIKGVPIELQVECFTWDKKLWCRHFCVLADSESGGHITHSGMVGMGVSCTVTREDG
TNRR

>sp|Q9WMB3|L_MEASC **RNA-directed RNA polymerase** L OS=Measles virus (strain Ichinose-B95a) GN=L PE=3 SV=1

MDSLSVNQILYPEVHLDSPIVTNKIVAILEYARVPHAYSLEDPTLCQNIKHRLKNGFSNQ

MIINNVEVGNVIKSKLRSYPAHSHIPYPNCNQDLFNIEDKESTRKIRELLKKGNSLYSKV
SDKVFQCLRDTNSRLGLGSELREDIKEKIINLGVYMHSSQWFEPFLFWFTVKTEMRSVIKSQ
THTCHRRRHTPVFFTGSSVELLISRDLVAIISKESQHVYYLTFELVLMYCDVIEGRLMTETAM
TIDARYAELLGRVRYMWKLIDGFFPALGNPTYQIVAMLEPLSLAYLQLRDITVELRGAFLNHC
FTEIHDVLDQNGFSDEGTYHELIEALDYIFITDDIHLTGEIFSFFRSFGHPRLEAVTAAENVRKY
MNQPKVIVYETLMKGHAIFCGIIINGYRDRHGGSWPPLTLPLHAADTIRNAQASGEGLTHEQ
CVDNWKSFAGVRFGCFMPLSLDSDLTMYLKDKALAALQREWDSVYPKEFLRYDPPKGTGS
RRLVDVFLNDSSFDPYDMIMYVVSGAYLHDPEFNLSYSLKEKEIKETGRLFAKMTYKMRAC
QVIAENLISNGIGKYFKDNGMAKDEHDLTKALHTLAVSGVPKDLKESHRGGPVLKTYSRSPV
HTSTRNVKAEKGFVGFPHVIRQNQDTDHPENIETYETVSAFITTDLKKYCLNWRYETISLFAQ
RLNEIYGLPSFFQWLHKRLETSVLYVSDPHCPPDLDAHVPLCKVPNDQIFIKYPMGGIEGYC
QKLWTISTIPYLYLAAYESGVRIASLVQGDNQTIAVTKRVPSTWPYNLKKREAARVTRDYFVI
LRQRLHDIGHHLKANETIVSSHFFVYSKGIYYDGLLVSQSLKSIARCVFWSETIVDETRAACS
NIATTMAKSIERGYDRYLAYSLNVLKVIQQILISLGFTINSTMTRDVVIPLLTNNDLLIRMALLPA
PIGGMNYLNMSRLFVRNIGDPVTSSIADLKRMILASLMPEETLHQVMTQQPGDSSFLDWAS
DPYSANLVCVQSITRLLKNITARFVLIHSPNPMLKGLFHDDSKEEDERLAAFLMDRHIIVPRAA
HEILDHSVTGARESIAGMLDTTKGLIRASMRKGGLTSRVITRLSNYDYEQFRAGMVLLTGRK
RNVLIDKESCSVQLARALRSHMWARLARGRPIYGLEVPDVLESMRGHLIRRHETCVICECGS
VNYGWFFVPSGCQLDDIDKETSSLRVPYIGSTTDERTDMKLAFVRAPSRSLRSAVRIATVYS
WAYGDDDSSWNEAWLLARQRANVSLEELRVITPISTSTNLAHRLRDRSTQVKYSGTSLVRV
ARYTTISNDNLSFVISDKKVDTNFIYQQGMLLGLGVLETLFRLEKDTGSSNTVLHLHVETDCC
VIPMIDHPRIPSSRKLELRAELCTNPLIYDNAPLIDRDATRLYTQSHRRHLVEFVTWSTPQLYH
ILAKSTALSMIDLVTKFEKDHMNEISALIGDDDINSFITEFLLIEPRLFTIYLGQCAAINWAFDVH
YHRPSGKYQMGELLSSFLSRMSKGVFKVLVNALSHPKIYKKFWHCGIIEPIHGPSLDAQNLH
TTVCNMVYTCYMTYLDLLLNEELEEFTFLLCESDEDVVPDRFDNIQAKHLCVLADLYCQPGT
CPPIRGLRPVEKCAVLTDHIKAEARLSPAGSSWNINPIIVDHYSCSLTYLRRGSIKQIRLRVDP
GFIFDALAEVNVSQPKVGSNNISNMSIKDFRPPHDDVAKLLKDINTSKHNLPISGGSLANYEIH
AFRRIGLNSSACYKAVEISTLIRRCLEPGEDGLFLGEGSGSMLITYKEILKLNKCFYNSGVSAN
SRSGQRELAPYPSEVGLVEHRMGVGNIVKVLFNGRPEVTWVGSIDCFNFIVSNIPTSSVGFI
HSDIETLPNKDTIEKLEELAAILSMALLLGKIGSILVIKLMPFSGDFVQGFISYVGSHYREVNLV
YPRYSNFISTESYLVMTDLKANRLMNPEKIKQQIIESSVRTSPGLIGHILSIKQLSCIQAIVGGA
VSRGDINPILKKLTPIEQVLISCGLAINGPKLCKELIHHDVASGQDGLLNSILILYRELARFKDN
QRSQQGMFHAYPVLVSSRQRELVSRITRKFWGHILLYSGNRKLINRFIQNLKSGYLVLDLHQ
NIFVKNLSKSEKQIIMTGGLKREWVFKVTVKETKEWYKLVGYSALIKD

A.3 – Model of MeV M protein structure

A model of the 3D structure of M was generated as described in **chapter 2 section 2.11.2** using SWISS-MODEL software and based on the protein structure of Newcastle disease virus matrix protein (RSCB PDB entry #4G1L). A 3D structure of MeV M is presented in **Fig.A-1**. Two dimers of MeV M adopt a typical cubic shape as seen in other paramyxoviral and pneumoviral matrix proteins. The N-terminus of M was located at the dimer interface while the C-terminal end locates to the outside face of the dimer (**Fig.A-1A**).

Fig.A-1. **Predicted 3D structure of MeV M protein.** (**A**) A dimer of MeV M (red and blue) forms a compact cubic shape with the top part likely to associate with the inner leaflet of the plasma membrane as it is a highly hydrophobic region of the complex. The N-terminal end of M is located inside the dimer, i.e. buried at the interface between the two monomers. The C-terminus of M locates to the side of dimer. (**B**) Top view of the MeV M dimer.

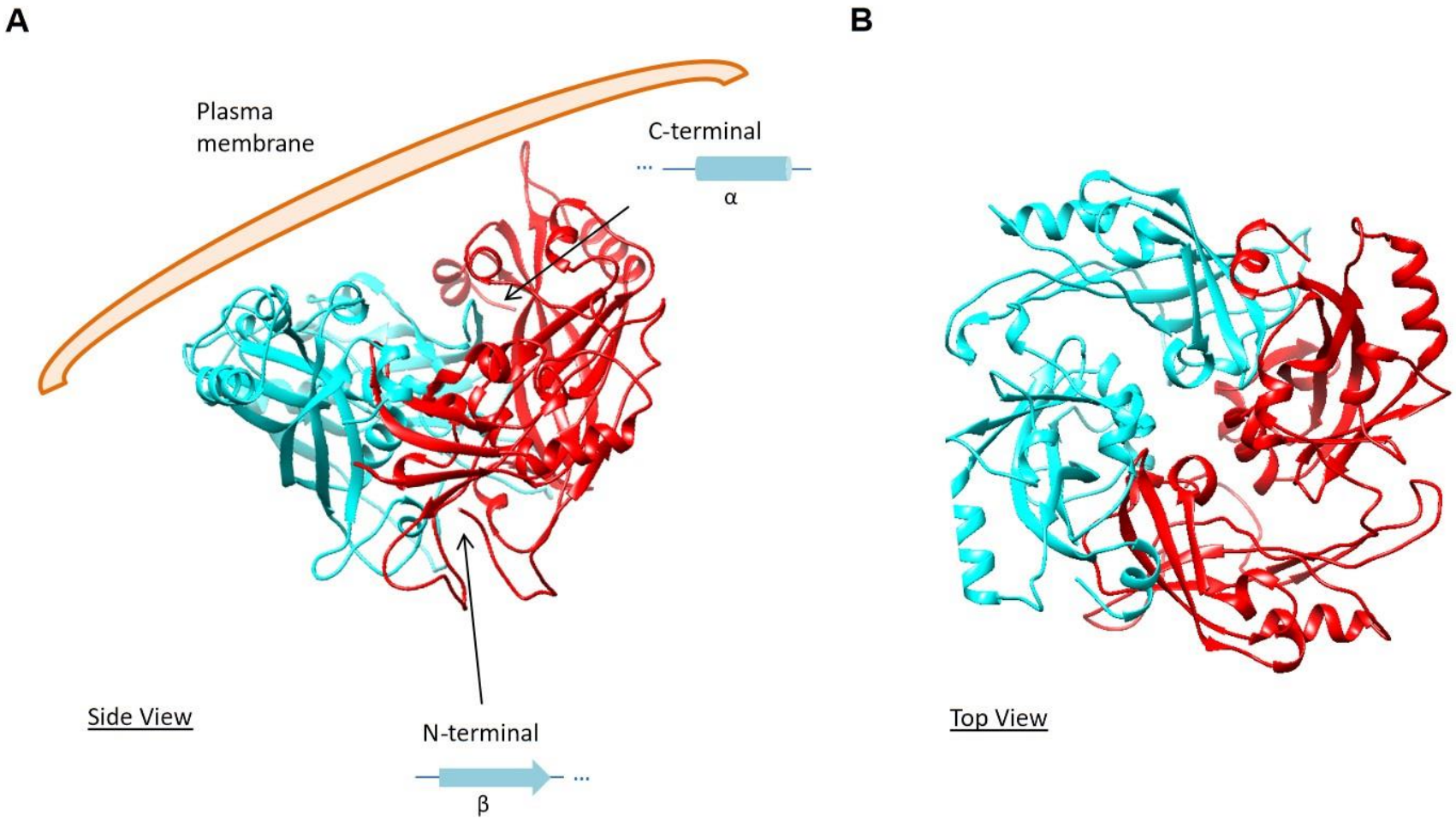
A
Plasma
membrane
C-terminal
α
Side View
N-terminal
β
B
Top View

A.4 – Blebbistatin and EIPA effectively block fluid-phase uptake in A549-SLAM

In chapter 4, I have used blebbistatin and EIPA to block MeV entry. As a control, I tested if these drugs will also block macropinocytosis as reported previously [401]. I pre-treated A549-SLAM with EIPA or blebbistatin at the indicated concentrations, washed and incubated with soluble fluorescent Dextran for 30min. Macropinocytosis was induced by the addition of PMA. Cells were bleached, fixed and prepared and observed by CSLM (**Fig.A-2**). The formation of macropinosomes was blocked by the two drugs at the indicated concentrations.

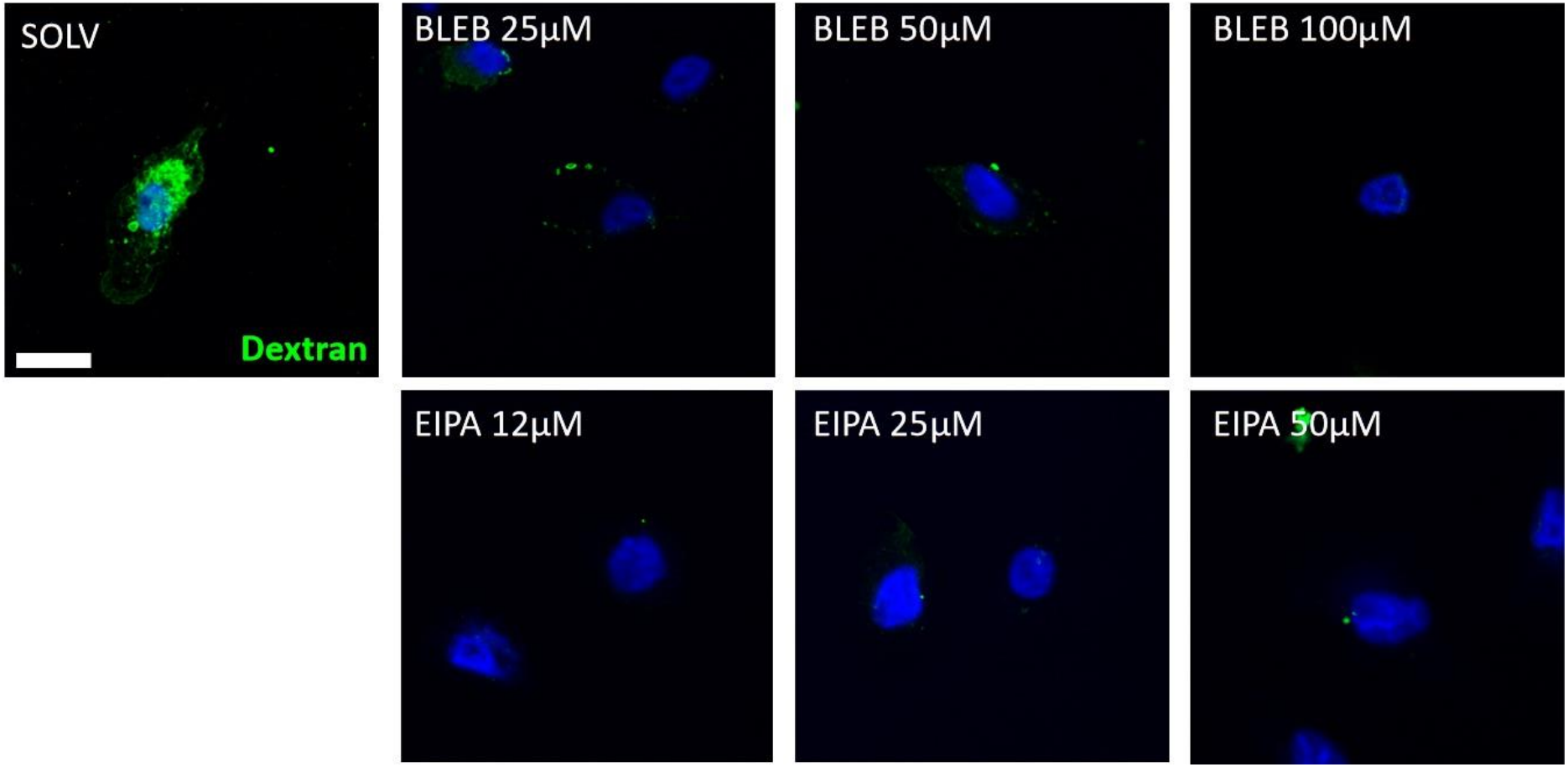
SOLV
Dextran
BLEB 25µM
BLEB 50µM
BLEB 100µM
EIPA 12µM
EIPA 25µM
EIPA 50µM

A.5 – Cytochalasin D and Jasplakinolide alter the pattern of the phalloidin-stained actin cytoskeleton

Similarly, I have used cytochalasin D and jasplakinolide to interfere with actin polymerisation. A549-SLAM cells were treated with drugs at indicated concentrations, fixed and stained with phalloidin (**Fig.A-3**). Cytochalasin D decreased the formation of actin filaments while jasplakinolide reduced staining with phalloidin due to the competitive binding of actin, as reported [439].

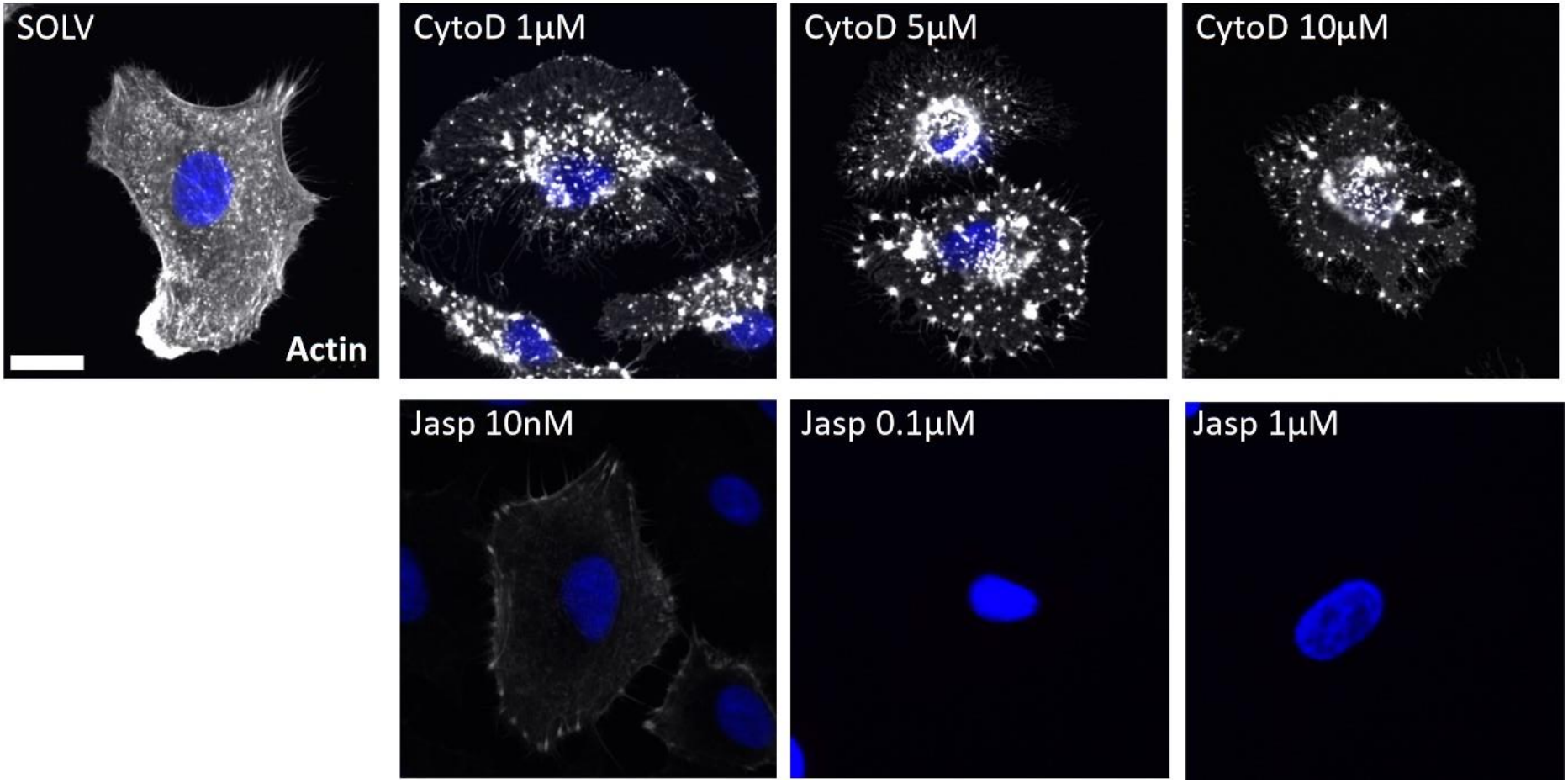
SOLV
Actin
CytoD 1µM
CytoD 5µM
CytoD 10µM
Jasp 10nM
Jasp 0.1µM
Jasp 1µM